2mip

June 1970

NVR-6431

(NASA-CR-134230) INVESTIGATION OF PREDICTION METHODS FOR THE LOADS AND STRESSES OF APOLLO TYPE SPACECRAFT PARACHUTES. VOLUME 1: LOADS (Northrop Corp.) 367 p HC CSCL 01B G3/02

N74-19673

Unclas 34747

NORTHROP

Investigation of Prediction Methods for the Loads and Stresses of Apollo Type Spacecraft Parachutes

Volume I - Loads

By

F. E. Mickey, A. J. McEwan,
E. G. Ewing, W. C. Huyler Jr.,
and B. Khajeh-Nouri

Prepared under Contract NAS 9-8131 for
National Aeronautics and Space Administration
Manned Spacecraft Center

Northrop Corporation, Ventura Division
Newbury Park, California, 91320

June 1970 NVR-6431

INVESTIGATION OF PREDICTION METHODS FOR THE LOADS AND STRESSES OF APOLLO TYPE SPACECRAFT PARACHUTES
VOLUME I - LOADS

Prepared for

NASA Manned Spacecraft Center
Houston, Texas
under Contract NAS 9-8131

Prepared by

F. E. Mickey, A. J. McEwan
E. G. Ewing, W. C. Huyler, Jr.
and B. Khajeh-Nouri

Approved by:

D. D. Warner, Manager
Engineering Department

NORTHROP CORPORATION, VENTURA DIVISION
1515 Rancho Conejo Boulevard
Newbury Park, California 91320

NV Project No. 0111

FOREWORD

This report presents the first volume of a two-volume final report on a one-year study entitled "Analysis of Apollo Spacecraft Parachutes." (The companion volume is listed as Reference 1.) This study was performed by Northrop Ventura for NASA/MSC under Contract NAS 9-8131. Messrs. M. A. Silveira, K. Hinson and C. Eldred of NASA/MSC monitored and reviewed the study.

This study, designated as Project 0111 at Northrop Ventura, was carried out with direction from the Systems Engineering Group under Mr. R. G. Lemm. Program direction was provided by Mr. T. W. Knacke of the Advanced Design Group, and the Project Engineer was Mr. F. E. Mickey of the Aerospace Landing Systems Project Office.

The different sections of the report were prepared by the various authors as follows: Mr. F. E. Mickey, Sections 3.2, 6.1, 6.2, 6.4 and 7.2-7.4; Mr. A. J. McEwan, Sections 1.1, 2.2, 3.1 and part of 4.2; Mr. E. G. Ewing, Sections 1.2, 2.3 and part of 4.2; Mr. W. C. Huyler, Jr., Sections 2.1, 4.1 4.3 and 7.1; Mr. B. Khajeh-Nouri, Sections 5.0 and 6.5. The authors gratefully acknowledge valuable assistance by Dr. D. F. Wolf, who prepared Section 6.3, and Mr. M. R. Bottorff, who prepared Section 7.5.

ABSTRACT

The results of a one-year study on the opening loads of Apollo type spacecraft parachutes are presented. A review is made of the flight test data that were obtained in the Apollo parachute development program to assess existing techniques and to upgrade the previously used load prediction methods. The results of this portion of the study are applied to an Apollo design case. Two new opening load methods are presented. One of these methods, referred to as the Mass/Time Method, is developed to a useful level for single Apollo type main parachutes; and a modified version of this method is applied to several Apollo cluster cases. An analysis of the longitudinal oscillations that occur in the Apollo parachutes indicates that they are caused by strong interactions with the wake of the forebody. A method for analyzing the flow about an inflating parachute is developed, and an algorithm for computing the complete inflation process is presented. The study establishes that the added mass of a parachute canopy cannot be directly inferred from typical flight test data; however, it may be measured by special techniques either in a wind tunnel or in free flight tests.

CONTENTS

CONTENTS (Concluded)

TABLES

TABLES (Concluded)

FIGURES

FIGURES (Continued)

FIGURES (Continued)

FIGURES (Continued)

FIGURES (Concluded)

SYMBOLS AND ABREVIATIONS

A	Canopy surface area	ft^2
A_1, A_2	Added mass coefficients	
BP	Boiler Plate vehicle	
b	Number of radial tapes	
C	Effective porosity	
$\underline{C}$	Nondimensional vehicle-parachute characteristics vector	
C_a	Nondimensional added mass coefficient	
C_DS	Drag area	ft^2
$\overline{\dot{C_DS}}$	Average rate of drag area growth	ft^2/sec
C_K	Opening load factor	
CM	Command Module	
$\underline{c}$	Vehicle-parachute characteristics vector	
D	Drag Diameter	lb ft
DCCS	Drogue Chute Canopy Stretch	
DCLS	Drogue Chute Line Stretch	
DOF	Degrees Of Freedom	
D_o	Nominal diameter ($= \sqrt{4S_o/\pi}$)	ft
D_r	Reefing line diameter	ft
DR1	Disreef, Stage 1	
DR2	Disreef, Stage 2	
E(c.r.)	Energy associated with canopy response	ft-lb
E(f.f.)	Energy associated with forcing function	ft-lb
ELS	Earth Landing System	
F	Force	lb
FN	Froude Number ($= v_o/\sqrt{r_o g}$)	
f_e	Observed (experimental) frequency	hz
f_κ	Canopy response frequency	hz

f_w	Forebody wake frequency	hz
g	Gravitational constant	ft/sec^2
h	Altitude Doublet Strength	ft ft^2/sec
$\underline{h}$	Doublet distribution vector	
ICTV	Instrumented Cylindrical Test Vehicle	
K, K_a	Added mass coefficient	
K_f	Dimensionless filling parameter	
k	Spring constant	lb/ft
$\underline{k}$	Wave number vector	
L	Characteristic length Lead canopy	ft
ℓ	Lag canopy number one	
$\ell\ell$	Lag canopy number two	
$\underline{l}$, $\underline{m}$, $\underline{n}$	Orthogonal unit vector set on canopy surface	
M	Mach number	
MCCS	Main Chute Canopy Stretch	
MCLS	Main Chute Line Stretch	
M, m	Mass	sl
$\dot{m}$	Mass flow function	sl/sec
m_a	Added mass	sl
NA	Not Available	
N_θ	Transverse load in radial tape per unit length along radial tape	lb/ft
n	Filling exponent Canopy growth factor	
PCCS	Pilot Chute Canopy Stretch	
PCLS	Pilot Chute Line Stretch	
P_R	Longitudinal load in radial tape	lb
PTV	Parachute Test Vehicle	
p	Pressure	lb/ft^2

q	Dynamic pressure	lb/ft^2
$\underline{q}$	Fluid velocity vector	
R	Radius Nondimensional radius $(= r/r_o)$ Radial coordinate of canopy surface	ft ft
R_{ij}	Correlation function	
R_o	Nominal radius $(= D_o/2)$	ft
R_ϕ	Meridional radius of curvature	ft
r	Radius	ft
$\underline{r}$	Canopy shape vector Separation vector (between two points)	
S_o	Nominal area of parachute	ft^2
s	Distance measured along flight path	ft
T	Fluid kinetic energy Nondimensional time $(= v_o t/r_o)$	ft-lb
t	Time	sec
Δt	Time to peak load	sec
t_f, t_{fill}	Fill time	sec
t^*	Ratio of Δt to t_{fill}	
U	Nondimensional velocity $(= v/v_o)$	
u	Amplitude of oscillation velocity	ft/sec
$\underline{u}_c$	Canopy surface velocity vector	
V	Volume	ft^3
v	Velocity along flight path	ft/sec
$\underline{v}$	Velocity vector	
W	Weight	lb
W/C_DS	Ballistic coefficient Unit canopy loading	lb/ft^2 lb/ft^2
W^*/C_DS	Effective unit canopy loading	lb/ft^2
w	Velocity normal to flight path (= 0)	ft/sec
w_c	Transport velocity of air through canopy surface	ft/sec
$\underline{X}$	Nondimensional state vector	
X, Z	Canopy surface coordinates	

x, y, z	Fixed coordinates	ft
x', y', z'	Moving coordinates	ft
$\underline{x}$	State vector	
Z	Coaltitude Longitudinal coordinate of canopy surface	ft ft
α	Angle defined by sketch on page 269	deg
γ	Flight path angle	deg
ε	Strain	
θ	Flight path angle, positive below horizontal plane (= $-\gamma$)	deg
Λ	Air inflow parameter	ft^3/sec
μ	Canopy mass per unit area	sl/ft^2
ν	Viscous damping coefficient Added mass ratio (= $v_o/\sqrt{r_o g}$)	lb-sec/ft
ξ	Damping factor	
ρ	Air (or fluid) density	sl/ft^3
σ	Meridional distance along canopy surface	ft
Φ	Energy spectrum function	
ϕ	Velocity potential	ft^2/sec
ϕ	Angle defined by sketch on page 271	deg
χ	Canopy surface azimuth angle	deg
Ψ	Drag area (= $C_D S$)	ft^2
Ω	Solid angle	steradians
ω	Angular velocity	rad/sec

Subscripts

av	Average
c	canopy
DCCS	Drogue Chute Canopy Stretch
DCLS	Drogue Chute Line Stretch
d	Disreef

dyn	Dynamic
i	Initial Inlet Inside
L	Lead canopy
MCCS	Main Chute Canopy Stretch
m	Maximum (or peak) mouth
o	Full open Outside
PCCS	Pilot Chute Canopy Stretch
PCLS	Pilot Chute Line Stretch
p	Parachute Projected
r	Reefed
s	Canopy skirt
se	Static equilibrium
ss	Steady state
tr	Transient
v	Vehicle Along flight path
w	Normal to flight path
1	Stage 1 At beginning of inflation
2	Stage 2 At end of inflation
∞	Infinity

SECTION 1.0

INTRODUCTION

The Apollo parachute landing system was designed, developed and qualified by Northrop Ventura during the period 1962-1968. In the normal course of this development, many flight tests were made, and extensive data on the performance of the Apollo spacecraft parachutes were collected. These data were used as the basis for developing the methods that were used during the course of the flight test program for estimating loads and in making structural analyses for the principal Apollo parachute assemblies: the drogue chutes, the pilot chutes and the main parachutes.

It was recognized that there would be substantial value in an analysis effort that would review all the flight test data at one time. In particular, it was seen that such an analysis effort would be free of the day-to-day pressures associated with a development program, and consequently that it could upgrade the loads and stress analysis methods used for the Apollo spacecraft parachutes in ways that had not been considered previously. The present study was therefore authorized with the objective of upgrading and improving loads, stress and performance prediction methods for Apollo spacecraft parachutes. Also included in this study were the tasks of developing (a) methods for a new theoretical approach to the parachute opening process, (b) new experimental-analytical techniques to improve the measurement of pressures, stresses and strains in inflight parachutes, and (c) a numerical method for analyzing the dynamical behavior of rapidly loaded pilot chute risers. In performing these tasks, emphasis was placed on analytical (as opposed to empirical) methods of analysis.

The results of the study are published in two volumes as follows:

INVESTIGATION OF PREDICTION METHODS FOR THE LOADS AND STRESSES OF APOLLO TYPE SPACECRAFT PARACHUTES
VOLUME I - LOADS

and

INVESTIGATION OF PREDICTION METHODS FOR THE LOADS AND STRESSES OF APOLLO TYPE SPACECRAFT PARACHUTES
VOLUME II - STRESSES

The present volume is VOLUME I - LOADS. The companion volume is listed as Reference 1.

Volume I presents the results of a study conducted for the purpose of analyzing Apollo parachute loads* data, upgrading loads prediction methods, and investigating advanced prediction methods. This includes a thorough analysis of an extensive amount of flight test data on the Apollo drogue and main parachutes. These data were used to upgrade the pertinent load prediction methods for both the drogue and main parachutes and to develop improved semiempirical methods directly applicable to Apollo type spacecraft parachutes. In addition, there is presented an investigation of vehicle-parachute interactions, a new parachute inflation theory, and concepts for new parachute test techniques.

Volume II presents the results of a study on parachute structural analysis methods which make extensive use of the test data accumulated during the Apollo development and qualification test programs. These study results include a literature review, refinement and extension of the Apollo structural analysis

* Unless otherwise indicated, the word "loads" in this report refers to the longitudinal loads transmitted through the parachute riser.

methods, corroboration of the methods by comparing analytical and test results, and application of the improved structural analysis methods to the Apollo parachutes. In addition, there is presented a study on dynamic loading effects in pilot parachute risers and an investigation of techniques for measuring loads, strains and differential pressures in parachutes.

SECTION 2.0

REVIEW OF APOLLO LOADS DATA AND REFINEMENT OF LOADS METHODS

This section contains the results of analyses that were undertaken to upgrade and improve the load prediction methods used in the Apollo development and qualification test programs. The scope of the material presented in this section is, in general, limited to Apollo parachute loads data and loads prediction methods. This portion of the report was completed prior to the evaluation and development of new loads methods presented in subsequent sections of the report.

Figure 1 illustrates the operational sequence of the Apollo Earth Landing System (ELS) for the normal entry mode. This system includes nine parachutes: an apex cover parachute, two drogue chutes, three pilot chutes and three main parachutes. A precise specification of this system including design and reliability criteria employed during its development is given in Reference 2.

Three test vehicles were used in the Apollo parachute development program. These vehicles, an Instrumented Cylindrical Test Vehicle (ICTV), a Parachute Test Vehicle (PTV) and a Boiler Plate vehicle (BP), are illustrated in Figure 2.

The data and loads analyses undertaken in this study were limited to the drogue, pilot and main parachutes. These analyses are documented in the three subsections that follow.

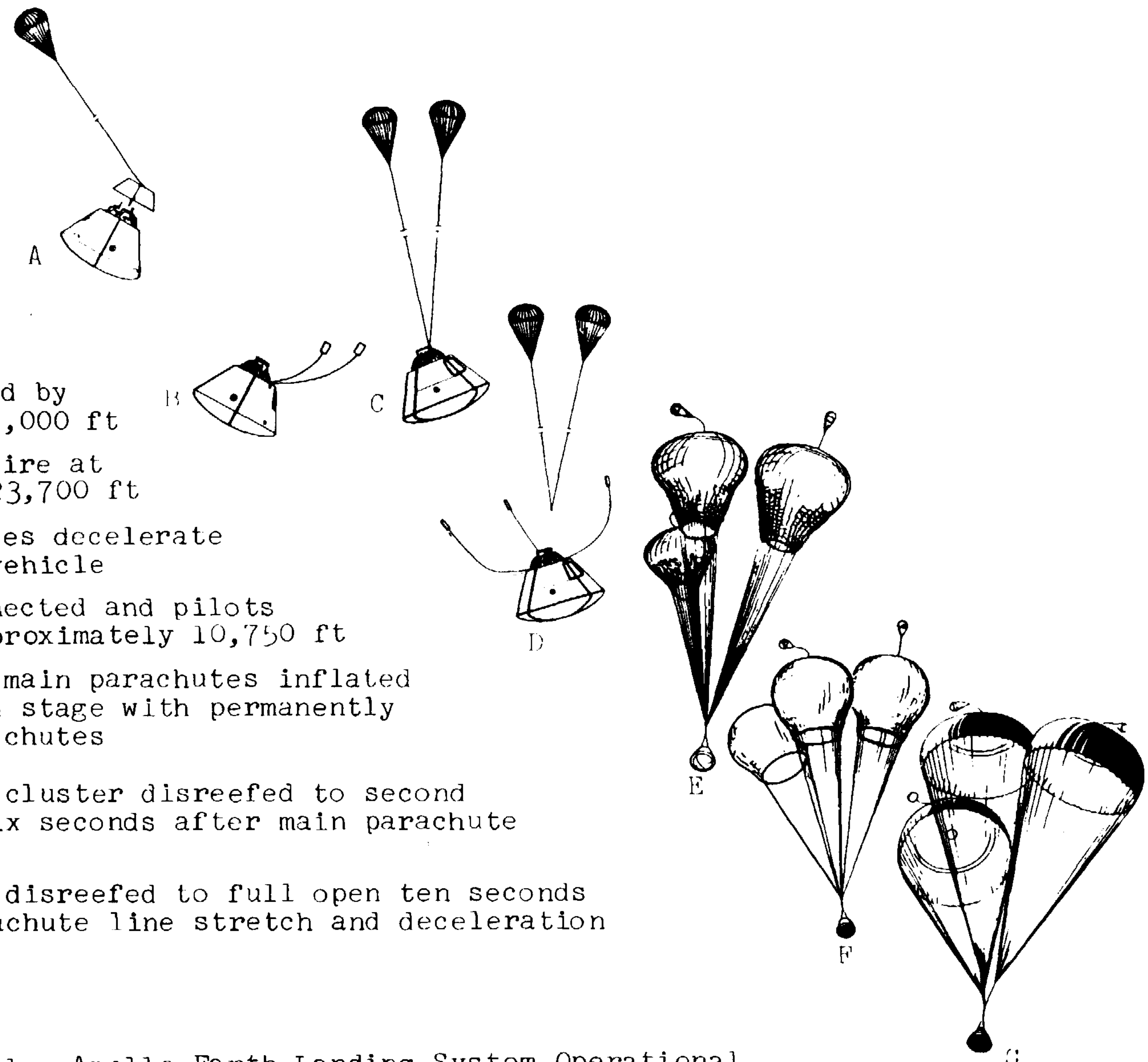

A. Apex cover separation aided by parachute at 24,000 ft

B. Drogue mortar fire at approximately 23,700 ft

C. Disreefed drogues decelerate and stabilize vehicle

D. Drogues disconnected and pilots mortared at approximately 10,750 ft

E. Pilot-deployed main parachutes inflated in first reefed stage with permanently attached pilot chutes

F. Main parachute cluster disreefed to second reefed stage six seconds after main parachute line stretch

G. Main parachute disreefed to full open ten seconds after main parachute line stretch and deceleration to impact.

Fig. 1. Apollo Earth Landing System Operational Sequence of Normal Entry Mode

ICTV	PTV	BP
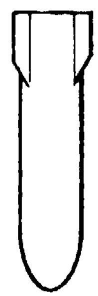	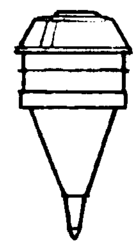	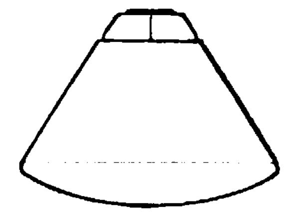
Instrumented Cylindrical Test Vehicle	Parachute Test Vehicle	Boilerplate
Length .... 160 in.	Length.............128 in.	Length............. 105 in.
Diameter .... 35 in.	Diameter .... 70 in.	Diameter .... 154 in.

Fig. 2. Vehicles Used in Apollo Parachute Development Program

2.1 DROGUE CHUTE LOADS

Each of the two drogue chute assemblies consists of a 16.5-foot diameter, conical ribbon parachute with a textile riser, a deployment bag, a steel cable riser, and a mortar tube assembly. The purpose of the drogue chutes is to provide drag, both to decelerate the Command Module (CM) and to stabilize it in the aft heat shield forward attitude. Each drogue chute features a reefing line with a nominal 10-second reefing interval to restrict the deployment loads to values that do not exceed the limits given in Reference 3 -- single drogue, 20,000 lb; two drogues, 20,000 lb each. Each 31.7-foot riser includes 15 ft of steel cable to provide protection against abrasion damage by the CM. The physical characteristics of a drogue chute including its riser and deployment bag are illustrated in Figure 3.

2.1.1 Loads Methods Used in Apollo Parachute Development Program

The loads methods used in the Apollo parachute development program are described in detail in Reference 3. Briefly, these methods were as follows.

The flight conditions at drogue mortar fire were the starting point for the parachute loads calculations. These conditions were determined by the Apollo prime contractor (the North American-Rockwell Corporation) by analyzing the dynamics of the CM for the normal entry mode and all possible abort modes. With these initial conditions, the flight conditions of the CM at drogue line stretch were calculated by using a three-degree-of-freedom (3-DOF) computer program. This computer program was used to compute the velocity difference between the drogue chute and the CM at the instant of line stretch. The snatch force, which occurs at this time, was then calculated with a snatch force computer program. Next, the opening load factor method was used

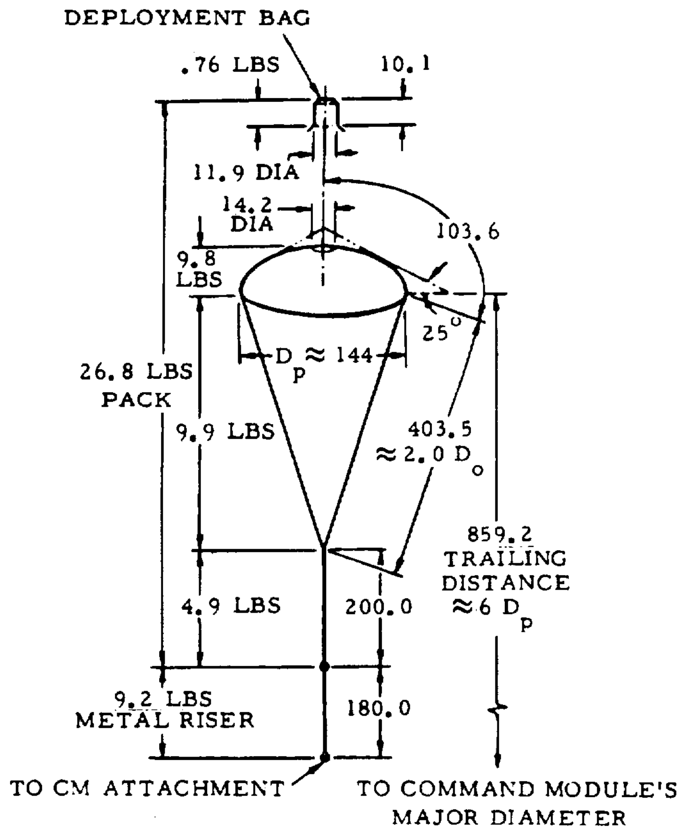

NOTE: The lengths shown above are fabrication dimensions (without strains)

General Data:

- Type - Conical ribbon with one-stage reefing
- Nominal diameter, D_o = 16.5 ft (198 in.)
- Nominal canopy area, S_o = 214 ft^2
- Number of gores = 20
- Canopy porosity = 22%
- Reefing line length = 266 in.
- Overinflation line length = 396 in.

Single Chute Characteristics:

- Reefed open drag area, $(C_D S)_r$ = 65 ft^2
- Full open drag area, $(C_D S)_o$ = 114 ft^2
- Pack weight = 26.8 lb (less metal riser)
- Pack volume = 1000 in.^{3}

Double Chute Characteristics:

Multiply the above single chute caracteristics by 2.0

Deployment Conditions:

Mortar muzzle velocity = 65.85 ft/sec (min)

At line stretch,	Minimum	Maximum
Altitude, ft	3,000	40,000
Dyn. pres., lb/ft^2	10	204
Mach number	0.10	0.67

Limit Loads (single chute):

- Reefed open, $(F_r)_{lim}$ = 17,200 lb
- Full open, $(F_o)_{lim}$ = 15,000 lb

Terminal Conditions:

For 13,000-pound CM,	One-Chute	Two-Chute
Altitude, ft	10,750	10,750
Dyn. pres., lb/ft^2	70	46
Mach number	0.265	0.214

Fig. 3. Configuration Drawing and Data for an Apollo Drogue Chute (Reference 2)

to calculate the reefed inflation load, F_r. That is, the following relation was used.

$$F_r = (C_K)_r \ (C_DS)_r \ q_{DCLS}$$

where $(C_K)_r$ denotes reefed opening load factor, $(C_DS)_r$ denotes reefed drag area, and q_{DCLS} denotes dynamic pressure at drogue chute line stretch. The value of $(C_K)_r$ used in this computation was estimated by giving careful consideration to the empirically derived values of $(C_K)_r$ associated with earlier reefed opening tests of the same parachute.

The next step in the computational sequence was to use the 3-DOF computer program to compute the flight conditions at the end of the 10-second interval of reefed drogue chute operation. Having thus established the conditions at the time of disreef, the opening load factor method was used to compute the disreef opening load, F_o. Namely, the following relation was evaluated.

$$F_o = (C_K)_o \ (C_DS)_o \ q_d$$

where $(C_K)_o$ denotes disreefed opening load factor, $(C_DS)_o$ denotes full open drag area, and q_d denotes dynamic pressure at disreef. The value of $(C_D)_o$ used in this computation was estimated by giving careful consideration to the empirically derived values of $(C_K)_o$ associated with earlier disreefed opening tests of the same parachute.

Reefing line load was evaluated as 4 percent of F_r, and over-inflation control line load was taken as 4 percent of F_o.

Table 1 is a summary of the drogue chute loads and methods used in the Apollo development program.

Table 1. Summary of Load Prediction Methods Used in Computing Apollo Drogue Chute Loads

Load	Method Used (see Ref. 3)
F_r	Opening Load Factor
F_o	Opening Load Factor
Snatch	Snatch Force Program
Reefing Line	0.04 x F_r
Overinflation Line	0.04 x F_o

2.1.2 Review and Refinement of Opening Load Factor Method

The drogue chute loads data from the Apollo parachute development and qualification tests were reviewed, and an analysis was made to upgrade the previously used opening load factor method. It was found that several improvements could be made in the opening load factor method described above. One improvement consists of using the dynamic pressure at drogue chute canopy stretch, q_{DCCS}, in the F_r calculation in place of q_{DCLS}. This is because the dynamic pressure at canopy stretch is more intimately connected with the opening process than the dynamic pressure at line stretch. (The dynamic pressure at the time of maximum load could also be used; however, this would be somewhat more difficult because of vehicle decelerations immediately prior to the time of maximum load.) The dynamic pressure at disreef, q_d, is still the best dynamic pressure for use in the F_o calculation. It was also found that an improvement could be made in the determination of values for the opening load factors. The following subsections discuss these results.

2.1.2.1 Conditions at Drogue Canopy Stretch. The time of drogue canopy stretch is defined as the instant when the parachute canopy starts to fill. It is measured on the telemetry force-time record as the point at the base of the opening load rise. At this time, the canopy is deployed and snatched, but it has not yet begun to open and there is no drag area except for the small amount due to the streaming canopy and lines.

For a test that has already been conducted, the vehicle flight conditions at drogue canopy stretch are determined through the use of combined observed and calculated data. It is felt that this approach, because it makes the best use of the available data, is an improvement over the previous approach of relying solely on observed data.

The reason for developing a new approach is that the cine-theodolite (Askania) data, which were used previously, are not accurate at the time of canopy stretch. Apollo Askania is designed to measure near-equilibrium flight conditions. In order to perform this function, the cine-theodolite cameras are run at 5 fr/sec, and 7-point data smoothing is used in data reduction. In a typical test, the drogue programmer parachute (referred to as the programmer) is disconnected, the vehicle accelerates in free fall until drogue canopy stretch (usually less than a second after programmer disconnect), and then the drogue chute inflates and decelerates the vehicle toward equilibrium. Thus, in a period of less than two seconds, the vehicle goes through a rapid acceleration and then begins a rapid deceleration. At the same time, the data are sampled at less than 10 points and these points are subsequently subjected to 7-point smoothing. The net result is that the peak velocity and dynamic pressure, which occur during parachute inflation, are reported in error and are furthermore reported as lower than the actual values. This error leads to the determination of values of C_K that are too large. This dynamic pressure error is somewhat random and therefore leads to random errors in C_K as well as bias errors.

The new approach uses Askania to determine flight conditions at programmer disconnect and then calls for calculating conditions at drogue canopy stretch with the equations of motion of the vehicle. Askania data are the only source of flight conditions at programmer disconnect. In some instances, the flight conditions data at disconnect are in error because of the effect of the post-disconnect acceleration through smoothing. In such cases, it becomes necessary to extrapolate data from several seconds prior to disconnect to the time of disconnect. The time of disconnect is accurately known from the electronic events recorder. Thus, vehicle flight path angle, velocity and altitude are known from Askania at disconnect. Rawin data provide air density as a function of altitude. Vehicle weight and mass are accurately known and vehicle drag area is also known. The time of canopy stretch is accurately known from the drogue chute load traces. Therefore, all pertinent parameters in the calculation of flight conditions at canopy stretch are known. With an ICTV or a PTV, the ballistic coefficient, W/C_DS, is so high that vehicle drag area is usually not a critical parameter. Thus, best available information is being used to calculate flight conditions at canopy stretch.

Several calculation methods are possible. The 3-DOF computer program could be used to provide a very accurate result for the flight conditions at canopy stretch. While less accurate a method, the solution of the vehicle acceleration under the assumptions of constant flight path angle and air density could be used. The trajectory equation,

$$\frac{dv}{dt} = \frac{W \sin \theta - \frac{1}{2} \rho v^2 C_D S}{m}$$

then has the solution (see Symbols Section for notation definitions):

$$v(t) = \sqrt{\frac{2W \sin \theta}{C_D S \rho}} \left[\frac{c \exp (2 \sqrt{g \sin\theta \, C_D S \, \rho/2m})t - 1}{c \exp (2 \sqrt{g \sin\theta \, C_D S \, \rho/2m})t + 1} \right]$$

At the next level of approximation, constant acceleration could be assumed. The change in velocity could then be shown to be equal to $\frac{W \sin \theta - C_D S q}{m}$ times the free fall interval, where q is the dynamic pressure at programmer disconnect. A sample calculation was performed using actual test conditions, and it was found that even with a BP having a drag area estimated at 90 ft^2, the three methods give almost identical results. Because the constant acceleration method is the simplest, it was chosen for the analysis.

The new method was applied to every Block II (H)* test for which $(C_K)_r$ could be analyzed. The calculated q_{DCCS} at drogue canopy stretch is presented in Table 2 along with the Askania provided q_{DCCS} for comparison. Almost without exception, the calculated q_{DCCS} is higher.

2.1.2.3 Discussion of Parameters Affecting C_K at Reefed Opening

Some of the parameters affecting $(C_K)_r$ of an Apollo drogue chute are the type of test vehicle (a wake effect), the Mach number, the deployment system, the vehicle attitude, the

---

* The Apollo parachute development and qualification tests were conducted in three blocks: Block I, Block II and Block II (H). The specific tests that were associated with each of these blocks are given in Appendix A of Volume II.

canopy fill rate, the ballistic coefficient, the flight path angle, and the magnitude of the loads developed. Knowing the relative effect of each parameter enables more precise opening load factor prediction, a definite improvement over the previous technique which used an ensemble average from past tests together with a scatter factor.

Table 2. Comparison of Calculated and Observed Dynamic Pressures at Drogue Chute Canopy Stretch

Test	Calculated q_{DCCS}	Askania q_{DCCS}	Difference (2)
83-6	154 lb/ft^2	153 lb/ft^2	+1%
84-1	199	193	+3
84-1R	238	239	-0.4
84-3	366	354	+3
84-4	175	172	+2
85-1	94 (1)	90	+4
85-2	68 (1)	62	+10
85-3	124 (1)	123	+1
85-4	105 (1)	97	+8
99-2	317	306	+4
99-3	203	192	+6
99-4	288	282	+2

NOTES: (1) Calculated values of q_{DCCS} for 85 Series tests are felt to be inaccurate due to drag area uncertainties (caused by vehicle oscillations).

(2) The following equation is used to compute the values given in the last column:

$$\text{Difference} = \left\{ \frac{\text{Calculated } q_{DCCS} - \text{Askania } q_{DCCS}}{\text{Askania } q_{DCCS}} \right\} (100\%)$$

The re-evaluation began with reviewing the test data from all Apollo test programs. An opening load factor for each drogue chute in each test was calculated and the associated telemetry and film coverage were studied. Each test's history was reviewed to identify the reasons for opening load factor differences. A trend was observed. Where no riser dynamics had occurred, it was found that the reefed opening load factor could be evaluated as follows:

$$
\begin{aligned}
(C_K)_r = \ & 1.00 \text{ plus the following factors as they apply:} \\
& + 0.00 \text{ if an ICTV is used} \\
& + 0.21 \text{ if a BP is used} \\
& + 0.18 \text{ if a PTV is used} \\
& + 0.07 \text{ if loads are high } (> \text{limit}) \\
& + 0.05 \text{ if mortar deployed} \\
& + 0.05 \text{ if only one drogue chute inflates} \\
& + 0.02 \text{ if test Mach number is high } (> 0.75)
\end{aligned}
\tag{1}
$$

For example, Equation (1) predicts a value of $(C_K)_r$ for Test 99-4 equal to 1.00 + 0.05 (because the drogues were mortar deployed) + 0.07 (because of the high loads) = 1.12. Likewise, $(C_K)_r$ for Test 84-4 is 1.00 + 0.18 (because it was a PTV test) + 0.05 (because only one drogue deployed) = 1.23, and $(C_K)_r$ for Test 50-12 is 1.00 + 0.21 (because it was a BP test) + 0.05 (because the drogues were mortar deployed) = 1.26.

In the specific case of Apollo drogue chutes, the ballistic coefficient is high enough to produce reefed opening load factors greater than one. In the general case, however, the ballistic coefficient, W/C_DS, may be considerably lower, allowing an appreciable velocity decay during opening and therefore opening load factors less than one.

It may be observed that the largest component in Equation (1) is due to the type of vehicle. This could be because the wake of each vehicle has different energy and frequency characteristics.

The second largest component is associated with the magnitude of the loads developed. The higher the loads, the higher the elongation of the canopy fabric. Elongations produce larger drag areas which in turn cause higher loads and, therefore, higher opening load factors. This is a nonlinear effect.

The deployment system used also influences the opening load factor. Mortar deployed drogue chutes may partially fill outside the vehicle wake, and they may have an increased velocity due to the observed transverse waves in the riser which travel to the vehicle and back just after canopy snatch.

The number of drogue chutes being inflated has an effect. This could be because of aerodynamic blanketing or because of differences in dynamic pressure decay during filling due to a lower ballistic coefficient, W/C_DS.

The Mach number seems to have a very small effect on $(C_K)_r$ at those conditions for which Apollo data are available.

A comparison of the measured reefed opening load factors and the predicted factors using Equation (1) appears in Table 3. This table shows all applicable Block II (H) data.

2.1.2.4 Presentation of Reefed Drogue Chute Test Data. All the applicable test data from the Apollo parachute development program are presented in Table 4. In this table, several peak loads and associated $(C_K)_r$ values are sometimes listed for the same test. The reasons for this are as follows. There may have been two drogue chutes, each experiencing a different riser load; there may have been duplicate riser load instrumentation, each indicating a slightly different riser load;

Table 3. Comparison of Reefed Drogue Chute Opening Load Factors As Predicted by Equation (1) And As Measured

Test No.	Trend Criteria					Opening Load Factors	
	PTV	Mortar Deployed	One Drogue Deployed	High Loads	High Mach	Eq. (1) $(C_K)_r$	Measured $(C_K)_r$
84-1	X					1.18	1.19
99-2				X		1.07	1.07
84-1R	X					1.18	1.18
84-4	X		X			1.23	1.22
84-3	X			X	X	1.27	1.28
99-4		X		X		1.12	1.13

Table 4. Reefed Opening Data for Drogue Parachutes

Test No. (1)	Chute No. Lead/Lag (2)	Drag Area Predicted $(C_DS)_r$ ft^2	Drag Area Actual $(C_DS)_r$ ft^2	Peak Opening Force F_r lb (3)	Initial Dynamic Pressure q_{DCCS} lb/ft^2	Opening Load Factor $(C_K)_r$ (4) (5)	Test Vehicle Type	Test Vehicle Weight W lb	Flight Path Angle γ_{DCCS} deg	Initial Mach Number M_{DCCS}	Type of Deployment	Type of Construction Lines	Unit Canopy Loading $\frac{W}{(C_DS)_r}$ lb/ft^2	Number of Parachutes	Reefing Diameter D_{r_2} % D_o	Drogue Chute Diameter D_o ft
85-1	-YL	Damaged Instrumentation														
	+Y	ℓ 65.	56. ± 2	6200.	94.	1.18	BP	13016.	-63	.37	Mortar	2500 lb Nylon	120	2	42.8	16.5
	+Y	ℓ (6)	52. ± 2	8000.		1.64		-								
85-2	+Y	L 65.	74. ± 2	5330.	68.	1.06	BP	13038.	-53	.25	Mortar	2500 lb Nylon	117	2	42.8	16.5
	+Y	L (6)	68.	4780		1.03		-								
	-Y	ℓ 65.	Broken Wire													16.5
	-Y	ℓ (6)	40. ± 1	3180		1.17		-								
85-3	+Y	65.	56±2 ft^2	8750.	124.	1.25	BP	13005.	-81	.45	Mortar	2500 lb Nylon	232.	1	42.8	16.5
	+Y	Not Readable														
85-4	-Y	65.	81±2 ft^2	9610.	105.	1.13	BP	13482.	-76	.40	Mortar	2500 lb Nylon	166.	1	42.8	16.5
	-Y	Not Readable														
85-5	+Y	65.	48 ± 2	12680.	172.	1.54	BP	12980.	-85	.48	Mortar	2500 lb Nylon	288.	1	42.8	16.5
	+Y	(6)	43 ± 1	10430.		1.41										
85-6		No Drogues														
85-7	+Y	No Calibration					BP				Mortar	2500 lb Nylon		1	42.8	16.5
	-Y	Broken Link														
50-12	#1		45 ± 3	6600.	118.	1.25	BP	9434.	-87		Mortar		107.	2		13.7
	#2		43 ± 2	6350.		1.25										
86-2	-Y		60	8900.	125.	1.19	BP	13035.	-81	.42	Mortar	2500 lb Nylon	217.	1	42.8	16.5
	+Y		Malfunctioned													
86-3	+Y		67.5	14525.	186.	1.16	BP	12995.	-88	.47	Mortar	2500 lb Nylon	96.5	2	42.8	16.5
	-Y		67.5	15500.		1.23										
86-4	+Y		66.5	2050.	25.4	1.22	BP	12985.	-89	.11	Mortar	2500 lb Nylon	103.	2	42.8	16.5
	-Y		60	2000.		1.31										

NOTES: See end of table

Table 4 Continued. Reefed Opening Data for Drogue Parachutes

Test No. (1)	Chute No.	Lead /Lag (2)	Drag Area Predicted $(C_DS)_r$ ft^2	Drag Area Actual $(C_DS)_r$ ft^2	Peak Opening Force F_r lb (3)	Initial Dynamic Pressure q_{DCCS} lb/ft^2	Opening Load Factor $(C_K)_r$ (4) (5)	Test Vehicle Type	Test Vehicle Weight W lb	Flight Path Angle γ_{DCCS} deg	Initial Mach Number M_{DCCS}	Type of Deployment	Type of Suspension Lines	Unit Canopy Loading $\frac{W}{(C_DS)_r}$ lb/ft^2	Number of Parachutes	Reefing Diameter D_{r_2} % D_o	Drogue Chute Diameter D_o ft
84-1	#1	ℓ	63.0	73.1	17300.	199.	1.19	PTV	12994.	-69.5	.57	Static Line	1400 lb. Dacron	91.44	2	40	16.5
	#2	L	63.0	69.0	15600.		1.14*										
99-2	#1		63.0	80.0	27200.	317.	1.07	ICTV	12999.	-70.2	.72	Static Line	2500 lb. Nylon		2	40	16.5
	#2		63.0	Failed													
84-1R	#1	L	63.0	60.0	16870.	238.	1.18	PTV	13026.	-65.8	.62	Static Line	2500 lb. Nylon	105.9	2	40	16.5
			(6)	59.0	16460.		1.17										
	#2	ℓ		63.0	16800/ 17750		1.14/ 1.20*										
			(6)	65.0	17900/ 18150		1.16/ 1.18*										
84-4	#1	L	58.0	57.0	12030	175.	1.21	PTV	12961.	-66.9	.55	Static Line	2500 lb. Nylon	227.4	1	36.5	16.5
			(6)	57.0	12130		1.22										
84-3	#1		58.0	50.0	23390.	366.	1.28	PTV	13009.	-69.1	.93	Static Line	2500 lb. Nylon		2	36.5	16.5
			(6)	50.0	23660.		1.29										
	#2			Failed													
99-3	#1	ℓ	55.0	64.	22160.	203.	1.70*	ICTV	13001.	-69.9	.83	Mortar	2500 lb. Nylon	100.0	2	36.5	16.5
			(6)	68.	21730		1.57*										
	#2	L	55.0	64.	20700		1.59*										
			(6)	64.	19950		1.54*										
83-6	#1	L	55.0	55.	9900/ 11100	154.	1.17/ 1.31*	PTV	12997.	-63.6	.52	Mortar	2500 lb. Nylon	114.0	2	36.5	16.5
	#2	ℓ	55.0	59.	9400/11100 /11400		1.04/1.21 /1.26*										
99-4	#1	ℓ	62.0	63.	18400/ 19510	288.	1.01/ 1.08*	ICTV	12989.	-61.9	.71	Mortar	2500 lb. Nylon	99.2	2	36.5	16.5
	#2	L	62.0	68.	22140		1.13										

Notes: See end of table

Table 4 Concluded. Reefed Opening Data for Drogue Parachutes

Test No. (1)	Chute No.	Lead /Lag (2)	Drag Area Pre-dicted $(C_DS)_r$ ft²	Drag Area Act-ual $(C_DS)_r$ ft²	Peak Opening Force F_r lb (3)	Initial Dynamic Pressure q_{DCCS} lb/ft²	Opening Load Factor $(C_K)_r$ (4) (5)	Test Vehicle Type	Test Vehicle Weight W lb	Flight Path Angle γ_{DCCS} deg	Initial Mach Number M_{DCCS}	Type of Deploy-ment	Type of Suspen-sion Lines	Unit Canopy Loading $\frac{W}{(C_DS)_r}$ lb/ft²	Number of Para-chutes	Reefing Diameter D_{r_2} % D_o	Drogue Chute Dia-meter D_o ft
48-1	#2		46.	52.0	9277.	q peak at 146.0 sec	1.22*	PTV	9441.	7.9	.57	Static		NA	2	39.3	13.7
	#1		No Telemetry Due To Broken Link									Line				Mid Gore	
48-2	#1	ℓ		47.0	9815.	184.1	1.13	PTV	9229.	8.5	.57	Mortar		103.7	2	39.3	13.7
	#2	L		42.0	9465.		1.22									Radial	
48-3	#1	ℓ		47.0	10030.	189.	1.13	PTV	9442.	8.0	.58	Mortar		101.5	2	41.2	13.7
	#2	L		46.0	9648.		1.12									Mid Gore	
48-4	#1	ℓ		42.0	9416.	183.	1.22*	PTV	10842.	~9.0	.57	Mortar		132.2	2	39.3	13.7
	#2	L		40.0	8992.		1.23*									Radial	
48-5	#1	L		49. ± 1	17175.	259.	1.35	PTV	10890.	9.0	.68	Mortar		113.4	2	39.3	13.7
	#2	ℓ		47. +1	13605.		1.12									Radial	

NOTES: (1) +Y and -Y denote the +Y bay parachute and the -Y bay parachute, respectively. #1 and #2 denote number one and number two parachutes, respectively

(2) L and ℓ denote the lead canopy and the lag canopy, respectively, during the disreef opening

(3) Multiple values separated by a virgule (/) are successive peak loads

(4) $(C_K)_r = F_r / q_{DCCS} (C_DS)_r$, where $(C_DS)_r$ is the measured reefed drag area (the third column of data)

(5) An asterisk (*) denotes an irregular deployment

(6) The second line of data for a parachute shows backup instrumentation values

and there may have been successive peak loads. For example, in Test 84-1R, there are six peak loads indicated. This is because there were two drogue chutes in this test, each of which had duplicate riser load instrumentation, and because one of the drogue chutes experienced two successive load peaks. In particular, the peak load for drogue chute No. 1 was 16,870 and 16,460 lb, as indicated by its two load sensors. The peak load for drogue chute No. 2 was 16,800 (first peak) and 17,750 (second peak), as indicated by one load sensor, and 17,900 (first peak) and 18,150 lb (second peak), as indicated by the other load sensor.

The data from the Apollo Block II (H) test program were studied first. Sufficient data were available from this program to permit a trend to be observed in effects due to vehicle type, Mach number, type of deployment, ballistic coefficient, and magnitude of loads developed. However, there were insufficient data to observe effects due to flight path angle, reefing ratio, and suspension line changes. All tests were conducted with a flight path angle about 60-70 degrees during drogue chute deployment; all drogue chutes were reefed to either 36.5% D_o or 40% D_o; also, all tests except one used drogue chutes having 2500-pound nylon suspension lines.

The Block II (H) drogue chute was a 16.5-ft D_o conical ribbon parachute with active radial reefing. Drogue chute loads were measured in Test 83-6 and Test Series 84, 85 and 99. One data point was used from each of Tests 84-1, 84-1R, 84-3, 84-4, 99-2 and 99-4 in the derivation of the components of $(C_K)_r$. These tests and their $(C_K)_r$ data are briefly reviewed on the following two pages.

Test

83-6: Both drogue chutes had load link dynamics.* The load link and riser motions were so extreme that one riser tied itself into a knot at the clevis fitting. Load link dynamics were identified visually in the onboard film coverage and by the presence of secondary and tertiary peaks in the telemetry load trace. The measured $(C_K)_r$ values for the two drogue chutes were 1.31 and 1.26 for this test.

84-1: The datum from one chute ($(C_K)_r$ = 1.19) could be used. The other chute came out of its bag during deployment and partially filled prior to line stretch. This chute produced a $(C_K)_r$ of 1.14 in this abnormal opening.

84-1R: One chute had a usable $(C_K)_r$ of 1.18. The other had load link dynamics, which were identified on both the film and the telemetry, and produced a $(C_K)_r$ of 1.19.

84-3: A $(C_K)_r$ of 1.28 for one drogue chute was used in the analysis. The other chute failed during reefed inflation.

84-4: This was a single drogue chute test which provided a usable $(C_K)_r$ of 1.22.

---

* Load link dynamics consists of high amplitude, high frequency, lateral oscillations of the load links and the riser that contains these links. The effect of load link dynamics is to introduce load oscillations which distort the true opening loads. The result is usually values of $(C_K)_r$ higher than normal, but occasionally a $(C_K)_r$ value is reduced by load link dynamics. At any rate, the effect of load link dynamics cannot be predicted prior to a test. (Load links are not part of the final configuration of the Apollo ELS).

85
Series: The 85 Series tests were qualification tests conducted with a BP vehicle. An attempt in this series of tests to measure riser loads without modifying the final ELS configuration, was unfortunately, not successful. (This conclusion was reached late in the series.)

Test
99-2: One drogue chute developed a $(C_K)_r$ of 1.07 and the other failed at reefed inflation. The $(C_K)_r$ of 1.07 was used in the analysis.

99-3: This test involved a configuration which proved to be prone to load link dynamics. The dynamics were severe and the $(C_K)_r$ values measured were in the range of 1.5 to 1.7. They were not used in the analysis.

99-4: This test involved a configuration change from Test 99-3 which was intended to reduce, if not eliminate, load link dynamics. One chute opened well with a $(C_K)_r$ of 1.13. The other chute exhibited load link dynamics, observed in both the film and telemetry, and produced a $(C_K)_r$ of 1.08.

99-5: Both drogue chutes failed.

99-5R: Both drogue chutes failed.

The usable $(C_K)_r$ values from the above tests were used to formulate Equation (1). This relation was then used to predict opening load factors for other tests of the Apollo parachute development program. This is discussed in the remaining portion of this subsection.

The 48 Series tests were conducted in late 1964 and early 1965. This series of tests was designed to assess the feasibility of reefing the Block I drogue chute, which was a 13.7-ft D_o conical ribbon parachute. The 48 Series was a development series, and several parameters were varied from test to test in an effort to optimize the configuration. Both midgore and radial reefing were used. The data strongly indicated that canopies with midgore reefing opened much more slowly in the reefed condition than did canopies with radial reefing. Whereas radially reefed drogue chute fill times were on the order of 0.1 to 0.2 sec, drogue chutes with midgore reefing required significantly longer fill times (0.5 - 1.2 sec).

The Block I drogue chute canopies with midgore reefing were dynamically dissimilar to those with radial reefing and are therefore not included in this analysis of reefed opening load factors. Only data points for radially reefed chutes are considered here. For all tests in which drogue chute loads had been measured since the start of the Apollo program in 1962, film sequences were studied, actual telemetry load traces were analyzed, and test reports were consulted. The results of this study are summarized below.

Test

48-1: One drogue chute had radial reefing, but its instrumentation failed. The other drogue chute had midgore reefing and opened very slowly.

48-2: Both drogue chutes had radial reefing. The $(C_K)_r$ values for the two chutes were 1.13 and 1.22. However, the telemetry trace from which the 1.13 was derived is illegible during the reefed opening (the trace from which the 1.22 was read is quite clear at this time). Because the value of 1.13 cannot be substantiated, a low level of confidence is attached to it.

48-3: Both drogue chutes had midgore reefing and opened quite slowly.

48-4: Both drogue chutes were radial reefed. The film sequences and the force traces both indicated load link dynamics. The $(C_K)_r$ values were 1.22 and 1.23.

48-5: Both drogue chutes were radial reefed. The film sequences and telemetry indicated load link dynamics. The $(C_K)_r$ values were 1.12 and 1.35.

The measured values of the opening load factors for the above tests are compared in Table 5 with predicted $(C_K)_r$ values obtained by using Equation (1). All of the tests listed in this table are 2-chute tests; hence, two opening load factors are listed for each test. Only one of the data points in Table 5 justifies high confidence. This is the C_K of 1.22 in Test 48-2. However, it may be noted that the opening load factors in Test 48-4, which had load link dynamics, are very close to the predicted values. It is also interesting that this test is the only one listed in Table 5 for which the values of measured $(C_K)_r$ are approximately the same for both drogue chutes.

Table 5. Comparison of Predicted and Actual Reefed Drogue Chute $(C_K)_r$ Values for the 48 Series Tests

Test Number	Predicted $(C_K)_r$ (1)	Measured $(C_K)_r$
48-2	1.23 1.23	1.13 1.22
48-4	1.23 1.23	1.22 1.23
48-5	1.30 1.30	1.12 1.35

NOTES: (1) Predicted $(C_K)_r$ is based on Equation (1)

Additional predicted and actual $(C_K)_r$ data are compared in Table 6. In all of the tests shown in this table, the vehicle was a BP, the drogue chutes were mortar deployed, and the opening loads and deployment Mach numbers were low. In fact, the only parameter that was varied and that affected the prediction of $(C_K)_r$ was the number of chutes deployed (Test 86-2 was a single drogue chute test). Thus, all $(C_K)_r$ values are predicted on the basis of Equation (1) to be 1.26 (1.00 + 0.21 (BP) + 0.05 (mortar deployment)), except that 1.31 is predicted for Test 86-2 (one drogue chute). It can be seen that the measured values compare poorly with the predictions. That is, the measured values are scattered from 1.16 to 1.31, including wide variations between the $(C_K)_r$ values for chutes in the same tests. This is because the drogue chute load fluctuations are greater in magnitude than the transient reefed opening loads when the BP was used. That is, the reefed opening loads seemed to be obscured by the load fluctuations. These fluctuations were probably due to the character of the BP wake. An indication of the extent of these load fluctuations is presented in Table 7. In this table, the maximum load during the first second after reefed inflation, F_m, is shown, and an associated load factor C_m is presented. Here, C_m is F_m divided by the average drag area and the observed dynamic pressure q_m at the time of occurrence of F_m. In each case, C_m is greater than C_K indicating that the magnitude of load fluctuations is greater than the magnitude of opening load overshoot. A third factor, C_m' is also presented in Table 7. This factor is F_m divided by the product of drag area and the dynamic pressure at canopy stretch q_{DCCS} (upon which $(C_K)_r$ is also based). A comparison of $(C_K)_r$ and C_m' shows that, in general, the highest load during the reefed interval is not the opening load, and also that the $(C_K)_r$ factors presently used to predict design case drogue chute loads -- 1.35, nominal; 1.41, worst case -- are conservative. Because the deployment

Table 6. Comparison of Predicted and Actual Reefed Drogue Chute $(C_K)_r$ Values for Tests Employing a BP Vehicle

Test Number	Predicted $(C_K)_r$ (1)	Measured $(C_K)_r$
50-12	1.26 1.26	1.25 1.27
86-2	1.31	1.19
86-3	1.26 1.26	1.16 1.23
86-4	1.26 1.26	1.22 1.31

NOTES: (1) Predicted $(C_K)_r$ is based on Equation (1)

Table 7. $(C_K)_r$, C_m and C_m' for Boilerplate Tests

Test No.	C_DS ft^2	q_{DCCS} lb/ft^2	q_m lb/ft^2	F_r lb	F_m lb	$(C_K)_r$ (1)	C_m (2)	C_m' (3)
50-12	43 45	118 118	110 110	6350 6750	6827 6864	1.25 1.27	1.45 1.39	1.36 1.30
86-2	60	125	123	8900	10000	1.19	1.35	1.32
86-3	67.5 67.5	186 186	162 162	14525 15500	15375 15350	1.16 1.23	1.40 1.40	1.22 1.22
86-4	66.5 60	25.4 25.4	- -	2050 2000	- -	1.22 1.31	- -	- -

NOTES: (1) $(C_K)_r = F_r/(C_DS)_r\ q_{DCCS}$

(2) $C_m = F_m/(C_DS)_r\ q_m$

(3) $C'_m = F_m/(C_DS)_r\ q_{DCCS}$

was at a very low dynamic pressure (25 lb/ft^2) in Test 86-4, and because the dynamic pressure and load both increased continually throughout the reefed interval, a determination of F_m was not attempted for this test.

2.1.2.5 Discussion of Parameters Affecting Disreef Opening

The test data from the two applicable Apollo test programs, Block I and Block II (H), were studied. In each test, a disreef opening load factor for each drogue chute was calculated. To explain scatter in these factors, telemetry and film coverage were analyzed. Trends were noted. As with the reefed opening load factors, it was found that the vehicle had the largest effect on the dynamic load factor. However, the larger factors were associated with the ICTV and the smaller factors with the PTV. This is opposite to the effect observed in the reefed opening load factor analysis. In the reefed case, it seems likely that the frequencies associated with the eddies in the PTV wake caused resonance of the canopy-air mass system. It is reasonable that the ICTV wake could not excite the disreefed chutes. The velocity defect in the wake apparently caused the lower factors to be associated with the PTV. The significant point here may be that the same wake could have a different effect on reefed and disreefed canopies because of their differences in size and added mass.

The other parameters affecting the disreef opening load factor, $(C_K)_o$ were less apparent than those affecting $(C_K)_r$. However, an intuitive mathematical model was made and used to yield some insight into this matter. This is discussed below.

Consider the forces on a drogue chute just before and following disreef as illustrated in Figures 4(a) and (b). The effective mass of the parachute is equal to the sum of the canopy, suspension line and the entrained air masses. The latter mass is referred to as the added mass. The drag is due to the shape of the canopy. Just before disreef, the riser load is equal to the canopy drag. (The parachute weight is relatively small and is neglected in this analysis.) Following disreef, the canopy shape changes, and the added mass and canopy drag increase. The riser force is now equal to the sum of the canopy drag and a reaction force due to the rate of change of the parachute momentum including its added mass. Equating the riser force with the force due to drag and the rate of change of momentum force gives the equation

$$D(t) + \frac{d(mv)}{dt} = F(t)$$

This may be integrated from disreef to the peak load point (Δt later) as follows:

$$(mv)_{\Delta t} - (mv)_o = \int_o^{\Delta t} F(t)dt - \int_o^{\Delta t} D(t)\,dt$$

The first integral represents the impulse of the riser force, as seen on the load traces. This force may be approximated as linearly increasing from disreef to maximum load (see Figure 4c)

$$\int_o^{\Delta t} F(t)dt = F_d\,\Delta t + \tfrac{1}{2}\left[\,F_m - F_d\,\right]\Delta t$$

$$= (C_DS)_r\,q_d\,\Delta t + \tfrac{1}{2}\left[(C_K)_o(C_DS)_o - (C_DS)_r\right]q_d\,\Delta t$$

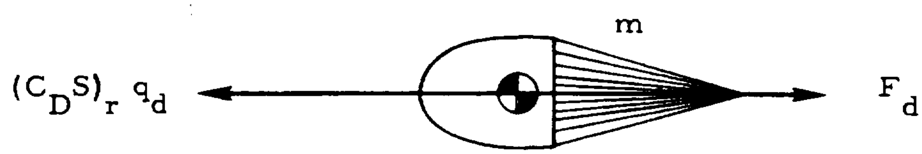

(a) Forces on drogue chute just before disreef.

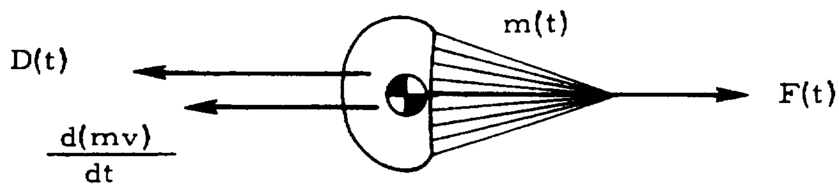

(b) Forces on drogue chute during disreef filling.

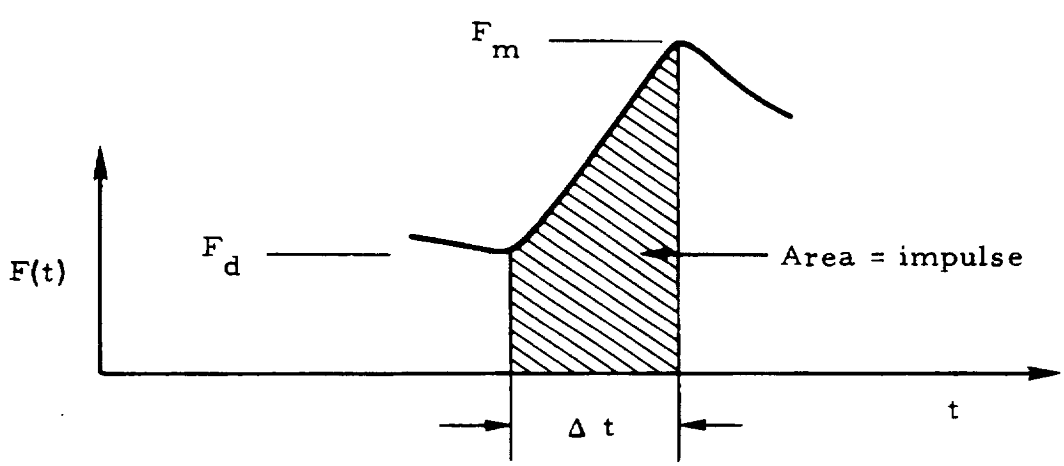

(c) Riser force versus time immediately before, during and immediately after disreef filling.

Fig. 4. Schematics of Drogue Chute Forces Associated with Disreef Filling

If it is assumed that the velocity decay is negligible during disreef opening, the velocity term may be factored from the two (mv) terms. For the Apollo drogue chutes, where the fill times are not long, this is a valid assumption. The force equation may now be solved for $(C_K)_o$ to give the following expression:

$$(C_K)_o = \frac{4B}{v\Delta t(C_DS)_o} + \frac{2\int_o^{\Delta t} D(t)dt}{q_d\Delta t(C_DS)_o} - \frac{(C_DS)_r}{(C_DS)_o}$$

where $B = \Delta m/\rho$.

Consider the remaining integral. Because the vehicle velocity is essentially constant, the term containing this integral may be approximated as

$$\frac{2}{\Delta t(C_DS)_o} \int_o^{\Delta t} C_DS(t)\, dt$$

Next, assume that $C_DS(t)$ increases linearly from $(C_DS)_r$ to $(C_DS)_o$ in time t_{fill} (not necessarily equal to Δt). Then

$$C_DS(t) = (C_DS)_r + \left[\frac{(C_DS)_o - (C_DS)_r}{t_{fill}}\right]t, \qquad 0 \leq t \leq t_{fill}$$

and

$$\frac{2}{\Delta t(C_DS)_o} \int_o^{\Delta t} C_DS(t)dt = 2\frac{(C_DS)_r}{(C_DS)_o} + \left(1 - \frac{(C_DS)_r}{(C_DS)_o}\right) t^*$$

where $t^* = \Delta t/t_{fill}$.

The disreef opening load factor may now be approximated as

$$(C_K)_o = \frac{4B}{(C_DS)_o} (1/v\ \Delta t) + \left(1 - \frac{(C_DS)_r}{(C_DS)_o}\right) t^* + \frac{(C_DS)_r}{(C_DS)_o}$$

Because the quantities $4B/(C_DS)_o$ and $(C_DS)_r/(C_DS)_o$ did not change during the Block II (H) drogue chute tests, it follows that $(C_K)_o$ was a linear function of $(1/v\ \Delta t)$ and t^*, at least for these tests.

The distance traveled by a parachute during the filling process is referred to as the fill distance. French[4] and others have indicated that the inflation of a parachute under incompressible flow conditions should take place over the same fill distance, irrespective of the vehicle, velocity, flight path angle or altitude. The reciprocal of the fill distance is the quantity $(1/v\ \Delta t)$, referred to as the inverted fill distance. Data that shows the dependence of disreef opening load factor on this quantity are shown in Figures 5 and 6. These data are also presented in Table 8.

Figure 5 indicates that a greater distance is required for a drogue chute to fill when it is deployed behind a PTV than when it is deployed behind an ICTV. This can apparently be explained as a wake effect. Namely, the velocity defect in a PTV wake is larger in magnitude than that in an ICTV wake. Because of this difference, the parachute behind a PTV would see less air velocity and, therefore travel less "air distance" than the vehicle in the same amount of time. If one were able to use air velocity at the canopy in calculating fill distance, the data points for the PTV's and ICTV's in Figures 5 and 6 might have the same fill distance. This explanation is compatible with that offered for the lower $(C_K)_o$ values associated with PTV's.

The ICTV data fell within 16 percent of their arithmetic mean fill distance. This is understandable since the fill times are accurate only to 10 or 20 percent.

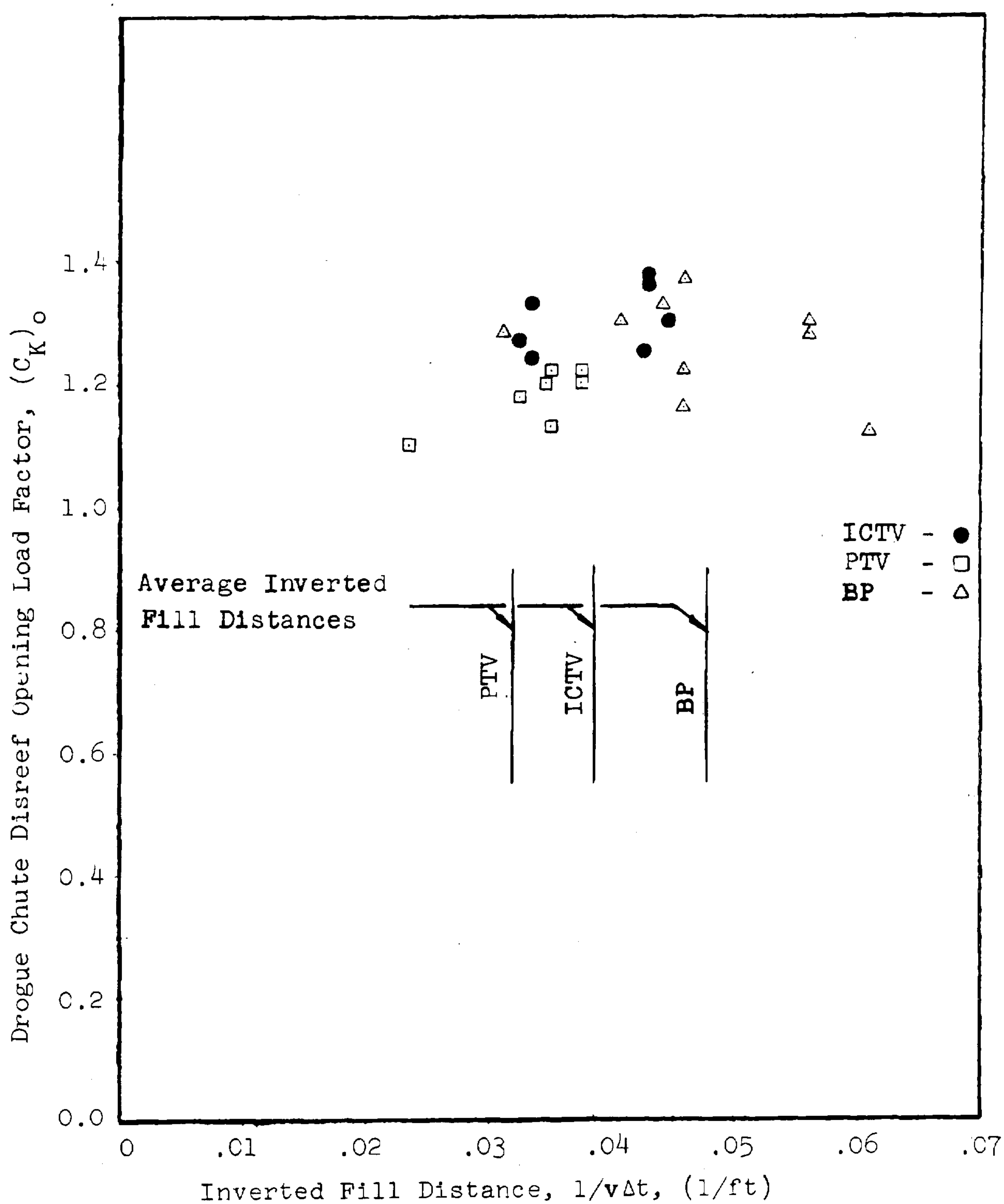

Fig. 5. Inverted Fill Distance versus Drogue Chute Disreef Opening Load Factors for the Three Test Vehicles

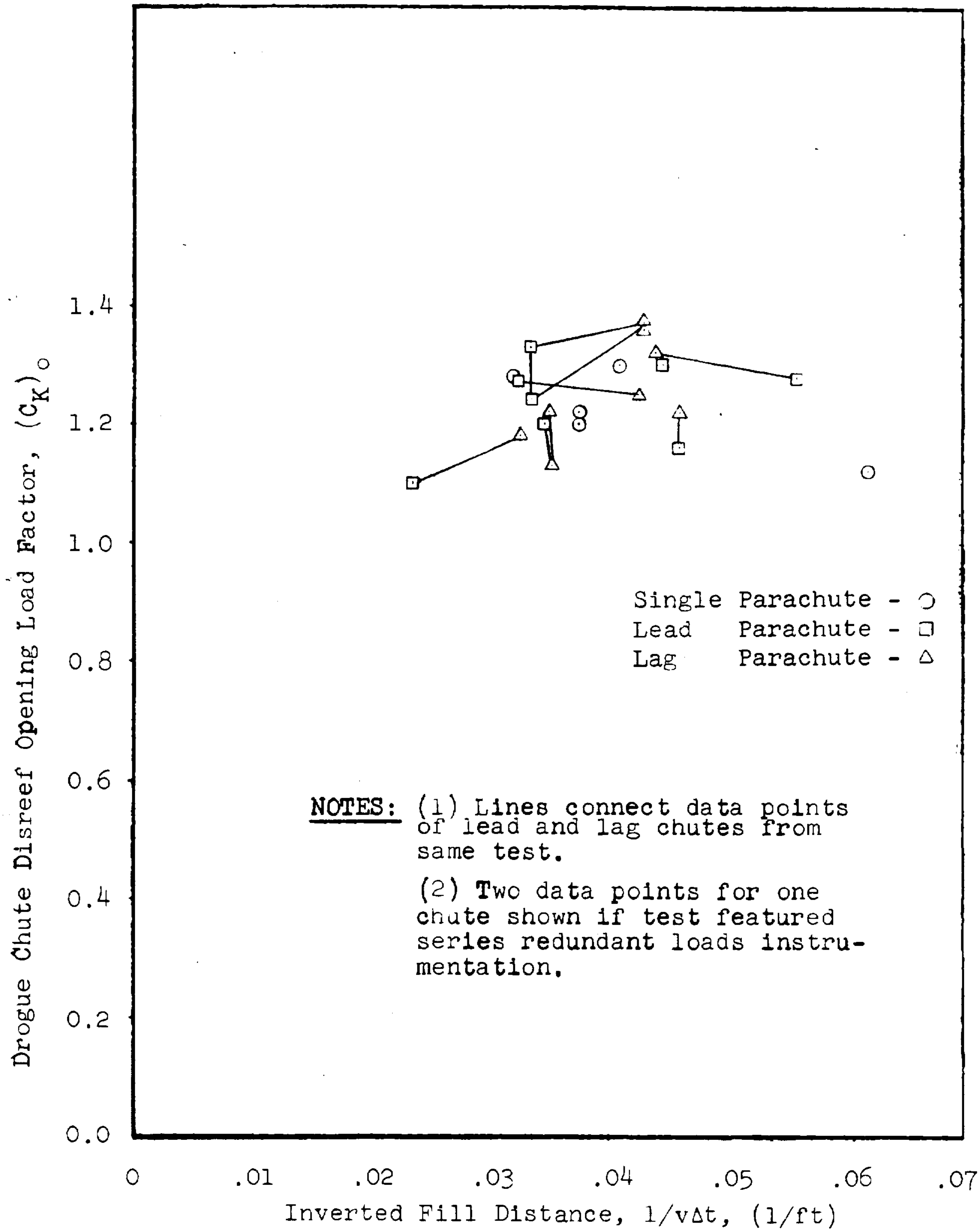

Fig. 6. Inverted Fill Distance Versus Drogue Chute Disreef Opening Load Factor for Lead, Lag and Single Parachutes

Table 8. Disreef Time and Load Data for Drogue Parachutes

Test No.	Chute No. Lead /Lag (1)	Initial Velocity v_d ft/sec	Time to Peak Load Δt sec	Fill Time t_{fill} sec	Fill Ratio t^* (2)	Fill Distance $(v_d t_{fill})$ ft	Peak Load Distance $(v\ \Delta t)$ ft	Inverted Fill Distance $\frac{1}{(v\ \Delta t)}$ 1/ft	Drag Area Ratio $\frac{C_D S_r}{C_D S_o}$	J (3)	Opening Load Factor C_{K_o} (4)
99-2	#1	560.	.04	.05	.8	28.0	22.4	.045	.62	.30	1.30
	#2	Drogue chute failed during reefed inflation									
84-1R	#1 L	412.	.07	.08	.87	33.0	28.8	.035	.342	.57	1.20
									.343	.57	1.20
	#2 ℓ	408.	.07	.09	.78	36.6	28.6	.035	.515	.39	1.13
84-4	#1	534.	.05	.07	.72	37.2	26.7	.038	.484	.37	1.22
									.494	.36	1.20
99-3	#1 ℓ	582.	.04	.07	.57	40.7	23.3	.043	.53	.27	1.36
									.55	.26	1.37
	#2 L	597.	.05	.08	.63	47.6	29.9	.033	.49	.32	1.33
									.48	.33	1.24
83-6	#1 L	447.	.095	.11	.87	49.0	42.5	.023	.412	.51	1.10
	#2 ℓ	440.	.07	.09	.78	40.0	30.8	.032	.485	.40	1.18
99-4	#1 ℓ	468.	.05	.09	.72	42.0	23.4	.043	.495	.36	1.25
	#2 L	475.	.065	.07	.72	33.2	30.9	.032	.48	.37	1.27
85-1	+Y ℓ	312.	.07	NA	NA	NA	21.8	.046	NA	NA	1.37 & 1.22
	-Y L	313.	.07	NA	NA	NA	21.9	.046	NA	NA	1.16
85-2	+Y L	254.	.07	NA	NA	NA	17.8	.056	NA	NA	1.28 & 1.30
	-Y ℓ	252.	.09	NA	NA	NA	22.7	.044	NA	NA	1.32
85-3	#1	410.	.06	NA	NA	NA	24.6	.041	NA	NA	1.30
85-4	#1	404.	.04	NA	NA	NA	16.2	.062	NA	NA	1.12
85-5	#1	388.	.08	NA	NA	NA	31.0	.032	NA	NA	1.28

NOTES: (1) L and ℓ denote lead canopy and lag canopy, respectively, during disreef opening

(2) $t^* = \Delta t / t_{fill}$

(3) $J = t^*(1 - C_D S_r / C_D S_o)$

(4) C_{K_o} values taken from Table 9

The PTV data fell within 25 percent of their arithmetic mean. This increase in deviation must be expected because of the preponderance of the PTV wake which is random in nature. Also, because of the greater load oscillation, the fill times are even less accurate, perhaps ± 30 percent.

The BP data are perplexing. Their mean fill distance is least and the deviation is greatest, being sometimes as much as ± 33 percent. There are two suggested explanations for this. First, because the loads fluctuate wildly, the times may be inaccurate. Second, the wake may not be homogeneous and centered behind the attach point. This could be due to the vehicle hang angle which could make the flow unsymmetrical.

Figure 6 compares the disreef opening load factors and inverted fill distances of lead, lag and single drogue chutes. Lead parachutes have greater fill distances than lag parachutes. Because of this, the lag parachutes tend to have higher load factors (as the equation indicates for parachutes with shorter fill distances).

Parachutes tend to align themselves parallel to the velocity vector, directly behind their attach points. When two parachutes are attached to the same point, both cannot occupy the same central position, and they stand off at an angle of attack, developing restoring side loads. An equilibrium is reached between the two. When one disreefs, its side load increases, pushing the reefed parachute farther out into the free stream. This change in equilibrium positions may take as much as 0.5 sec to accomplish. The greater the time difference in a nonsynchronous disreefing, the greater the position shift and the amount of free stream air that the lag chute sees when it disreefs. This decreases the lag chute's fill distance and increases its load factor. There is a definite correlation in the test data between the difference in fill distance and time lag. In only one case did the lag chute have a greater fill distance (Test 85-2). (This may be a bad data point due to the poor load traces or due to inaccurate fill times.)

The effect of the time ratio t^* ($= \Delta t/t_{fill}$) was also studied. Values of Δt were obtained from telemetry traces and values of t_{fill} were estimated from films of the disreefing drogue chutes. Some correlation was found to exist between the higher values of t^* and higher opening load factors. The difficulty in seeing good correlation is that $t^* \left(1 - \frac{C_D S_r}{C_D S_o}\right)$, the product of two fractions, is smaller than either $4B/v\Delta C_D S_o$, or $C_D S_r / C_D S_o$ and, therefore, has less effect. This effect may, in fact, be of the same order of magnitude as the parameters that are ignored by the model (elasticity, etc.), thus making it difficult to detect.

2.1.2.6 Presentation of Disreefed Drogue Chute Test Data. All applicable test data are presented in Tables 8 and 9 and are discussed below.

Test

84-1: Both drogue chutes failed in a premature disreef, providing no applicable data.

99-2: This was a two-drogue, ICTV test. One drogue chute failed before disreef; the other disreefed but split a gore. This decreased the drag area and increased the measured opening load factor.

Table 9. Disreef Opening Load Data for Drogue Parachutes

Test No. (1)	Drag Area Predicted $(C_DS)_o$ ft^2	Drag Area Actual $(C_DS)_o$ ft^2	Peak Load F_o lb	Initial Dyn. Press q_d lb/ft^2	Opening Load Factor $(C_K)_o$ (2) (3)	Test Vehicle Type	Test Vehicle Weight W lb	Flight Path Angle γ_d deg	Mach Number M_d	Altitude h ft	Suspension Lines	Unit Canopy Loading $\frac{W}{(C_DS)_o}$ lb/ft^2	Number of Parachutes	Fill Time t_{fill} sec (4)	Reefing Diameter D_{r_2} % D_o
84-1 #1	Failed														
#2	Failed														
99-2 #1	109.	130.	35920.	212.	1.30*	ICTV	12999.	-78	.53	18170.	2500 lb Nylon	100.	1 Open & 1 Stream	.05	40.0
#2	Failed														
84-1R L#1	109.	117.	16810.	120.	1.20	PTV	13026.	-75	.40	17600	2500 lb Nylon	54.4	2(1 at a time)	.08	40.0
L#1	109.	122.	17500.		1.20									.08	
ℓ#2	109.	126.	16790.	118.	1.13				.39		2500 lb Nylon			.09	
ℓ#2	109.	115.	16600.		1.22									.09	
84-4 #1	109.	124.	27400.	181.	1.22	PTV	12961.	-76	.51	20200	2500 lb Nylon	104.	1	.07	36.5
#1	109.	125.	27100.		1.20										
84-3 #1	Failed														
#2	Failed														
99-3 L#1	109.	124.	22310.	135.	1.33	ICTV	13001.	-65	.59	35040	2500 lb Nylon	51.	2(1 at a time)	.08	36.5
L#1	109.	136.	22790.		1.24									.08	
ℓ#2	109.	127.	22030.	128.	1.36				.61		2500 lb Nylon			.07	
ℓ#2	109.	124.	21730.		1.37									.07	
83-6 L#1	109.	126.	16280.	117.	1.10	PTV	12997	-71	.43	22050	2500 lb Nylon	51	2(1 at a time)	.11	36.5
ℓ#2	109.	130.	17290.	113.	1.18				.43		2500 lb Nylon			.09	
99-4 L#1	126.	125.	22260.	140.	1.27	ICTV	12989.	-77	.47	20700	2500 lb Nylon	49.	2(1 at a time)	.09	36.5
ℓ#2	126.	137.	23346.	136.	1.25				.46		2500 lb Nylon			.07	

NOTES: See end of table

Table 9 Concluded. Disreef Opening Load Data for Drogue Parachutes

Test No. (1)		Drag Area Predicted $(C_DS)_o$ ft^2	Drag Area Actual ft^2	Peak Load F_o lb	Initial Dyn. Press q_d lb/ft^2	Opening Load Factor $(C_K)_o$ (2) (3)	Test Vehicle Type	Test Vehicle Weight W lb	Flight Path Angle γ_d deg	Mach Number M_d	Altitude h ft	Suspension Lines	Unit Canopy Loading $\frac{W}{(C_DS)_o}$ lb/ft^2	Number of Parachutes	Fill Time t_{fill} sec (4)	Reefing Diameter D_{r_2} % D_o
85-1 +Y	ℓ	NA	98.	7700.	64.5	1.22	BP	13016.	-83	.29	18600.	2500 lb Nylon	58.1	2	.13	42.8
+Y	ℓ	(5)	94.	8300.		1.37										
-Y	L	NA	128.	9550.	64.5	1.16						2500 lb Nylon			.11	
-Y	L	(5)	NA	NA												
85-2 +Y	L	NA	120.	9000.	58.	1.28	BP	13038.	-78	.23	8300.	2500 lb Nylon	68.8	2	.10	42.8
+Y	L	(5)	110.	8300.		1.30										
-Y	ℓ	NA	≈75.	5710.	58.	1.32						2500 lb Nylon			.14	
-Y	ℓ	(5)	NA	NA												
85-3 +Y		NA	102.	14500.	109.	1.30	BP	13005.	-81	.36	18500	2500 lb Nylon	128.	1	.10	42.8
+Y		(5)	NA	NA												
85-4 -Y		NA	132.	14630.	99.	1.12	BP	13482.	-77	.36	20700	2500 lb Nylon	102.	1	.09	42.8
-Y		(5)	NA	NA												
85-5 +Y		NA	78.	10970.	110.	1.28	BP	12980.	-84	.35	14700.	2500 lb Nylon	167.	1	.11	42.8
+Y		(5)	NA	NA												

NOTES: (1) L and ℓ denote lead canopy and lag canopy, respectively, during disreef opening

(2) $C_{K_o} = F_o/q_d\,(C_DS)_o$ where $(C_DS)_o$ is the measured equilibrium descent drag area (the third data column)

(3) An asterisk (*) denotes a damaged canopy

(4) t_{fill} is time from disreef event to instant when overinflation line becomes taunt

(5) Second line of data for a parachute shows backup instrumentation values

84-1R: This was a two-drogue, PTV test and was the last test to have drogue chutes reefed to 40 percent. Due to nonsynchronous disreefing, the lead drogue chute completely filled before the lag chute disreefed. Because the loads were high, the decelerations were also high, significantly decreasing the dynamic pressure between the lead and lag parachutes' disreef times.

(Due to inaccuracies in the Askania data during periods of high deceleration, it was necessary to compute the dynamic pressure of the lag parachute at the time of its disreef for Test 84-1R. This was accomplished by integrating the equation of motion of the vehicle-parachute system. The equation used was

$$\frac{dv}{dt} = g \sin \Theta - F_L/m - C_D S \rho v^2/2\,m$$

where $C_D S$ is the drag area of the vehicle and lag drogue chute and F_L is the force applied by the lead drogue chute. The force F_L was computed as the impulse of the lead drogue chute force between disreef times, divided by the elapsed time. This procedure permitted an easy solution of the differential equation and subsequent calculation of dynamic pressure at lag drogue chute disreef.)

84-4: This was a one-drogue chute test using a PTV. It was the first test in which a drogue chute was reefed to 36.5 percent.

84-3: Both drogue chutes failed, providing no applicable test data.

99-3: This was a two-drogue chute test using an ICTV.

83-6: This was a two-drogue chute test using a PTV.

99-4: This was a two-drogue chute test using an ICTV. It was the last test in which a drogue chute was reefed to 36.5 percent.

2.1.3 Drag Area Study

Because of fabric elasticity and hysteresis, parachute drag area is a function of both load and time. The higher the load, the more a canopy stretches. This, in turn, affects the load, the opening load factor and the trajectory. It is essential to understand these effects and to be able to predict them.

Usually, the opening load is the highest load experienced by a parachute canopy during a particular opening stage. The canopy typically deforms under this load, giving a large initial drag area. After the opening load, the canopy loading typically decreases and the canopy tends to relax. This relaxation may not be instantaneous due to viscoelastic characteristics inherent in the canopy fabric. A measure of this effect is indicated by a canopy growth factor, n. This factor is the ratio, minus 1.0, of the drag area at the beginning of a stage, $(C_DS)_i$, to the average drag area over the stage, $(C_DS)_{av}$.

$$n = (C_DS)_i/(C_DS)_{av} - 1$$

A positive value of n indicates that the drag area decreases, and a negative value indicates that the drag area increases. This is illustrated in Figure 7.

After the opening load, the loads typically decrease with time, allowing the materials to relax and the drag area to decrease. In some cases, however, the loads remain very high, preventing relaxation. In fact, the material may even creep under a sustained high loading, increasing the drag area with time. This is the trend: n decreases with increased loads (increasing q).

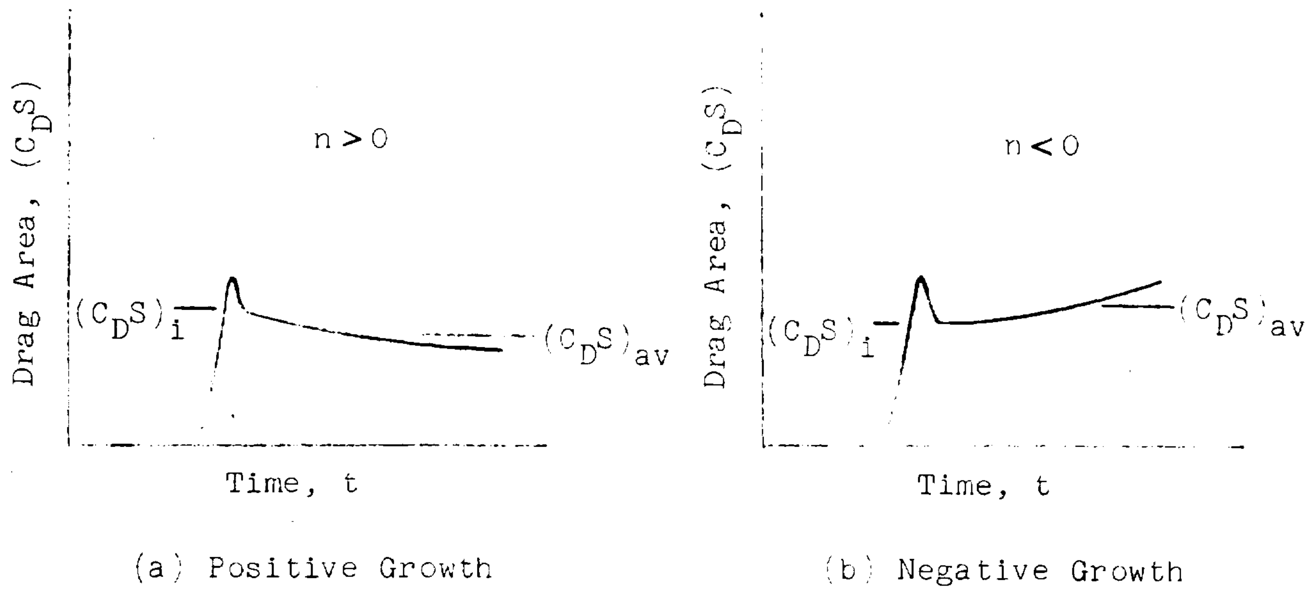

Fig. 7. Schematics of Typical Drag Area Growth Curves

All applicable data are presented in Tables 10 and 11. Much of the reefed drogue chute data was unusable because of load link dynamics. This phenomenon made it impossible to measure the initial forces and prevented calculation of the canopy growth factor. (Because this phenomenon existed only during the reefed stage, it had no effect on the full open data.) The canopy growth factor was approximated by first dividing the opening load factor by the ratio of the maximum force to the initial force and then subtracting one.

The reefing lines pass through twenty rings and assume the shape of a twenty-sided polygon. The relationship between each chord of the polygon and the radius of the circumscribed circle is linear. Hence, the area of the circle is a constant times the reefing line length (the sum of the chords) squared. The reefing line length increases with the reefing line load, which is about 4 percent of the riser load. Because there are two reefing lines, each line carries about 2 percent of the riser load. In the Block II (H) ICTV and PTV tests, the reefing lines were 2500-lb nylon cord. Because the riser loads were always less than 28,000 lb, the reefing line loads were always less than 560 lb. With these low loads, the slope of the load versus percent elongation curve of the material is nearly constant. The elongation is a constant times the reefing line load which, in turn, is a constant times the riser load. The length of the stretched reefing line is the original length plus the elongation. It

Table 10. Drag Area Data for Reefed Drogue Chutes

Test No.	Chute No.	Drag Area $(C_DS)_r$ ft^2	Flight Conditions q_{DCCS} lb/ft^2	M_{DCCS}	Peak Force F_r lb	Initial Force F_1 lb	Opening Load Factor $(C_K)_r$ (1)	Force Ratio F_r/F_1	Canopy Growth n_r (2)	Vehicle Type	Reefing Diameter D_r % D_o
84-1	# 1L	73.1	199.	.57	17300		1.19			PTV	40.0
	# 2L	69.0	199.	.57	15600		1.14*				40.0
99-2	# 1	80.0	317.	.72	27200	26000	1.07	1.05	.02	ICTV	40.0
	# 2	Failure									40.0
84-1R	# 1L	60.0	238.	.62	16870	15000	1.18	1.12	.05	PTV	40.0
		59.0	238.	.62	16460	14500	1.17	1.13	.03		
	# 2L	62.0	238.	.62	16800/17750		1.14/1.20*				40.0
		65.0	238.	.62	17900/18150		1.16/1.18*				
84-4	# 1	57.0	175.	.55	12030	10600	1.21	1.14	.06	PTV	36.5
		57.0	175.	.55	12130	10800	1.22	1.13	.08		
84-3	# 1L	50.0	366.	.93	23390	19000	1.28	1.23	.04	PTV	36.5
		50.0	366.	.93	23660	19000	1.29	1.24	.04		
	# 2	Failure									36.5
99-3	# 1L	64.0	203.	.83	22160		1.70*			ICTV	36.5
		68.0	203.	.83	21730		1.57*				
	#2 L	64.0	203.	.83	20700		1.59*				36.5
		64.0	203.	.83	19950		1.54*				
83-6	# 1L	55.0	154.	.52	9900/11100		1.27/1.31*			PTV	36.5
		NA									
	# 2L	59.0	154.	.52	9400-11100/11400		1.04/1.21/1.26*				36.5
		NA									
99-4	# 1L	63.0	288.	.71	18400/19510		1.01/1.08*			ICTV	36.5
	# 2L	68.0	288.	.71	22140	19000	1.13	1.165	-.03		36.5

NOTES: (1) $(C_K)_r = F_r/q_{DCCS}(C_DS)_r$, where $(C_DS)_r$ is measured reefed drag area (the third data column)

(2) $n_r = \left\{(C_K)_r/(F_r/F_1) - 1\right\}$

follows that the geometric projected area A of the canopy may be written in the form:

$$A = C_o\,[C_1 + C_2 P]^2 = C_3 + C_4 P + C_5 P^2$$

where the C's are constants and P is the riser load. If both sides of this equation are multiplied by a drag coefficient, it becomes drag area as a function of riser load. This relation

Table 11. Drag Area Data for Disreefed Drogue Chutes

Test No.	Chute No.	Drag Area $(C_D S)_o$ ft^2	Initial Conditions q_d lb/ft^2	M_d	Peak Force F_o lb (1)	Initial Force F_1 lb	Opening Load Factor $(C_K)_o$ (2)	Force Ratio F_o/F_1	Canopy Growth n_c (3)	Vehicle Type	Reefing Diameter D_r D_o
84-1	# 1 L	Failed								PTV	40.0
	# 2 ℓ	Failed									40.0
99-2	# 1	130	212	.53	35920.*	26000.	1.30	1.38	-0.06	ICTV	40.0
	# 2	Failed									40.0
84-1R	# 1L	117	120	.40	16810.	14000.	1.20	1.20	0.0	PTV	40.0
		122			17500.	14500.	1.20	1.20	0.0		
	# 2ℓ	126	118	.39	16790.	14500.	1.13	1.14	0.0		40.0
		115			16600.	13600.	1.22	1.22	0.0		
84-4	# 1S	124	181	.51	27400.	23200.	1.22	1.18	0.03	PTV	36.5
		125			27100.	24400.	1.20	1.11	0.08		
84-3	# 1 L	Failed								PTV	36.5
	# 2	Failed									36.5
99-3	# 1ℓ	124	135	.59	22310.	18400.	1.33	1.21	0.1	PTV	36.5
		136			22790.	19000.	1.24	1.20	0.03		
	# 2L	127	128	.61	22030.	17500.	1.36	1.26	0.08		36.5
		124			21730.	17300.	1.37	1.26	0.09		
83-6	# 1 L	126	117	.43	16280.	14700.	1.10	1.11	0.0	PTV	36.5
	# 2 ℓ	130	113	.43	17290.	14600.	1.18	1.18	0.0		36.5
99-4	# 1 L	125	140	.46	22260.	18300.	1.27	1.22	0.04	ICTV	36.5
	# 2 L	137	136	.47	23340.	19000.	1.25	1.23	0.02		36.5

NOTES: (1) An asterisk (*) denotes a damaged canopy

(2) $(C_K)_o = F_o / q_d\,(C_D S)_o$, where $(C_D S)_o$ is measured disreefed drag area (third data column)

(3) $n_c = \left\{(C_K)_o / (F_o/F_1) - 1\right\}$

has the form of a parabola. No definite correlation of this relation with test data could be found because of a lack of data. In a further study, the coefficients of the equation could be determined theoretically. Good correlation with new test data would provide a means of drag area prediction.

Reefed canopy growth is plotted against dynamic pressure in Figure 8. Because of load link dynamics, there are insufficient data to detect a correlation.

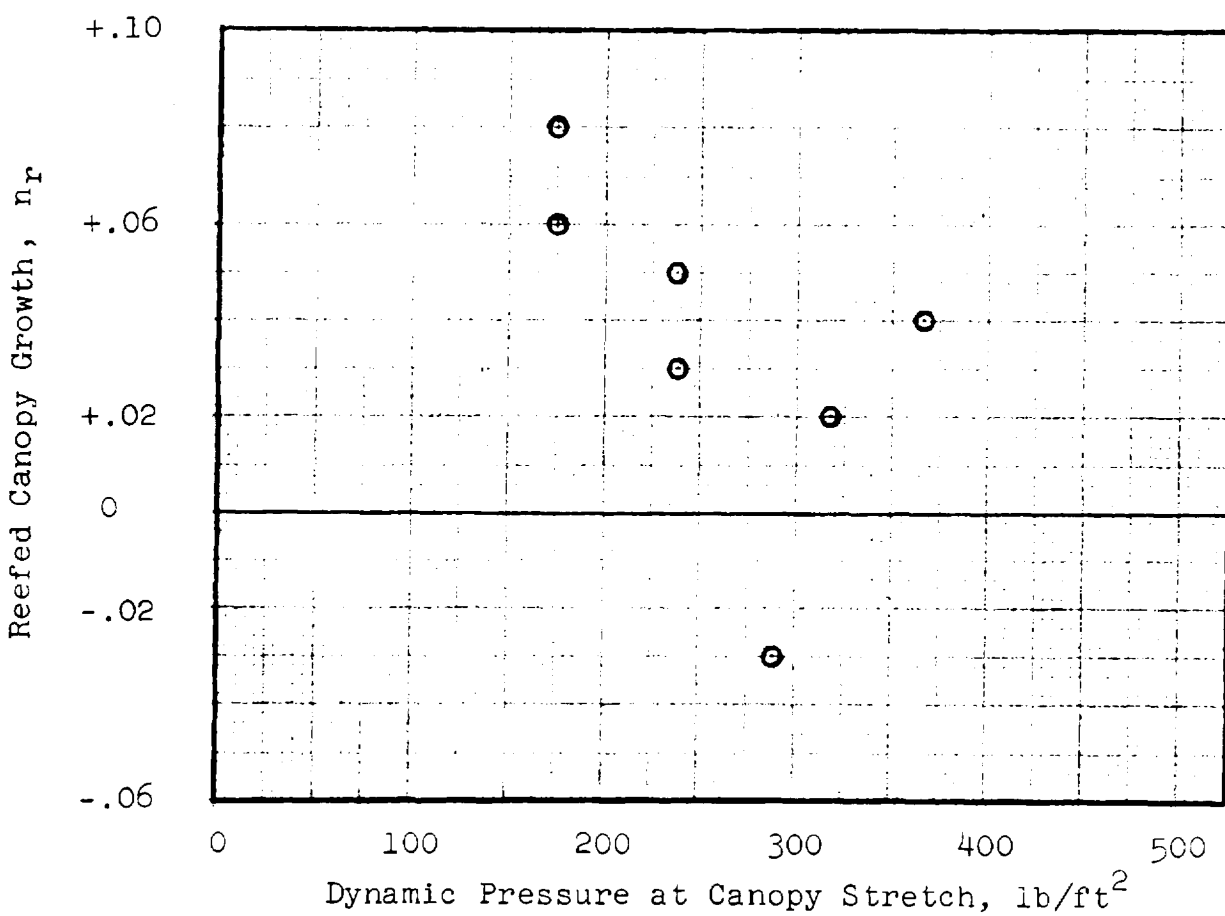

Fig. 8. Drogue Chute Reefed Canopy Growth Factor Versus Dynamic Pressure at Canopy Stretch

The full open drag area and canopy growth factor are plotted versus the dynamic pressure at disreef in Figures 9 and 10, respectively. Because the dynamic pressure variations shown in these figures are relatively small, nothing conclusive regarding the effect of this variable may be discerned.

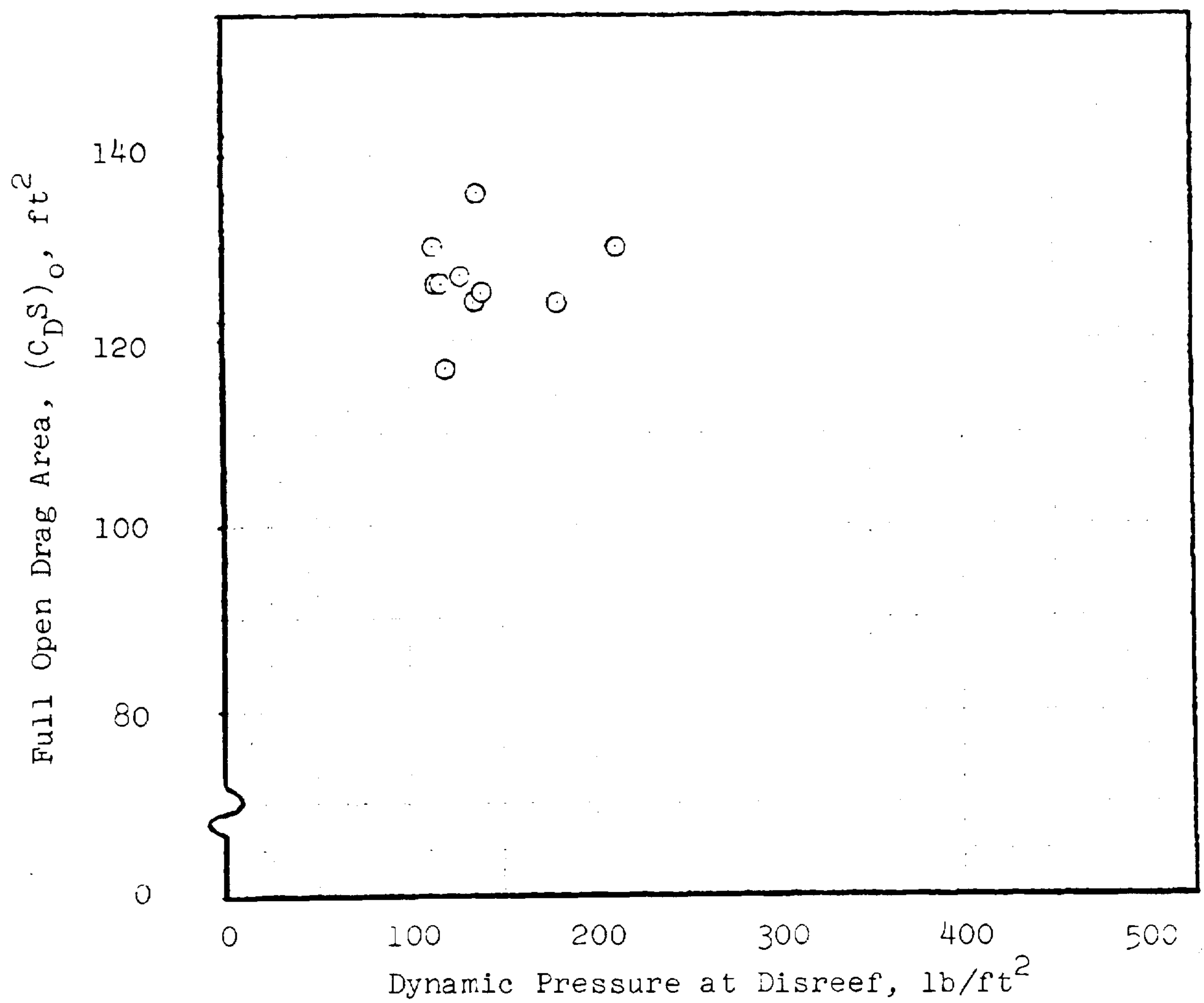

Fig. 9. Drogue Chute Full Open Drag Area Versus Dynamic Pressure at Disreef

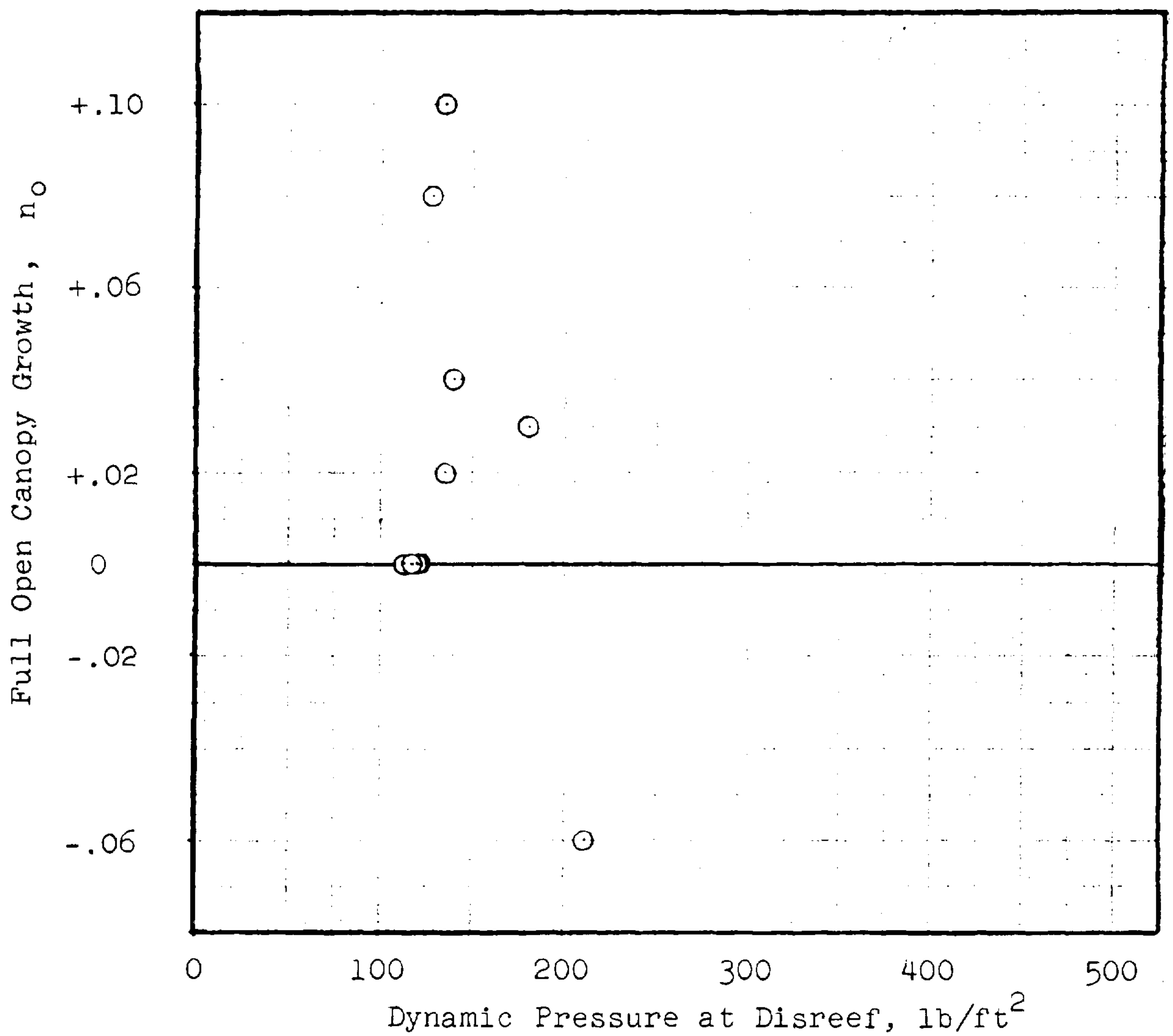

Fig. 10. Drogue Chute Full Open Canopy Growth Factor Versus Dynamic Pressure at Disreef

2.1.4 Wake Study

The mechanism by which a wake may cause riser load fluctuations was studied. It was hypothesized that the frequencies associated with the turbulent wake could cause oscillations of the system with the added air mass providing an intermediate transfer function. It was further suspected that the strong fluctuations observed behind the PTV and BP were indicative of resonant conditions in the system. An order of magnitude check on the hypothesis was sought through data analysis and is presented in Section 5.0.

2.2 PILOT CHUTE LOADS

Each of the three pilot chute assemblies consists of a ringslot parachute with textile riser, a deployment bag, a steel cable and a mortar tube assembly. The function of a pilot chute is to pull a main parachute pack away from its stowed position on the CM, to quickly stretch this parachute's riser, suspension lines and canopy into a lineal configuration behind the CM, to stabilize the apex of the main canopy during reefed inflation, and to control the canopy shape during the reefed interval.

The pilot chute canopy is a twelve-gore, 7.2-foot diameter ringslot parachute. For the normal entry mode of operation, the pilot chutes are mortar deployed at the same instant that the drogue chutes are disconnected from the CM. A sabot weight is permanently attached to the deployment bag to increase its inertia and assist in "strip-off" of the bag from the canopy. After deploying the main parachutes from their stowed positions, each pilot chute remains attached, through a main parachute bag, to the apex of a main parachute. The physical characteristics of a pilot chute including its riser and deployment bag are illustrated in Figure 11.

2.2.1 Loads Methods Used in Apollo Parachute Development Program

The loads methods used in the Apollo parachute development program are described in detail in Reference 3. Briefly, these methods were as follows.

A pilot chute snatch load was calculated for the pilot chute line stretch event with a snatch force computer program. A pilot chute opening load, F_o was calculated using the opening load factor method,

$$F_o = C_K \, (C_D S)_o q_{PCLS}$$

where C_K, $(C_D S)_o$ and q_{PCLS} denote opening load factor, full open drag area (24.4 ft^2) and dynamic pressure at pilot chute line

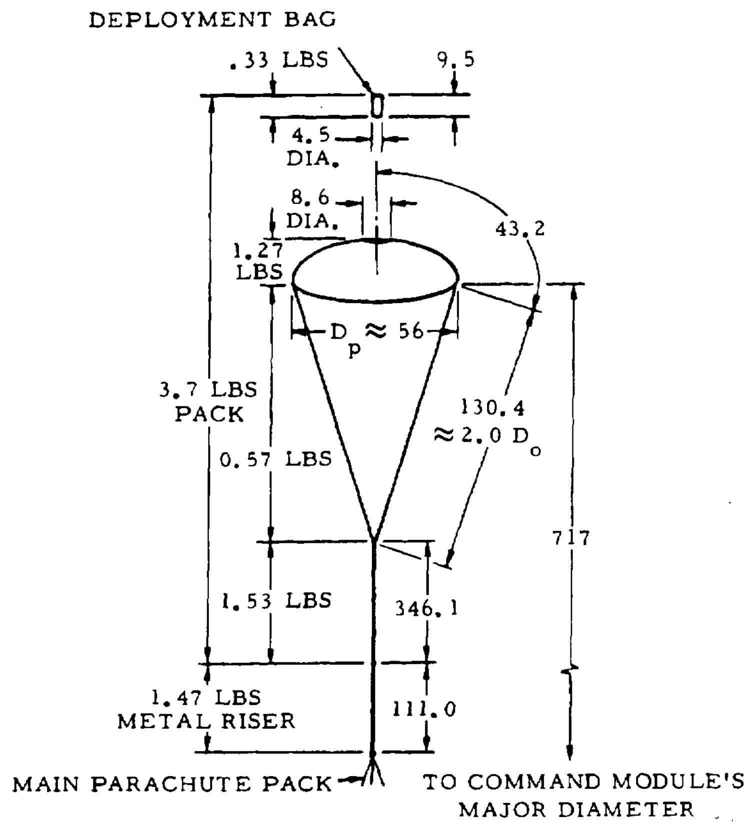

NOTE: The lengths shown above are fabrication dimensions (without strain)

General Data:

Type - Ringslot

Nominal diameter, D_o = 7.2 ft

Nominal canopy area, S_o = 40.7 ft^2

Number of gores = 12

Canopy porosity = 24%

Single Chute Characteristics:

Full open drag area, $(C_DS)_o$ = 24.4 ft^2

Pack weight = 3.7 lb (less metal riser)

Pack volume = 150 $in.^3$

Deployment Conditions:

Mortar muzzle velocity = 90 ft/sec (min)

At line stretch,

	Minimum	Maximum
Altitude, ft	2,500	18,000
Dyn. pres., lb/ft^2	30	70

Mass extracted (main parachute pack) = 136 lb_m

Fig. 11. Configuration Drawing and Data for an Apollo Pilot Chute (Reference 2)

stretch, respectively. The value of C_K used in this computation was established by giving careful consideration to the values of C_K associated with earlier tests of the same parachute.

Each pilot chute deploys one main parachute; and, being permanently attached, each pilot chute is snatched to the vehicle velocity when its respective main parachute canopy becomes fully stretched. This event, occurring at main chute canopy stretch (MCCS), subjects the pilot chute to higher loads than those occurring at either pilot chute line stretch or at pilot chute opening. The pilot chute loads associated with MCCS were calculated using the equation,

$$F_{MCCS} = 1.75\ (C_D S)_o q_{MCCS}$$

where q_{MCCS} denotes the dynamic pressure of the vehicle at MCCS. The coefficient 1.75 is a value that was determined to be appropriate for permanently attached pilot chutes based on a wide range of previous experience with deployable nonrigid aerodynamic decelerators.

The pilot chute overinflation line load was taken as 4 percent of F_{MCCS}. Table 12 is a summary of different types of pilot chute loads and methods that were computed in the Apollo development program.

Table 12. Summary of Load Prediction Methods Used in Computing Pilot Chute Loads

Load	Method Used (Ref. 3)
F_{MCCS}	$1.75\ (C_D S)_o q_{MCCS}$
F_o	Opening Load Factor
Snatch	Snatch Force Program
Overinflation Line	$0.04 \times F_{MCCS}$

2.2.2 Review and Refinement of Opening Load Factor Method

The pilot chute loads data from the Apollo parachute development and qualification tests were reviewed, and an analysis was made to upgrade the opening load factor method. The results of this work are presented below.

2.2.2.1 Explanation of the Calculation of Flight Conditions During Vehicle Free Fall. There were only four tests in the Apollo parachute development program for which both Askania and loads information were obtained for the pilot chutes. Each of these tests used static line deployment immediately after a horizontal launch. Starting from a horizontal trajectory caused the initial rate of change of the flight path angle to be significant. Therefore, the analysis procedure included consideration of flight path angle at launch. The velocity was then separated into horizontal and vertical components. Knowing the time to canopy stretch after launch, the change in vertical velocity due to gravity, and the change in horizontal velocity due to drag were calculated. A drag area of 2.0 ft^2 was used for the ICTV. The total velocity and the flight path angle at canopy stretch were then calculated, as well as a dynamic pressure based on Rawin data. The calculated dynamic pressures are presented in Table 13 along with the Askania values for comparison. The calculated flight path angles at canopy stretch were between six and eight degrees below horizontal in all four tests.

Table 13. Comparison of Calculated and Askania Dynamic Pressure at Pilot Chute Line Stretch

Test	Dynamic Pressure (lb/ft^2)		
	Calculated	Askania	% Difference
80-3R1	114	114	0
80-3R2	95	97	-2
81-2	93	90	+3
81-4	120	119	+1

2.2.2.2 <u>Determination of Pilot Chute Opening Load Factor</u>. All data for the tests in which pilot chute loads were measured are presented in Table 14.

The opening load factor method was used to analyze the pilot chute opening loads data in order to determine values of C_K. Of the six factors measured, five fell witin 0.02 of 0.85 and one fell at 0.72.

All of the factors are significantly less than 1.00. It is believed that this is because the main packs, in weighing only about 140 lb, produced relatively light loadings for the pilot chutes. An attempt was made at using the force traces to compute acceleration-time histories for the main parachute packs and integrating these to obtain calculated dynamic pressures for the pack (and therefore the pilot chute) and opening load factors at the time of peak load. The results are shown in Table 14 as "calculated pack q" and "resulting C_K'". There are four C_K' within 0.02 of 1.06 and two lower ones at 0.94 and 0.91. It may be noted that the main parachute packs are initially tied to the ICTV, and that there is not a good means of estimating the time history of the forces on each pack opposing the pilot chute forces. It is interesting that four of the six factors calculated in this manner come out very close to the value 1.05 recommended in Reference 5 for ringslot canopies under infinite mass conditions.

An explanation was sought for the low (0.72) C_K measured on the No. 2 pilot chute in Test 81-4. One observation made was that chute No. 2 opened about 30 percent slower than No. 1, and about 100 percent slower than the single pilot chute in Test 80-3R1, which was the other test at a q over 110 lb/ft^2. It was also observed that both pilot chutes in Test 81-4 were above the ICTV at pilot canopy stretch and swung into the wake during inflation, causing the velocity vector to be skewed to the canopy centerline. While it is possible that these observations, based on telemetry and film analysis, may be connected to the low factor, no quantitative explanation was found.

Table 14. Opening Loads Data for Pilot Parachutes

1	2	3	4	5	6	7	8	9	10	11	12
Test No.	Chute No.	Vehicle Weight W lb	Calc'd Vehicle $(\gamma)_{PCCS}$ deg	Altitude h ft	Opening Load F_o lb (1)	Calc'd Vehicle $(q)_{PCCS}$ lb/ft^2	Pilot Chute C_K (2)	Calc'd Pack $(q)_{F_o}$ lb/ft^2	Resulting C_K' (3)	Askania Listed $(q)_{PCCS}$ lb/ft^2	Pilot Chute C_K'' (4)
80-3R1	1	7,500	6	10,700	2340	114	0.84	102	0.94	114	0.84
80-3R2	1	7,500	7	10,300	1930	95	0.83	73	1.08	97	0.82
81-2	1	13,000	8	10,600	1900	93	0.84	75	1.04	90	0.87
	2				1975	93	0.87	76	1.07	90	0.90
81-3 (5)	1	13,000	NA	NA	2230	NA	NA	NA	NA	NA	NA
	2				2350	NA	NA	NA	NA	NA	NA
81-4	1	13,000	7	10,500	2475	120	0.85	98	1.04	119	0.85
	2				2110	120	0.72	95	0.91	119	0.73

NOTES:
(1) Average values of F_o are shown for tests that had two load sensors
(2) $C_K = F_o/(C_DS)_o q_{PCCS}$ where q_{PCCS} is listed in Column 7
(3) $(C_K)' = F_o/(C_DS)_o q_{F_o}$ where q_{F_o} is listed in Column 9
(4) $(C_K)'' = F_o/(C_DS)_o q_{PCCS}$ where q_{PCCS} is listed in Column 11
(5) No Askania data were available for Test 81-3

A third opening load factor, C_K'', is presented in Table 14. The values of q at pilot canopy stretch, read from Askania and shown in Table 14, were used to define this factor. The reason for showing C_K'' is to illustrate the reduction in data scatter resulting from using calculcated values of dynamic pressure, as opposed to using values read directly from Askania. The advantage in doing this is evident. (It is believed that this approach is even more beneficial when applied to drogue and main parachute reefed opening loads. This belief rests on the knowledge that the decelerations due to drogue and main parachute opening cause Askania errors, whereas there is no vehicle deceleration due to pilot chute loads.) The Table 14 data are also presented in Figures 12 (a) and (b) in the form of measured load versus the load computed by using the factor 0.85, a drag area of 24.4 ft^2 and dynamic pressure values (a) read from Askania and (b) calculated.

No evaluation of effects of parameters such as drag area ratio, vehicle shape, vehicle attitude, flight path angle and Mach number on opening loads was possible in the data analysis because these parameters did not vary significantly in the tests for which pilot chute data are available.

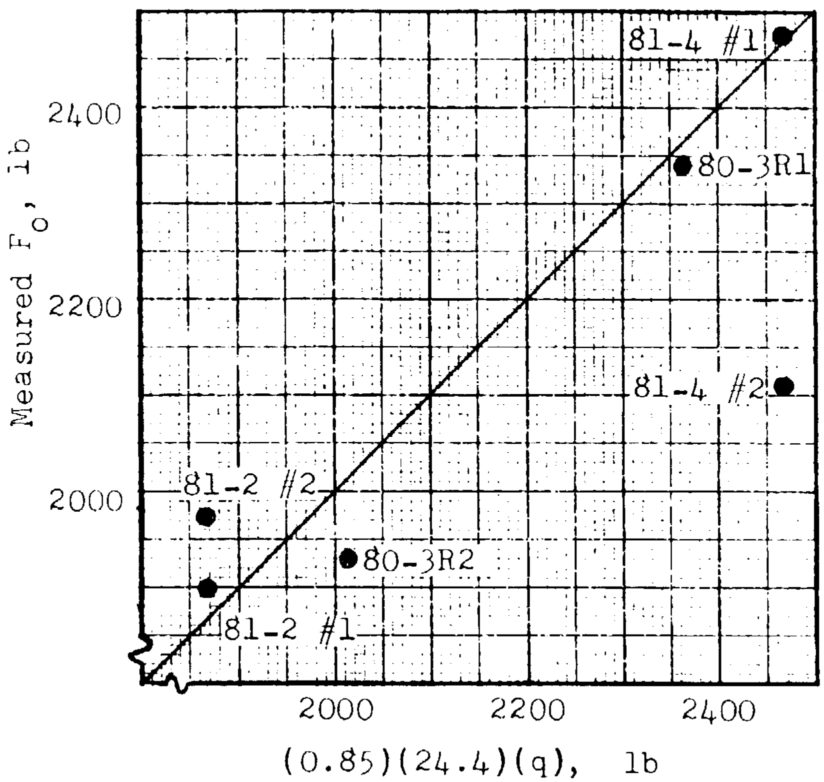

(a) Dynamic pressure at pilot canopy stretch taken from Askania data

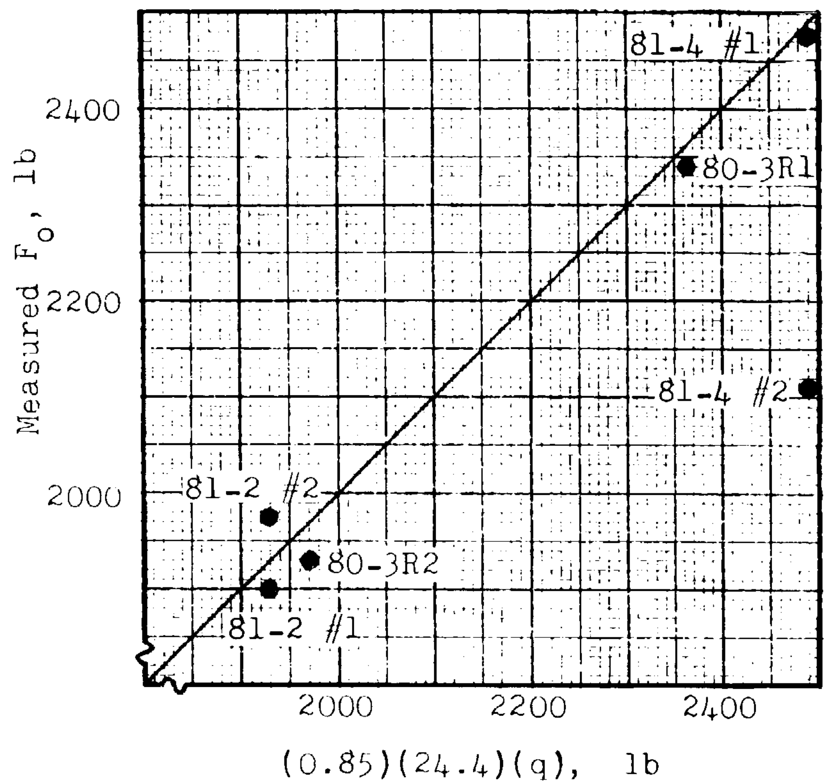

(b) Dynamic pressure at pilot canopy stretch based on trajectory computations

Fig. 12. Comparison of Measured Pilot Chute Loads and Calculated Pilot Chute Loads

2.3 MAIN PARACHUTE LOADS

Each of the three main parachute assemblies consists of an 83.5-foot diameter, modified ringsail parachute with a riser assembly and a deployment bag. The purpose of the main parachutes is to safely recover the CM with any two of the three parachutes at a maximum water impact velocity of 38 ft/sec.

Each main canopy is constructed of 68 fabric gores and has 68 suspension lines, 120 ft in length. The riser is a two-part assembly of plied textile webbing at the upper end and multiple steel cables at the lower end to provide protection against abrasion damage by the CM. The physical characteristics of a main parachute including its riser and deployment bag are illustrated in Figure 13.

The ringsail modification consists of a wide slot added to the crown of the canopy through removal of 75 percent of the cloth width from the top of the 5th ring, counting downward from the central vent. This slot increases the geometric porosity of the canopy from 7.2 to 12.0 percent of S_o. Also, the conical apex makes an angle of 19 deg below the horizontal, instead of 15 deg, because it was developed by removal of 4 gores from the original 72 in a spherical surface. Although the cloth removed from the 5th ring was replaced by heavy bands on the upper and lower edges of the slot, this area was subtracted from the total in determining the nominal diameter of 83.5 ft.

The governing design limit loads were derived from operational conditions in which one of the drogue chutes and one of the main parachute canopies were assumed to be inoperative. Nonsynchronous stretchout, disreefing and filling of the clustered canopies augmented the opening loads in the first canopy to open at each stage in the opening process. Therefore, the method of load prediction used in the Apollo parachute development program allowed for the effects of probable variations in the pertinent time differentials. These effects were found to be most important in the final opening phase after disreefing.

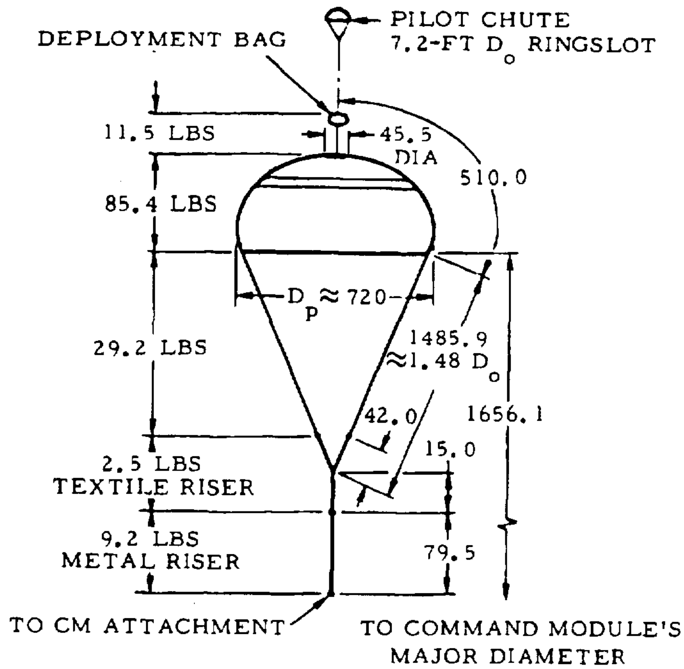

NOTE: The lengths shown above are fabrication dimensions (without strains)

General Data:

Type - Slotted ringsail with two-stage reefing

Nominal diameter, D_o = 83.5 ft

Nominal canopy area, S_o = 5478 ft^2

Number of gores = 68

Canopy porosity = 12%

Stage 1 reefing line length = 22.0 ft

Stage 2 reefing line length = 65.0 ft

Single Parachute Characteristics:

Stage 1 reefed open drag area, $(C_DS)_{r_1}$ = 285 ft^2

Stage 2 reefed open drag area, $(C_DS)_{r_2}$ = 1080 ft^2

Full open drag area, $(C_DS)_o$ = 4200 ft^2

Pack weight = 128.6 lb (less metal riser)

Pack volume = 5500 $in.^3$

Multiple Parachute Characteristics:

The characteristics of 2-parachute clusters and 3-parachute clusters are discussed in Section 2.3; see also Reference 2

Deployment Conditions:

Deployment is initiated by pilot chutes (one for each main parachute)

At line stretch,

	Minimum	Maximum
Altitude, ft	2,500	13,000
Dyn. pres., lb/ft^2	30	90

Limit Loads (per parachute):

Stage 1 reefed open, $(F_{r_1})_{lim}$ = 21,830 lb

Stage 2 reefed open, $(F_{r_2})_{lim}$ = 22,925 lb

Full open, $(F_o)_{lim}$ = 20,910 lb

Terminal Conditions:

For 13,000-pound CM,

	Two-Chute	Three-Chute
Altitude	Sea Level	Sea Level
Max. vel., ft/sec	38.0	31.4

Fig. 13. Configuration Drawing and Data for an Apollo Main Parachute (Reference 2)

The main parachutes are reefed in two stages as follows:

Stage	Reefing Line Diameter	Working Interval	Reefing Line Cutter Delay Time (Initiated at MCCS)
1	8.4% Do	6 sec	6 sec
2	24.8	4	10

Midgore skirt reefing is used; i.e., the reefing rings are attached to the skirt band on the centerline of each gore, instead of at the radial intersection. Average drag areas for the different reefing ratios tested are given in Figure 14. Since reefing ratio is given in terms of D_o = 83.5 ft, a fully inflated canopy has a nominal reefing ratio of roughly 0.68.

2.3.1 Loads Methods Used in Apollo Parachute Development Program

The loads methods used in the Apollo parachute development program are described in detail in Reference 3. These methods are very briefly summarized below.

The first stage opening loads were calculated with a 2-DOF computer program which computed the trajectory of the CM during the approximately 6-second interval of this opening stage. Basic inputs to the program were empirically derived schedules of drag area versus time for each main parachute in the cluster. Dissimilar schedules were used to simulate unequal loading situations due to nonsynchronous deployment of the main parachutes by their respective pilot chutes. Effects due to vehicle dynamics were accounted for by multiplying the 2-DOF computer program loads by a "vehicle dynamic factor" of 1.05. In addition, the loads were multiplied by a "dispersion factor" of 1.10 to account for basic uncertainties in this loads prediction technique.

Second stage opening loads were calculated by the same method used to calculate first stage opening loads. In particular, the 2-DOF computer program was used to compute the trajectory data and associated loads during the approximately 4-second interval of the second opening stage.

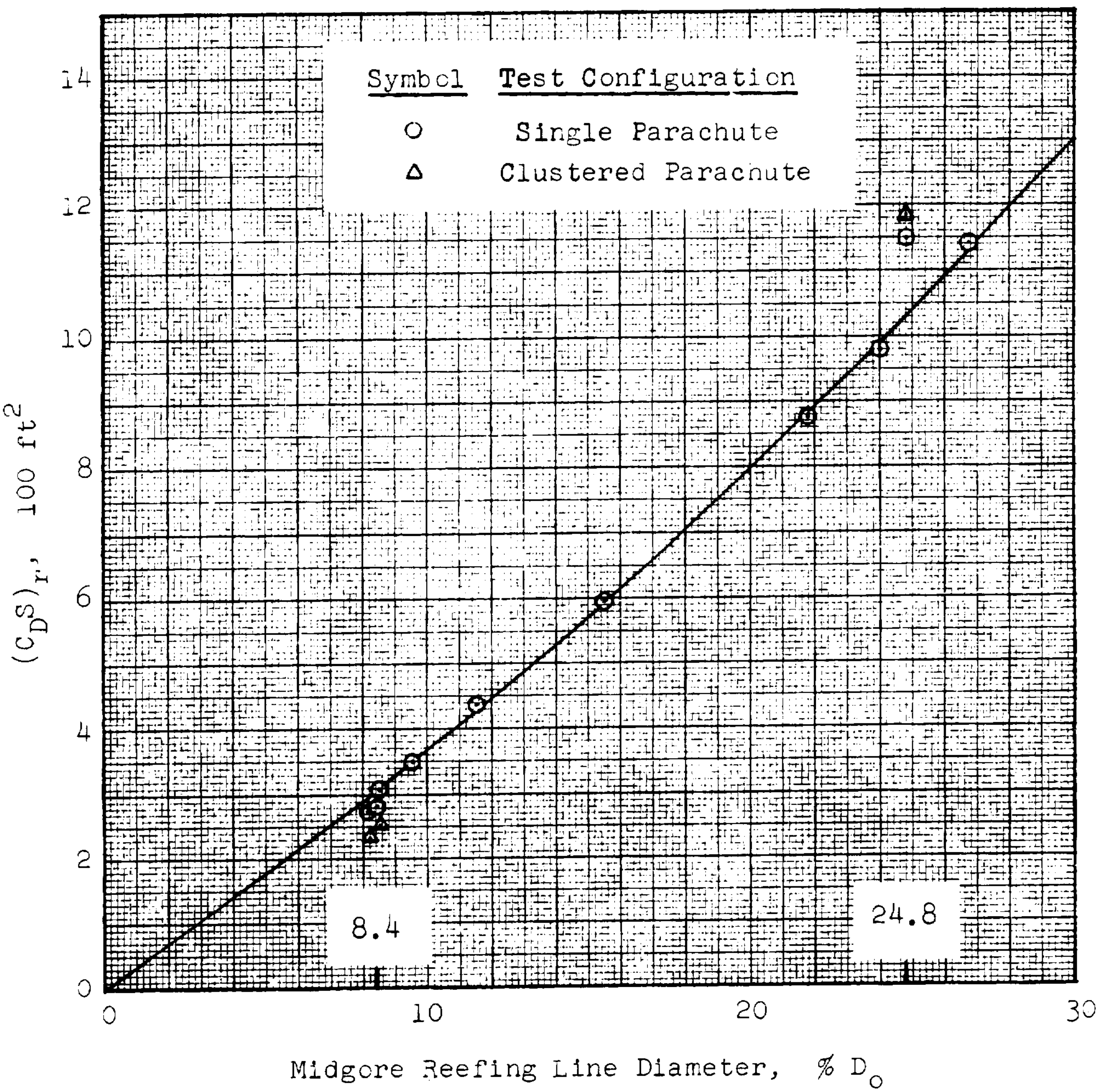

Fig. 14. Main Parachute Reefed Drag Area Versus Midgore Reefing Line Diameter (D_o = 83.5 ft)

The third stage (disreef) opening loads were calculated by an opening load factor method modified for clustered parachutes. Due to the presence of reefed "aerodynamic blanketing" (aerodynamic interference between parachutes) and nonsynchronous disreefing, the disreef loads experienced by different parachutes, even within the same cluster, were not the same. In order to use the opening load factor method, the unit canopy loading had to be determined for each parachute separately. This was accomplished by an iterative technique which was generally as follows: Values for the unit canopy loadings were assumed, calculations were made using these unit loadings and test data, and unit canopy loadings were determined. The cycle was repeated until the assumed and determined values matched. Knowing the unit canopy loadings, opening load factors could then be found from previous test data.

Snatch loads of the main parachute, being relatively low, were not calculated. Table 15 is a summary of the main parachute loads and methods that were computed in the Apollo parachute development program.

Table 15. Summary of Load Prediction Methods Used in Computing Main Parachute Loads

Load	Method Used (see Ref. 3)
F_{r_1}	2-DOF Computer Program
F_{r_2}	2-DOF Computer Program
F_o	Opening Load Factor (Modified)
Snatch	Not Calculated ($<F_{r_1}$)

2.3.1.1 Review of Reefed Opening Loads Prediction Method Used During Block II (H) Testing. Flight conditions were determined with a three-degree-of-freedom computer program, along with average parachute reefed drag areas and filling times, and supplied to a 2-DOF computer program. With this program, parachute forces were computed as the product $(C_D S)q$. Peak loads so determined were further augmented by special factors to cover vehicle dynamic effects in the prediction technique. Thus, the basic input parameters for Stage 1 were:

1) Initial flight conditions after main parachute stretchout when filling first begins
2) Deployment time differential between parachutes
3) Reefed filling time
4) Average reefed drag area (Stage 1)
5) Vehicle dynamic load factor (1.05 used)
6) Scatter factor (1.10 used)

The basic input parameters for Stage 2 were:

1) Initial flight conditions at first stage disreef
2) Disreef time differential between parachutes (0.34 to 0.85 sec used)
3) Reefed filling time
4) Average reefed drag area (Stage 2)
5) A combined vehicle dynamics and scatter factor (1.05 used)

All of the foregoing parameters are explained in greater detail in Reference 3. Of particular interest here are the methods of evaluating reefed drag areas and filling times.

2.3.1.2 Reefed Drag Areas. The appraisal of test data made for the load analysis of Reference 3 justified the use of the following reefed drag areas:

Canopy	$(C_DS)_{r_1}$	$(C_DS)_{r_2}$
Lead canopy in 2-chute cluster or first two canopies in 3-chute cluster	285 ft^2	1080 ft^2
Lag canopy in 2- or 3-chute cluster	257 ft^2	972 ft^2

Inconsistencies in the measurements obtained during the Block II (H) tests were large at the selected reefing ratios, necessitating reliance on the results of the Block I tests to establish the Stage 1 values and the drag area ratio of lag/lead canopies of 0.9. It may be noted that the Stage 1 drag areas selected fall below the average curve of Figure 14, but are in good agreement with test values obtained with single and clustered canopies. The Stage 2 values straddle the average data curve, but are far below measured values. The high measured values, if correct, are believed to have resulted from unusual canopy expansion due to heavy overloads.

It is difficult to find anything in the measured drag areas and opening forces of the two reefed stages that would justify the use of a smaller drag area for the lag canopy than for the lead canopy. This is because in many cluster tests, a reverse correlation existed between drag area and peak load. It was noted that the longest Δt measured was only 0.2 sec, compared to 0.8 sec and longer in the Block I tests, and it therefore appeared desirable to use a correction factor for the lag canopy. In seeking to improve the method, the following assumptions and evaluations were made:

1) Assume the reefed drag area is the same for all canopies in the cluster.

2) Evaluate the drag area at the time of reefed opening (rather than as the average value between reefed opening and disreef).

3) Evaluate the drag area growth rate during the reefed intervals.

4) Evaluate the reefed drag area at disreef as an initial condition for the following stage.

2.3.1.3 <u>Reefed Filling Time and Drag Area Growth</u>. The reefed filling time is calculated from the drag area and average area growth rate as

$$t_{f_r} = \frac{\Delta C_D S}{\overline{\dot{C}_D S}}$$

Where: $\Delta C_D S = (C_D S)_r - (C_D S)_i$

$(C_D S)_r$ = reefed drag area

$(C_D S)_i$ = initial drag area (= C for Stage 1)

$\overline{\dot{C}_D S}$ = average rate of growth for a given set of conditions

The area growth rate is related to the initial velocity, v_i, through the air inflow parameter

$$\Lambda = (C_D S)_r \, v_i$$

Use of the reefed drag area, rather than the canopy inlet area, is justified because the latter is usually irregular in shape and poorly defined. $(C_D S)_r$ accurately reflects the effectiveness of the actual air inflow in filling out the canopy volume.

The relationship between the drag area growth rate and the air inflow parameter for each Block II (H) test is shown in Figure 15 for both reefing stages. Pertinent data derived from the test results are summarized in Tables 16 and 17. The values of $\overline{\dot{C}_D S}$ were determined by parametric computer analysis. A plot was then

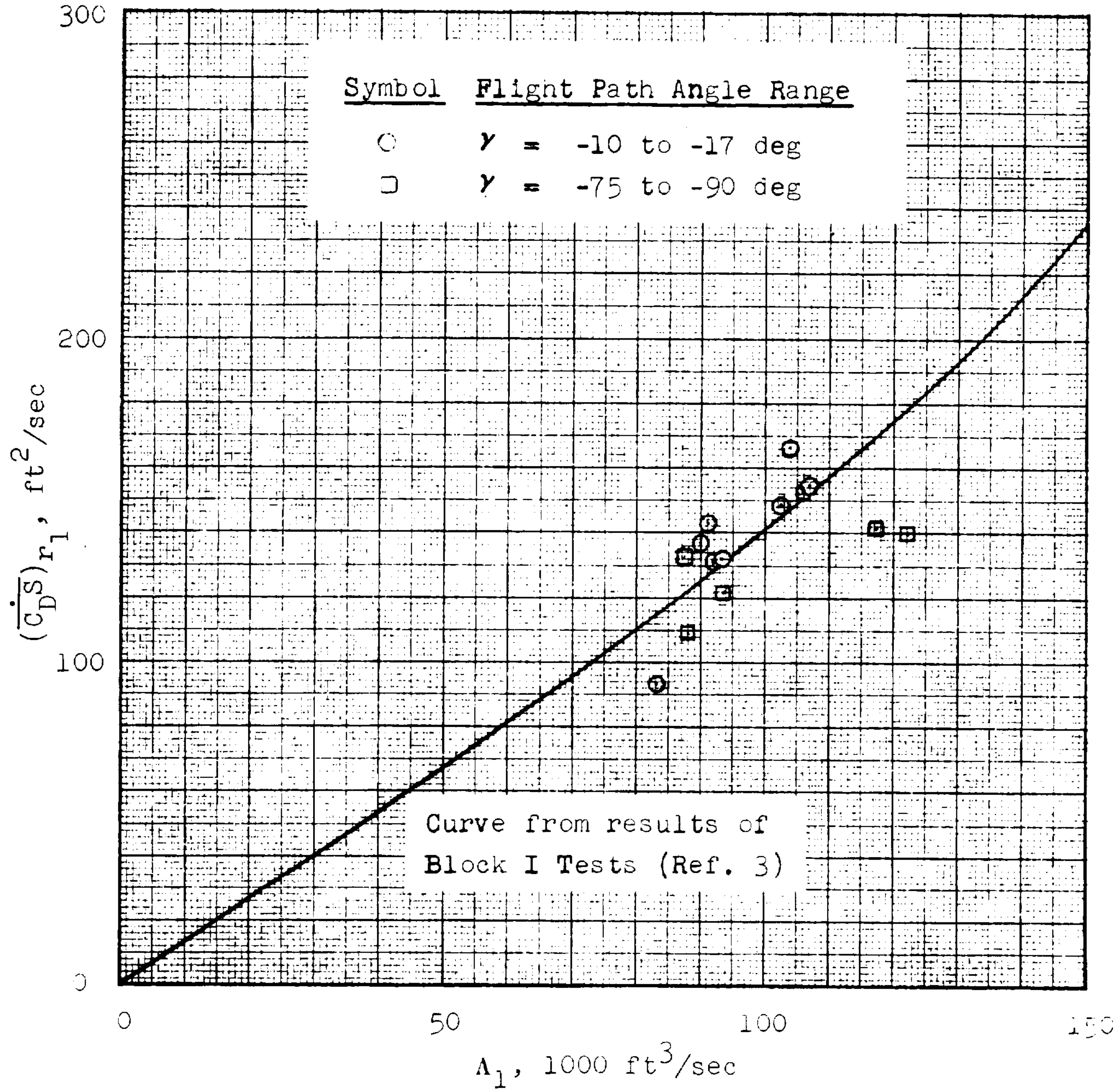

(a) Reefing Stage 1

Fig. 15. Drag Area Growth Rate Versus Air Inflow Parameter. Data Points Are from Block II (H) Tests; See Table 16

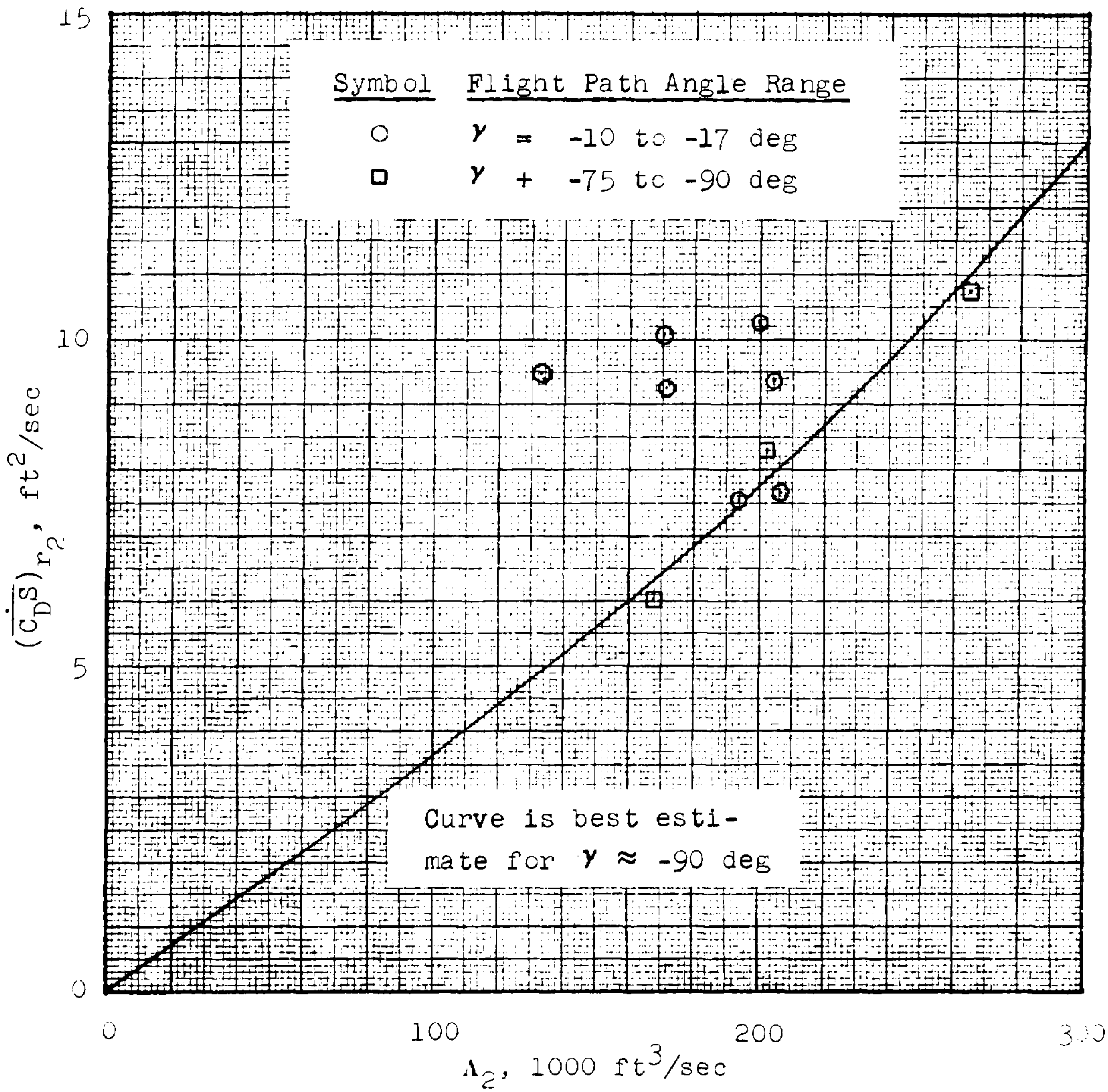

(b) Reefing Stage 2

Fig. 15 Concluded. Drag Area Growth Versus Air Inflow Parameter. Data Points Are from Block II (H) Tests; See Table 17

Table 16. First Reefing Stage Opening Data for Single and Clustered Main Parachutes

① Test No.	② Initial Conditions V_{MCCS} ft/sec	③ γ_{MCCS} deg	④ Stage 1 Peak Force F_{r_1} lb	⑤ Filling Time $t_{f_{r_1}}$ sec (1)	⑥ Average Drag Area $(C_DS)_{r_1}$ ft^2 (2)	⑦ Inflow Parameter Λ_1 ft^3/sec (3)	⑧ Area Growth $(\dot{\overline{C_DS}})_{r_1}$ ft^2/sec (4)	⑨ Reefing Diameter D_{r_1} % D_o
80-1R	328.8	-17	13,554	1.92	275	90,400	143	8.2
80-2	305.8	-10	18,700	1.86	278	101,600	149	8.2
80-3R1	367.5	-10	19,885	1.68	280	103,000	167	8.4
80-3R2	321.5	-13	16,195	2.15	288	92,600	134	8.4
81-1 (5)	346.7	-14	16,200	1.88	257	89,100	137	8.2
81-2 (5)	335.5	-15	13,720	2.66	247	82,800	93	8.4
81-3 (5)	372.0	-16	18,438	1.84	285	106,000	151	8.4
81-4 (5)	371.7	-11	17,157	1.85	246	91,400	133	8.4
82-1	382.4	-76	27,830	2.15	305	110,700	142	8.4
82-1R	407.3	-75	30,410	2.11	297	121,000	141	8.4
82-2	305.9	-83	20,375	2.59	285	87,100	110	8.4
82-4	296.7	-83	22,900	2.31	355	105,300	154	9.5
84-1R (5)	288.2	-82	12,410	2.64	322	92,800	122	8.4
84-4 (5)	305.3	-83	17,830	2.14	285	87,000	133	8.4

NOTES: (1) $t_{f_{r_1}} = (C_DS)_{r_1} / (\dot{\overline{C_DS}})_{r_1}$

(2) $(C_DS)_{r_1}$ is average value of F/q during latter portion of first reefed interval in which reefing line is taunt

(3) $\Lambda_1 = (C_DS)_{r_1} V_{MCCS}$

(4) $(\dot{\overline{C_DS}})_{r_1}$ is the drag area growth rate that, when used in a 2-DOF point-mass trajectory computation, produces the same F_{r_1} that is shown in Column (4)

(5) These were cluster tests. Presented data are for canopy that became the lead canopy after Stage 2 disreef (the corresponding data for the lag canopies are not available)

Table 17. Second Reefing Stage Opening Data for Single and Clustered Main Parachutes

(1) Test No.	(2) Initial Conditions v_{d_1} ft/sec	(3) γ_{d_1} deg	(4) Stage 2 Peak Force F_{r_2} lb	(5) Filling Time $t_{f_{r_2}}$ sec (1)	(6) Stage 1 Drag Area $(C_DS)_{r_1}$ ft^2 (2)	(7) Stage 2 Drag Area $(C_DS)_{r_2}$ ft^2 (3)	(8) Delta Drag Area $\Delta(C_DS)$ ft^2 (4)	(9) Inflow Parameter Λ_2 ft^3/sec (5)	(10) Area Growth $(\dot{C_DS})_{r_2}$ ft^2/sec (6)	(11) Reefing Diameter D_{r_2} % D_o
80-1R	151.6	-49	12,906	0.632	275	875	600	132,600	949	21.8
80-2	173.4	-52	18,205	0.767	278	985	707	170,000	922	24.0
80-3R1	176.4	-46	19,491	0.824	280	1125	845	198,500	1025	26.7
80-3R2	166.3	-64	18,684	0.996	288	1222	934	203,300	938	26.7
81-1 (7)	184.1	-48	19,407	0.657	257	920	663	169,500	1009	24.0
81-2 (7)	164.4	-51	18,597	1.310	247	1250	1003	205,800	767	26.7
81-4 (7)	169.6	-54	16,420	1.187	245	1135	891	192,700	750	26.7
82-2	223.5	-84	32,800	0.830	285	1180	895	264,000	1078	24.8
82-4	177.7	-88	24,300	0.936	355	1130	775	201,000	828	24.8
84-1R (7)	125.5	-85	11,140	1.675	322	1330	1008	167,000	602	24.8

NOTES:

(1) $t_{f_{r_2}} = (C_DS)/(\dot{C_DS})_{r_2}$

(2) $(C_DS)_{r_1}$ taken from Column (6) of Table 16

(3) $(C_DS)_{r_2}$ is average value of F/q during latter portion of second reefed interval in which reefing line is taunt

(4) $\Delta(C_DS) = (C_DS)_{r_2} - (C_DS)_{r_1}$

(5) $\Lambda_2 = (C_DS)_{r_2} v_{d_1}$

(6) $(\dot{C_DS})_{r_2}$ is drag area growth rate that, when used in a 2-DOF point-mass trajectory computation, produces the same F_{r_2} that is shown in Column (4)

(7) These were cluster tests. Presented data are for canopy that became the lead canopy after Stage 2 disreef (the corresponding data for the lag canopies are not available.

made of $(C_DS)q$ as a function of $\overline{\dot{C_DS}}$ based on the initial velocity and altitude observed in each test. The value of $\overline{\dot{C_DS}}$ selected was that corresponding to the measured opening force. In cluster tests, it was possible to do this only for the lead or most highly loaded parachute.

Stage 1 Data

For Stage 1, the data, though few in number and scattered, were consistent with those obtained from the Block I tests with a single stage of reefing. Therefore, the Block I data curve was superimposed and used as shown in Figure 15 (a). This curve falls reasonably well among the data points which are separated into two groups depending on the flight path angle. Presumably, the near-vertical data would be most applicable to the design cases, but confidence in the accuracy of the few measurements shown is low.

Stage 2 Data

The Stage 2 data points plotted in Figure 15 (b) appeared at first to afford no meaningful correlation, so a constant area growth rate of 1000 ft^2/sec was adopted as the one yielding the best load prediction for most cases. Subsequently, the correlation shown for near-vertical tests results was detected, but, as yet, had not been checked out in the computer.

A typical linear drag area growth schedule for one of the two-canopy design cases is illustrated in Figure 16. The curves after Stage 2 disreef were estimated.

Plots of measured C_DS versus time for reefing Stage 1 were re-examined, and the slopes of the growth curves were carefully measured. These average growth rates are plotted with the air inflow parameter, based on the drag area at reefed opening, in Figure 17. Fair correlation of the data results, and the separation relative to flight path angle disappears. This is an improvement for the near-vertical trajectory data, because if the constant

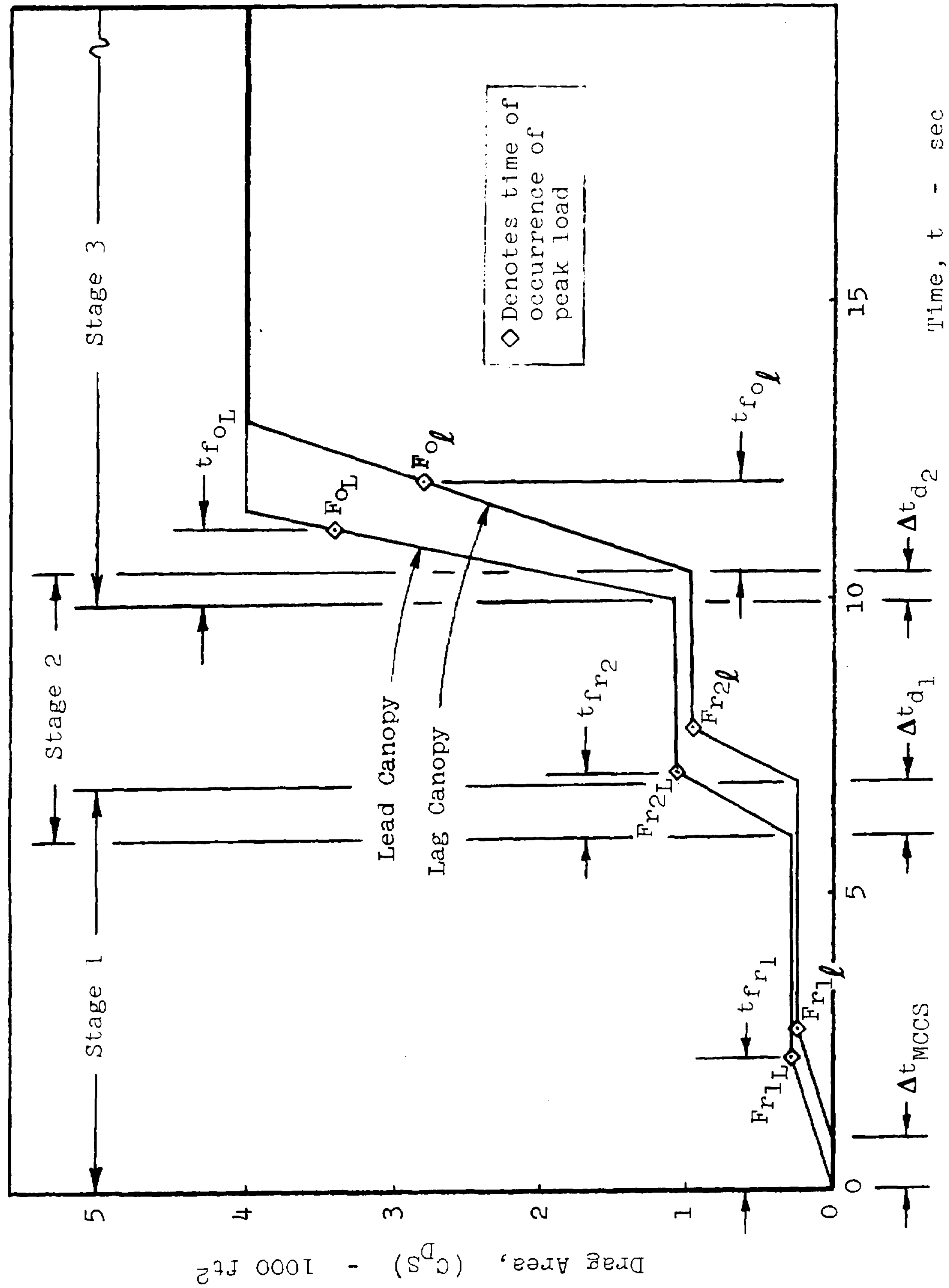

Fig. 16. Typical Drag Area-Time Relationship Assumed for the Parachutes in a Two-Chute Cluster of Main Parachutes

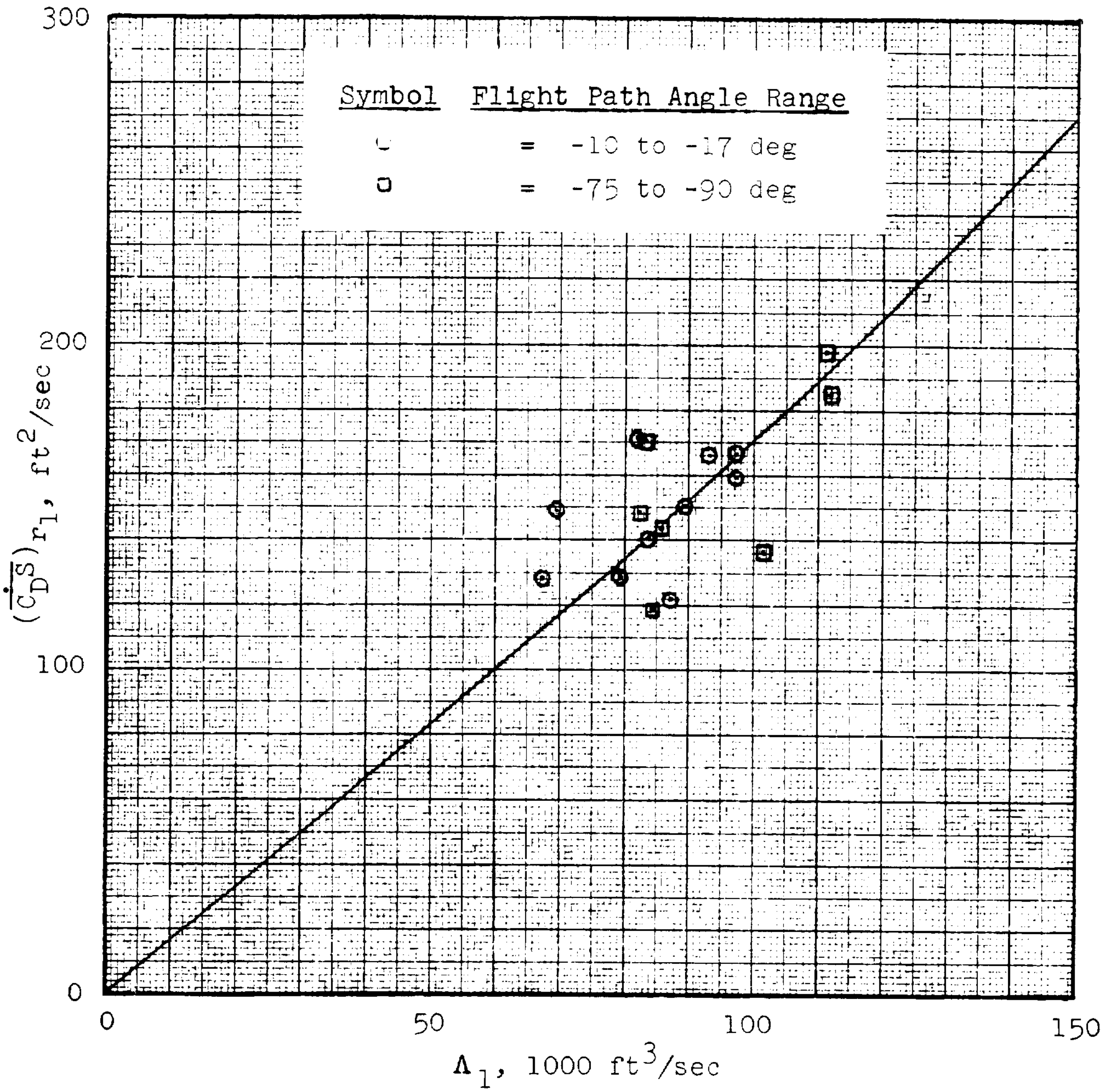

Fig. 17. Corrected Drag Area Growth Rate Versus Air Inflow Parameter for Reefing Stage 1. Data Points Are from Block II (H) Tests; See Table 18

filling distance theory discussed on page 73 is valid, one would expect vertical growth rates to be higher than those in near-horizontal flight.

The velocities at main canopy stretch used in constructing Figure 17 were determined and corrected by a method similar to that employed for the drogue and pilot chutes. The corrected velocities and other pertinent test data are summarized in Table 18. The average growth rates are substantially higher than those the computer requires to reproduce the measured opening forces. The resultant shorter filling times generate higher than measured opening forces when linear growth rates are employed in the computer program. Examination of the plotted C_DS versus time data derived from Askania and telemetry records shows a roughly linear growth rate in about half the tests; but, in most cases, the upper part of the curve shifts gradually to a lower rate as reefed inflation is approached. Since the peak opening force occurs at about the same time, this has an attenuating effect. However, the magnitude of the load reduction between computed values, based on reported filling times and the measured values, appears to be disproportionately large for the small time differential represented by the transition from one growth rate to another. The computer results indicate that a filling time 18 percent longer than the actual is required, on the average, when a linear growth rate is assumed for the first reefing stage.

Nonlinear Drag Area Growth

The data indicate that the drag area growth rate is nonlinear and not accurately represented by the ratio F/q derived from the Askania and telemetry data. Therefore, an investigation was made to find a suitable growth function to accurately represent the process. This was particularly needed for Stage 2 where it is known that at the instant of disreef the canopy mouth

Table 18. Corrected Data for First Reefing Stage of Single and Clustered Main Parachutes

① Test No.	② Chute No.	③ Initial Conditions v_{MCCS} ft/sec	④ γ_{MCCS} deg	⑤ Stage 1 Peak Force F_{r_1} lb	⑥ Filling Time $t_{f_{r_1}}$ sec (1)	⑦ Average Drag Area $(C_DS)_{r_1}$ ft^2 (2)	⑧ Inflow Parameter Λ_1 ft^3/sec (3)	⑨ Area Growth $(\dot{C_DS})_{r_1}$ ft^2/sec (4)	⑩ Reefing Diameter D_{r_1} % D_o
80-1R	1	335	-17	13,554	1.785	250	83.7	140	8.2
80-2	1	374	-10	18,700	1.633	260	97.2	159	8.2
80-3R1	1	374	-10	19,885	1.555	246	97.4	167	8.4
80-3R2	1	339	-13	16,195	1.655	275	93.2	166	8.4
81-1	1	350	-14	16,200	1.374	235	82.2	171	8.2
	2			12,860	1.355	199	69.7	149	8.2
81-2	1	339	-16	13,720	1.830	235	79.7	128	8.4
	2			13,480	1.560	200	67.8	128	8.4
81-4	1	380	-11	15,780	1.885	230	87.4	122	8.4
	2			17,157	1.565	235	89.3	150	8.4
82-1	1	385	-76	27,830	1.464	290	111.7	198	8.4
82-1R	1	409	-75	30,410	1.480	274	112.1	185	8.4
82-2	1	306	-84	20,375	1.823	270	82.6	148	8.4
82-4	1	295	-87	22,900	2.537	345	101.9	136	9.5
83-6	1	312	-88	12,360	1.922	275	85.8	143	8.4
84-1R	1	287	-85	12,100	2.520	290	83.2	115	8.4
	2			12,410	2.500	294	84.4	118	8.4
	3			12,000	2.500	294	84.4	118	8.4
84-4	1	310	-83	17,830	1.587	270	83.7	170	8.4
	2			NA	NA	NA	NA	NA	NA

NOTES:

(1) $t_{f_{r_1}} = (C_DS)_{r_1} / (\dot{C_DS})_{r_1}$

(2) $(C_DS)_{r_1}$ is average value of F/q during latter portion of first reefed interval in which reeefing line it taunt

(3) $\Lambda_1 = (C_DS)_{r_1} v_{MCCS}$

(4) $(\dot{C_DS})_{r_1}$ is the drag area growth rate that, when used in a 2-DOF point-mass trajectory computation, produces the same F_{r_1} that is shown in Column (4)

snaps open to a larger diameter and the air inflow rate increases suddenly. At the same time, the riser load drops due to momentary relaxation of the suspension lines. Therefore, the measured force is not simply $(C_D S)q$ during this critical part of the opening, when the velocity is a maximum, but the result of aeroelastic dynamics. Because the filling time is relatively short, added air mass effects are also present so that the riser load does not correspond to $(C_D S)q$ until after full inflation is reached. It was found that an exponential growth rate function based on measured drag areas and filling times would produce results similar to the opening load factor method of relating $(C_D S)q$ to the measured peak load. Because an exponential growth rate was suited to computer programming, it was investigated in some detail.

Dimensionless Filling Time Parameter

French[4] and others have shown that the distance traveled during the filling of a given parachute tends to be a constant. This led to the definition of a dimensionless filling parameter, K_f. This parameter is defined as,

$$K_f = \frac{v_i t_f}{D}$$

where v_i is the initial velocity (v_{MCCS} for Stage 1), t_f is the filling time, and D is a characteristic dimension of the canopy such as the nominal diameter, D_o, or the reefing line diameter, D_r. Dimensionless filling times, based on D_{r1}, were computed from the Stage 1 test data. These are summarized in Table 19 and plotted against the initial velocity, v_{MCCS} in Figure 18. These data suggest a mean value for the dimensionless filling time parameter, K_f = 83.9. This number could be used in the

Table 19. Dimensionless Filling Time Parameter Data for First Reefing Stage of Main Parachutes

①	②	③	④	⑤	⑥	⑦	⑧
Test No.	Chute No.	Reefing Diameter D_{r_1} % D_o	ft	Initial Conditions v_{MCCS} ft/sec	MCCS deg	Filling Time $t_{f_{r_1}}$ sec (1)	Filling Parameter K_f (2)
80-1R	1	8.2	6.85	335	-17	1.785	87.2
80-2	1	8.2	6.85	374	-10	1.633	89.2
80-3R1	1	8.4	7.01	374	-10	1.555	83.0
80-3R2	1	8.4	7.01	339	-13	1.655	80.0
81-1	1	8.2	6.85	350	-14	1.374	70.2
	2	8.2	6.85			1.335	68.2
81-2	1	8.4	7.01	339	-16	1.830	88.5
	2	8.4	7.01			1.560	75.5
81-4	1	8.4	7.01	380	-11	1.885	102.1
	2	8.4	7.01			1.565	84.8
82-1	1	8.4	7.01	385	-76	1.464	80.4
82-1R	1	8.4	7.01	409	-75	1.480	86.5
82-2	1	8.4	7.01	306	-84	1.823	79.6
82-4	1	9.5	7.93	295	-87	2.537	94.3
83-6	1	8.4	7.01	312	-88	1.922	85.5
84-1R	1	8.4	7.01	287	-85	2.520	103.0
	2	8.4	7.01			2.500	102.3
	3	8.4	7.01			2.500	102.3
84-4	1	8.4	7.01	310	-83	1.587	70.2
	2	8.4	7.01			NA	NA

NOTES: (1) $t_{f_{r_1}}$ values taken from Table 18

(2) $K_f = v_{MCCS} t_{f_{r_1}} / D_{r_1}$

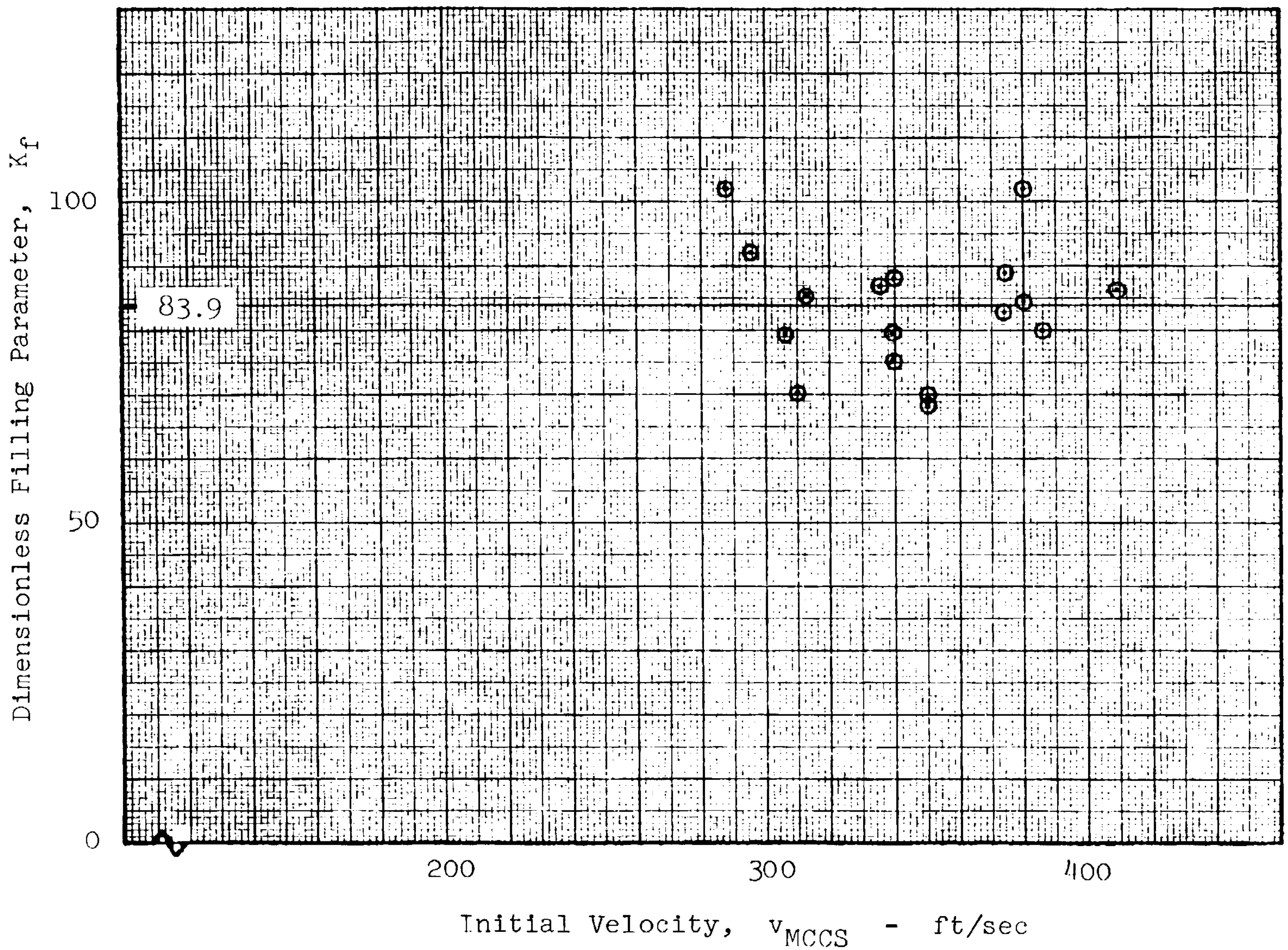

Fig. 18. Dimensionless Filling Parameter Versus Initial Velocity for First Stage Opening of Main Parachutes. Data Points Are from Table 19

calculation of reefed filling times for any reefing ratio within the range tested for Stage 1 in place of the more complicated procedure associated with using Figure 15 (a).

In re-evaluating the test data for both reefing stages, it was found that several good measurements obtained with clustered canopies had been omitted from Figures 13 and 14. This resulted from overemphasis on the importance of the lead canopy in the final opening phase, which in several instances was actually the lag canopy during one or both reefed stages. In consequence, the growth rates of the other canopies were not evaluated. This oversight was corrected in the calculated results presented in Figures 17 and 18. Also, after careful examination, all the data of Test 81-3 were rejected as unreliable.

2.3.1.4 Opening Loads Following Stage 2 Disreefing

Background

In parachute tests performed prior to 1960, two important quantities, the dynamic pressures at canopy stretch and at disreef, were seldom reported, because, in most cases, the corresponding velocities had not been measured. Therefore, only a fraction of the available data was usable: that in which the delay from launch to canopy stretch was very short, and that from which the velocity or dynamic pressure at canopy stretch and disreef could be deduced. In addition, it was necessary to have some means of calculating the reefed and full open drag areas of each canopy, and only approximate drag coefficients were available in many cases. For example, reefed drag areas were derived from an old empirical relationship that proved to be wrong most of the time, but consistent application of the resultant curve minimized this source of error.

The following quantities were generally calculated using standard atmospheric density (for want of aerological data at the time of each test).

$$\text{Opening Shock Factor,} \qquad X = \frac{F_o \text{ (measured)}}{(C_D S)\, q_i}$$

$$\text{Ballistic Coefficient,} \qquad \frac{W}{C_D S} = \frac{\text{System Weight}}{\text{Drag area (reefed or full open)}}$$

$$\text{Initial Dynamic Pressure,} \quad q_i = \tfrac{1}{2}\, \rho_o v_i^2$$

A plot was made of X versus $W/C_D S$ with initial flight velocity and altitude at launch noted. A large fraction of the data was for various ringsail parachutes tested at altitudes of 10,000-15,000 ft. These showed some correlation with launch velocity and a family of curves were drawn in by visual inspection of the trends for different equivalent airspeeds.

Whenever the deployment conditions of a new parachute design fell within the scope of the empirical data curves, it was possible to predict the probable opening force with fair accuracy as

$$F_o = X(C_D S)q_i$$

However, it was not always certain that the conditions were indeed comparable because of the large variations in vehicle ballistic coefficients and in the time intervals from launch to canopy stretch. Also, the variation of X with altitude was often obscured by insufficient and scattered data.

This background is given to bring out the considerable refinement of method represented by the Apollo load prediction technique and to clarify the reason it is unnecessary to use EAS as the controlling variable at a given altitude when the appropriate dynamic pressure is known with reasonable accuracy. The "opening shock factor" is now called the "opening load factor" and denoted as C_K. The complexity of the cluster parachute filling problem made it more expedient to employ this approach to load prediction for the Apollo main parachute disreef opening stage than to undertake development of an adequate computer program similar to that employed for the reefed opening stages.

Physical Basis

The filling of clustered canopies is an unstable process that leads to nonuniform opening and disparate load sharing more often than not. This effect is most pronounced in the final opening phase and starts with nonsynchronous disreefing of the canopies at the end of the second stage. Because the normal filling time of the ringsail canopy from Stage 2 disreef to full open is relatively short, the disreef time differential between "lead" and "lag" canopies has a strong effect on subsequent inflation. If the disreef Δt is favorable to the lagging canopy of Stage 2, this lage canopy may recover and take the lead in the final opening phase. Here, the lead canopy is defined as the one receiving the highest peak load, the lag canopy (or lag canopy No. 1) second highest, and the lag-lag canopy (or lag canopy No. 2) the lowest. The disreef Δt is not the only factor that causes the canopies to fill at different rates, so good correlation of results with this parameter cannot be expected.

Summary of Method

The load prediction method of Reference 3 for the opening loads following Stage 2 disreefing is summarized as follows:

Opening Force

The empirical opening force relationship, as applied to the Apollo main parachute cluster, is used in the form

$$F_o = C_{K_o}(C_D S)_o \, q_{d_2} \tag{2}$$

where:

F_o = peak opening force of full open stage

C_{K_o} = opening load factor of full open stage

$(C_D S)_o$ = drag area of full open canopy (4000 ft^2)

q_{d_2} = dynamic pressure at Stage 2 disreef

When values of C_{K_o} were calculated for the tests performed with two-stage reefing, it was found that the single canopies provided more drag area than the cluster canopies at the same effective unit loading. Therefore, only the cluster data presented in Table 20 were available to support development of the curves given in Figure 19.

Effective Unit Canopy Loading

The method of evaluating the effective unit canopy loading for each parachute in the cluster is one of apportioning the total system weight (W) in accordance with the ratio of the instantaneous dynamic drag area (F/q) of each canopy to the combined dynamic drag area of all canopies in the cluster measured at the time of maximum force in the lead canopy.

$$\left[\frac{W^*}{C_D S_o}\right]_j = \frac{(C_D S_m)_j}{\Sigma (C_D S_m)} \left[\frac{W}{4000}\right] \tag{3}$$

Table 20. Disreef Opening Load Factor Data for Single and Clustered Main Parachutes

① Test No.	② Chute No.	③ Lead /Lag (1)	④ System Weight W lb	⑤ Eff. Unit Loading (W^*/C_DS_o) lb/ft^2 (2)	⑥ Initial Dyn. Pres. q_{d_2} lb/ft^2	⑦ Dynamic Drag Area C_DS_m ft^2 (3)	⑧ Total Dyn. Drag Area $\sum(C_DS_m)$ ft^2	⑨ Opening Load F_o lb	⑩ Opening Load Factor C_{K_o} (4)	⑪ Reefing Diameter D_{r_2} % D_o
80-1R	1	-	5,422	1.36	7.05	4660	4660	13,737	0.487	21.8
80-2	1	-	7,501	1.88	9.70	5513	5513	21,790	0.562	24.0
80-3R1	1	-	7,598	1.88	7.30	5880	5880	21,185	0.718	26.7
80-3R2	1	-	7,497	1.88	6.43	6635	6635	20,546	0.799	25.7
81-1	1	ℓ	12,989	1.56	7.95	2870	5960	14,020	0.441	24.0
	2	L		1.68	8.35	3090		15,120	0.453	24.0
81-2	1	L	12,989	2.58	5.41	5650	7130	17,518	0.810	26.7
	2	ℓ		0.674	3.81	1480		6,568	0.431	26.7
81-3	1	ℓ	13,054	1.51	7.70	2930	6300	14,170	0.460	26.7
	2	L		1.74	7.37	3370		16,060	0.545	26.7
81-4	1	L	12,989	1.91	6.24	4340	7400	17,161	0.687	25.7
	2	ℓ		1.34	5.82	3060		12,200	0.524	25.7
82-2	1	-	9,687	2.42	≈8	7500	7500	28,135	≈.88	24.8
82-4	1	-	10,486	2.62	9.15	6980	6980	32,200	0.880	24.8
84-1R	1	ℓ	13,026	0.41	1.78	1120	8850	5,140	0.722	24.8
	2	L		1.37	3.86	3720		9,300	0.602	24.8
	3	ℓℓ		1.47	3.75	4010		10,040	0.669	24.8
84-4	1	L	12,961	≈1.6	6.17	4120	NA	15,320	0.620	24.8
	2	ℓ		NA	NA	NA		NA	NA	24.8

NOTES: (1) L, ℓ and ℓℓ denote lead canopy, lag canopy number one and lag canopy number two, respectively, of Stage 3

(2) (W^*/C_DS_o) defined by Equation (3)

(3) $(C_DS_m) = F_o/q_m$, where q_m is dynamic pressure at time of occurrence of F_{o_L}

(4) $C_{K_o} = F_o/q_{d_2}(C_DS_o)$, where (C_DS_o) is 4000 ft^2

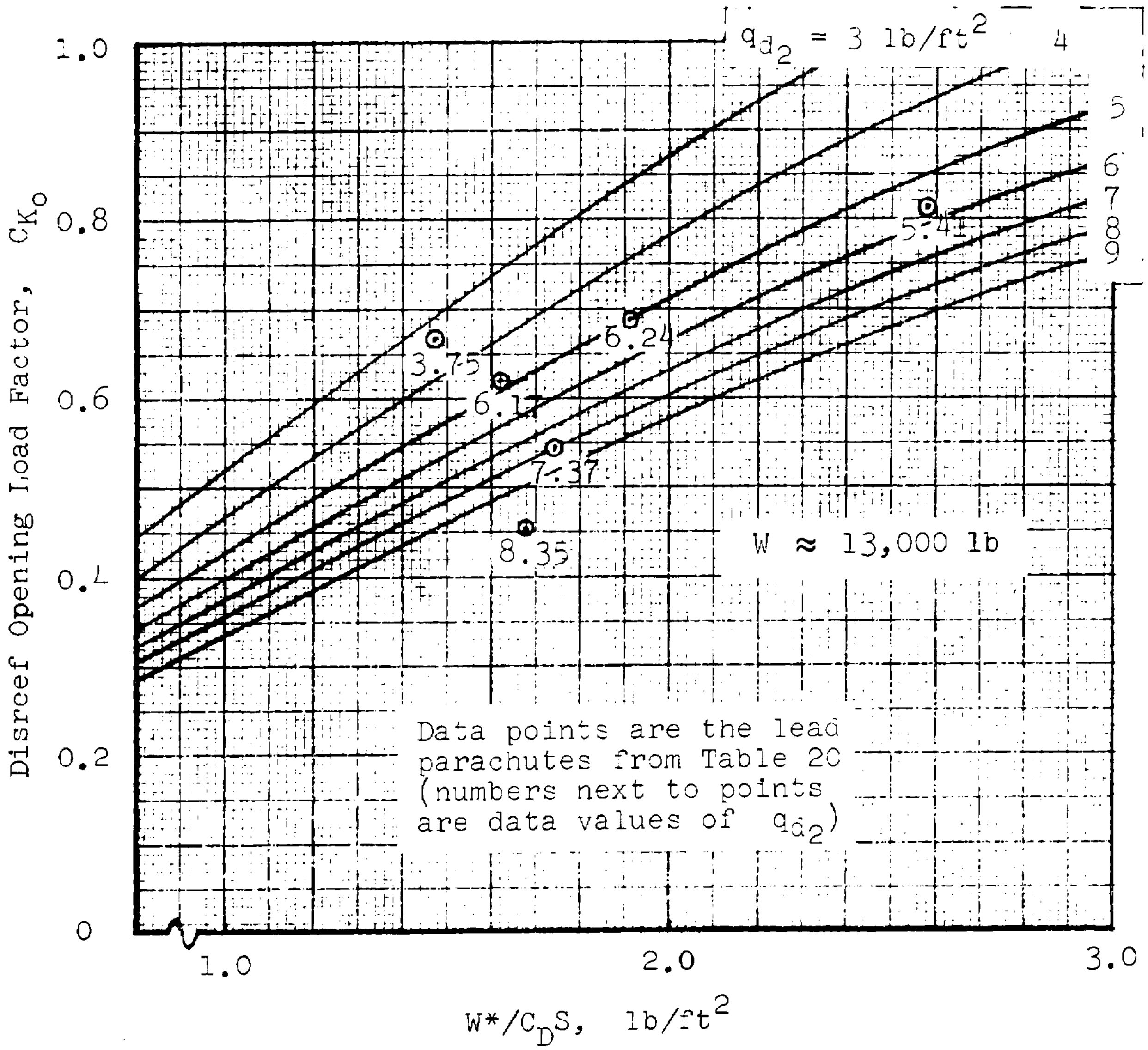

Fig. 19. Disreef Opening Load Factor Versus Effective Unit Canopy Loading for Main Parachutes

where:

j = one of n canopies in the cluster, $j = 1, \ldots, n$

W^* = portion of weight carried by j canopy

$(C_D S_m)_j$ = dynamic drag area of j canopy = F_j/q_m

F_j = instantaneous force of j canopy

q_m = dynamic pressure at time of lead canopy maximum force

$$\Sigma(C_D S_m) = (C_D S_m)_1 + \ldots + (C_D S_m)_n$$

The term "dynamic drag area" is employed to distinguish the instanteous ratio of force to dynamic pressure from the steady-state value because mass inertia and aeroelastic effects may be present and contribute to data variations. The assumption is made in Equation (3) that the steady state values are directly proportional to the dynamic values measured for each canopy. The calculated results are summarized in Table 20 and plotted in Figure 20. The curve indicated for clustered canopies is used in the load calculation.

Lead/Lag Canopy Inflation Characteristics

Canopy growth is characterized by a nondimensional ratio $C_D S_m / C_D S_{r_2}$ in which the numerator is the dynamic drag area of a given canopy in the cluster at the time the lead canopy load reaches its maximum value, and $C_D S_{r_2}$ is the average reefed drag area of a given canopy during Stage 2 after inflation.

A dimensionless time parameter is defined as $\Delta t_{d_2}/t_{f_o}$, the ratio of the time differential between lead and lag canopy disreefing to the time required after disreefing for the lead canopy load to reach its maximum value. The signs of Δt_{d_2} are opposite for lead and lag canopies. A positive Δt_{d_2} for either canopy means that the other disreefed first and inhibited the growth of the second-to-disreef, irrespective of its later development as a leading or lagging canopy. A negative Δt_{d_2} for a given canopy indicates that

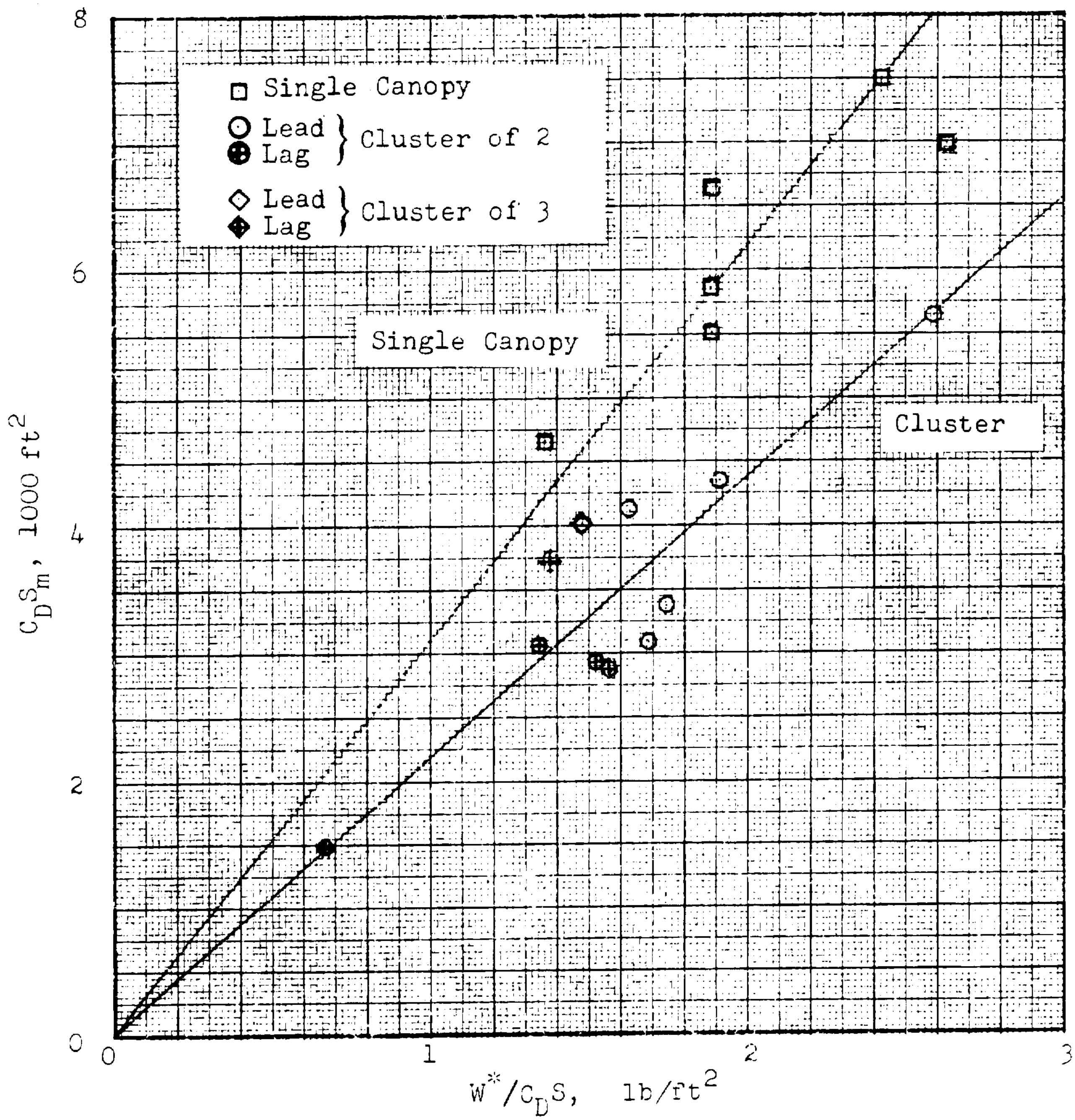

Fig. 20. Drag Area at Time of Lead Canopy Peak Load Versus Effective Unit Canopy Loading for Main Parachutes

it disreefed first, and consequently, its initial growth was less inhibited by the presence of the other still reefed canopy.

Calculated values of these parameters, derived from the test data summarized in Table 21, are plotted in Figure 21(a). The scatter around $\Delta t_{d_2}/t_{f_o} = 0$ shows that the dynamic drag area at the time of the lead canopy maximum load is not much affected by small disreefing time differentials between lead and lag canopy. Although the distribution of the data is not necessarily symmetrical about zero, it tends to fit this pattern better than any other; however, since only positive values of $\Delta t_{d_2}/t_{f_o}$ are used in calculating the drag area ratio of the lag canopy, the principal value of the negative data is in helping to establish the slope of the right hand portion of the curve in Figure 21(a).

The canopy continues to fill, but at a greatly reduced rate, during the latter portion of the reefed interval and causes the effective drag area at disreef to be greater than the average value in most cases. Because the initial phase of reefed opening is subject to wide variations due to dynamic effects, it appears that the end value of the reefed drag area determined at near-equilibrium conditions, being the starting point of subsequent growth, should show better correlation of the inflation parameters developed. This approach is tested with the data plot of Figure 21(b). At $\Delta t_{d_2}/t_{f_o} = 1.0$, the lag canopy drag area equals its end value, and consequently the area ratio is unity. This is not necessarily the case when the average reefed drag area is used, for the reason given. At $\Delta t_{d_2}/t_{f_o} = -1.0$, the drag area ratio approaches that of the single canopy, but Figure 20 shows that the presence of the lag canopy reefed for the entire interval will change the filling characteristic significantly, so that the peak load occurs at a smaller level of growth, if not earlier in the filling process.

Table 21. Canopy Growth and Disreef Time Lag Data for Single and Clustered Main Parachutes

①	②	③	④	⑤	⑥	⑦	⑧	⑨
Test No.	Chute No.	Lead /Lag (1)	Stage 2 Drag Area $(C_DS)_{r_2}$ ft^2	Drag Area Ratio $\frac{(C_DS)_m}{(C_DS)_{r_2}}$	Filling Time t_{f_o} sec (2)	Time Lag Δt_{d_2} sec (3)	Time Lag Ratio $\frac{\Delta t_{d_2}}{t_{f_{o_L}}}$	Reefing Diameter D_{r_2} % D_o
80-1R	1	-	875	5.32	1.41	-	-	21.8
80-2	1	-	985	5.60	1.10	-	-	24.0
80-3R1	1	-	1125	5.24	1.02	-	-	26.7
80-3R2	1	-	1222	5.43	1.05	-	-	26.7
81-1	1	ℓ	920	3.12	1.02	0.29	+0.23	24.0
	2	L	860	3.60	1.26	-.29	-0.23	24.0
81-2	1	L	1250	4.52	1.24	-1.10	-0.89	26.7
	2	ℓ	1210	1.24	2.64	1.10	+0.89	26.7
81-3	1	ℓ	945	3.09	0.91	-.07	-0.075	26.7
	2	L	1050	3.21	0.94	0.07	+0.075	26.7
81-4	1	L	1075	4.03	1.12	-.35	-0.313	26.7
	2	ℓ	1135	2.69	0.84	0.35	+0.313	26.7
82-2	1	-	1180	6.36	1.03	-	-	24.8
82-4	1	-	1130	6.18	0.95	-	-	24.8
84-1R	1	$\ell\ell$	≈550	NA	NA	NA	NA	24.8
	2	L	1145	3.46	1.20	-.25	-0.208	24.8
	3	ℓ	1330	3.21	1.11	0.25	+0.208	24.8
84-4	1	L	1075	3.83	1.03	NA	NA	24.8
	2	ℓ	NA	NA	NA	NA	NA	24.8

NOTES: (1) L, ℓ, and $\ell\ell$ denote lead canopy, lag canopy number one and lag canopy number two, respectively, of Stage 3

(2) t_{f_o} denotes the time interval between second stage disreef and the time of occurance of F_o

(3) Δt_{d_2} denotes second stage disreef lag time

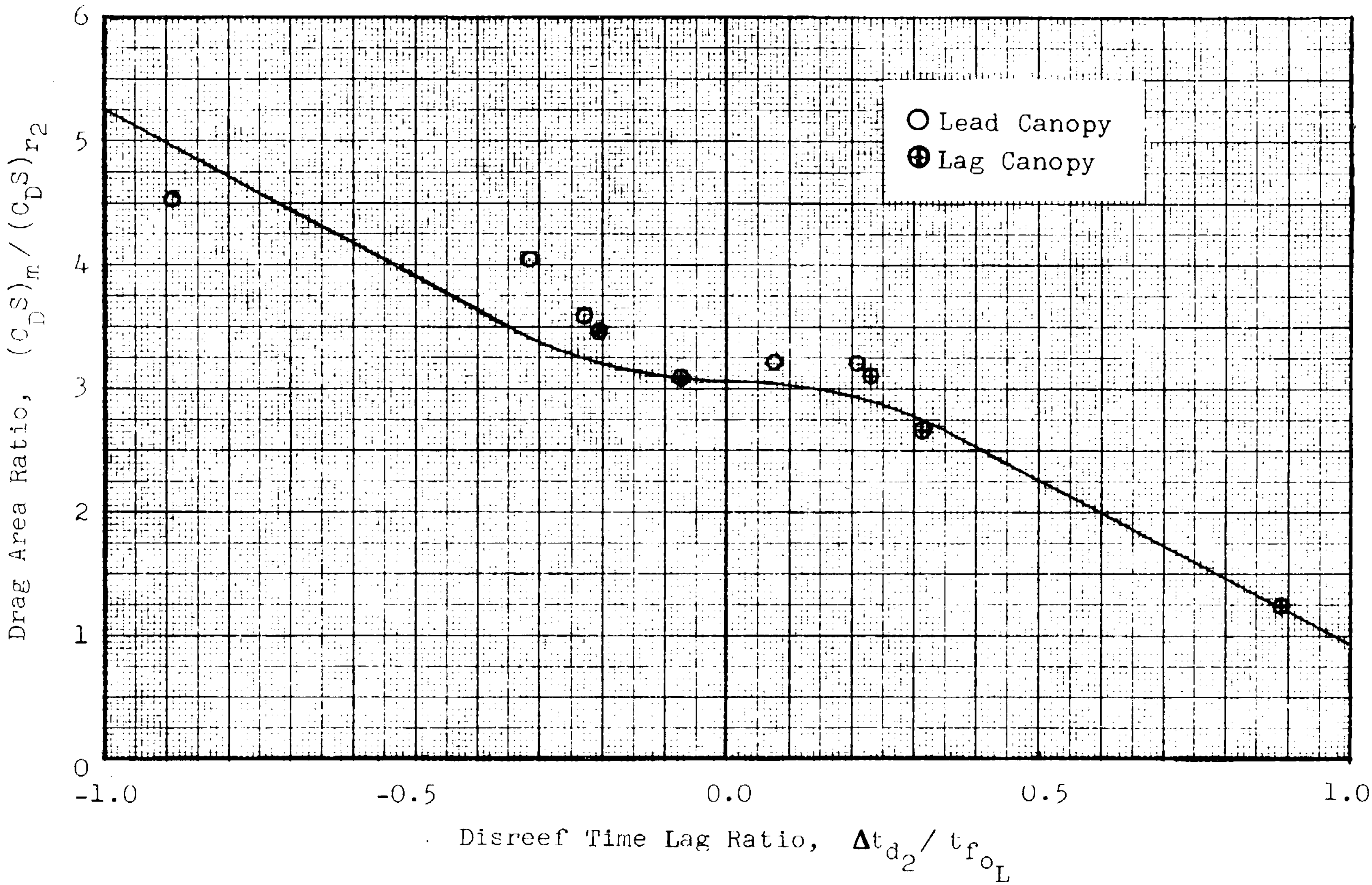

(a) Drag Area Ratio Based on $(C_DS)_{r_2}$

Fig. 21. Cluster Canopy Drag Area Ratio Versus Disreef Time Lag Ratio

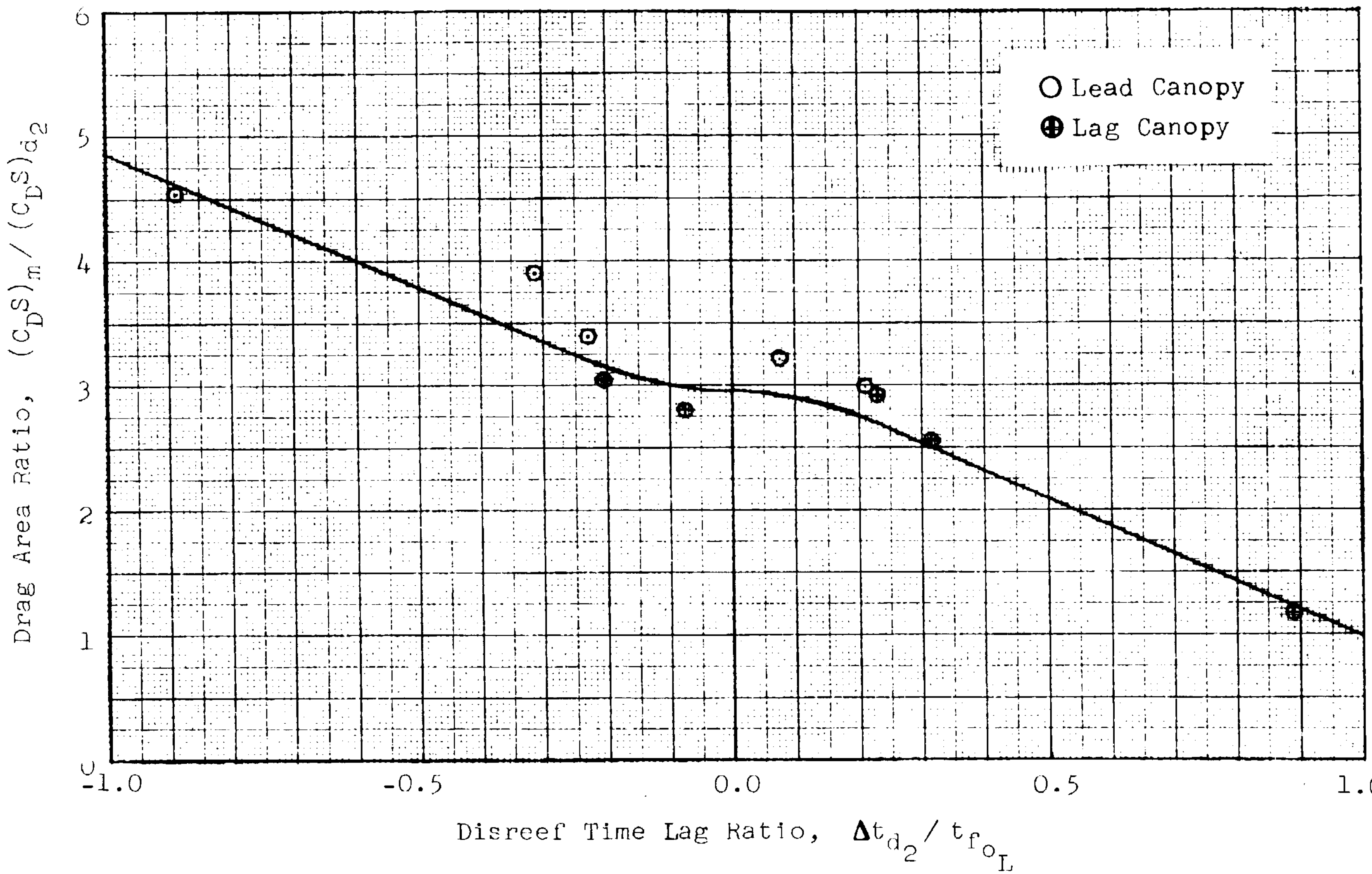

(b) Drag Area Ratio Based on $(C_D S)_{d_2}$

Fig. 21 Concluded. Cluster Canopy Drag Area Ratio Versus Disreef Time Lag Ratio

Canopy Filling Time from Stage 2 Disreef to F_o

The canopy filling time after Stage 2 disreef, t_{f_o}, is treated as a function of a mass flow function, $\dot{m}$, and the effective unit canopy loading. The mass flow function is considered to be proportional to the initial value and is defined by the relation

$$\dot{m} = \rho v_{d_2} (C_D S)_{r_2} \tag{4}$$

where:

ρ = air density, sl/ft^3

v_{d_2} = velocity at Stage 2 disreef, ft/sec

$(C_D S)_{r_2}$ = average drag area of one canopy during latter portion of Stage 2 opening, ft^2

The use of $(C_D S)_{r_2}$ rather than the reefed inlet area in Equation (4) is justified because the latter is usually poorly defined and the former is proportional to the volume at the time of disreefing. The calculated results derived from pertinent test data are presented in Table 22 and Figure 22. Because of data scatter, considerable judgment was required to establish the unit canopy loading curves. This was aided by extrapolation of a similar set of curves developed from the Block I test data in Reference 6.

At disreefing, the canopy mouth quickly snaps open to a larger inlet area (due to tension in the reefing line) and then continues to expand at an exponential rate until inflation is completed. Although the disreef drag area accurately reflects the bulbous development of the canopy, which produces the reefing line tension, and causes the mouth to snap open, the subsequent filling characteristic is not determined solely by the initial inflow rate. Apart from canopy shape and porosity factors, there is a lead/lag canopy dynamic interplay called "blanketing" that causes unequal filling rates even though disreefing may be synchronous. The existence of this interplay is emphasized by the occurrence of lag canopies with negative disreef time differentials.

Table 22. Disreef Filling Time Data Obtained During Single and Clustered Main parachute Tests

①	②	③	④	⑤	⑥	⑦	⑧	⑨	⑩
Test No.	Chute No.	Lead /Lag (1)	Altitude h ft	Air Density ρ sl/ft^3	Initial Conditions v_{d_2} ft/sec	$(C_DS)_{r_2}$ ft^2	Filling Time t_{f_o} sec (2)	Mass Flow Function $\dot{m}$ sl/sec (3)	Reefing Diameter D_{r_2} % D_o
80-1R	1	-	9635	.001698	91.5	875	1.41	136	21.8
80-2	1	-	9713	.001680	106.5	985	1.10	176	24.0
80-3R1	1	-	9760	.001698	93.0	1125	1.02	178	26.7
80-3R2	1	-	9007	.001748	86.0	1222	1.05	183	26.7
81-1	1	ℓ	9610	.001704	96.5	920	1.02	151	24.0
	2	L			99.0	860	1.26	145	24.0
81-2	1	L	9345	.001736	79.0	1250	1.24	171	26.7
	2	ℓ			66.3	1210	2.64	139	26.7
81-3	1	ℓ	9620	.001701	95.1	945	0.91	153	26.7
	2	L			93.1	1050	0.94	166	26.7
81-4	1	L	9310	.001752	84.4	1075	1.12	159	26.7
	2	ℓ			81.6	1135	0.84	162	26.7
82-2	1	-	8276	.001804	94.2	1180	1.03	200	24.8
82-4	1	-	7548	.001826	100.1	1130	0.95	207	24.8
84-1R	1	$\ell\ell$	8100	.001913	NA	≈550	NA	NA	24.8
	2	L			63.6	1145	1.20	139	24.8
	3	ℓ			62.9	1330	1.11	160	24.8
84-4	1	L	6732	.001970	79.1	1075	1.03	167	24.8
	2	ℓ			NA	NA	NA	NA	NA

NOTES: (1) L, ℓ, and $\ell\ell$ denote lead canopy, lag canopy number one and lag canopy number two, respectively, of Stage 3

(2) t_{f_o} denotes the time interval between second stage disreef and the time of occurance of F_o

(3) $\dot{m} = \rho v_{d_2} (C_DS)_{r_2}$

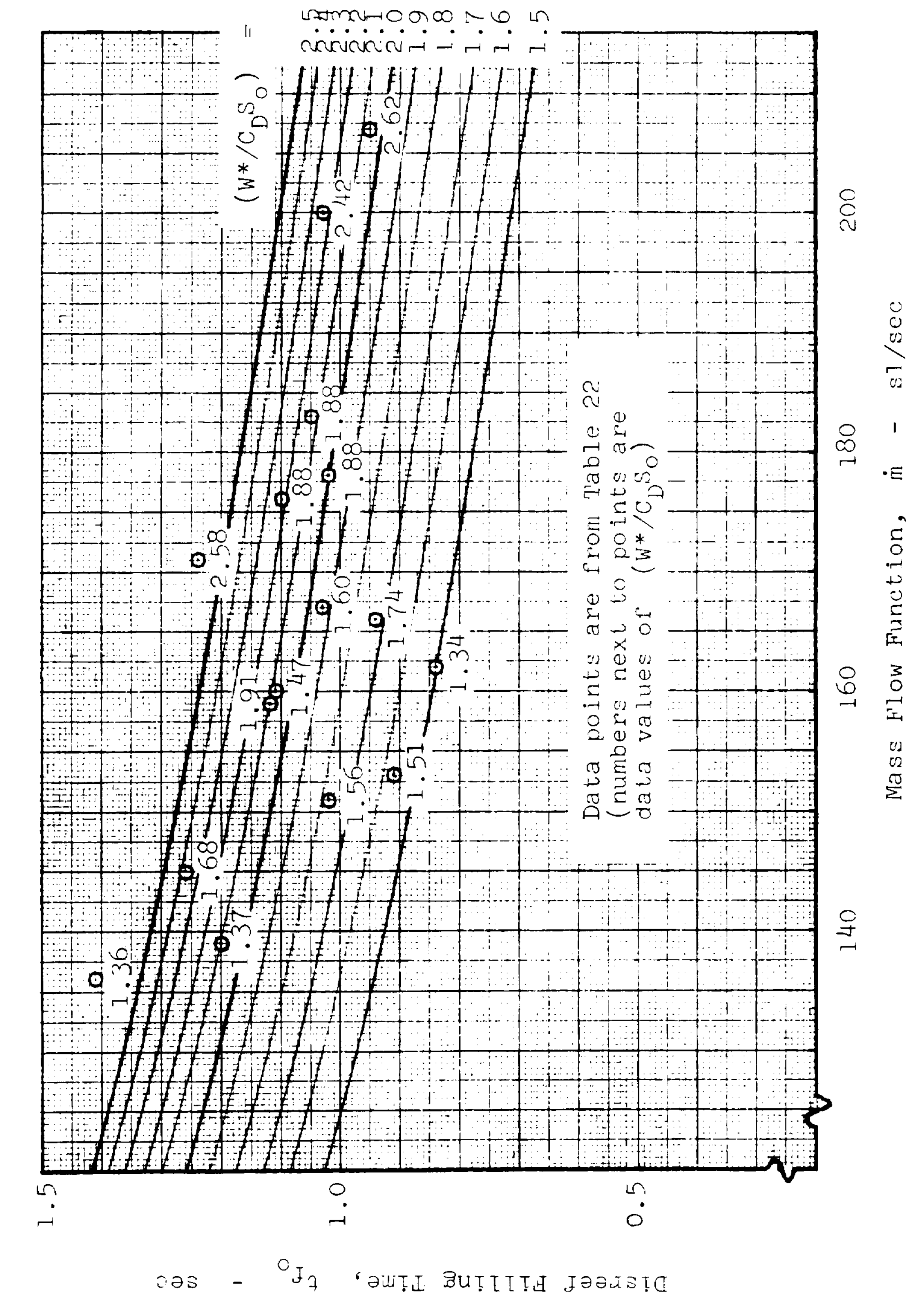

Fig. 22. Disreef Filling Time Versus Mass Flow Function for Main Parachutes

Procedure for Calculating the Disreef Opening Loads

The peak opening loads of the individual parachutes in two- and three-canopy clusters of 83.5-ft D_o ringsails is determined as follows:

1) Establish the conditions at Stage 2 disreef for each parachute in the cluster (lead, lag and lag-lag). These are q, v, γ, h, ρ and Δt (with subscript d_2).

2) Using $(C_DS)_{r_2}$ = 1080 ft^2, calculate the value of the mass flow function for the lead canopy ($\dot{m}_L$).

3) Estimate the value of W^*/C_DS_o for the lead canopy.

4) Determine the value of C_DS_m for the lead canopy in Figure 20 corresponding to the estimated value of W^*/C_DS_o.

5) Determine the value of the lead canopy filling time (t_{f_o}) in Figure 22 corresponding to W^*/C_DS_o and $\dot{m}_L$.

6) Calculate $\Delta t_{d_2}/t_{f_o}$ for the lag parachute(s).

7) Determine the corresponding value of $(C_DS_m)/(C_DS)_{r_2}$ for the lag parachute(s) from Figure 21(a).

8) Calculate C_DS_m for the lag parachute(s) using a value of $(C_DS)_{r_2}$ from page 62 and $(C_DS_m)/(C_DS)_{r_2}$ from Figure 21(a)

9) Calculate W^*/C_DS_o for the lead parachute. Compare this value with the estimated value in Step (3) above. Using the calculated value of W^*/C_DS_o, repeat Steps (3) through (9) until initial and final values are equal.

10) Calculate the unit canopy loading(s) of the lag parachute(s).

11) Determine the opening load factor C_{K_o} in Figure 19 for each parachute for the corresponding values of W^*/C_DS_o and q_{d_2}.

12) Using C_DS_o = 4000 ft^2, calculate the opening force of each parachute.

2.3.2 Example Opening Loads Calculations

The main parachute loads for one Apollo design case are presented, on an example basis, in Appendix C. This case, referred to as Case 410, is a normal entry case for which one drogue chute and two main parachutes operate. Conditions at the time of lead parachute line stretch for this case are as follows: vehicle weight, 12,960 lb; flight dynamic pressure, 85.0 lb/ft^2; flight path angle, -90 deg; altitude, 10,750 ft; time from drogue chute disconnect to lead MCLS 1.6 sec; time from drogue chute disconnect to lag MCLS, 1.8 sec. The area growth method is used to predict the Stage 1 and Stage 2 lead parachute maximum loads, F_{r_1} = 18,650 lb and F_{r_2} = 18,350 lb; and the opening load factor method is used to predict the Stage 3 lead parachute maximum load, F_{r_o} = 18,680 lb. These values are compared with those from the final Apollo ELS loads report[3] for the same case. It is noted that whereas the new values for Stages 1 and 3 are approximately 0.8 percent higher, the new value for Stage 2 is approximately 14.8 percent lower than the corresponding load from Reference 3.

SECTION 3.0

BACKGROUND STUDIES ON IMPROVED LOAD PREDICTION METHODS

3.1 GENERAL LITERATURE SURVEY

A review of available literature pertinent to the prediction of opening loads for the Apollo spacecraft parachutes is presented in this section.

The analysis and data review reported on in Section 2.0 brought about an awareness of the details of the methods used to make these load predictions. Also, it improved the accuracy of these specific methods to close to their limits. In order to further increase the accuracy with which Apollo parachute loads could be predicted, it was felt that new methods must be developed. Rather than start such a development from basic principles and derive these new methods, it was decided to review the parachute literature on load prediction methods. Such an approach allows the present study to benefit from the many thousands of hours that have been spent, around the world, on the problem at hand. The specific benefit was expected to be in the form of either complete methods which could be adapted to the Apollo parachutes, or considerations which would aid in any methods formulated within the present study. Both benefits have been derived from the literature review, and a summary of that review follows.

3.1.1 Early Analyses (1942 through 1949)

The analyses published between 1942 and 1949 present a rapid evolution of the understanding of the parachute opening process. During World War II there was much development work in mancarrying parachutes for use at altitudes up to 40,000 ft. Such applications of parachutes at altitudes far above sea level were apparently rare enough, prior to this period, that altitude effects on parachute opening loads were unknown. It was the development work at higher altitudes conducted during this period that brought about the discovery of altitude effects and fostered the analytical work on parachute opening loads which advanced so far by 1949.

Prior to 1942, it was apparently believed that velocity was the parameter that determined the opening shock of a particular parachute/payload system. Wildhack[7] presented a report that dealt with the minimization of opening loads following ejection from an airplane in horizontal flight. His recommendation was that the parachutist deploy the parachute at the minimum velocity point in his trajectory. The basis was that trajectories are controlled by weight and drag and that initially drag would predominate and decelerate the free-falling man, but that soon the man's flight path would have curved enough towards vertical that the weight would predominate and accelerate the man. Wildhack's recommendation that the parachutist deploy his parachute at the minimum velocity point, occurring at the time weight first predominates over drag, indicates an awareness of the effect of velocity on parachute opening loads and, at the same time, a lack of awareness of the effect of altitude. Wildhack's only mention of altitude effects was the (presumably tongue in cheek) recommendation that the parachute deployment not be so delayed during ejections close to the ground.

During the same year (1942) Pflanz[8] published an analysis dealing with the calculation of parachute loads during the opening process. Representing the instantaneous parachute load as C_DSq, he calculated system velocity as a function of time by the equation*

$$m \frac{dv}{dt} = -C_DSq = -\frac{1}{2} \rho v^2 C_DS.$$

This equation was solved numerically for several forms of the drag area growth (linear, exponential, sinusoidal, etc), as well as for several velocities. The resulting time histories of parachute force (C_DSq), which were presented, illustrated the effects of these parameters on these force histories. In 1943 Pflanz[9] published another report in which the approach was the same as

* The symbols used herein are chosen to be compatible with those in the symbols section of this report and are therefore not generally those used by the original authors.

in his first report, except that the gravity term was added to the velocity equation prior to the re-evaluation of the results. That is

$$m \frac{dv}{dt} = -\frac{1}{2} \rho v^2 C_D S + W \sin \theta.$$

As emergency ejections at high altitudes became frequent during World War II, parachutists reported unusually high opening shocks at high altitudes. Because the resulting forces and accelerations approached and even exceeded the limits of human tolerance, the Army Air Force conducted a test program to investigate the phenomenon. The results were published by Hallenbeck in Reference[10] which showed that, for altitudes up to 40,000 ft, opening force did indeed increase with increasing altitude when the true airspeed at dummy drop was held constant (parachute deployment was almost immediately after dummy drop). Hallenbeck also showed that the time from "initial shock" (line stretch) to peak force decreased with increasing altitude.

The problem came to the attention of von Karman[11] who, in 1945, published a paper dealing with the observed altitude effect. He concluded that the observations would be explained if the apparent mass of the parachute were considered in analysis. Without actually analyzing the opening process, he described how the density variation with altitude would cause a similar variation in the apparent mass. He qualitatively described the mechanism of the effect of apparent mass variation on opening force.

In 1946 a report written by Scheubel[12] was published. In it, Scheubel presented a very comprehensive treatment of the parachute opening process. A description of some of the contents of this report will bear witness to both the insight of the author and the advance in technical understanding represented by this report. Scheubel credited Mueller with being the first to recognize that the opening of a parachute is really an inflation process. Scheubel reported that Mueller, in 1927, equated the parachute volume change rate to the product of the mouth area and parachute airspeed. Scheubel pointed out that while he believed Mueller's approach to be correct, he disagreed with Mueller's formulation. The reason for disagreement was that Mueller would have had to conclude that at full open, when the parachute volume change rate is zero (and mouth area has a nonzero value) parachute velocity would be zero. To correct this problem, Scheubel introduced a velocity ratio for the inflowing air such that

$$\frac{dV}{dt} = \frac{vi}{v} \; A_i \frac{ds}{dt} \; .$$

Based on transformation of this equation, Scheubel observed that the distance "necessary for the complete inflation of a given canopy, is a constant and is proportional to the linear dimensions of the parachute." He then noted that the ratio $\frac{vi}{v}$ should be nearly one at the beginning of inflation and decrease towards zero at the end of inflation. He also commented that the solution of his equation would depend on a knowledge of the basic principles governing the ratio $\frac{vi}{v}$, and that this knowledge was not available in 1946.

To obtain a rough estimate of the opening process, Scheubel suggested as a model of the inflating canopy a right circular cylinder open at one end (Figure 23a) whose radius increases (and height decreases) as it inflates. Scheubel went on to discuss apparent mass which, together with the included mass, constitutes the parachute added mass. He wrote Newton's law of momentum

$$\frac{d \; \Sigma \; mv}{dt} = F$$

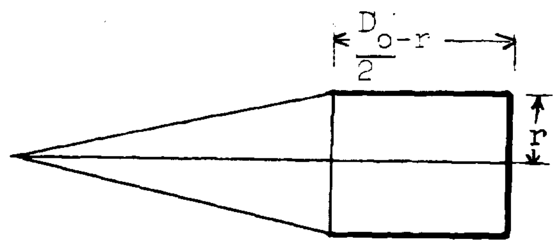

(a) Scheubel's Model

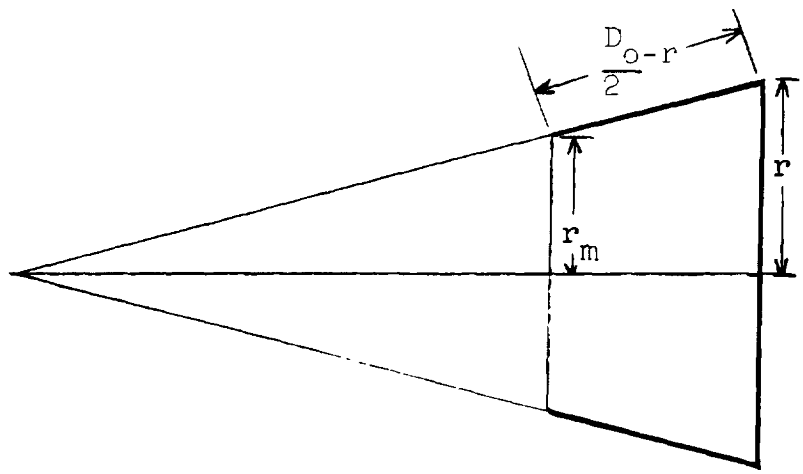

(b) O'Hara's Model

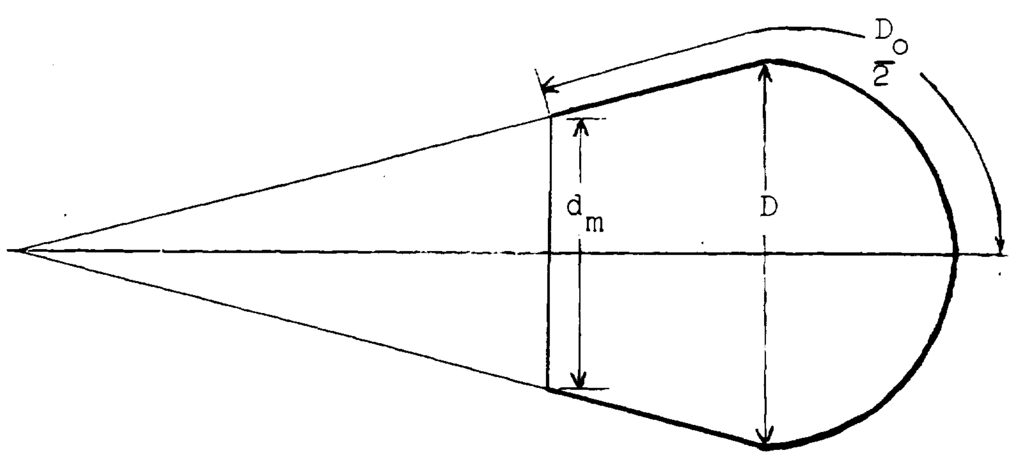

(c) Heinrich's Model

Fig. 23. Various Canopy Models Used in Parachute Analyses

and noted that the mass term should include both the system mass and the added mass. He specified that the force F should be the drag force. (In dealing with man-carrying parachutes in near horizontal trajectories, as Scheubel was, it is permissable to neglect the gravity term.) He pointed out that his calculations indicated opening shock force should increase as the square of velocity. He then commented that the effect of altitude on force and inflation time was related to the added mass, and mentioned the dependence of shock factor (opening load factor) on the weight of the payload.

While the foregoing material does not fully describe the important technical content of Reference 12 it is believed that it is sufficient to both display the knowledge of its author and to emphasize the importance of the work in the evolution of parachute opening load technology. Also, it is probably correct to say that the material presented in Reference 12 represents the composite German technology of opening load analysis and therefore includes contributions of others, in addition to the contributions of Scheubel himself. And credit is certainly due to Scheubel for the lucidity and comprehensiveness of the presentation.

O'Hara[13] presented a paper in 1949 which described a very comprehensive, aggressive analysis of the parachute opening process. His model is shown in Figure 23b The approach he chose was to select a simple enough shape for a model of the inflating parachute that many canopy characteristics (volume, areas, etc.,) could be mathematically described by simple geometrical considerations, and then use an extension of Scheubel's flow equation to account for the rate of change of volume. That is, for incompressible flow, the rate of change of the canopy geometric volume equals the rate of net increase of air enclosed within the canopy. The rate of increase in air volume was represented by O'Hara as

$$\frac{dV}{dt} = v_i \pi r_m^2 - v_o \pi r^2$$

where v_i and v_o were defined by O'Hara as the mean inflow and outflow velocities through the canopy mouth and crown, respectively. It can be seen that the extension of Scheubel's flow equation is the addition of the outflow term, due to porosity. It should be noted that both r and r_m are functions of canopy geometry, and are related by the similar triangles they define.

Having established his basic model for the parachute, O'Hara wrote the equation of motion for the system

$$\frac{d}{dt}\left\{\left(m + K\rho r^3\right)v\right\} = -\tfrac{1}{2}\rho v^2 C_D \pi r^2 .$$

(O'Hara noted the neglect of gravity and of system elasticity.) Values for K, C_D and the mean inflow and outflow velocities were still required. By making some reasonable, though unproven, estimates of inflow and outflow velocities, O'Hara was able to solve the flow equation for $\frac{dr}{dt}$ and insert the solution into the equation of motion.

He also estimated K and C_D to complete the solution. He thus had an equation which could be evaluated by numerical techniques and through which values of the parachute force and opening time could be calculated. In his paper he presented the results of some calculations showing the effect of altitude on opening force and time and commented on such effects as porosity, variation of C_D with porosity, effect of the number of suspension lines and the constraining effect of the suspension lines on opening rate.

Like Scheubel's paper, O'Hara's paper represented a significant advance in published parachute technology; and together they define an understanding of the basic principles of the parachute opening process almost as complete as that understanding at our disposal today.

3.1.2 Further Development of O'Hara's Model

The analyses published subsequent to the publishing of O'Hara's paper in 1949 generally advanced the understanding of parachute opening, either by suggesting improvements in O'Hara's analysis, or by developing a new model. Several papers in the former category will be commented on here, followed by a discussion of the latter category. It is noted that all of the analyses from the former category that are mentioned here were either authored by Dr. H. G. Heinrich of the University of Minnesota or by other individuals from that institution.

The first of these analyses was presented by Heinrich[14] in 1961. This analysis appeared in a report on the status of research on parachute operation. Heinrich used the model shown in Figure 23c. He credits this model to O'Hara, although O'Hara used the flat-ended model shown in Figure 23b. Heinrich used O'Hara's equation for the rate of increase in air volume during opening. He also used the relation

$$\frac{v1}{v} = 1 - T, \quad (T \equiv t/t_f)$$

which, as Scheubel suggested, goes from a value of one to zero as the parachute opens. Heinrich then suggested that projected diameter should increase parabolically with respect to time as

$$D = \frac{2D_o}{\pi} \; T^{\frac{1}{2}}$$

This assumption on projected diameter is the major difference between this analysis and O'Hara's. With this, and other simplifying assumptions, the inflation time was solved through numerical integration. Then the maximum opening force was expressed in terms of the fill time. Heinrich presented some comparisons between calculated values of fill time and opening force and corresponding experimental data for a 28-foot flat circular parachute. The comparisons show very good agreement in fill time and reasonable accuracy in opening force.

This analysis was republished in 1961 under the co-authorship of Heinrich and Bhateley.[15] It was subsequently republished in a somewhat more complete form in Reference 16 in 1963.

Bhateley[17] presented a thesis on the fill time and opening force of reefed canopies. The treatment is fairly similar to that of Reference 14, except that outflow through the canopy vent is included in the mass flow equation. As in Reference 14, the simplifying assumption was made here that the suspension line length is equal to the canopy nominal diameter D_O. This assumption reduces the generality of the solution, for, as we know, many parachutes do not fit this assumption. As an example, the Apollo Block II (H) drogue has a suspension line length of 2 D_O. In this particular case, the error might not be significant; but the point is made here because References 14-17 all contain many simplifying assumptions which reduce the generality of these analyses. Of course, the value of these assumptions is that they permit fairly simple solutions in cases where they are valid.

Buchanan[18] presented a report in 1965 in which the approach was very similar to that of Reference 14 This analysis extended the mass balance equation. In Reference 14, Heinrich expressed the mass balance as

$$\frac{\pi}{4} d^2 v_1 \rho - \frac{\pi}{2} D^2 v_O \rho = \frac{d}{dt} (\rho V),$$

which is essentially the same as O'Hara's formulation. Buchanan used the relation

$$\frac{\pi}{4} d^2 \; v_1 \; \rho - \lambda_g \left(\frac{\pi D^2}{2} - \frac{d_V{}^2}{4}\right) v_O \rho - \frac{\pi d_V{}^2}{4} \; v_V \rho = \frac{d}{dt} (\rho V) \qquad (5)$$

which separates outflow through the vent from that due to geometric porosity λ_g. Buchanan then presented the results of wind tunnel testing in the form of v_V and v_1 as functions of T.

These data were obtained through the use of pressure surveys at the vent and mouth. These data were then curve-fit, and the resulting function was substituted into the mass balance equation. It is interesting to note that where previous investigators had often used the assumption that

$$\frac{v_1}{v} = 1 - T,$$

Buchanan found the relation

$$\frac{v_1}{v} = 0.91 - 0.31\,T$$

to be more exact for the particular wind tunnel model he used. He also found that a good approximation for the ratio v_v/v was 1. However, because of its dependence on the unknown pressure distribution, Buchanan was unable to present values for v_g/v and calculate fill times for different flight velocities.

Heinrich and Noreen[19], in 1968, presented an excellent paper dealing with the separate terms in the filling equations. Having selected the model from Reference 14, and writing the equation for the parachute force as a function of time (for finite mass operation),

$$F = \tfrac{1}{2}\,\rho C_D S\, v^2 - v\,\frac{dm_a}{dt} - (m_p + m_a)\,\frac{dv}{dt}\,, \qquad (6)$$

the authors set about determining values for the various terms through wind tunnel tests. Velocity and acceleration were measured directly during the tests and time histories of canopy area and volume were estimated from film pictures of the inflating canopy. Added mass m_a was estimated from the canopy volume and the results presented in Reference 20. The values of these parameters were then substituted into the force equation, and time histories of force were calculated. The results compared quite favorably with the measured values, indicating both the soundness of the approach and the accurate work of the investigators.

Heinrich[21], in 1968, presented a paper on parachute opening time for infinite mass conditions using an extention of O'Hara's model. The content is essentially the same as that of Reference 18.

3.1.3 Other Models

While O'Hara's model was being developed at Minnesota, several investigators proposed different models of the parachute inflation process.

Weinig[22] derived the equations for the unsteady motion of an expanding, decelerating sphere by using potential flow. In his report, published in 1951, he proposed this expanding sphere as an analog of the inflating parachute. He pointed out that through the use of such an analog, the radial component of the air acceleration in the canopy would be treated, as well as the axial component. Weinig set up the equations of motion of this model and obtained a solution. However, he did not attempt to estimate the various parameters and so could not compare his model with any test data. Foote and Scherberg [23] published an analysis in 1952 in which they used Weinig's drag coefficient for the expanding, decelerating sphere. As described above, Weinig's drag coefficient included added mass terms. Foote and Scherberg used a mass balance equation which included a term for outflow due to canopy porosity and a choking factor to limit inflow through the canopy mouth. They obtained solutions for system motion and parachute force that appeared reasonable. Foote and Giever[24, 25] presented two reports, in 1956 and 1958, in which they attempted to reduce the analysis of Reference 23 to a simple engineering method for predicting opening loads. In the first of these two reports, the authors reported on their sensitivity studies of various parameters. They concluded that the mouth inflow choking factor, which determines the efficiency of the mouth and therefore the fill rate, was of critical importance. They then established a test program (Reference 25) to determine values of the choking factor and attempted to conduct this program. Unfortunately, the test program was plagued by failures and errors, and the desired information was not obtained. While the effort was generally unsuccessful, it contained some good analysis and especially established the strong dependence of the opening process on mouth inflow in models of this sort.

Scheubel[12] was apparently the first to point out that a parachute should inflate in a constant distance in 1946. French [4] derived the same result for incompressible flow in a paper presented in 1963. He also demonstrated that test data supported this conclusion. French [26] presented another paper in 1968, in which he separated the inflation process into two phases, as Berndt had proposed in Reference 27 (1964). French showed that the first of these two phases should take place in a constant distance, and that this fact provided a scaling law for (first phase) fill time. He used Berndt's data to show the hypothesis to be valid. Although French did not apply the concept of a constant filling distance to the calculation of loads, Schilling [28] had made such an application in 1957. He chose the distance traveled as the independent variable, noting that opening would occur in the constant filling distance. He then assumed that the projected radius would be directly proportional to the distance the canopy had traveled since the beginning of inflation. These assumptions allowed Schilling to solve the equation of motion for the system and calculate opening force. He compared some calculations with experimental data and found fair agreement.

Rust [29] presented an excellent analysis of the dynamics of the opening parachute in 1965. His analysis is more complete and general than most other models, and yet he showed how opening loads may be calculated through the use of the model. Rust represented the opening of a parachute with reefing as a succession of five stages. With projected radius as the independent variable, two equations of motion were derived (for flight path angle and velocity). The canopy was not modeled with a specific geometric shape, but related terms such as the rate of change of volume with projected radius were left in mathematical form. The author then suggested several shapes for the investigator to choose from. Having chosen the shape which most closely matches the actual shape of the inflating canopy, the investigators could then evaluate the unspecified parameters, such as rate of change of canopy volume with projected radius. Recalling that Foote and Giever established effective mouth inflow area as a critical parameter, the benefit is apparent. The investigator who applies Rust's method can choose the canopy shape that most accurately matches the particular type of parachute he is analyzing, and therefore is not forced to use a geometrical model which opens unlike the actual canopy being studied. Naturally, Rust's analysis necessitates a numerical solution, but this is not a significant disadvantage in the present era of the computer. Rust's model includes consideration of added mass, vehicle drag, canopy porosity and vent size. While these terms were represented mathematically, Rust presented procedures for the evaluation of all terms in his equations through wind tunnel testing. While the comprehensiveness and generality of the method make it more cumbersome than many of the other models, they also make it potentially more accurate. With the estimation of some parameters, the method can be applied to the Apollo parachutes now; but a fair evaluation of the method will probably not be possible until the wind tunnel testing Rust proposed is performed. Rust, in Reference 29, does present a numerical calculation of the inflation of the Mercury Ringsail (with reefing). Although he had to estimate several parameters, the results compare well with test data.

Bloetscher[30] used a model in 1967 like that in Reference 16 to calculate opening loads. He obtained accurate results for peak force, but poor results (compared to test data) for filling time, by letting inflow and outflow velocity equal free stream velocity. Reference 16 specifies mean values of inflow and outflow velocities in the solution.

Asfour[31] in 1967 proposed a model which, like Weinig's,[22] included both axial and radial components of air velocity. However, where Weinig's model was derived from theory, Asfour's model was largely intuitive. Asfour assumed that the canopy contained a volume of air that was stagnated with respect to the canopy, and that the lower surface of this volume moved toward the canopy skirt as the parachute inflated. He reasoned that air entering the canopy would reach this lower surface, turn, and flow from the axis toward the canopy walls. He then reasoned that this radial flow would force the canopy material out until that material became taut and arrested the radial airflow. Asfour then derived a "snap stress" involved in absorbing the kinetic energy of the radially flowing air and showed it to be significant.

Roberts[32] in 1968 presented a paper treating the opening process as "a complex, intimate connection between a stress analysis and pressure distribution via the application of Newton's second law of motion." Roberts derived equations for canopy stress-strain-shape equilibrium as functions of pressure distribution for a vertically descending, opening parachute. He showed how the equations could be solved, in principle, but made no attempt to obtain numerical results with this complicated model.

3.1.3 Added Mass

In addition to the direct analysis of the parachute opening process, there have been results developed in the study of added mass which promise to help complete the understanding of this process in the future. These results will be described briefly. The results of studies on parachute scaling which will help complete the understanding of the process in a similar manner will be discussed in Section 3.2.

As described above, von Karman[11] and Scheubel[12] both identified the parachute added mass as an important parameter in the analysis of parachute opening force. In 1945 von Karman discussed the apparent mass of parachutes in relation to simple bodies, such as spheres and disks, for which its value can be derived. Scheubel suggested the representation of added mass by

$$m_a = K\rho\pi r^3,$$

where K is a shape factor, in 1946. As mentioned above, Weinig[22] proposed a decelerating, expanding sphere as an analog of the inflating parachute. In his report, dated 1951, he derived the drag terms of the shape which included added mass terms.

An experimental technique for determining the added mass was proposed by von Karman[11] and subsequently used by Heinrich.[20] The technique consisted of dropping parachutes with two separate payload weights, attached such that one weight would come to rest on the ground before the other. When the lower weight hit the ground (while the system was in equilibrium descent) the gravity force was reduced and then the unbalanced drag force decelerated the remaining mass. This remaining mass included both the actual system mass and the added air mass. The decelerations and forces were measured, and the added mass was then calculated through the application of Newton's law. The tests were conducted with variations in canopy porosity and type, and Heinrich made the surprising observation that apparent mass decreased very rapidly as effective porosity increased. Rust,[33] published an analysis in 1965 on the determination of apparent mass from infinite mass wind tunnel data. Ibrahim,[34] who has done much recent work on added mass, presented a paper in 1966 on the added mass of an idealized parachute. In this paper, he treated the theoretical flow about imporous spherical cups of varying concavity. The flow was idealized to a potential flow. In a report[35] presented in 1965, the same investigator gave the results of an experimental study of the apparent moment of inertia of parachute canopies. The method Ibrahim used was to study the oscillations of canopy-shaped, metal models in both air and water. The change in frequency of the particular mode of oscillation being studied, in going from air to water, determined the apparent moment of inertia for that mode. Among his results was an indication that apparent moment of inertia decreases rapidly as canopy porosity increases. This trend is in agreement with Heinrich's observations in Reference 20. Ibrahim suggested the usage of the term "added mass" to describe the included air and apparent air masses (of the canopy) together. By this definition, added mass comprises both fluid that is inside and outside the canopy

3.1.4 Summary

This general literature review has traced the evolution of parachute opening load prediction methods during the past quarter century. It has shown that the present concept of parachute inflation was developed in the period 1946 to 1949, although several papers published during the past five years represent some advances in the understanding. However, it is concluded that most investigators have either oversimplified their analytical models, or left more complex models unsolved.

The survey has resulted in several specific benefits to the present study. The importance of added mass in the calculation of opening loads has been reinforced. All of the work studied has contributed to the understanding of the process and its analysis in a general way; and some of the work has contributed in specific ways. Rust's analysis has offered the most specific contribution in that it is now held to be the analytical technique worthiest of development for Apollo parachutes.

3.2 PARACHUTE PARAMETERS STUDY

It can be observed that most of the data plots used to correlate Apollo parachute flight test data are expressed in terms of variables which possess dimensions. For example, force is plotted versus time, opening force shock factor is plotted versus W/C_DS (unit canopy loading) for constant values of dynamic pressure, and filling time is plotted versus mass inflow rate for constant values of unit canopy loading. Thus, most of the variables used in these plots have units; e.g., force is in pounds, time is in seconds, unit canopy loading is in pounds per square foot, etc. The question quite naturally arises: Wouldn't these plots be more meaningful if they were expressed in terms of nondimensional variables? Also, what might these nondimensional variables be? These questions are the subject of this section.

3.2.1 Introductory Discussion

The question of how to make free flight tests with scale models such that data from the models would be directly applicable in predicting the flight characteristics of full scale flight vehicles was studied by Scherberg and Rhode[36] in 1927. They concluded that "the maneuvers of a full scale airplane under the action of gravity alone may be completely simulated by a model ..." They gave both scaling laws for constructing models and scaling laws for predicting full scale flight characteristics from the observed flight characteristics of scale models.

Kaplun[37] analyzed the special case of a parachute opening in a wind tunnel, the so-called infinite mass case. He used dimensional analysis to deduce that there are six basic parameters which should have the same values on reduced scale model tests as on full scale tests in order for the tests to be dynamically similar. He identified these parameters as a canopy Reynolds number, a fabric Reynolds number, a Mach number, a shroud line elasticity parameter, a canopy rigidity parameter, and a canopy inertia parameter. Kaplun indicated that a nondimensional quantity such as the maximum opening force coefficient, $(F_r/q_oS_o)_{max}$ will have the same value provided that the set of these six parameters is the same. Kaplun then pointed out that there are many practical limitations which preclude perfect similitude in reduced scale model tests.

French[38] analyzed the case of a parachute opening in free flight. He indicated that the parachute opening process is governed by two nondimensional parameters: $gD_o \sin \Theta/v_1^2$ and $\rho D_o^3/m$. He stated that a nondimensional quantity such as $(F_r/q_oS_o)_{max}$ will have the same value when the set of these two parameters is the same. French presented data which supported this similarity law but concluded that more and better data would be required to verify the law.

Rust[29] developed a theory for free-falling, opening parachutes by developing a set of three differential equations to define the process. These equations featured nondimensional variables and a set of nondimensional parameters. The nondimensional parameters given by Rust were an added mass ratio, a ratio of parachute drag area to vehicle drag area, a quantity $r_g g/v_1^2$, and a quantity $r_g g/v_o^2$. These nondimensional parameters, together with a volume rate of change with respect to distance quantity, were specified as correlation parameters for the equations governing the process. Also, Rust showed that an additional correlation parameter, m_v/m is required for correlating opening force data with a maximum opening force coefficient $(F_r/q_1S_o)_{max}$.

Barton[39] analyzed the free-falling opening parachute and showed how the model scale and the air density ratio can be used to predict full scale test results from properly scaled model tests. Barton's results extended those of Scherberg and Rhode by making air density an additional test variable.

It is interesting that the ideas developed in the investigations described above were apparently arrived at independently. Also, it is interesting to note that two apparently different approaches are in evidence. On the one hand, Scherberg and Rhode[36] and Barton[39] devised scaling laws to specify both how models should be built and tested, and how the results from the model tests should be used to make predictions on the characteristics of the full scale flight vehicles. On the other hand, Kaplun[37], French[38] and Rust[29] identified dimensionless parameters which must have the same values on model tests as on full scale tests; this being the case, the test results, when expressed in terms of appropriate nondimensional variables, should be directly applicable to the full scale flight vehicle. It therefore seems reasonable to ask: Are the different approaches equivalent? Another interesting observation is the complete disparity between the correlation parameters identified by Kaplun, French and Rust. A total of twelve were identified; and no two were the same! Therefore, another interesting question might be: Is there a correct set of correlation parameters?

In order to resolve the questions just posed, a simple mathematical model for an opening parachute is formulated. This model is represented by three ordinary differential equations-- one equation for each of three dependent variables -- and a statement of the initial conditions associated with these questions. The first two equations are force balance equations along and normal to the flight path; and, the third equation is a canopy volume rate of change equation. The three dependent variables are the total flight velocity v, the flight path angle θ, and the parachute radius r. Next, the governing equations and the initial conditions are transformed by replacing the variables v, Θ, r and t by a set of nondimensional variables U, Θ, R and T. The functional form of the solution then obtained is used as a basis for showing how more meaningful data plots can be made. Also, answers are developed for the other questions raised in the foregoing paragraphs.

3.2.2 Analysis

Figure 24 presents a schematic of a vehicle-parachute system at a point on the flight path where the parachute is in the process of opening. A simple mathematical model for the opening process is developed in Appendix A. This model is based on the assumption that the state of the process can be defined at any instant of time by a state vector $\underline{x} = \underline{x}(t)$ where t denotes time. This state vector, for the mathematical model analyzed, is

$$\underline{x} = (v, \Theta, r)^T \qquad (7)$$

It is shown in Appendix A that corresponding to the three components of $\underline{x}$ are three governing equations for the opening process which can be represented as

$$\dot{\underline{x}} = \underline{f}(\underline{x}, \underline{c}, g, m, \rho) \qquad (8)$$

where the dot denotes differentiation with respect to t. The quantity $\underline{c}$ is a vehicle-parachute characteristics vector. This vector $\underline{c}$ is actually a function of r but is treated as a function of $\underline{x}$. Specifying a particular vehicle-parachute system is equivalent to specifying $\underline{c} = \underline{c}(\underline{x})$. Vehicle parachute systems that are different in any respect (type, diameter, number of gores, suspension line length, etc.,) will, in general, have different vehicle-parachute characteristics vectors. The quantities g, m, ρ are taken to be constants during the opening process. The initial conditions associated with Equation (8) are

$$\underline{x}(0) = \underline{x}_i \qquad (9)$$

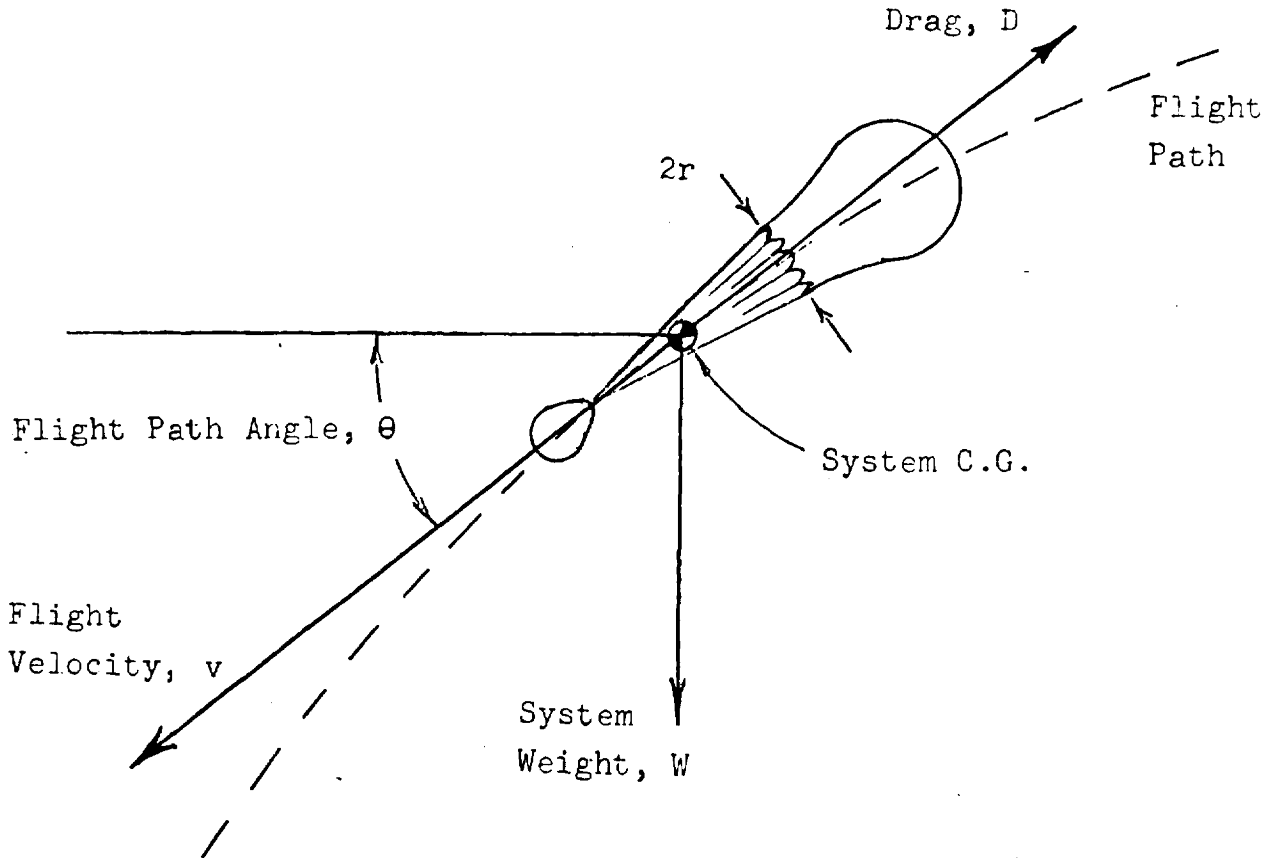

OTHER NOTATION

g	Gravitational constant
m	System Mass ($= m_v + m_p$)
r_o	Parachute nominal radius ($= \sqrt{S_o/\pi}$)
r_v	Vehicle radius
V	Canopy air volume
ρ	Air density

Fig. 24. Schematic of Vehicle-Parachute System

where $\underline{x}_i = (v_i, \theta_i, r_i)^T$ denotes the flight velocity, the flight path angle, and the radius of the parachute at t = 0 when the opening process is assumed to start.

It is known by the Cauchy-Lipschitz theorem[40] that Equation (8), together with the initial conditions given in Equation (9), has a unique solution of the form

$$\underline{x} = \underline{x}(t)$$

In general, $\underline{x}(t)$ is different for every different combination of c, g, m, ρ and $\underline{x}(0)$.

Once $\underline{x}(t)$ is known, it is a simple matter to compute the other quantities associated with the opening process. For example, the force in the parachute riser, F_r is given by

$$F_r = m_v(g \sin \theta - \dot{v}) - D_v$$

The opening time, t_o is given simply as the time at which r(t) first becomes equal to the parachute full-open radius, r_{fo}.

The foregoing results can be made more general by introducing the nondimensional state vector

$$\underline{X} = (U, \theta, R)^T$$

where $U = v/v_o$ and $R = r/r_o$. The quantities v_o and r_o are defined as the full-open, equilibrium velocity associated with g, m and ρ, and one-half the parachute nominal diameter, D_o, respectively. In addition, the independent variable t is replaced by the nondimensional variable T defined as

$$T = v_o t/r_o$$

It is shown in Appendix A that substituting these nondimensional variables into Equation (8) results in a new set of three governing equations which can be represented as

$$\underline{\dot{X}} = \underline{F}(\underline{X}, \underline{C}, FN, \nu) \qquad (10)$$

where the dot now denotes differentiation with respect to T, and where

$$FN = v_o/\sqrt{r_o g}$$

$$\nu = (C_a \rho r^3/m)_o$$

The quantities FN and ν (nu) are referred to as Froude number and added mass ratio respectively. They represent natural groupings of dimensional quantities; however, both quantities are themselves dimensionless. The vector $\underline{C}$ is actually a function of R but is treated as a function of $\underline{X}$. Specifying a class of vehicle-parachute systems is equivalent to specifying $\underline{C} = \underline{C}(\underline{X})$. Vehicle-parachute systems that are different with respect to type, number of gores, suspension line length-to-diameter ratio, etc., (but not size per se) will, in general, have different $\underline{C}$ vectors. The quantities FN and ν are constant by definition during the opening process.

The transformed initial conditions are

$$\underline{X}(0) = \underline{X}_i$$

where $\underline{X}_i = (U_i, \theta_i, R_i)^T$ denotes conditions at $T = 0$ when the opening process is assumed to start. When in addition to $\underline{C}$ and $\underline{X}_i$, the parameters FN and ν are also specified, then it is known by the Cauchy-Lipschitz theorem[40] that Equation (10) has a unique solution of the form

$$\underline{X} = \underline{X}(T)$$

In general, $\underline{X}(T)$ is different for every different set of $\underline{C}$, $\underline{X}_i$, FN, ν.

Having once obtained $\underline{X}(T)$, other quantities having significance may be computed. For example, a force coefficient for the parachute riser, defined as

$$C_F = \frac{F_r}{q_o S_o}$$

is readily computed from the equation

$$C_F = (2C_a m_v/\pi \nu m)_o(\sin \theta /FN^2 - \dot{U}) - C_{D_v}\frac{r_v^2}{r_o^2} \qquad (11)$$

Likewise, the nondimensional opening time, T_o is given as the value of T at which $R(T)$ first becomes equal to $R_{fo} = r_{fo}/r_o$.

It is notationally convenient to define an individual parachute opening process as the solution

$$\underline{x} = \underline{x}(t;\ \underline{x}_i,\ \underline{c},\ g,\ m,\ \rho) \qquad (12)$$

This denotes that $\underline{x}$ varies with t, but is dependent in this variation on $\underline{x}_i$, $\underline{c}$, g, m, ρ. It has been shown that the governing equation for an individual process can be transformed into a more general form. It is now apparent that each solution of this transformed equation represents a group of individual processes. Let a process group be denoted as solution

$$\underline{X} = \underline{X}(T;\ \underline{X}_i,\ \underline{C},\ FN,\ \nu) \qquad (13)$$

In other words, each group solution (<u>set</u>) having the form of Equation (13) has corresponding to it many individual solutions (<u>elements</u>) having the form of Equation (12).

Are the variables associated with the elements of any one set related in specific ways? To answer this question, consider a specific set as defined in Equation (13). Fixing the Froude number and the added mass ratio, say as FN_o and ν_o, is equivalent to specifying two equations in four unknowns (g is assumed fixed); viz., the equations

$$FN_o = v_o / \sqrt{r_o g}$$
$$\nu_o = C_a \rho_o r_o^3 / m_o$$

provide two relations between the four variables: v_o, r_o, m_o, ρ_o. It is shown in Appendix A that there are four ways in which an element of the set may be specified. The most interesting of these is the one which specifies r_o, ρ_o and solves for v_o, m_o with the relations

$$v_o = FN_o \sqrt{r_o g}$$
$$m_o = C_a \rho_o r_o^3 / \nu_o$$

Now let the variables of another element of the same set be distinguished by the subscript 1. Being an element of the same set is equivalent to saying

$$\underline{X}_{1i} = \underline{X}_{oi}$$
$$\underline{C}_1 = \underline{C}_o$$
$$FN_1 = FN_o$$
$$\nu_1 = \nu_o$$

The latter two equations expand as

$$v_1 / \sqrt{r_1 g} = v_o / \sqrt{r_o g}$$

$$c_a \rho_1 r_1^3 / m_1 = c_a \rho_o r_o^3 / m_o$$

and it then follows that

$$v_1 / v_o = (r_1 / r_o)^{\frac{1}{2}} \tag{14}$$

$$m_1 / m_o = (\rho_1 / \rho_o)(r_1 / r_o)^3 \tag{15}$$

Also useful is the knowledge that similar events of the two elements must occur in time according to the relation

$$T_1 = T_o$$

That is,

$$v_1 t_1 / r_1 = v_o t_o / r_o$$

This relation, when combined with Equation (13) gives the result

$$t_1 / t_o = (r_1 / r_o)^{\frac{1}{2}} \tag{16}$$

Equation (10) provides a means for relating the forces in the two elements; in particular, it is readily shown that

$$F_1 / F_o = (\rho_1 / \rho_o)(r_1 / r_o)^3 \tag{17}$$

Equations (14) - (17) give the scaling laws for the velocities, masses, times and forces in terms of the density ratio and the radius ratio. Scaling laws for other variables such as angular velocity, pressure, moment of inertia, etc., are readily determined by combining the above derived relations.

3.2.3 Discussion of Correlation Concepts

In the Section 3.2.1 it was noted that two quite different approaches have been proposed by previous investigators to aid in the correlation of free-flight data, and it was asked: Are the different approaches equivalent? Also, it was noted that some twelve different dimensionless parameters have previously been proposed, and it was asked: What are the correct dimensionless parameters? Attention will now be given to these questions.

The approach used by Scherberg and Rhode[36] and Barton[39] was to define scaling laws for constructing models, for conducting tests with models, and for predicting full scale vehicle characteristics from the observed flight characteristics of models. The scaling laws proposed by these investigators for the four basic dimensions of length, time, force and mass are compared in Table 23.

It may be noted that the scaling laws proposed by Scherberg and Rhode are the same as those of Barton for the special case of constant density. Also, it may be noted that Barton's

Table 23. The Basic Scaling Laws Proposed by Several Investigators

Quantity	Scherberg and Rhode[36]	Barton[39]
Length	$r_1/r_o = r_1/r_o$	$r_1/r_o = r_1/r_o$
Time	$t_1/t_o = (r_1/r_o)^{\frac{1}{2}}$	$t_1/t_o = (r_1/r_o)^{\frac{1}{2}}$
Force	$F_1/F_o = (r_1/r_o)^3$	$F_1/F_o = (\rho_1/\rho_o)(r_1/r_o)^3$
Mass	$m_1/m_o = (r_1/r_o)^3$	$m_1/m_o = (\rho_1/\rho_o)(r_1/r_o)^3$

scaling laws are identical with those derived in the previous section. Thus, it is now seen that Barton's scaling laws of dynamic similitude are precisely those relations which correctly relate the variables associated with individual parachute opening processes which have the same nondimensional initial conditions $\underline{X}_i$, the same nondimensional vehicle-parachute characteristics vector $\underline{C}$, the same Froude number FN, and the same added mass ratio ν.

The second approach was that used by Kaplun[37], French[38] and Rust[29]. They identified dimensionless parameters which they required to be the same on model tests as on full scale tests. The model data, when expressed in nondimensional form, were then said to be directly applicable to the full scale flight vehicle. The dimensionless parameters proposed by these investigators are compared in Table 24 . This table uses the notation used in this discussion with several additions. The quantities d_o and r_g are, respectively: the thread diameter (or ribbon width), and the parachute radius measured along the gore. The quantities a_o, k and EI are the speed of sound (in air), the spring constant for the suspension lines, and a characteristic canopy rigidity respectively. It is interesting to note that every one of the twelve parameters presented in Table 24 are different.

Several observations may be made regarding the dimensionless parameters listed under Kaplun in Table 24 . Kaplun's list does not include Froude number, one of the most important parameters which govern the operation of parachutes. The first two parameters listed are Reynolds number and the third is Mach number; these are important only in so far as they affect the vehicle-parachute aerodynamic characteristics. For large subsonic parachutes such as those in the Apollo system, Reynolds number and Mach number are believed to be of secondary importance to Froude number and added mass ratio. The fourth and fifth

Table 24. Correlation Parameters Proposed by Several Investigators

Kaplun[37]	French[38]	Rust[29]
$\frac{\rho_o D_o v_o}{\mu_o}$	$\frac{g D_o \sin\theta}{v_i^2}$	$\frac{\pi C_a' \rho_o r_g^3}{3m}$
$\frac{\rho_o d_o v_o}{\mu_o}$	$\frac{\rho_o D_o^3}{m_o}$	$\frac{C_{D_p} S_o}{C_{D_v} S_v}$
$\frac{v_o}{a_o}$		$\frac{r_g g}{v_i^2}$
$\frac{k}{\rho_o v_o^2 D_o}$		$\frac{r_g g}{v_o^2}$
$\frac{EI}{\rho_o u_o^2 D_o^4}$		
$\frac{m_o}{\rho_o D_o^3}$		

parameters in Kaplun's list govern flexing and stretching type displacements of the parachute structure. Whereas the flexing parameter has little importance in relation to the Apollo parachutes, the stretching parameter is known to be important. It may be shown, using the scaling laws derived earlier, that the strain ratio scales as follows (assuming the same materials are used to construct both parachutes):

$$\epsilon_1/\epsilon_o = (\rho_1/\rho_o)\ (r_1/r_o)$$

This shows that variations in the test altitude and/or size of the parachute will, in general, lead to mismatching of this stretching parameter. The last parameter in Kaplun's list may be recognized as $C_a/8\nu$.

The two parameters listed under French in Table 24 suggest several comments. First, the two parameters are recognized to be $(\sin\theta/FN^2)/U_i^2$ and $8\,\nu/C_a$. For <u>any one</u> stage of parachute opening, the flight path angle, θ typically varies by only a small amount and may therefore be considered a constant. Thus, as regards a single stage of opening, two equations in the two variables v and r are sufficient to define the process. In this case, it may be shown that individual parachute opening processes belonging to the same set must have the same initial conditions U_i, R_i; the same characteristics vector $\underline{C}$; the same added mass ratio ν (or $\rho_o D_o^3/m_o$); and the same value of the parameter $FN/\sqrt{\sin\theta}$ (or $\sin\theta/FN^2$). Thus, it is apparent that French had the right idea but did not go quite far enough in specifying similarity requirements. It is also interesting that whereas French suggested only the two parameters given in the table to correlate the parachute opening force coefficient C_{F_r}, Equation (11) clearly shows that this coefficient is also a function of (m_v/m).

The following observations may be made regarding the four parameters listed under Rust in Table 24. The first and last parameters are equivalent to ν_o and FN_o, respectively. The second parameter is a vehicle-parachute characteristic, and the third parameter is equivalent to $1/FN^2U_i^2$.

It is now apparent that the analysis results given by Kaplun, French and Rust are quite different. However, it may be observed that the analysis presented by Rust is compatible with the relations given by Barton.

The most difficult question of all is: What are the correct correlation parameters? This is difficult to answer because it depends on the process and what one is interested in correlating. Therefore, let the scope of the question be restricted to the Apollo parachute and flight conditions, and let it be the state vector $\underline{X} = (U, \Theta, R)$ that one is interested in correlating. Under these restrictions, the results of the present investigation are believed to be directly applicable. These results are shown in Table 25 for two cases: (a) Θ equals a constant, and (b) Θ equals a variable. It is acknowledged that correlations based on Table 25 may not be adequate in all cases. In particular, it is suspected that both compressibility and riser stretching may sometimes be important enough to cause anomolous second order effects.

Table 25. Correlation Parameters Proposed in the Present Investigation

(a) Θ = Constant	(b) Θ = Variable
U_1	U_1
R_1	Θ_1
$\underline{C}$	R_1
$FN_o / \sqrt{\sin \Theta}$	$\underline{C}$
ν_o	FN_o
	ν_o

SECTION 4.0
NEW LOAD PREDICTION METHODS

The most important impact of the general literature survey (Section 3.1) on parachute opening loads was probably the reinforcement of the importance of including the consideration of parachute added mass in the opening load calculations. Of the prior Apollo load prediction methods, the only one that accounted for the added mass was the opening load factor method, and the consideration was indirect there. It was decided that it would therefore be appropriate to undertake the development of a simple engineering method that included added mass, for the prediction of opening loads and trajectories, and to develop it for the particular case of the Apollo main parachute. This method came to be called the Mass/Time Method and is the subject of Section 4.2.

Another result of the general literature survey was the conviction that Rust's theory,[29] of all known work, represented the most promising approach for developing a good, general model of the parachute opening process. The assets of the method are 1) generality, 2) completeness, 3) freedom from restricting assumptions, 4) simplicity, 5) applicability to an Apollo type recovery system and 6) that it requires only the appropriate wind tunnel data to be applied to a new parachute system. Because of its promise, and because it was derived from basic principles, it was decided that it would be appropriate to develop the theory as an effort parallel to the Mass/Time Method. It was recognized however, that the complete development of Rust's theory would not be possible during the present study, and so the pursuit of this theory alone was not feasible. The method developed from Rust's theory is called the Shape/Distance Method, and its state of development is discussed in Section 4.3.

Because some important questions remained at the end of the development of the Mass/Time and Shape/Distance Methods, a short study was conducted to help answer these questions. This study is reported in Section 4.4. Its objectives were 1) the assessment of the applicability of the Mass/Time Method to clustered parachutes, 2) the verification of the basic assumptions of the Shape/Distance Method and 3) the inclusion of the forms of the trajectory equations containing the added mass terms (Section 6.3).

In addition to the work on the opening load prediction methods, a new method was developed for predicting the deployment times for Apollo parachutes, and the fill times of Apollo drogue chutes. This new method is described in Section 4.1.

4.1 IMPROVED TECHNIQUE FOR DETERMINATION OF PARACHUTE DEPLOYMENT AND FILL TIMES

Because of vehicle acceleration during parachute deployment, the dynamic pressure at canopy stretch depends upon the deployment time. In this way, accurate opening load prediction depends upon accurate deployment time prediction. A discussion of techniques for the determination of parachute deployment times is presented below. The inadequacies of the present method are identified and a new technique, using extant computer programs, is proposed.

During the Apollo Block II (H) program, the predicted deployment times (from mortar fire or disconnect to line stretch) were obtained from averages of empirical data from the Block I and Block II programs and the fill times (from line stretch to the peak load point) were considered constant (except for the main parachutes).

This method is inaccurate for the following reasons:

a) The technique ignores the effects of the type of deployment system used, the type of vehicle, the altitude, the flight path angle, the changes in mortar muzzle velocities with temperature (if mortar deployed), the changes in mortar muzzle velocities with altitude (if mortar deployed), the changes in the deployment parachute (if static line deployed), and the test-to-test differences in the parachute configuration.

b) Using a constant filling time is not accurate, for the times will change with the test condition.

A better technique, which accounts for all the important parameters ignored by the old method, is available using extant computer programs (GT03, WG305 and SNAT).

Computer program WG305 is similar to SNAT except that it allows for flight path angle variations.

The new technique is as follows:

a) The flight conditions at parachute initiation (mortar fire or disconnect) are determined by GT03.

b) The time to canopy stretch is determined by SNAT (if static line deployment) or by WG305 (if mortar deployment).

c) The fill times are taken from empirical data curves.

d) Finally, these deployment and fill times are used as imputs to the final trajectory computer run using GT03.

For example, Tests 83-6, 99-4 and 85-5 had mortar-deployed drogue chutes. Computer program WG305 was used to determine the deployment times from mortar fire to canopy stretch. Then, the times from canopy stretch to the peak load point were obtained from Figure 25. A comparison of the predicted and actual times appears in Table 26.

Test 84-4 had mortar-deployed pilot chutes which static line-deployed the main parachutes. Computer programs WG305 and SNAT were used to predict the pilot chute and main parachute deployment times, respectively. A comparison of the predicted and actual times appears in Table 26.

Figure 25 is a plot of the time from canopy stretch to the peak load point versus the vehicle velocity at drogue chute canopy stretch. The parameters are the type of deployment system used and the reefing ratio. Two things can immediately be seen: 1) the greater the reefing ratio, the longer the fill times; and 2) mortar-deployed drogue chutes had shorter fill times than static line-deployed drogue chutes. This latter observation is attributed to the mortar-deployed drogues starting to fill in the free stream; whereas, static line-deployed drogue chutes fill in the vehicle wake.

Two tests in the Block II (H) program had static line-deployed drogue chutes which were reefed to 40% D_O. One of them exhibited load link dynamics. This phenomenon alters the fill time in a random way and makes discerning the fill time very difficult. This left only one good test point.

In order to obtain a curve for static line, 40% D_O drogue chutes, a parachute inflation theory was used. French's paper[4] states "Theoretical considerations of the inflation of a parachute in incompressible flow indicate that a given parachute should open

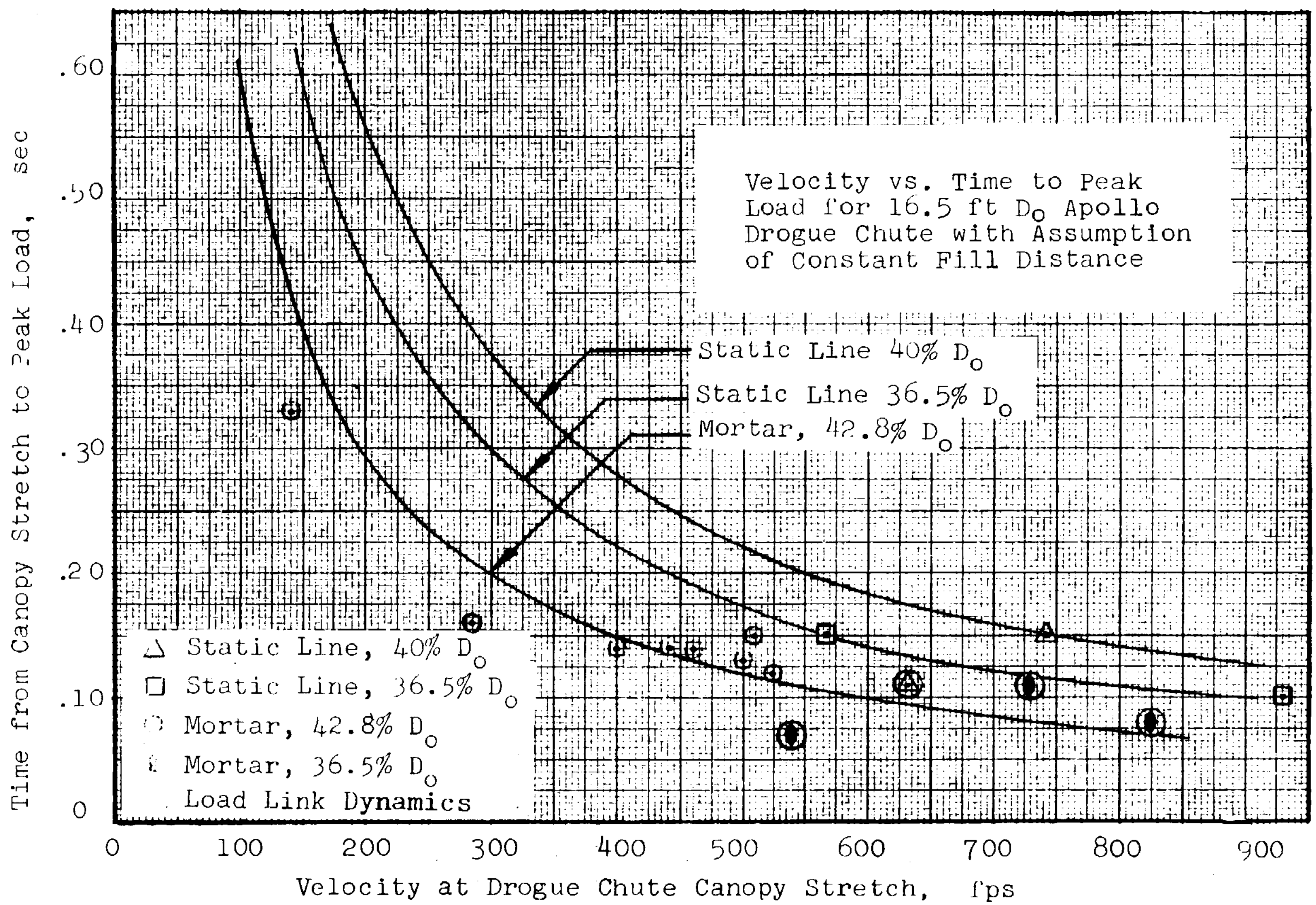

Fig. 25. Time to Peak Load Versus Velocity at Drogue Chute Canopy Stretch

Table 26. Comparison of Prediction Methods

Test No.	Type of Deployment	Reefing Diameter	Velocity at Drogue Chute Canopy Stretch	Drogue Chute Time Intervals								Pilot Chute Time Intervals			
		D_r	v_{DCCS}	$(t_{DCCS} - t_I)$		$(t_M - t_{DCCS})$			$(t_M - t_I)$			$(t_{PCLS} - t_{PMF})$		$(t_{MCLS} - t_{PCFO})$	
				New Method	Actual	Old Method	New Method	Actual	Old Method	New Method	Actual	New Method	Actual	New Method	Actual
		% D_o	ft/sec	sec		sec			sec			sec		sec	
(1)	(2)			(3)		(4)			(5)			(6)		(7)	
83-6*	M	36.5	539.	0.84	0.83	0.10	-	0.07	0.65	-	0.90	-	-	-	-
84-1R*	SL	40.0	631.	0.88	1.21	0.10	-	{0.10 0.13	0.75	-	{1.34 1.47	-	-	-	-
84-3	SL	36.5	931.	0.82	1.02	0.10	0.10	0.10	0.80	0.92	1.12	-	-	-	-
84-4	SL	36.5	567.	0.85	0.86	0.10	0.15	0.15	0.80	1.00	1.01	0.34	0.33	1.37	1.42
85-1	M	42.8	400.	0.93	0.98	0.10	0.15	0.14	0.70	1.08	1.12	-	-	-	-
85-2	M	42.8	284.	-	1.44	0.10	0.21	0.16	0.70	-	1.60	-	-	-	-
85-4	M	42.8	441.	-	0.89	0.10	0.14	0.14	0.70	-	1.03	-	-	-	-
85-5	M	42.8	524	0.84	0.84	0.10	0.12	0.12	0.60	0.96	0.96	-	-	-	-
85-7	M	42.8	508.	-	0.88	0.10	0.12	0.15	0.70	-	1.03	-	-	-	-
86-2	M	42.8	460.	-	-	0.10	0.13	0.14	-	-	-	-	-	-	-
86-3	M	42.8	499.	-	-	0.10	0.12	0.13	-	-	-	-	-	-	-
86-4	M	42.8	140.	-	-	0.10	0.42	0.33	-	-	-	-	-	-	-
99-2	SL	40.0	742.	0.60	0.69	0.10	0.15	0.15	0.70	0.75	0.84	-	-	-	-
99-3*	M	36.5	825.	-	0.81	0.10	-	0.08	0.70	-	0.89	-	-	-	-
99-4*	M	36.5	729.	0.77	0.75	0.10	-	{0.09 0.13	0.55	-	{0.84 0.88	-	-	-	-

NOTES:

(1) An asterisk (*) indicates that the drogue chute riser experienced "load link dynamics"

(2) M and SL denote "Mortar" and "Static Line"

(3) $(t_{DCCS} - t_I)$ denotes the time interval from drogue chute Initiation to Drogue Chute Canopy Stretch

(4) $(t_M - t_{DCCS})$ denotes the time interval from Drogue Chute Canopy Stretch to Maximum/peak opening load (multiple values are for successive peak loads)

(5) $(t_M - t_I)$ denotes the time interval from drogue chute Initiation to Maximum/peak opening load (multiple values are for successive peak loads)

(6) $(t_{PCLS} - t_{PMF})$ denotes the time interval from Pilot Mortar Fire to Pilot Chute Line Stretch

(7) $(t_{MCLS} - t_{PCFO})$ denotes the time interval from Pilot Chute Full Open to Main Chute Line Stretch

in a fixed distance.....". Knowing this, fill distance isolines were superimposed on the data in Figure 25. There were two tests using static line deployed drogue chutes reefed to 36.5% D_o. The data fell on one isoline.

There were eight tests using mortar deployed drogue chutes reefed to 42.8% D_o. These data also followed an isoline. There was some scatter, however, which can be expected because, as mentioned before, a fill time depends upon the parachute's location relative to the vehicle wake. The eight data were from BP tests and a Boilerplate can be in any orientation at drogue mortar fire, placing the drogue chutes in or out of the vehicle wake. In this way, the scatter can be understood.

There were four tests using mortar-deployed drogue chutes reefed to 36.5%. All of them, however, had load link dynamics. It is anticipated that an isoline for this series of tests should fall below that of the Boilerplate data by virtue of its smaller reefing ratio.

As can be seen in Table 26, this new technique is very accurate and should be incorporated into future load prediction methods. Because the same computer programs are used for snatch load calculation, one computer run will produce the deployment time prediction and the Δv's needed for the snatch load calculation.

4.2 MASS/TIME OPENING LOAD METHOD

During this study the simplified analytical approach to parachute opening load prediction, referred to as the Mass/Time Opening Load Method, was developed in a digital computer program to a useful level for the single Apollo ringsail test cases. With the input of initial conditions and empirically derived parachute drag area and growth parameters, the computer solves the equations of motion and generates, along with vehicle trajectory elements, the parachute force applied to the vehicle through the riser connection as a function of time.

4.2.1 Approach

Before describing the development of the Mass/Time Method, it will be useful to discuss some preliminary considerations.

In the computer method for the Stage 1 and 2 opening loads, it had previously been necessary to employ false filling times and growth rates in order to obtain good agreement with measured opening loads. It appears that one of the reasons for this was the use of an "average" reefed drag area which in most cases was much larger than the effective value at reefed opening. It is recognized that the most dependable determination of reefed drag area is made at the end of the reefed interval where near-equilibrium conditions prevail. Therefore the following procedure was implemented in order to improve the model of the first two stages of opening, and the associated deceleration of the system. The time to the peak load was used in place of the reported filling time. The former could be determined accurately from telemetered force traces, while the latter was subject to observational errors. Also, the assumed linear growth rates in conjunction with unit canopy loads of 5 psf and greater caused computed peak loads to be coincident with full opening in each stage. (This was not true of the final opening stage following disreefing where the unit canopy loading was small.) Using the time to peak load in first stage, and a linear drag area growth, the peak drag area which gave a duplication of peak measured force was found. The drag area growth was then changed to a value which gave the drag area that had been observed at the end of the first reefed interval. The procedure was repeated from this point for the second stage of reefing. The resulting drag area history has a rapid linear increase during first stage opening, a slower increase during the first reefed stage, and another rapid increase followed by a slower increase during second stage. The slower increases reflect the continued filling during a reefed stage after the reefing line becomes taunt but before the canopy filling has been completed.

The same approach was not applicable to the calculation of third stage opening loads. In this case, it was necessary to include consideration of the canopy added mass in the equations of motion.

From the work of Heinrich and Noreen[22], the following equations for vehicle motion and cluster parachute force may be derived:

$$\frac{W_v}{g}\dot{v} + W_v \sin\gamma + \tfrac{1}{2} C_D A \rho v^2 + (F_{p1} + F_{p2} + \dots F_{pn}) = 0 \qquad (18)$$

$$F_p = \tfrac{1}{2}\rho C_D S v^2 + v\dot{m}_a + (m_a + m_p)\dot{v} \qquad (19)$$

where n is the number of parachutes in the cluster and m_a is the added air mass defined as the sum of the two quantities identified by Heinrich as the apparent and the included air masses.

The practical problem presented by the added mass terms is how to derive values for the characteristic parameters and time functions from the test data that have accuracies commensurate with the other empirically derived parameters (drag areas, filling times, etc.,) and still maintain the simplicity required of a useful engineering tool. The decision was made to develop a new 2-DOF computer program, rather than attempt to modify the existing program (which embodied many special features not required for solution of the present problem). The equations of motion used in this program were as follows:

$$\dot{x} = v\cos\gamma$$

$$\dot{y} = v\sin\gamma$$

$$\dot{v} = -\frac{F_p + D_V + W_V\sin\gamma}{m_V}$$

$$\dot{\gamma} = -\frac{g\cos\gamma}{v}$$

where the parachute force $F_p = F_{p1} + F_{p2} + \dots + F_{pn}$ as in Equations (18) and (19).

Letting $\psi = C_D S$ and $q = \frac{1}{2} \rho v^2$, Equation (19) takes the form

$$F_p = \psi q + v \frac{\Delta m_a}{\Delta t} + (m_a + m_p) \frac{\Delta v}{\Delta t} \tag{20}$$

Data analysis indicated the feasibility of representing the drag area growth function by the following relationship

$$\psi = \psi_1 + (\psi_2 - \psi_1) \left[\frac{t - t_1}{t_2 - t_1}\right]^n \tag{21}$$

Scheubel[8] and others have shown that the added air mass is a function of the shape and radius of the canopy. He was among the first to use the general relationship

$$m_a = K \rho r^3$$

where K is a shape factor and r is the radius of the inflated canopy. Both can be taken into account without knowing either precisely by determining an empirical expression for the added air mass as a function of the drag area ψ .

Since $\psi = C_D S_p$, $S_p = \pi r^2$, and none of the components of ψ are known as accurately as their product, it is convenient to rewrite Scheubel's relationship in the form

$$m_a = \rho K_a \psi^{3/2} \tag{22}$$

The new shape factor K_a is treated as a constant for the present because the inflated portion of the canopy, together with its boundary layer and wake, does not appear to vary in shape throughout the later stages of filling. This premise derives from the observation that the elongated portion of the canopy upstream of the pressurized crown appears to be functioning mainly as a flow duct with small momentum losses.

Differentiating Equation (22) with K_a constant,

$$\dot{m}_a = \frac{3}{2} \rho K_a \psi^{\frac{1}{2}} \dot{\psi} \qquad (23)$$

and from Equation (8)

$$\dot{\psi} = \frac{n(\psi_2 - \psi_1)}{t_2 - t_1} \left[\frac{t - t_1}{t_2 - t_1}\right]^{n-1} \qquad (24)$$

Trial calculations showed that, using Equation (21) alone, the position of the peak load could be shifted in time by varying the exponent n, when the unit canopy loading is held constant. For the two reefed stages n = 1 gave good results, and it appeared that the added air mass had a small effect and could be neglected.

In order to aid evaluation of the added air mass-time function over the entire filling process, the computer program was made double-ended so that measured force-time data could be used as inputs. With this approach to Equation (20), only m_a and $\Delta m_a/\Delta t$ remain as unknowns. And since

$$m_a(t_2) = \int_0^{t_2} \frac{\Delta m_a(t)}{\Delta t} dt = \int_{t_1}^{t_2} \frac{\Delta m_a(t)}{\Delta t} dt + m_a(t_1)$$

it is possible to perform an iterative solution in the computer for $m_a(t)$.

The nature of the empirical filling time parameter poses another problem when dealing with reefing Stage 2 and the final opening stage. A dimensionless filling parameter is

$$K_f = \frac{v_1 t_f}{D} \qquad (25)$$

where D is a characteristic diameter. The dimensionless parameter, K_f thus defined is applicable only to reefing Stage 1 or to a nonreefed canopy; the other filling stages start from a partially inflated condition which has a strong effect on the stage filling time. Also, it will be noted that the reefing line diameter is not a good characteristic length to use because it has no well-defined relationship to the volume of the inflated portion of the canopy, i.e., the pressurized crown region. The projected diameter D_p could be used, but this is seldom known or derivable with good accuracy (even from wind tunnel data) and traditionally has been one of the intangible parameters that have been avoided in engineering practice. Therefore, a more general definition of the filling time parameter was considered as follows:

$$K_f = \frac{v_1 t_f}{\psi_2^{\frac{1}{2}} - \psi_1^{\frac{1}{2}}} \tag{26}$$

Since v_1 is the initial velocity, i.e., at the start of the filling process, this is unknown for the second reefed and final opening stages until trial calculations have been made for the preceding stage(s). Both initial and final drag areas are known from the averaged test data for all stages based on the given reefing parameters (D_r/D_o and ψ_r/ψ_d). The square root of the drag area provides a characteristic length which has a logical relationship to the volume of the added air mass as justified in the development of Equation (22).

4.2.2 Preliminary Work

Several avenues of approach were taken during the evolution of the Mass/Time Method. These avenues are discussed below.

An attempt was made to develop a new approach for predicting the loads of the opening main parachute on the computer by using measured filling times and adjusting initial drag area and drag area growth rate inputs (added mass was neglected) in a way that would yield peak loads equal to the measured values. It was reasoned that if the results of each test could be duplicated by this means, a basis for calculating mean values of the performance parameters would be established. These mean parameters would define the coefficients for the equations of motion used in the two-degree-of-freedom computer program wherewith the opening loads for any given set of initial conditions could be predicted. Probable variations of actual opening loads about the predicted value could be evaluated by utilizing the initial conditions of the source tests as inputs to predict loads for comparison with the measured values. A determination of the standard deviation for all usable test results could then be made.

The approach described above was found to be feasible for reefing Stages 1 and 2, but the same success was not achieved in the final opening stage. Here, although the peak load could be predicted on the basis of the reported filling time (with an adjusted dynamic drag area and a linear growth rate) the time of occurrence could not be duplicated.

Two factors could be identified in the final opening phase that would cause the actual force peak to occur later in the filling cycle than the computer results indicated; viz.,

1) A nonlinear growth rate accelerating exponentially near the end of the process, and

2) A large inertial component of the force due to the rapidly changing acceleration imposed on the inflowing air mass.

Approximation of an exponential growth rate with a two-step linear program gave improved results with an adjusted dynamic drag area that was relatively large, indicating that a substantial inertial force component, beyond the increment due to aeroelastic expansion, could exist.

Although the effective drag area of the full open canopy was known to be close to 4300 ft^2, it was necessary to employ a value of 9500 ft^2 and a three-step linear growth schedule to obtain reasonably good prediction of the force-time history of the final opening stage as the product of $C_D Sq$ only. This indicated that the added air mass effect was large and must be accounted for.

The effort described above was quite useful in that it both proved the feasibility of using dynamic drag areas (and neglecting direct consideration of added mass) in Stages 1 and 2, and proved the unfeasibility of not considering added mass directly in Stage 3. To meet this requirement, a computer program was developed around the set of equations described in the foregoing discussion and summarized here for convenience. Note that the parachute weight component has been added to Equation (31) in the interest of completeness.

$$\dot{x} = v \cos \gamma \tag{27}$$

$$\dot{y} = v \sin \gamma \tag{28}$$

$$\dot{v} = -\frac{F + D_V + W_V \sin \gamma}{m_v} \tag{29}$$

$$\dot{\gamma} = -\frac{g \cos \gamma}{v} \tag{30}$$

where the parachute force, including the effects of the added air mass, is expressed in this form:

$$F_p = \psi q + v\dot{m}_a + (m_a + m_p)\,\dot{v} + W_p \sin\gamma \tag{31}$$

Both the effective drag area of the canopy ψ and the added air mass m_a are expressed as functions of time in equations having empirically based coefficients and exponents as follows:

$$C_D S(t) = \psi = \psi_1 + (\psi_2 - \psi_1)\left[\frac{t - t_1}{t_2 - t_1}\right]^n \tag{32}$$

$$m_a = \rho K_a \psi^{3/2} \tag{33}$$

$$\dot{m}_a = \frac{3}{2} \rho K_a \psi^{\frac{1}{2}} \dot{\psi} \tag{34}$$

$$\dot{\psi} = n \frac{\psi_2 - \psi_1}{t_2 - t_1} \left[\frac{t - t_1}{t_2 - t_1}\right]^{n-1} \tag{35}$$

The new computer program[41] for the Mass/Time Method was developed to its present status during this study. It uses Equations (31) through (35) to determine the values of the variables in Equations (27) through (30) as functions of time for each parachute in a cluster. It then numerically integrates Equations (27) through (30) during the time interval of interest to produce a time history of riser load (for each parachute) and a trajectory of the vehicle. The program uses air density values from a standard day density-altitude function. The approach used in the program is to sum the individual parachute loads and apply them to the vehicle mass. In addition to this pretest version of the prediction program, there is a posttest version of the program that uses Equations (27) through (32) to determine the time rate of change of added masses and then integrates these derivatives to yield added masses as functions of time. To obtain the masses as outputs, it is necessary to input the canopy drag area-time histories and measured riser loads for each parachute, as well as initial conditions. This posttest version is an integral part of the prediction program, thereby making the program double-ended; i.e., it features both a pretest and a posttest version. The posttest version may be used to aid in the determination of the parameters in Equations (32) and (33). However, these parameters may be optimized by trial and adjustment using the pretest version as well. Incorporation of the iterative procedure required for complete data reduction in the computer was deferred in the interest of testing the basic program.

In preparation for development of the single parachute characteristic parameters to be employed in the Mass/Time Method, the new 2-DOF computer program, being double-ended, was employed to determine the approximate magnitude of the added air mass terms by inputting the force-time history and estimated drag area growth schedule of Test No. 80-1R. The results indicated a mass value for the full open parachute of approximately 400 slugs. In addition, a careful film analysis of the opening canopy showed that a good fit of projected area growth was obtained with area as a function of time to the 1.5 power. Also, since it was known from previous ringsail experience that C_{Dp} increased from approximately $C_{Dp} = 1.1$ at disreef to $C_{Dp} = 1.75$ at full open, the value of n in Equation (32) might be expected to fall in the range of 2.5 to 3.0, provided the time function of C_{Dp} had an exponent of 1.0 or greater.

A fairly detailed film analysis of the opening Apollo main parachute (in Test 80-1R) was conducted to support the load prediction methods being developed. This film analysis sought to study the sequence of events during all three opening stages, and to define the parachute area growth with time. The analysis has satisfied these objectives and led to several important new observations about the opening of an Apollo main parachute.

The method of analysis was to trace the parachute shape from frames of the test films spaced at suitable intervals of time, and then to derive the desired information from these tracings. Canopy mouth area and projected area were obtained from onboard film for all three stages. For third stage, these parameters were also measured from a ground-to-air sequence.

The results of the analysis are presented in Figures 26 through 29. These figures show canopy projected area versus time after launch and, where important and available, canopy mouth area

Pertinent Event Times

Event	Time After Launch, sec
Line stretch	2.20
First stage peak load	3.80
First stage disreef	7.59
Second stage peak load	8.20
Second stage disreef	10.39
Third stage peak load	11.80

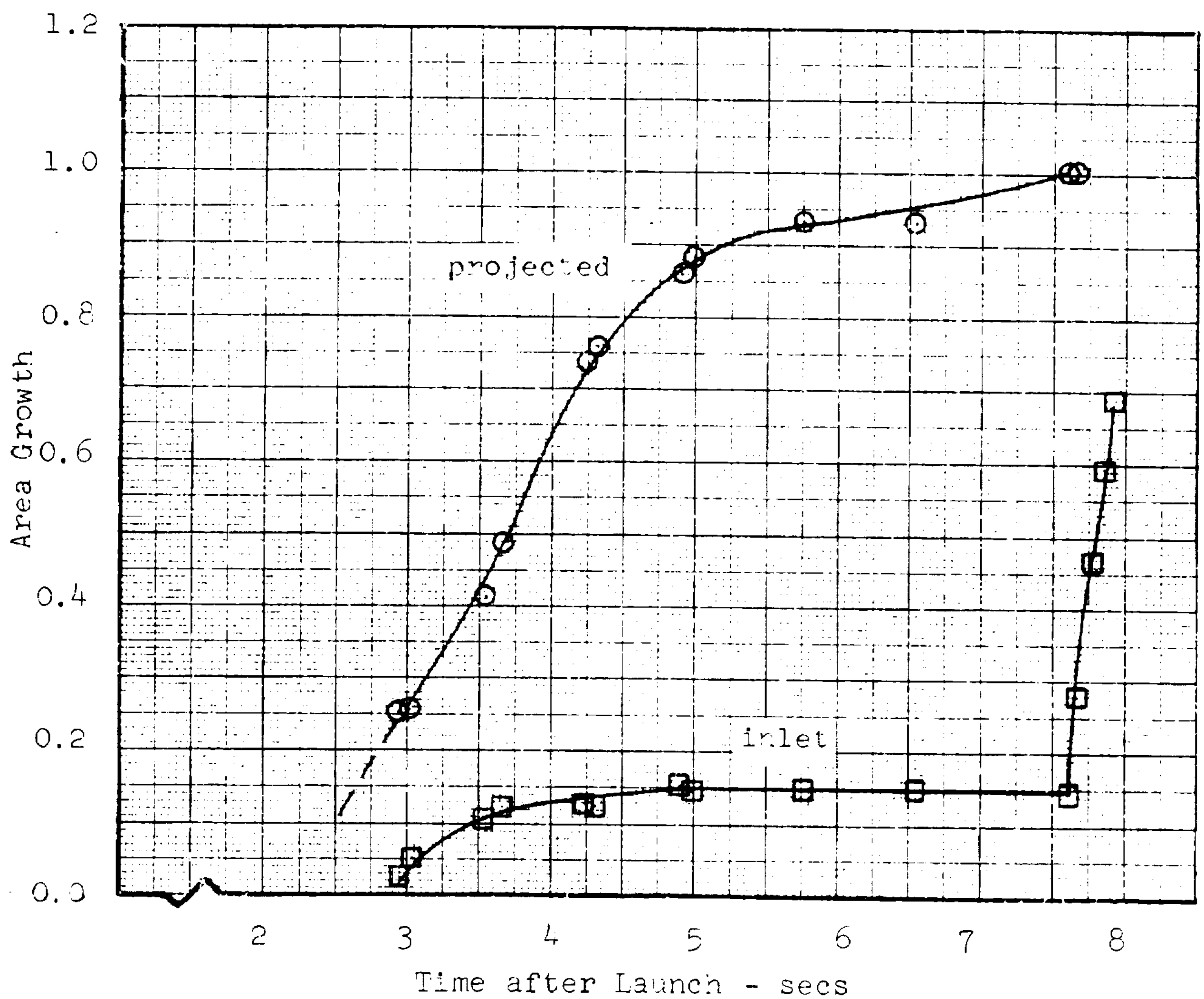

Fig. 26. Area Growth During First Stage of Test 80-1R

Pertinent Event Times

Event	Time After Launch, sec
Line stretch	2.20
First stage peak load	3.80
First stage disreef	7.59
Second stage peak load	8.20
Second stage disreef	10.39
Third stage peak load	11.80

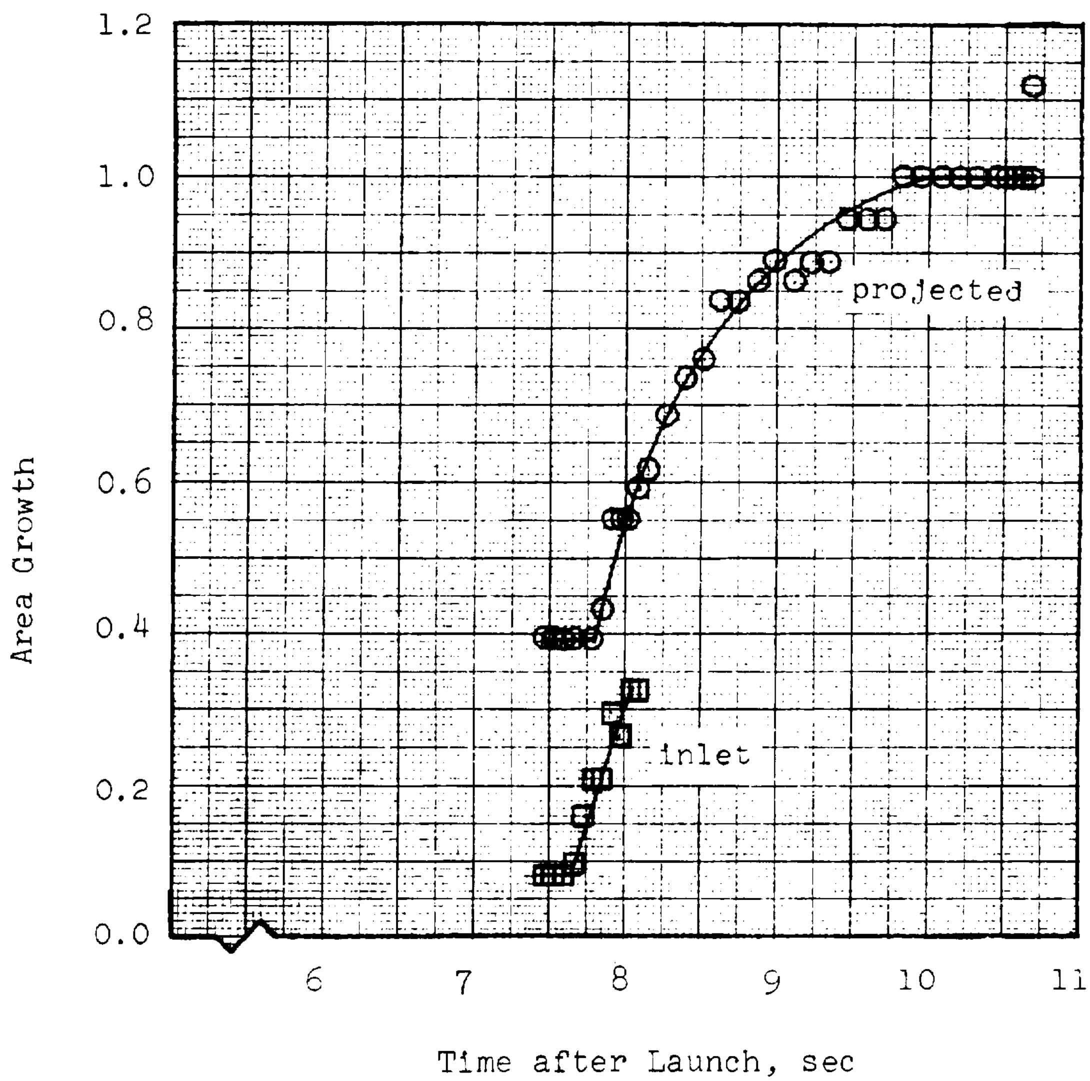

Fig. 27. Area Growth During Second Stage of Test 80-1R

Pertinent Event Times

Event	Time After Launch, sec
Line stretch	2.20
First stage peak load	3.80
First stage disreef	7.59
Second stage peak load	8.20
Second stage disreef	10.39
Third stage peak load	11.80

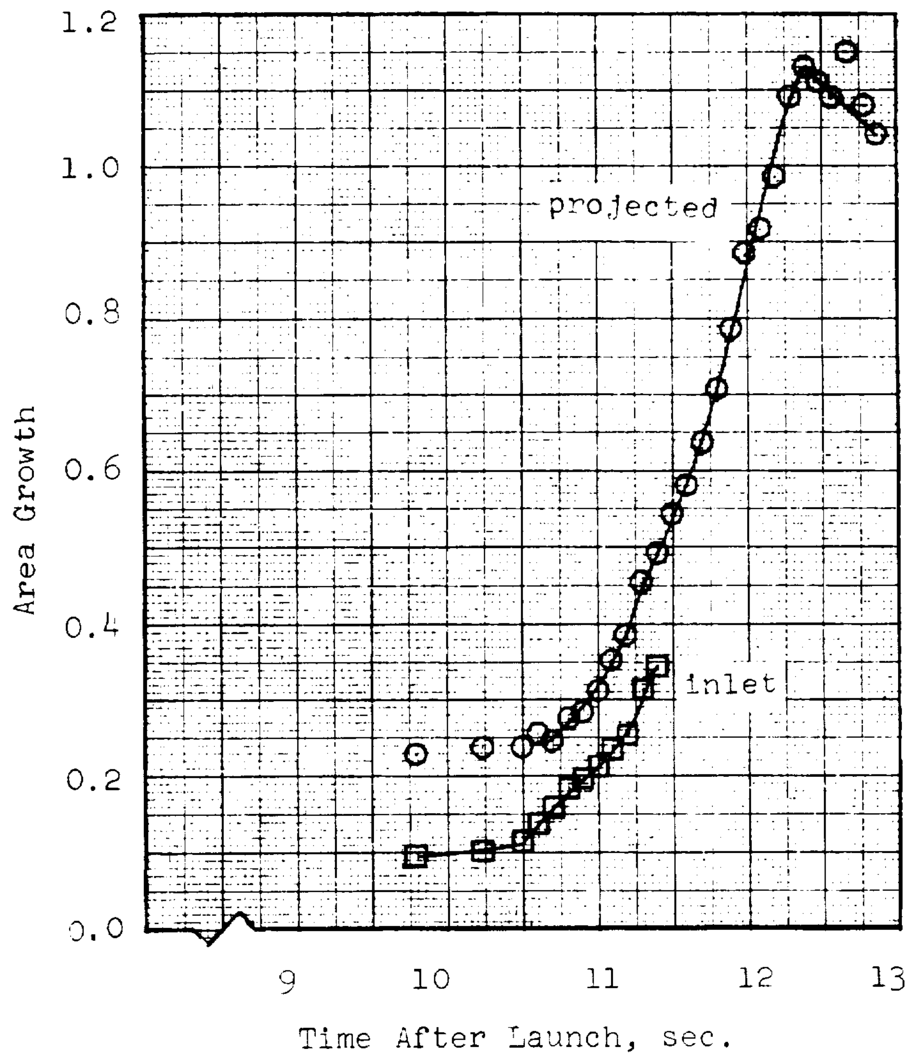

Fig. 28. Area Growth During Third Stage of Test 80-1R (Ground-Air)

Pertinent Event Times

Event	Time After Launch, sec
Line stretch	2.20
First stage peak load	3.80
First stage disreef	7.59
Second stage peak load	8.20
Second stage disreef	10.39
Third stage peak load	11.80

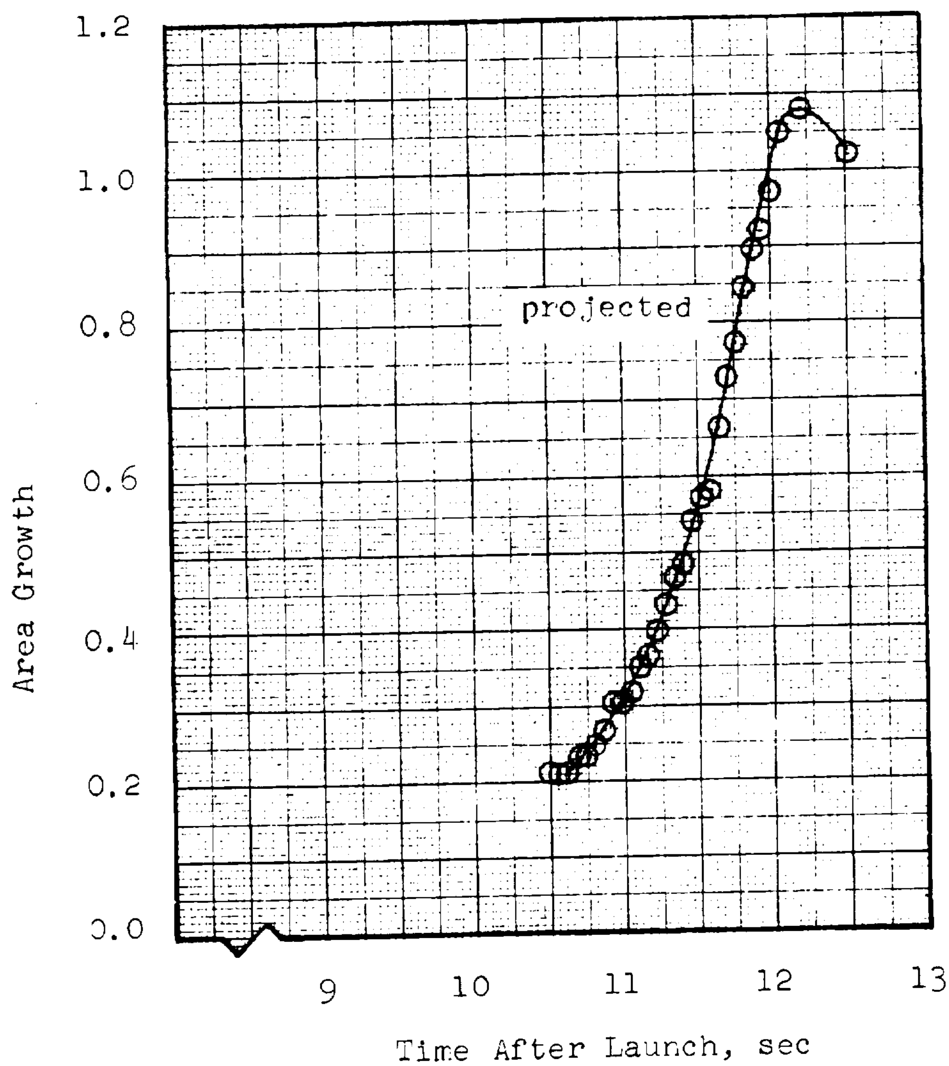

Fig. 29. Area Growth During Third Stage of Test 80-1R (Onboard)

versus time. The areas have been normalized to the equilibrium projected area for a stage, as no attempt was made to evaluate the areas in square feet. Also, in order to provide an indication of the data scatter, every point read from the film is presented.

As can be seen, the filling is markedly different in first and second stages from the inflation to full open. In the two reefing stages (see Figures 26 and 27) the canopy grows rapidly at first, until the reefing lines become taut, and then grows at a slower rate until the reefing lines are cut. In third stage, the canopy begins to grow rather slowly, but this growth rate increases until the canopy reaches full open, as shown in Figures 28 and 29. The area growth that occurs in the two reefed stages after the reefing lines become taut constitutes a significant portion of the final drag areas in both stages. As previously pointed out, and verified by Figures 26 and 27, this continued filling, and the resulting bulging over the reefing line, is significant for a ringsail, and therefore ought to be considered in analysis.

The delay between the time the mouth area begins to grow after the reefing lines are cut and the time the canopy projected area begins to grow seems to be about 0.2 sec in both second and third stages. (See Figures 27 and 28.) This amount of time, while not excessive, is significant when compared to the time to peak load in both stages. It is probable that during this interval the canopy added mass is changing percentage-wise more rapidly than the canopy drag area. Rust, in Reference 29, identified this interval as Phase IV in the inflation of a parachute with reefing. His assumption that this phase occurs instantaneously appears to be a good simplification from a practical point of view, and may not require modification. At the same time, the knowledge of an actual value for the duration of Phase IV could be beneficial in the interpretation of results obtained through the Shape/Distance Method (Section 4.3).

Figures 28 and 29, which depict the same events measured from different sources, show the same general characteristics. However, an unresolved problem exists with respect to the difference in the times at which maximum projected area was observed. The problem probably indicates inherent difficulties in the analysis method due to such things as timing errors, camera speed variations and the fact that the line of observation is skewed from the canopy centerline in the ground-to-air film. It is felt that the general observations and curve shapes are valid.

In addition to the analysis of Test 80-1R, the third stage of test 82-4 was studied to verify the variation in n with filling time that will be discussed below. This film analysis, which is presented in Figure 30, substantiates the trend observed in the calculations; the value of n decreases with the filling time.

Estimates of K_a, using Equation (33), ranged from approximately 0.3 to 0.75. Accordingly, a series of four computer runs was made with $n = 2.5$ and $K_a = 0.2, 0.4, 0.6$ and 0.8. Single parachute Test 80-1R was employed as a model. Since the film analysis showed the filling time to be close to 1.81 sec, instead of 1.94 sec, this new value was substituted. Good results were obtained with $K_a = 0.65$.

It is interesting to note that the added air mass associated with the fully inflated canopy with $C_DS = 4300\ ft^2$ and $K_a = 0.65$ is 320 slugs or approximately 10,300 lbs at the test altitude. This is equivalent to a sphere of air somewhat greater in diameter than the inflated canopy.

Since the peak load can be shifted in time by varying n, two additional computer runs were made with $K_a = 0.65$ and $n = 2.5$ and 3.0. The result for $n = 3.0$ was a nearly perfect fit of the measured force-time history with $F_o = 13,754$ lbs (measured $F_o = 13,737$ lbs) and $tf_o = 9.56$ sec.

Pertinent Event Times

Event	Time After Programmer Disconnect, sec
Second Stage Disreef	39.01
Third Stage Peak Load	39.96

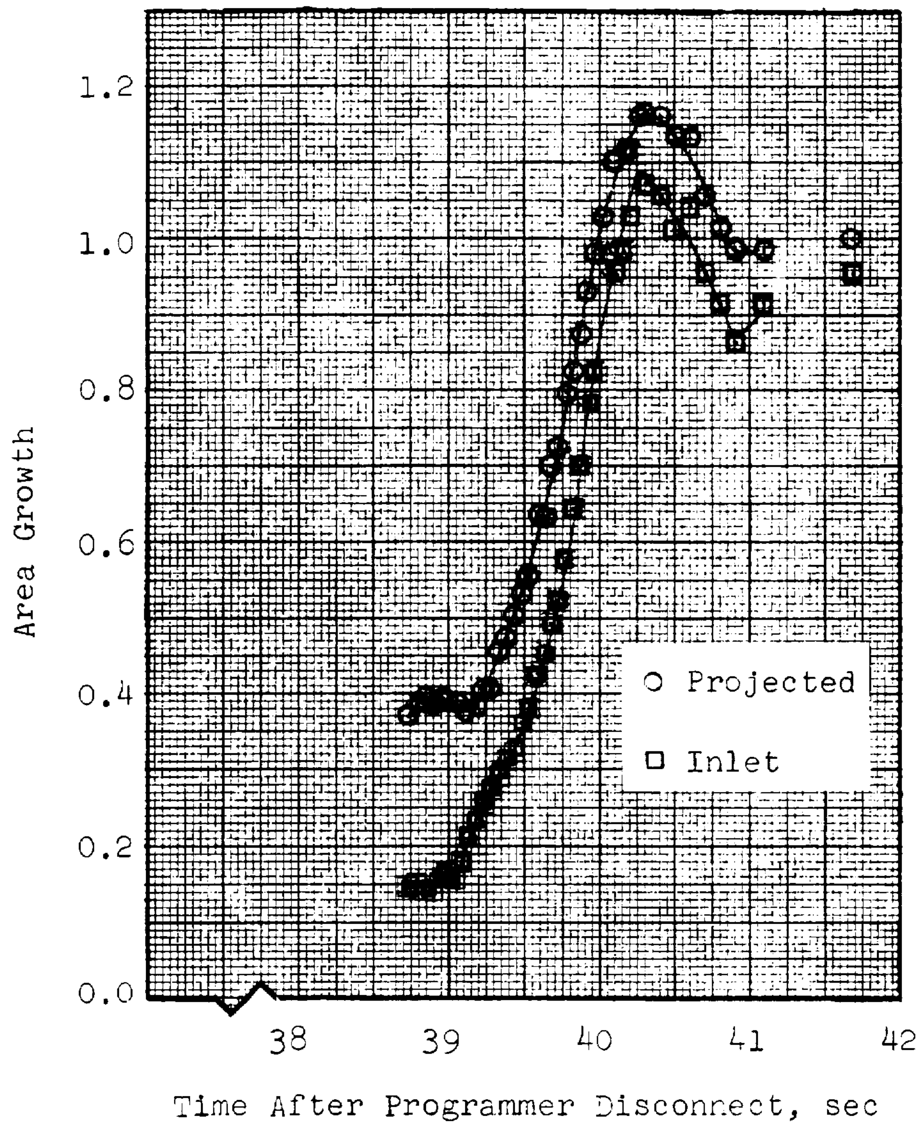

Fig. 30 . Area Growth During Third Stage of Test 82-4

At the same time, an experiment was performed in the computation of the force-time history of the two reefed stages. Instead of removing the added mass terms with $K_a = 0$ as had been done previously, the entire program was run with $K_a = 0.65$, letting $n = 1.0$ for the reefed opening stages only. This produced a nearly perfect fit for the first stage with $F_{r_1} = 13{,}524$ lbs (measured $F_{r_1} = 13{,}554$ lbs) at $t = 1.6$ sec, but trouble developed in the second stage; namely, large discontinuities appeared in the force-time plot due to abrupt changes in $\dot{m}_a$. It will be noted that Stage 1 opening was attended by a sharp drop in load after the peak was reached, due to a drop in $\dot{m}_a$ attending the transition from rapid to slow filling. This happens to match the measured data with high fidelity, and is found repeated in other test runs. But at Stage 1 disreef, $\dot{m}_a$, being tied to $\dot{\psi}$ through Equation (34), suddenly increased from 0.61 to 25.27 sl/sec and again at the load peak suddenly decreased from 41.58 to 1.48 sl/sec. The resultant distortion of the force-time plot made it clear that the use of a linear growth rate for ψ in Stage 2 was a poor approximation because it lacked the smooth transitions that could be detected in the film records. Two courses of action were open: (1) for the sake of simplicity return to the original treatment of the first two stages without the added mass terms in the force equation, and (2) develop a $\psi(t)$ function for the second stage that would accurately represent the actual process. After testing of the second approach led to undesirable complications in reefing Stage 2, the first course of action was chosen, and pursued to completion for the single parachute case, because its feasibility had already been demonstrated.

Effort was then focused on establishing the best values of the input parameters for each of the Block II(H) single parachute tests, so that the average values could be determined for the single parachute case.

The program with inputs changed to the conditions of Test 80-2 produced reasonably good results. The predicted load-time history of Stages 1 and 2 was in good agreement with measured data; the peak load of Stage 3 was high by 10 percent and occurred 0.06 sec late. Correction of the Stage 3 peak load calculation for Test 80-2 posed a problem because the initial dynamic pressure was only 3 percent above the measured value and the load onset agreed exactly with the measured data. The fact that the peak was higher and occurred later than the actual indicated that the exponent n should be less than 3. Because this might compromise the load calculation for Test 80-1R, further confirmation was sought by inputting the conditions of the third single canopy Test 80-3R1 and rerunning Test 80-2, both with n = 2.5 and n = 3. The results of these computer runs showed that n = 2.5 gave the best force-time match for both tests. Similar results were found for the other single canopy tests, with the result that n varied from test to test between 2.0 and 3.0 approximately. It was found that the variation in n correlated well with the filling time of the third stage.

The six single parachute tests (Tests 80-1R, 80-2, 80-3R1, 80-3R2, 82-2 and 82-4) provided information on the input parameters, and it was possible to tentatively formulate a method for predicting the loads for all three opening stages for single main parachutes. This method is described in Section 4.2.3, and its accuracy is demonstrated in Section 4.2.4

4.2.3 Mass/Time Method for Single Chutes

In order to use the Mass/Time Method for single parachute tests, the following procedure is carried out:

a) Initial conditions must be provided to the program. These are vehicle weight and drag area, altitude, velocity and flight path angle.

b) A parachute drag area-time history must be provided. Drag areas at the end of each stage are determined from Figure 31 as functions of reefing ratio. Drag area at the completion of reefed inflation in Stage 1 is evaluated as 80 percent of the drag area at the end of Stage 1. Drag area at the completion of reefed inflation in Stage 2 is evaluated as 90 percent of the drag area at the end of Stage 2. Drag area at the completion of filling in Stage 3 is 4300 sq ft. Filling times are calculated for each stage from the relation

$$t_f = K_f \left(\Psi_2^{\frac{1}{2}} - \Psi_1^{\frac{1}{2}}\right) / v_1$$

where Ψ_1 is the parachute drag area at the end of the previous stage, Ψ_2 is the drag area at the end of inflation in the stage under consideration, v_1 is the vehicle velocity at the end of the previous stage, and values of K_f are 34.1, 8.64 and 4.06 for Stages 1, 2 and 3 respectively. Reefing cutter times must be specified for the method to be used. The exponent n is determined from Figure 32 as a function of t_{f_o}, the filling time in third stage.

c) The added mass factor K_a is 0.66 for Stage 3.

In this rudimentary form the Mass/Time program must be computed stage-by-stage to determine the velocity v_1 at the end of each stage. Its application would be simplified by including the filling time calculations in the program for the second and third stages, inputting K_f along with the drag areas. By further augmentation of the computer program with a table of n versus t_{f_o} (Figure 32) the complete opening process may be computed in a single run. However, implementation of these refinements was deferred in the interest of completing the evaluation of the single parachute test cases.

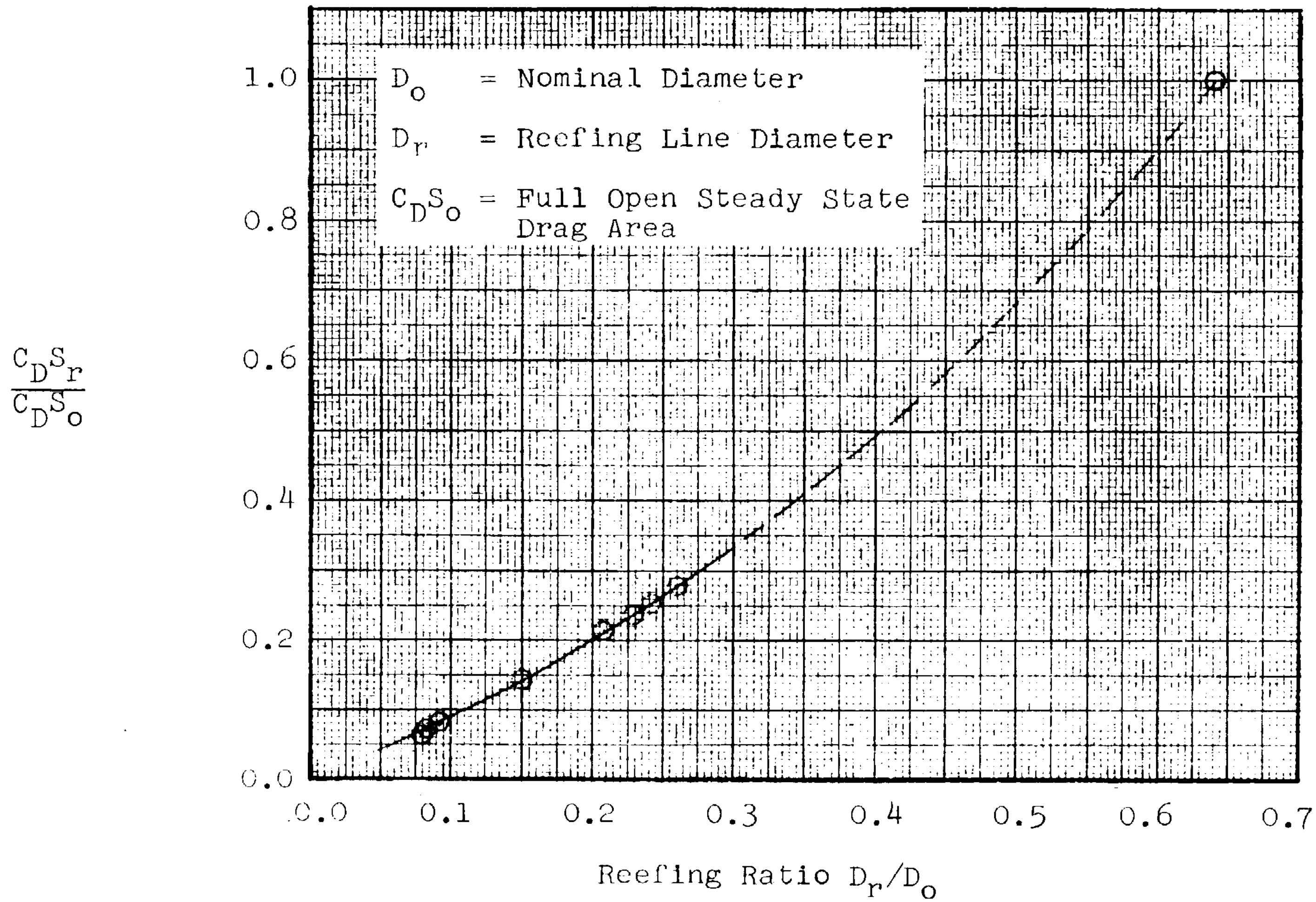

Fig. 31. Ringsail Effective Drag Area With Midgore Skirt Reefing (Apollo Test Data)

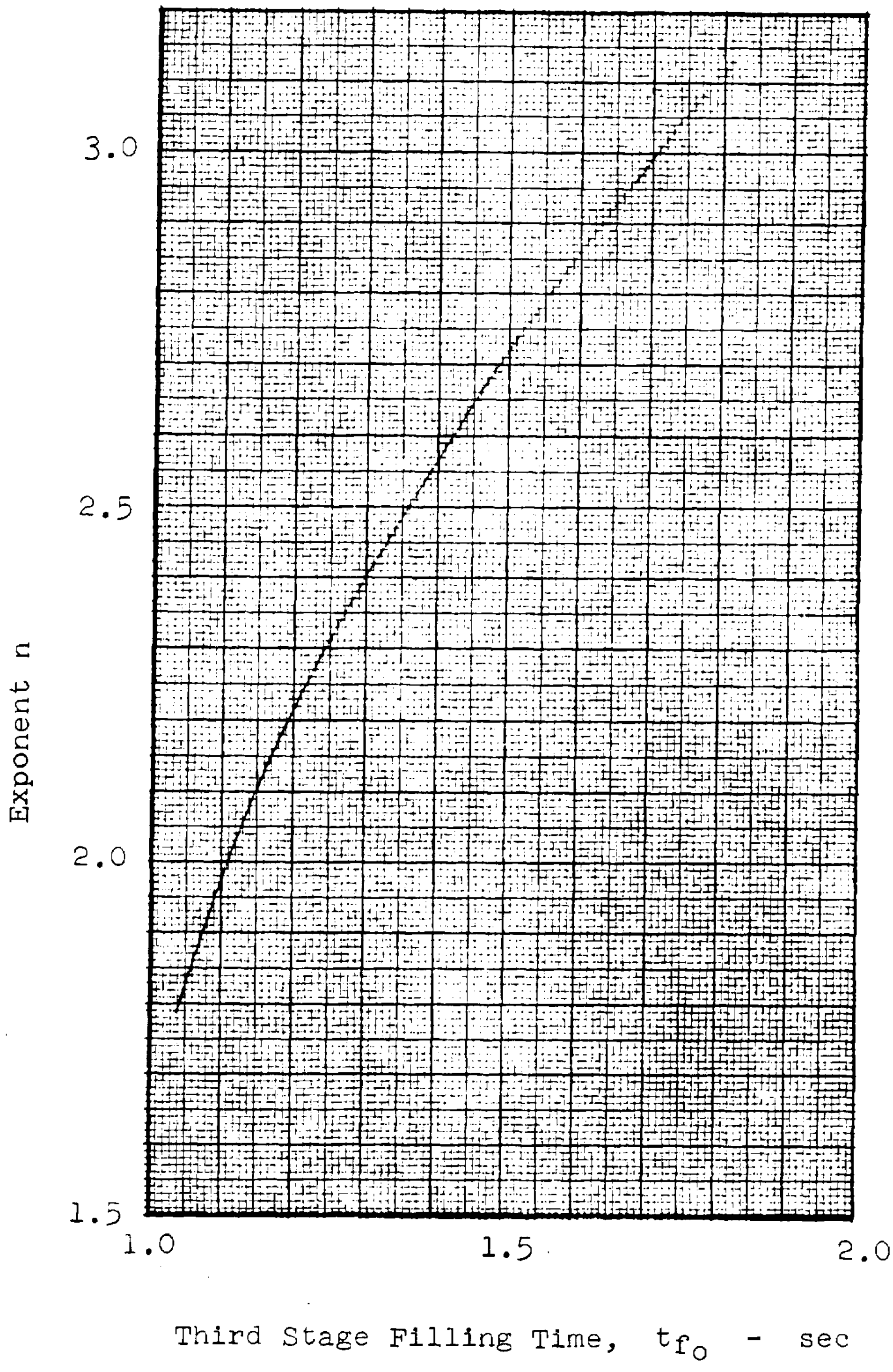

Fig. 32. Exponent n as a Function of Third Stage Filling Time

4.2.4 Accuracy

The method described in Section 4.2.3 was applied to single parachute tests 80-1R, 80-2, 80-3R1, 80-3R2, 82-2 and 82-4. These tests present a range of vehicle weights from 5300 lb to 10,300 lb, variations in first and second stage reefing ratios, opening loads of from 14,000 lb to 23,000 lb in Stage 1, 13,000 lb to 33,000 lb in Stage 2 and 14,000 lb to 32,000 lb in Stage 3, initial flight path angles ranging from nearly horizontal to nearly vertical, and initial flight velocities ranging from 295 to 375 ft/sec. In spite of the many, wide variations in test parameters, the accuracy of the method is excellent as demonstrated in Figures 33 through 38. When errors are measured from the nearest of the load measurements established by the two load links used in each test, they are within ± 5 percent for 17 of the 18 data points (6 tests x 3 opening loads/test) and 12 percent in the eighteenth case. These ranges in measurements are indicated by pairs of short horizontal lines for each stage in Figures 33 through 38.

It should be noted that this work represents the first successful attempt at calculating a time history of force for third stage, rather than only predicting peak load.

After the results of the six single parachute tests had been studied, it was decided to apply some of the assumptions of the Mass/Time Method to a two-parachute cluster test and find out how well the model could accommodate the cluster situation. An ICTV test (81-2) was chosen. Drag areas were determined by the procedure for single parachutes. Because applicable values of K_f remained to be determined by cluster data analysis, actual filling times were used. The results presented in Figure 39 illustrate in a general way the effects of cluster operation on the parameters of interest:

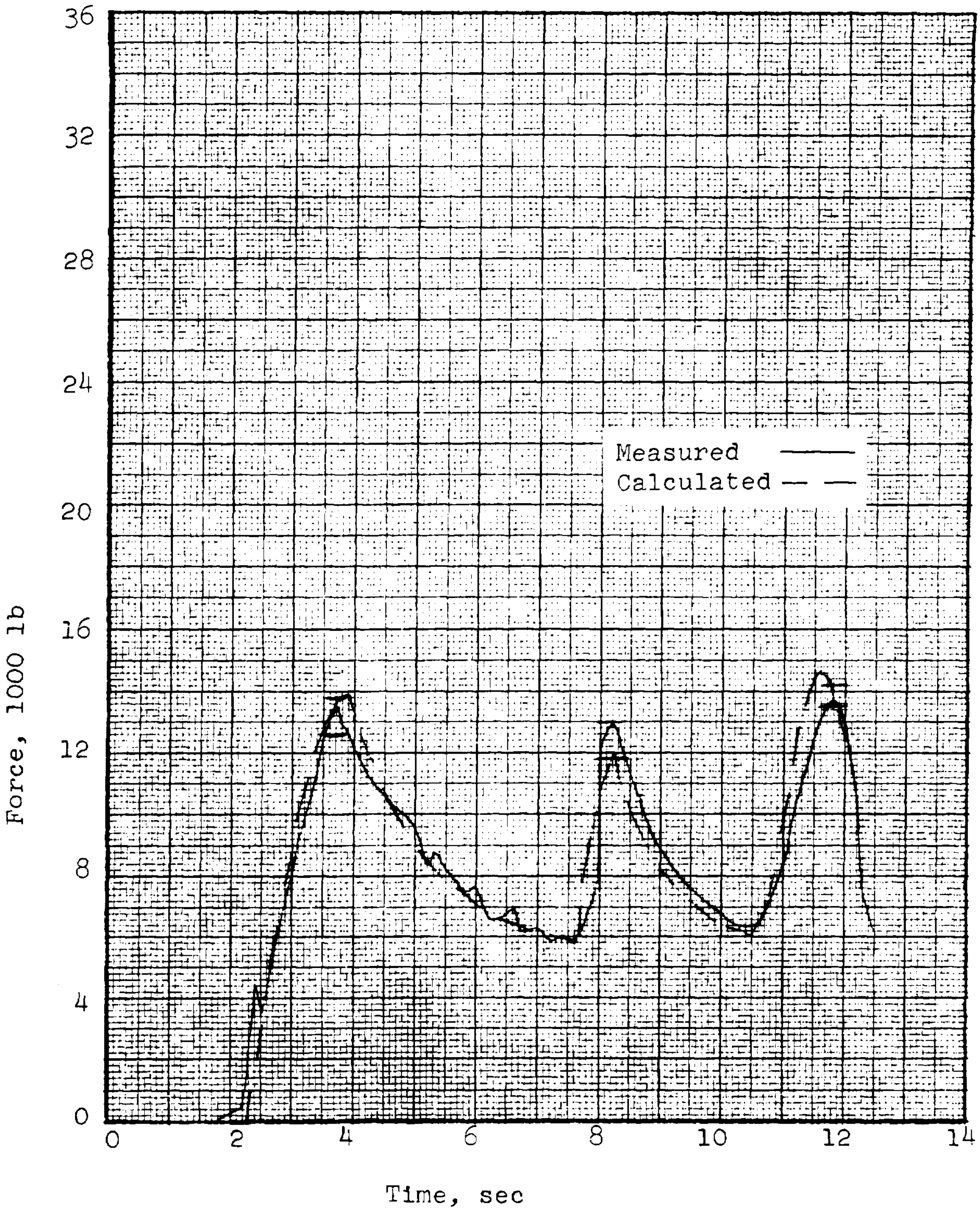

Fig. 33. Mass/Time Method, Test 80-1R

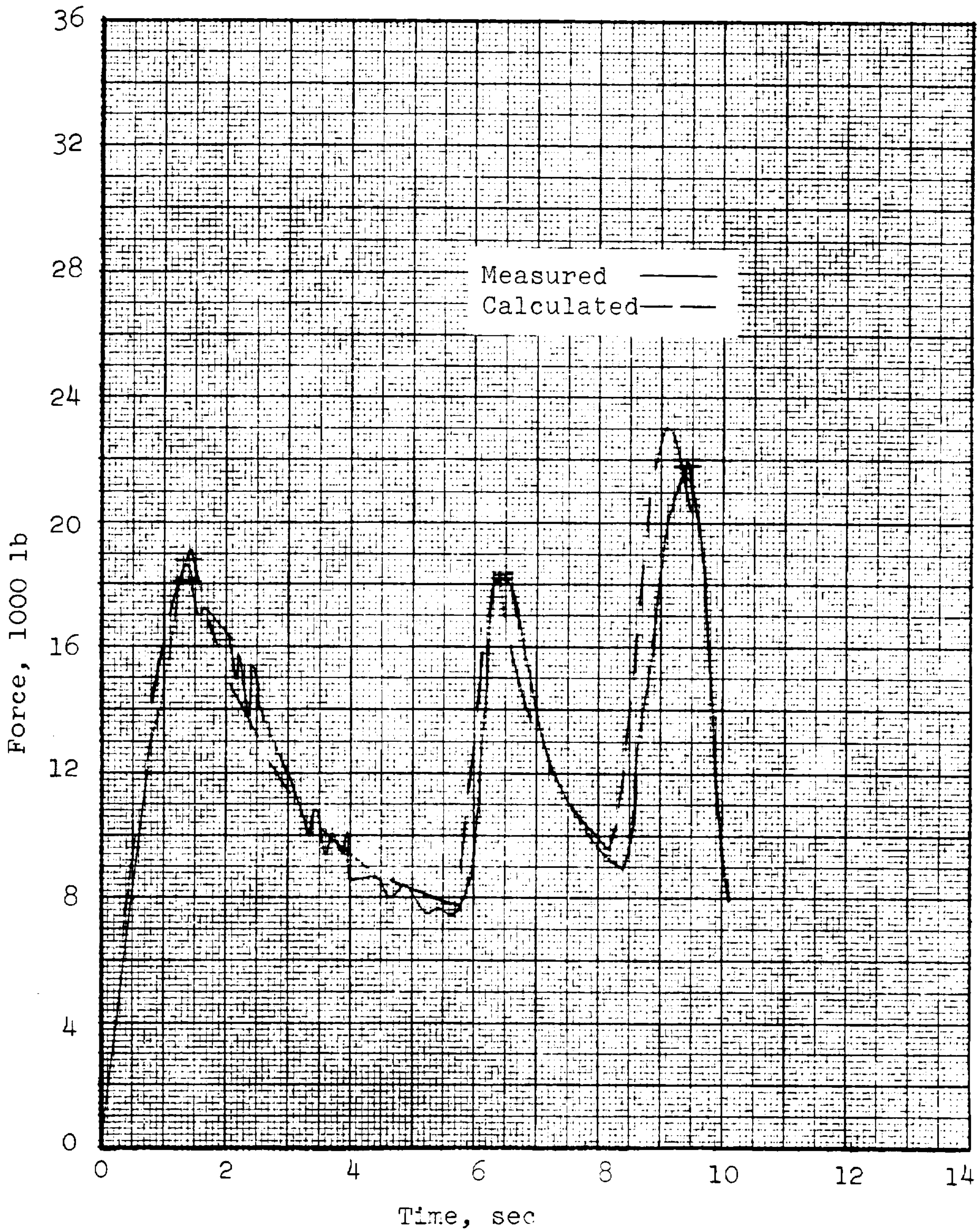

Fig. 34. Mass/Time Method, Test 80-2

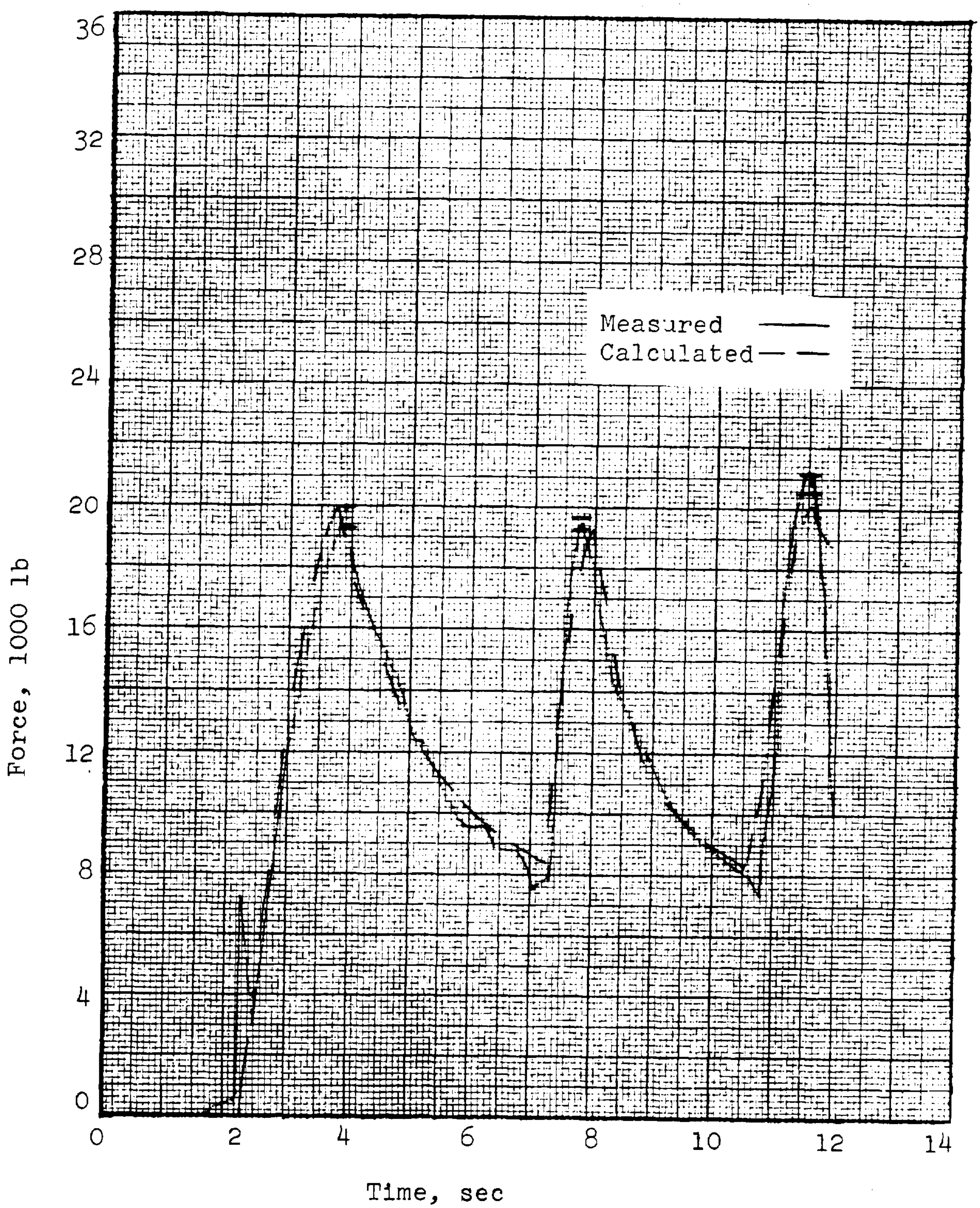

Fig. 35. Mass/Time Method, Test 80-3R1

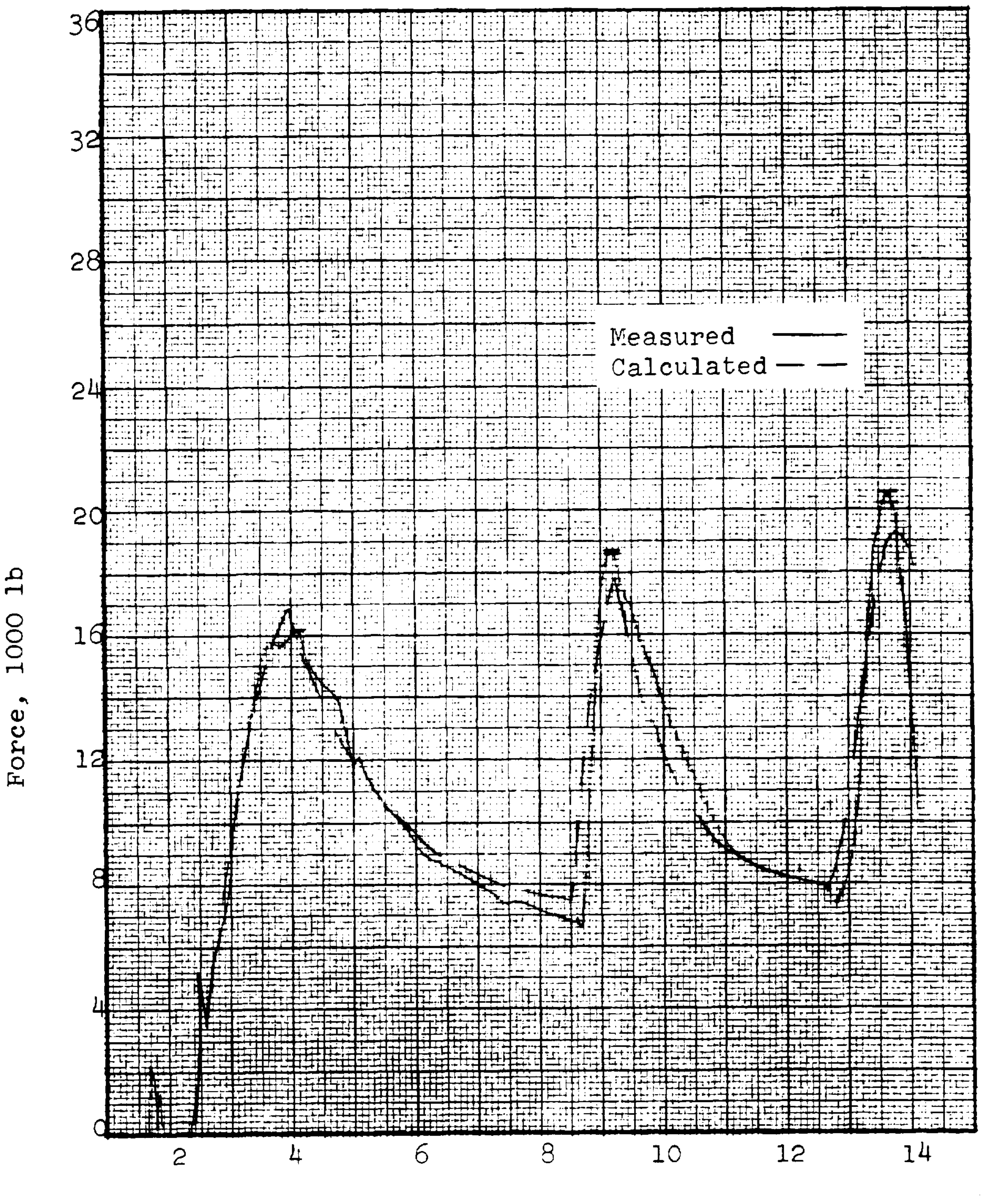

Fig. 36. Mass/Time Method, Test 80-3R2

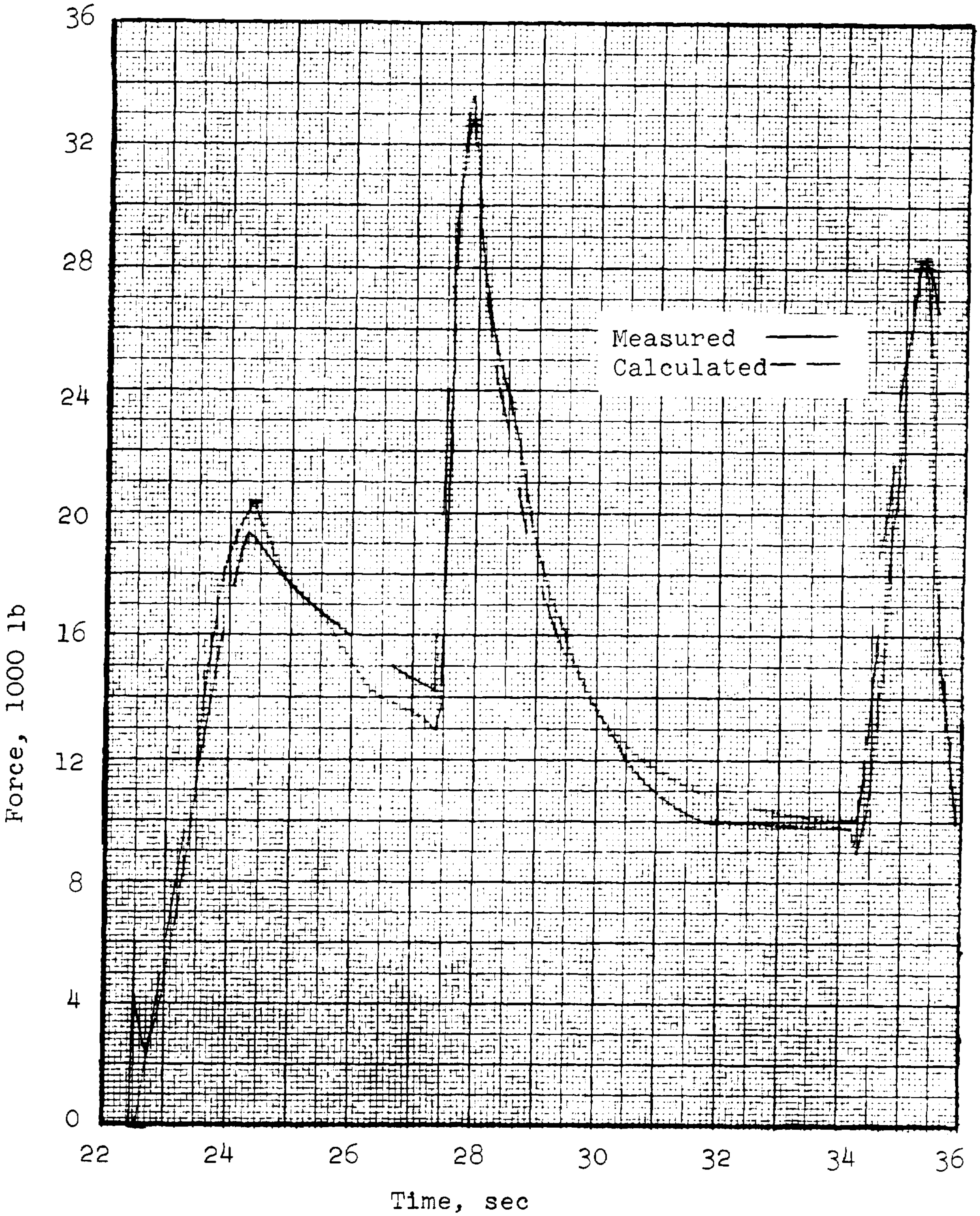

Fig. 37. Mass/Time Method, Test 82-2

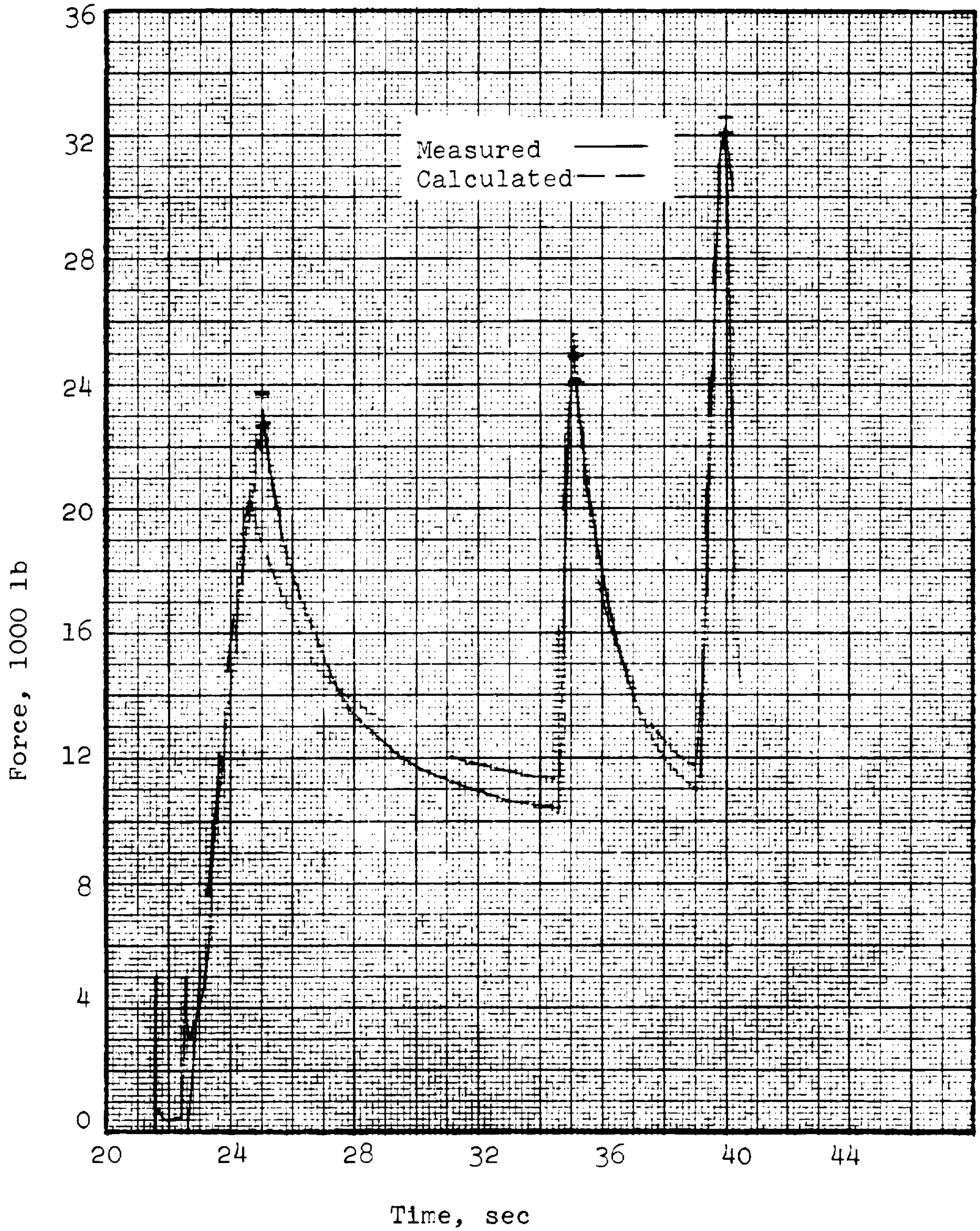

Fig. 38. Mass/Time Method, Test 82-4

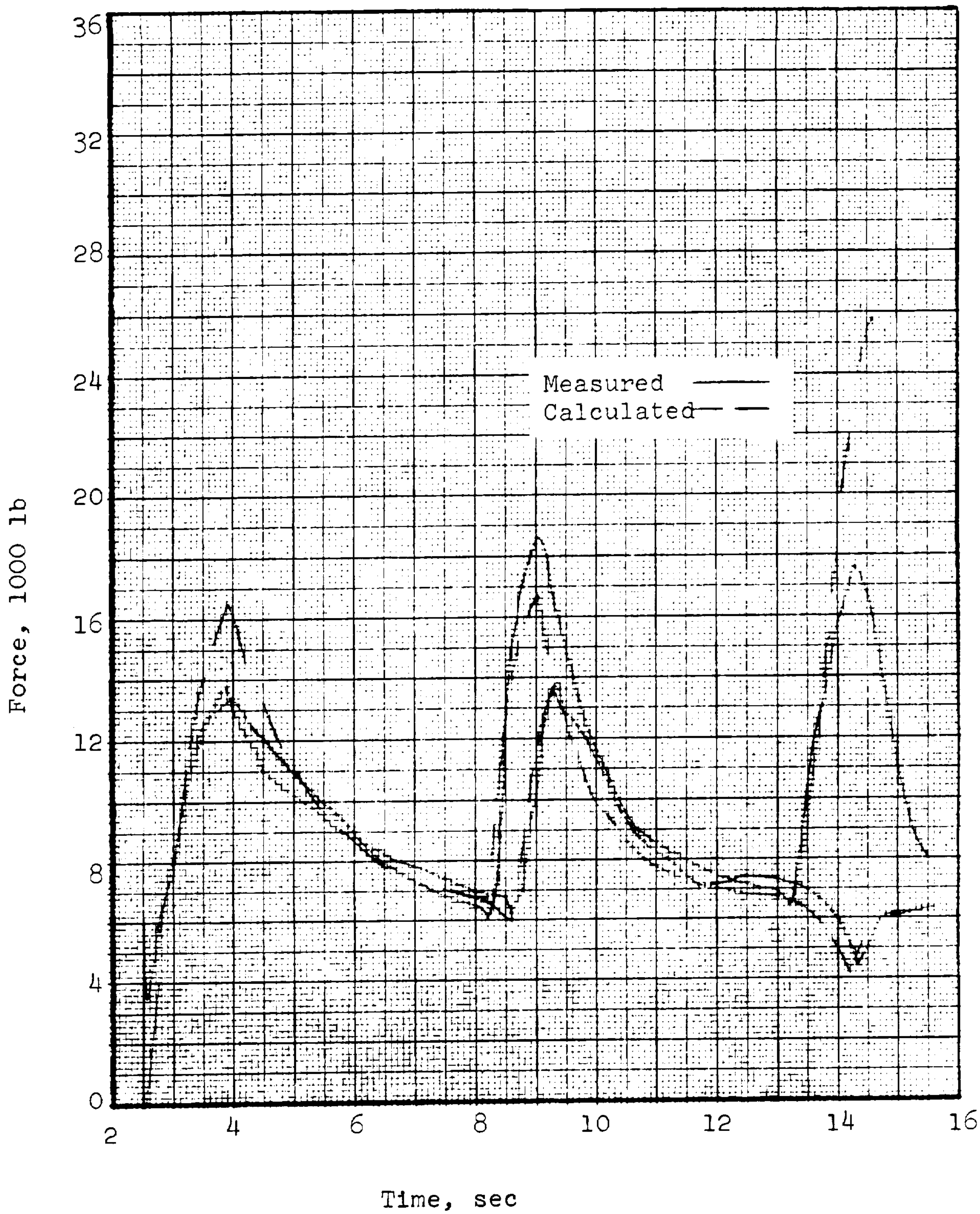

Fig. 39. Mass/Time Method, Test 81-2

a) Nearly synchronous reefed opening of the two canopies during Stage 1 is attended by measured peak loads about 20 percent less than predicted on the basis of single canopy drag areas. With allowance for small inertial effects, the interference between canopies can be accounted for by a reduction in effective drag area of about 18 percent in this case. This is consistent with both film observations and the geometry of two circles of equal area expanding side by side, with progressive flattening of the interface, approaching as a limit two half circles with rounded corners.

b) With a smaller than predicted total drag area at Stage 1 disreef the dynamic pressure would have been higher than predicted. This would account for part of the difference between measured and predicted peak loads for Stage 2 of canopy No. 1, but the effective drag area is uncertain and added mass effects undoubtedly are present. If the predicted drag area was close to actual, as indicated by the measured F/q at Stage 2 disreef, the added mass effect on canopy No. 1 was substantial. This view is supported by the near equality of Stage 2 peak loads indicated for canopy No. 2 which disreefed one half second later, and being the lag canopy most probably would have a smaller drag area than canopy No. 1. This would offset the higher than predicted dynamic pressure at disreef. Verification of these surmises requires a second computer run with revised reefed drag area in both stages.

c) During final opening the lag canopy disreefed 1.1 seconds after the lead canopy (No. 1), and good agreement between measured and predicted loads is shown. The lead canopy predicted peak load is 50 percent greater than measured and is anomalous in that it is still rising at the cutoff point where the canopy reaches full inflation; the measured peak occurred prior to full inflation. No explanation for this anomaly has been found because it was necessary to conclude the investigation with this single computer run.

4.3 SHAPE/DISTANCE METHOD

The Shape/Distance Opening Load Prediction Method is a potential tool for both loads and trajectory prediction. Adapted to a computer, the method provides continuous loads and trajectory prediction throughout a test. The method was chosen for development because it adapts easily to the Apollo ELS parachutes; the method accommodates reefing, load drag, and canopy added mass. The development is not complete, however, for specific parachute parameters required by the method are not, at this time, available. In their absence approximations have been used, and encouraging results have been obtained.

A brief review of the theory and, in more detail, the progress made to date in its implementation to single Apollo main parachutes is presented in this subsection.

4.3.1 Review of Rust's Theory

The method was developed from Rust's "Theoretical Investigation of the Parachute Inflation Process."[29] The opening load theory presented in this report is summarized on the following next few pages.

Rust derived the governing differential equations by considering the free body diagram of the vehicle-parachute system in Figure 40. By equating the force sum to the system's rate of change of momentum, Rust obtained two trajectory equations: one normal and one parallel to the flight path

$$\frac{d}{dt}\left[(m_\ell + m_c + m_a)\ v\right] = (W_\ell + W_c)\ \sin\Theta - D_\ell - D_c$$

$$v\,\frac{d\Theta}{dt} = g\ \cos\Theta.$$

The variables were then nondimensionalized and the independent variable was changed from time to projected radius using the relationship

$$\frac{d}{dt}\ (\ldots) = \frac{d\ (\ldots)}{d\overline{R}}\ .\ \frac{d\overline{R}}{d\overline{s}}\ .\ \frac{d\overline{s}}{dt} = \overline{v}\ \frac{d\overline{R}}{d\overline{s}}\ .\ \frac{d(\ldots)}{d\overline{R}}$$

where $\overline{s}$, $\overline{v}$, and $\overline{R}$ are dimensionless trajectory distance, velocity, and projected canopy radius, respectively. The change of independent variable was to obviate the need for an assumed diameter-time relationship.

Upon expansion and rearrangement, the two equations are of the form

$$\frac{d\overline{v}}{d\overline{R}}^{2} + f_1\ (\overline{R})\ \overline{v}^{2} = f_2\ (\overline{R})\ \sin\Theta$$

$$\overline{v}^2\ \frac{d\Theta}{d\overline{R}} = f_3\ (\overline{R})\ \cos\Theta$$

These trajectory equations, which must be solved simultaneously, yield velocity and flight path angle as functions of $\overline{R}$.

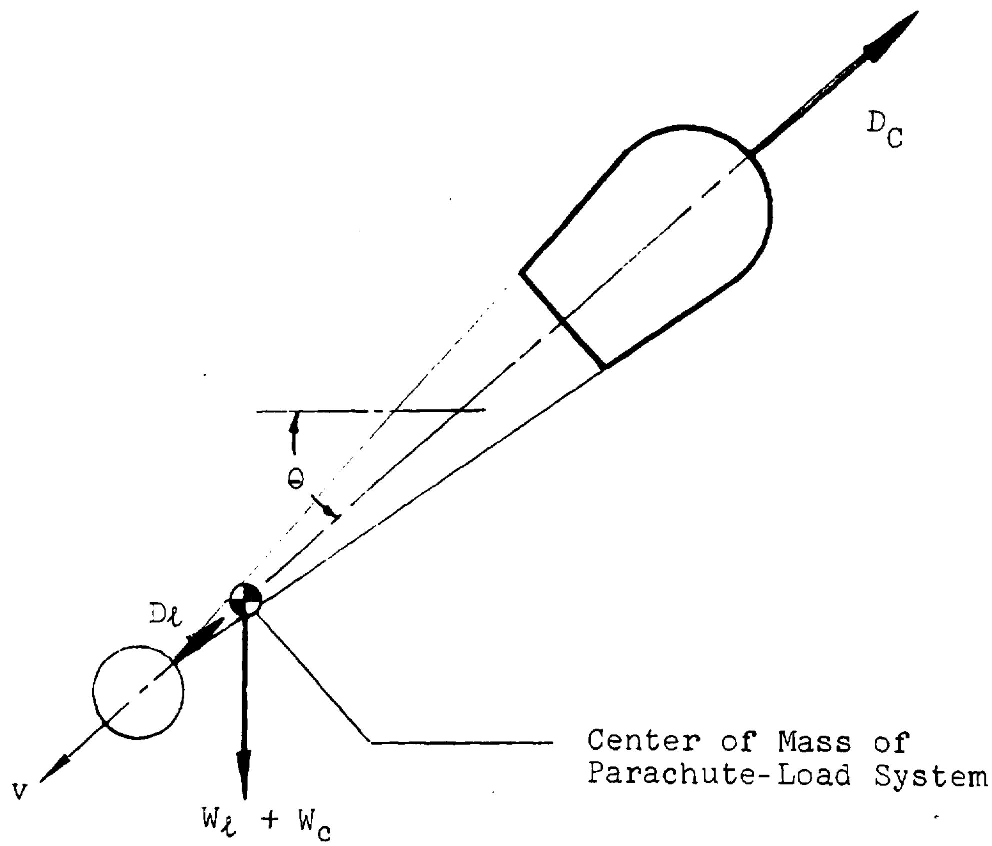

a) Parachute-Load System

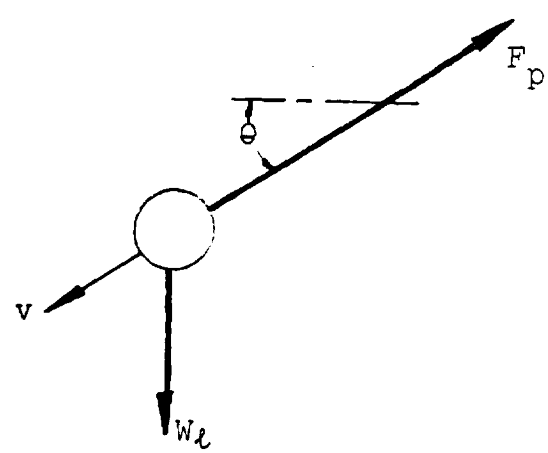

b) Load

Fig. 40. Free Body Diagrams Used in Rust's Theory

To get a relationship for time, Rust used the chain rule.

$$\frac{dt}{d\bar{R}} = \frac{dt}{d\bar{s}} \cdot \frac{d\bar{s}}{d\bar{R}} = \frac{1}{\bar{v}} \cdot \frac{d\bar{s}}{d\bar{R}}$$

or

$$\frac{dt}{d\bar{R}} = f_5 (\bar{R}) / \bar{v}$$

Rust redefined the free body diagram to get a relationship for riser force. Equating the forces acting on the vehicle in Figure 40 to the vehicle mass times acceleration and rearranging results in

$$F_p = W_\ell \sin \theta - D_\ell - m_\ell \frac{dv}{dt}$$

or

$$F_p = W_\ell \sin \theta - D_\ell - m_\ell \left[f_4 (\bar{R}) \frac{d\bar{v}}{d\bar{R}}^2 \right].$$

This is an auxiliary equation which, when used with the trajectory equations, provides riser force, velocity, flight path angle, and time as functions of $\bar{R}$.

One other relationship is needed to determine the coefficients, $f_n (\bar{R})$. In each of these terms, $d\bar{s}/d\bar{R}$ appears (it results from the independent variable change using the chain rule). Rust showed how to obtain this by considering

$$\frac{d\bar{s}}{d\bar{R}} = \frac{d\bar{V}}{d\bar{R}} \bigg/ \frac{d\bar{V}}{d\bar{s}}$$

where $\bar{V}$ is canopy volume. The numerator can be obtained by considering the canopy as a truncated cone topped by an ellipsoid. A relation between volume and radius is determined geometrically and differentiated to obtain $d\bar{V}/d\bar{R}$.

The denominator can be obtained as follows:

$$\frac{d\overline{V}}{d\overline{s}} = \frac{d\overline{V}}{dt} \cdot \frac{dt}{d\overline{s}} = \frac{1}{\overline{v}} \cdot \frac{d\overline{V}}{dt}$$

Where $d\overline{V}/dt$ is gotten by mass balance. The rate of change of enclosed mass must equal the flow rate in, less the flow rate out. Or

$$\frac{d}{dt}\left[\rho V\right] = (\rho Av)_{in} - (\rho Av)_{out}$$

$$\frac{dV}{dt} = (Av)_{in} - (Av)_{out}$$

By assumption or wind tunnel test, the velocities can be found. The areas are known.

Collecting the equations for inspection, it can be seen that there are three differential equations and one auxiliary:

$$\frac{d\overline{v}^2}{d\overline{R}} + f_1 (\overline{R}) \overline{v}^2 = f_2 (\overline{R}) \sin \theta$$

$$\overline{v}^2 \frac{d\theta}{d\overline{R}} = f_3 (\overline{R}) \cos \theta$$

$$\frac{dt}{d\overline{R}} = f_5 (\overline{R}) / \overline{v}$$

$$F_p = f_6 (\overline{R}).$$

The three differential equations have to be solved simultaneously, an appropriate task for a computer. Besides containing $d\overline{s}/d\overline{R}$, the coefficients $f_n (\overline{R})$ have terms like canopy drag, vehicle weight, and canopy added mass.

When integrated, the equations provide velocity, flight path angle, time, and riser load.

4.3.2 The Computer Program

The computer program[41] was designed to provide continuous loads and trajectory prediction, using Rust's inflation theory, throughout a test. All phases of inflation have been programmed and checked against Rust's hand-calculated example, given in Appendix C of Reference 29.

The computer program is composed of a main program with six subroutines. For a given set of initial conditions, canopy parameters, and vehicle weight and drag; the program yields velocity, altitude, dynamic pressure, riser load, canopy drag area, flight path angle, projected radius, and time. The main program provides the coefficients of Rust's differential equations, as well as input and output. The first subroutine computes continuous density change with altitude by means of a curve fit to the 1959 Standard Day Atmosphere. The second subroutine calculates a "potential flow" added mass of the canopy at each integration step. The third and fourth subroutines control the integration. The fifth subroutine presents the proper differential equations, as they apply to each phase of inflation, to the sixth subroutine, which does the numerical integration (fourth order Runge-Kutta technique).

4.3.3 Application of the Method to an Apollo Main Parachute Test

The Shape/Distance Opening Load Method has been applied to Apollo main parachute Test 80-1R. A discussion of the approach to providing the necessary input to the computer program and of the results is presented here.

4.3.3.1 Computer Program Input. Consider the inputs which are needed by the computer program. First, relationships peculiar to the parachute being modeled; drag coefficient, added mass, and canopy shape information must be supplied. Then, those conditions peculiar to the test being simulated; initial density altitude and velocity, vehicle weight and drag, percent reefing, and cutter times must be provided.

The latter are obtained from test plans. The former are more difficult; some of the parachute parameters should be obtained from wind tunnel testing (one of the advantages of the Shape/Distance Method is that they can be obtained in such a way). In lieu of accurate knowledge of some of the parachute parameters, approximations have been made, using the best available information.

4.3.3.1.1 Canopy Drag Coefficient. As a parachute inflates, its drag area changes, not only because of an increasing projected area, but also because the canopy shape is changing. It is not enough to assume a constant drag coefficient. The drag coefficient as a function of projected radius and eccentricity is needed, but is not available. However, the equilibrium drag area as a function of reefing ratio is available (Figure 41), and was obtained from the end point dynamic drag areas (instantaneous riser force/dynamic pressure at end of a reefing stage) of numerous main parachute tests.

Unfortunately, the use of this function produced unrealistically high first stage loads. This is understandable because of the shape differences between two canopies having the same inlet radius, one inflating and the other not inflating (at equilibrium).

This shape difference can be seen in Figure 42. This effect is especially pronounced at small reefing ratios. Near full open, the shapes are almost identical.

Because of this problem, a new approach was tried. Different curves of C_DS versus R/R_o were generated. It is known that added mass manifests itself as drag. During the first stage of inflation the added mass is small, so the resultant first stage loads can be attributed to canopy drag alone. This is an aid to determining the true C_DS curve, that curve which

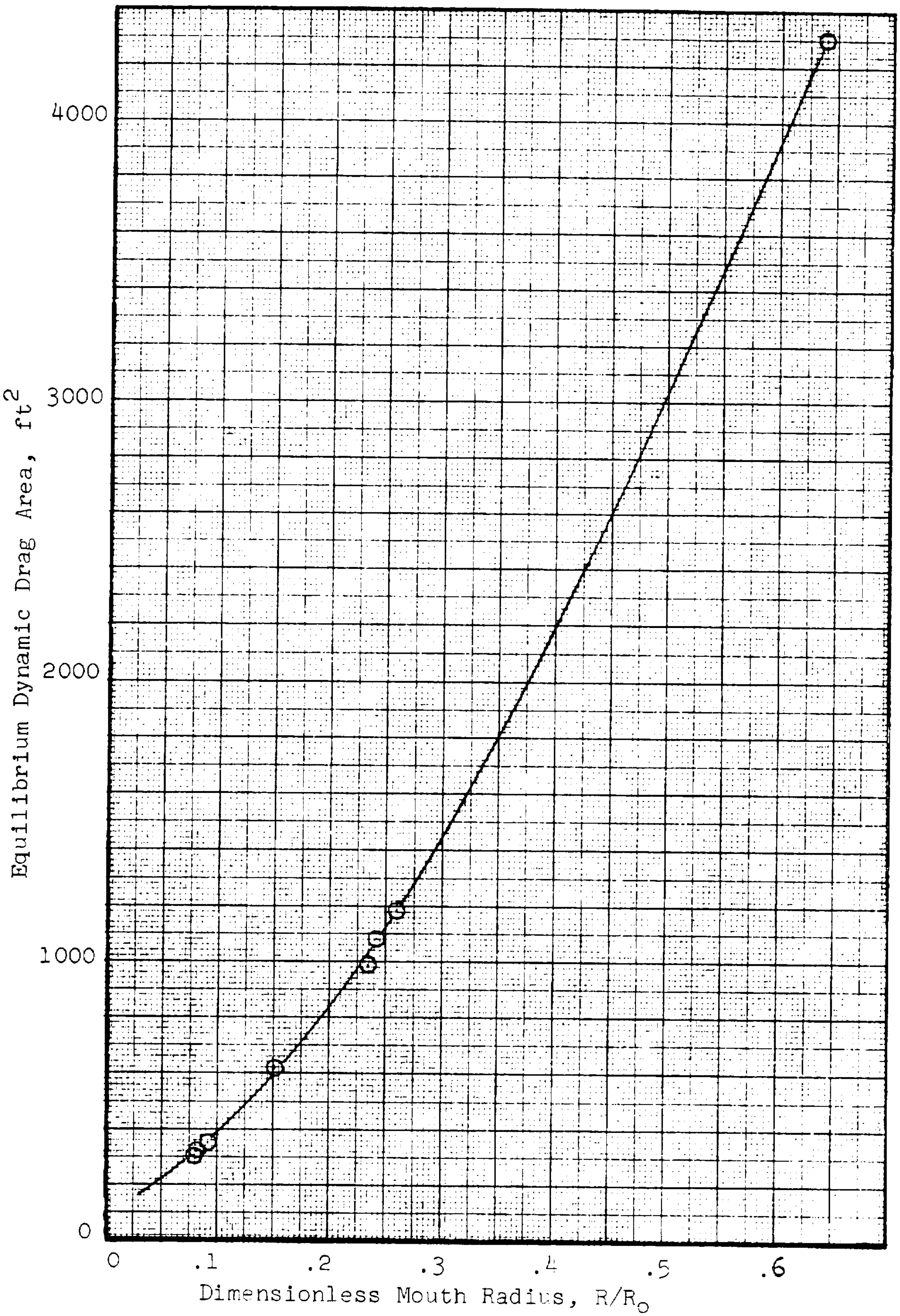

Fig. 41. Equilibrium Dynamic Drag Area Versus Dimensionless Mouth Radius

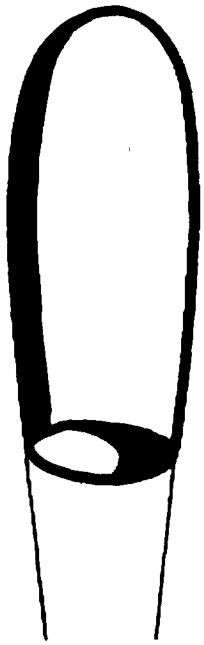

(a) Before Equilibrium

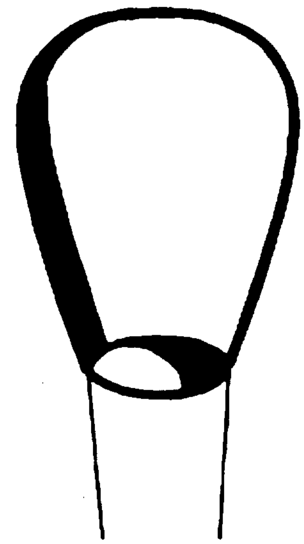

(b) At Equilibrium

Fig. 42. Comparison of Canopy Shapes at Same Mouth Diameter Before and At Equilibrium

generates first stage loads best. During the second reefing stage the effect of added mass is more significant. As a boundary condition, it was reasoned that the true inflation curve must approach the equilibrium curve as full open is approached. These two aids provided points at low reefing ratios and one point at full open through which the true curve must pass.

Because canopy drag is associated with added mass effects, further discussion will be postponed until after the added mass is presented.

4.3.3.1.2 Canopy Added Mass. The added mass analysis began with a literature review. While von Karman[11] provided insight into the physics of the phenomenon and Heinrich[20] performed von Karman's proposed experiment and studied the effect of porosity on the coefficient, Neustadt[42] provided the most immediately practical, quantitative approach. Neustadt assumed the canopy could be represented by an ellipsoid having the same volume and projected diameter and used the well-established relations for the added mass of ellipsoids of revolution from potential flow theory.

Both Heinrich and Neustadt assume the mass is a function of volume. With this assumption, the relative amounts of added mass in each reefing stage can be estimated. Because the mass is quite small during the first reefing stage, it was decided to attribute the entire parachute load to the drag coefficient. The air mass is more significant in the second and third reefing stages because the volume is greater.

The computer program was made to calculate the canopy's "Neustadt ellipsoid" at each integration step. Using potential flow theory, the program calculates the added mass of each ellipsoid. Because of Neustadt's assumptions (potential flow, imporous cloth, equivalent shape), the resultant mass coefficients had to be modified by some factor. This factor was determined by iteration, using the riser load unaccounted for by the drag coefficient.

Figure 43 shows several canopy shapes assumed by the main parachute in Test 80-1R and their equivalent ellipsoids as calculated by the program and drawn to scale.

4.3.3.1.3 Determining $d\overline{s}/d\overline{R}$. Rust's theory requires knowledge of the rate of change of distance with radius, $d\overline{s}/d\overline{R}$. This can be obtained through the radius-time relationship ($d\overline{s}/d\overline{R} = \frac{v}{d\overline{R}_p/dt}$). Rust stated that if the canopy inflow and outflow velocities are known, $d\overline{s}/d\overline{R}$ can be calculated. He showed how it can be done using mass balance to get $d\overline{V}/d\overline{s}$ and combining it with $d\overline{V}/d\overline{R}$ by chain rule. Unfortunately, these velocities are not now known, leaving two alternatives: (1) assume the velocities and adjust to get the correct output (iterative approach), or (2) determine the radius-time relationship from film analysis.

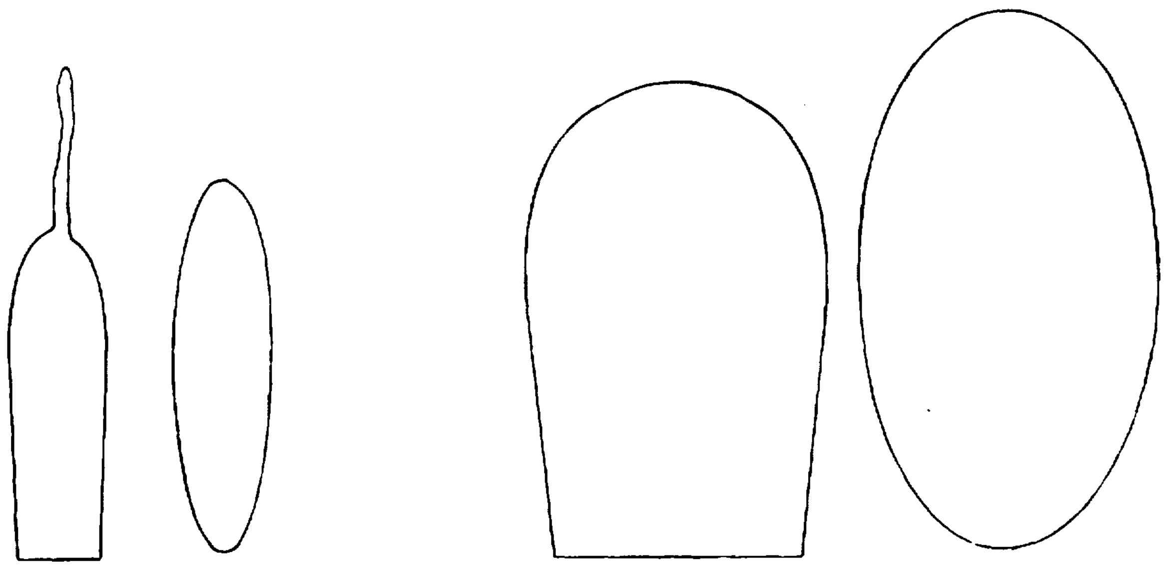

(a) During Phase I

(b) During Phase V

Fig. 43. Comparison of Canopy Shapes with Their Equivalent Ellipsoids

The latter is chosen because an iterative approach is already being used for the drag and added mass coefficients. The diameter-time data are determined from the film analysis and used by the computer program to calculate instantaneous values of dR_p/dt and then $d\overline{s}/d\overline{R}$.

4.3.3.1.4 Film Analysis. Films from Test 80-1R were analysed to determine the canopy shape parameters. Measurements of the eccentricity of the elliptical portion of the canopy, the characteristic radii defining the phases of inflation, and the inflated length of the canopy in the first phase were obtained from the flight test films. This analysis required more detail than the film analysis described in Section 4.2.

Eccentricity versus time for the first three phases of inflation was taken from air-to-air and ground-to-air film coverage (See Figure 44). Because of the obliqueness of the parachute axis

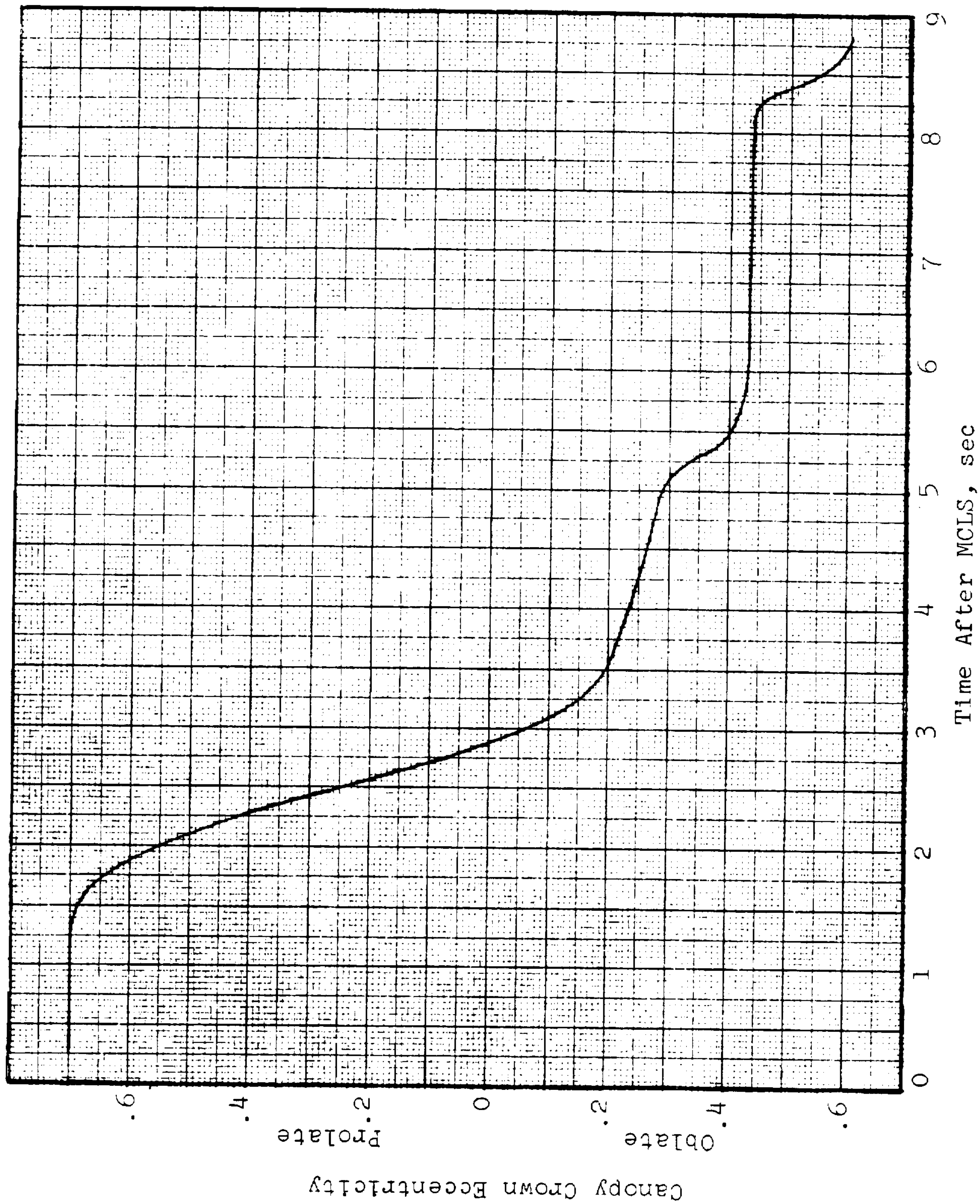

Fig. 44. Canopy Crown Eccentricity Versus Time After MCLS

to the camera line of sight, the eccentricities could not be precisely measured. This obliqueness is not excessive during the first two phases but becomes considerable after that.

During the first two phases, the canopy crown shape is similar to a prolate hemispheroid. The transition to an oblate hemispheroid occurs during the third phase. During this phase, the inlet radius is restricted by the reefing line, yet the canopy continues to inflate by bulging out, causing the crown to pull in and become oblate. After the transition from prolate to oblate, the canopy remains oblate.

Rapid breathing of the canopy was observed in the middle of Phase III at a time when severe fluctuations of eccentricity and dynamic drag area occurred. The cause is not known. Perhaps the increasing projected radius makes the parachute more responsive to the vehicle wake. This breathing was not observed at any other time. Figure 44 presents faired data.

The parachute projected radius was measured as a function of time from onboard films. These values appear in Figures 45, 46, and 47. Because of a lack of any accurate reference lengths in the films, the radii may not be exact. The dimensions were based on known unloaded reefing line lengths. The characteristic radii defining each phase of inflation are tabulated in Table 27.

The distance the airball has progressed as a function of dimensionless projected radius during Phase I is used to calculate inflated volume during that phase. It can be seen in Figure 48 that the relation is linear. No change in the rate of progress of the airball can be detected near the vent.

4.3.3.2 Results. Those parachute parameters which were determined by iteration and the final loads and trajectory prediction of Test 80-1R are presented here.

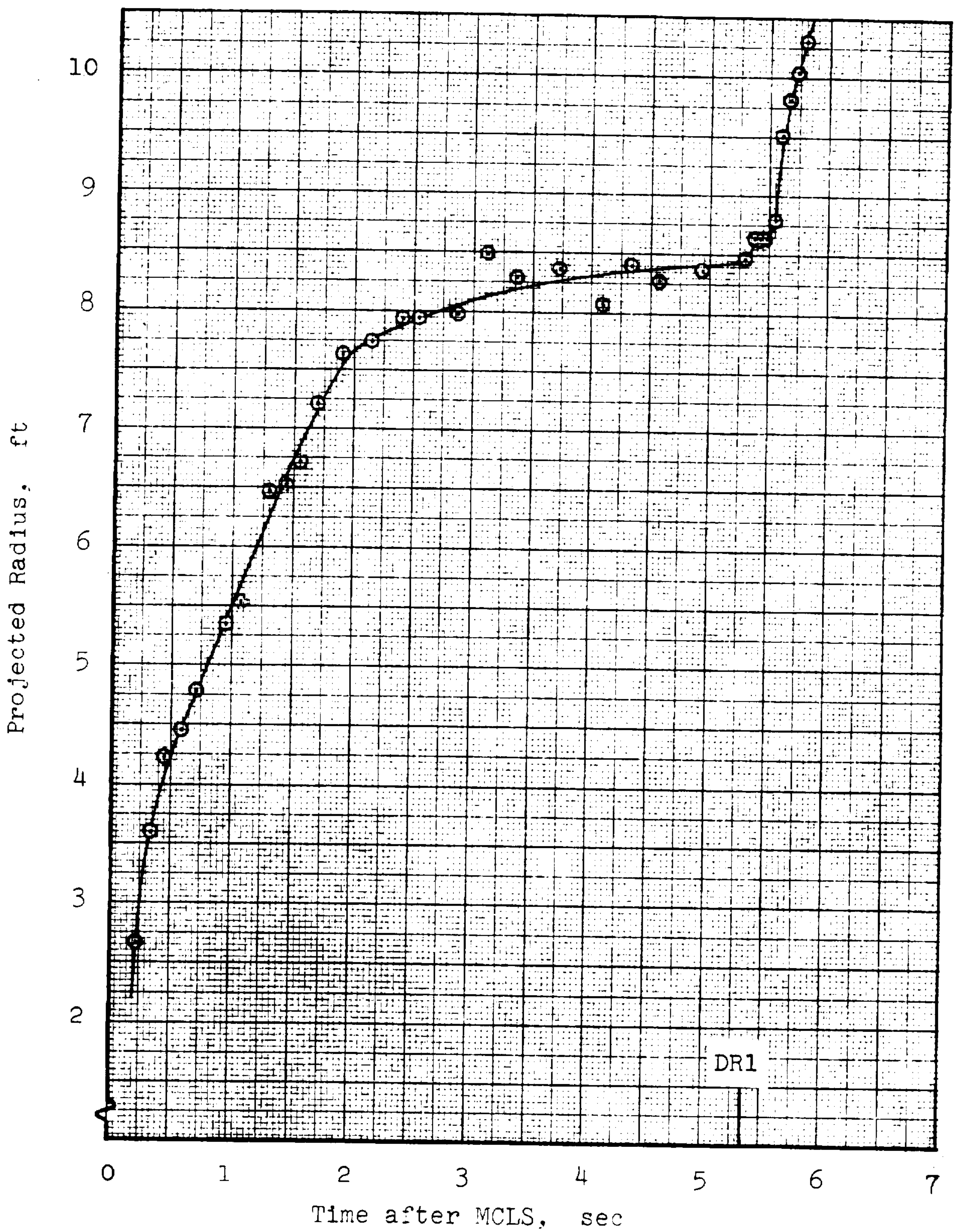

Fig. 45. Main Parachute Canopy Projected Radius Versus Time after MCLS for First Stage Opening

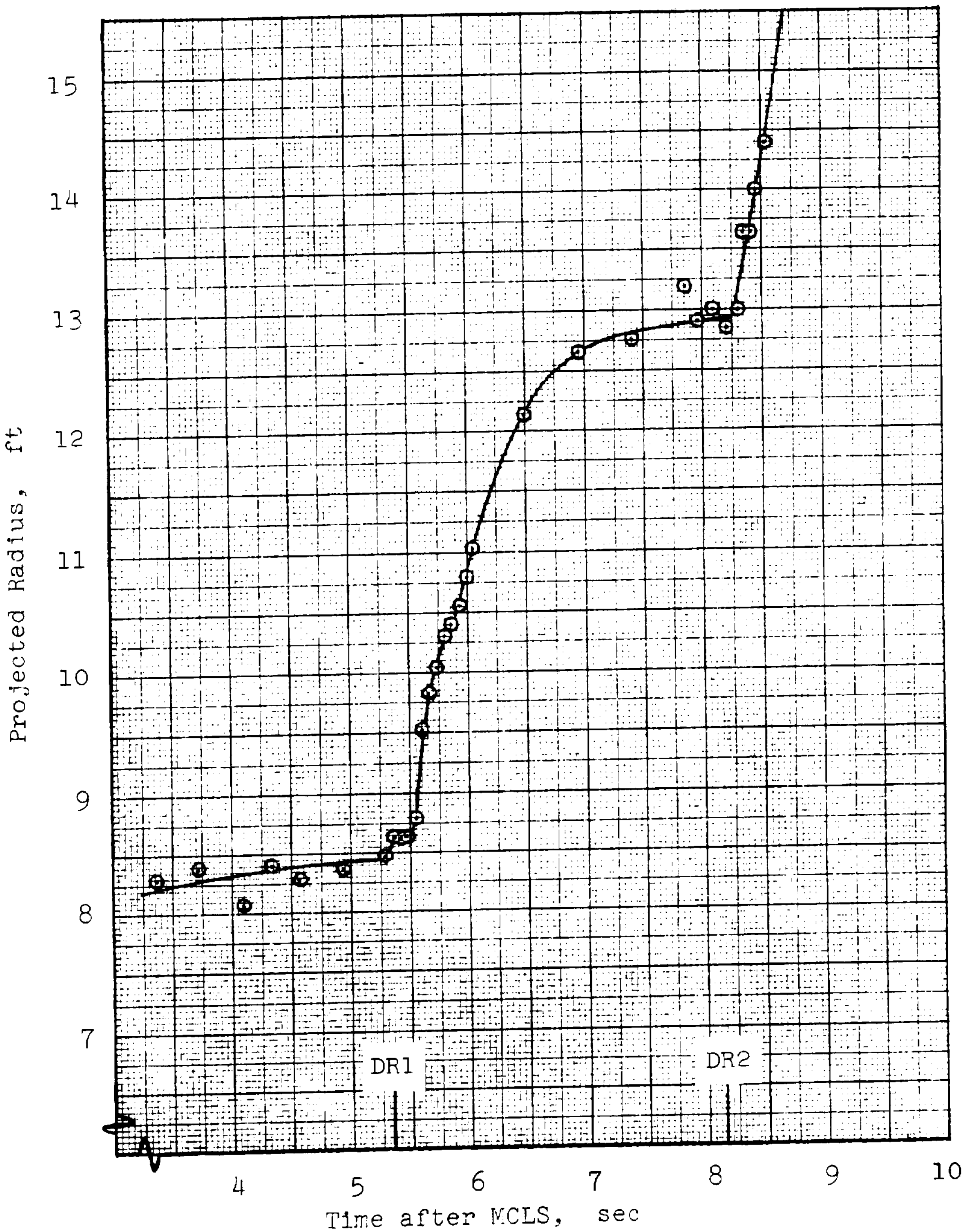

Fig. 46. Main Parachute Canopy Projected Radius Versus Time after MCLS for Second Stage Opening

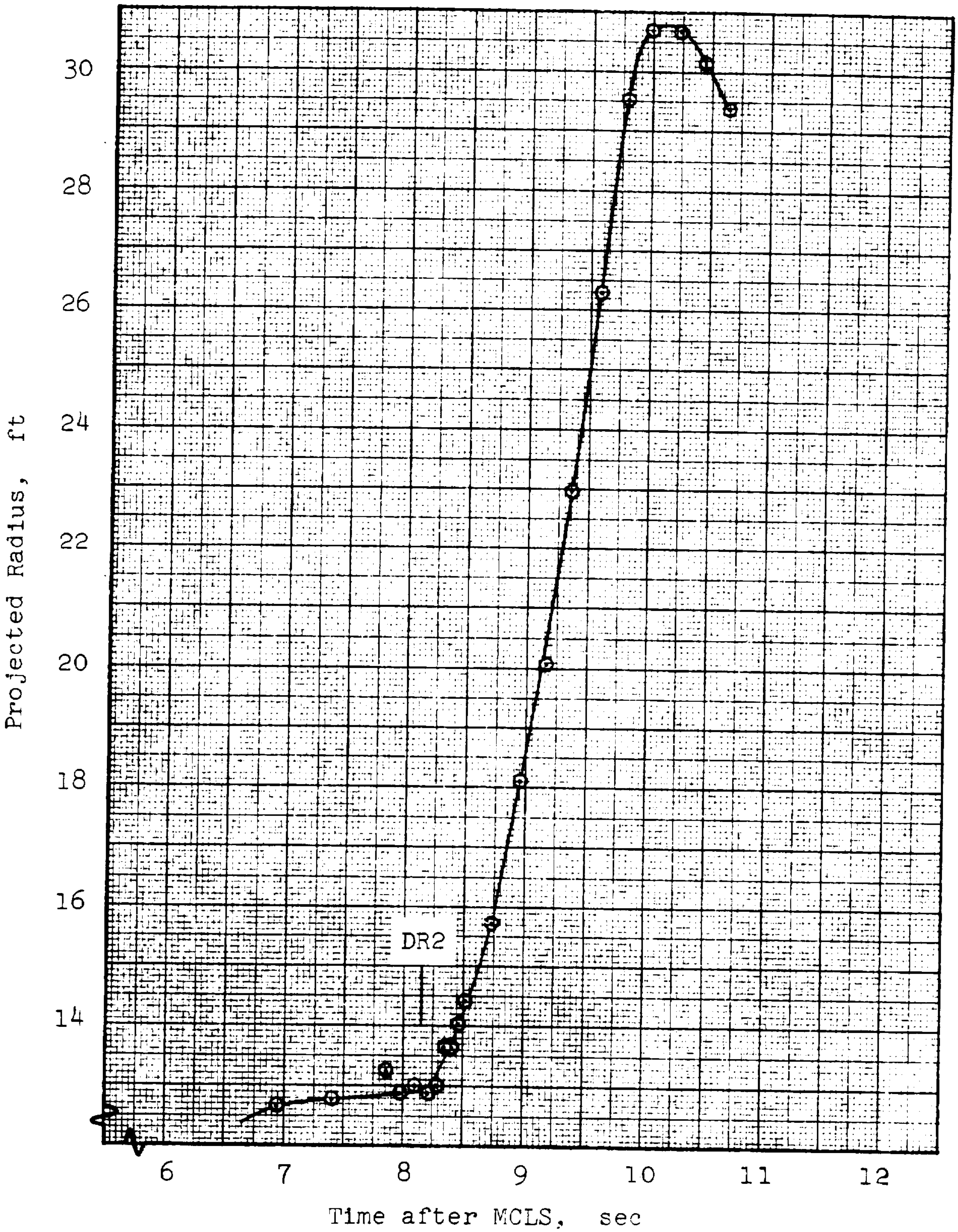

Fig. 47. Main Parachute Canopy Projected Radius Versus Time after MCLS for Third Stage Opening

C-3

Table 27. Characteristic Radii

Characteristic Radius	Dimensionless Radius
$\overline{R}*$	.105
$\overline{R}_{r_{i_1}}$	.154
$\overline{R}_{r_{f_1}}$	.20
$\overline{R}_{r_{i_2}}$	.274
$\overline{R}_{r_{f_2}}$	.304
$\overline{R}_o$	.704 (Steady State) .725 (Overinflation)

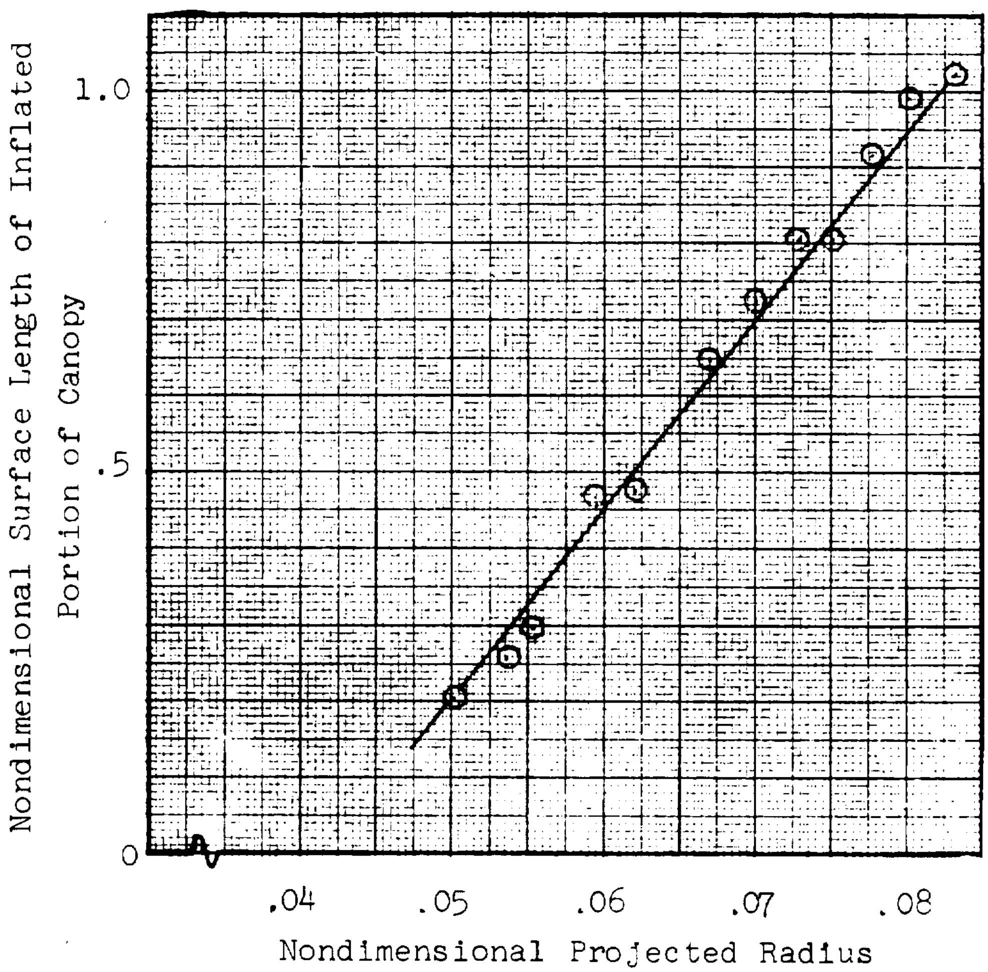

Fig. 48. Nondimensional Surface Length of Inflated Portion of Canopy Versus Nondimensional Projected Radius

Two canopy drag area functions were used:

a) for the first stage

$$C_DS_c = 5363.\ (R/R_o)^{1.3} - 10.\ \text{and}$$

b) for all other reefing stages

$$C_DS_c = 7980.\ (R/R_c)^{1.385}$$

These functions are compared with the equilibrium dynamic drag area, discussed in Section 4.3.3.1.1, in Figure 49.

The first function gave good dynamic drag area results, with no added mass, during the first stage of inflation (see Figure 50). The second function gave reasonable dynamic drag area results, with added mass, during the second stage of inflation. (see Figure 51).

Some difficulty arose because drag area was based upon canopy inlet size (reefing ratio). Rust's idealized canopy geometry does not allow for skirt bunching, which alters the crown eccentricity observed in flight test films. Use of the observed eccentricity with Rust's relations results in large inlet sizes and larger C_DS than actual.

This problem would not exist if drag as a function of projected radius were known (as would be the case with wind tunnel experiments).

The added mass of the parachute canopy as predicted by the method of equivalent ellipsoids is presented in Figure 52. Predictions are made only during the inflation phases; no prediction is needed during the reefed phases, which accounts for the gaps in Figure 52. In an attempt to compensate for Neustadt's assumptions, computer runs were made with the added mass from the theory modified by a factor to determine what factor gave the best results (multiplying factors of 0.0, 0.5, 1.0, 1.5 and 2.0 were used).

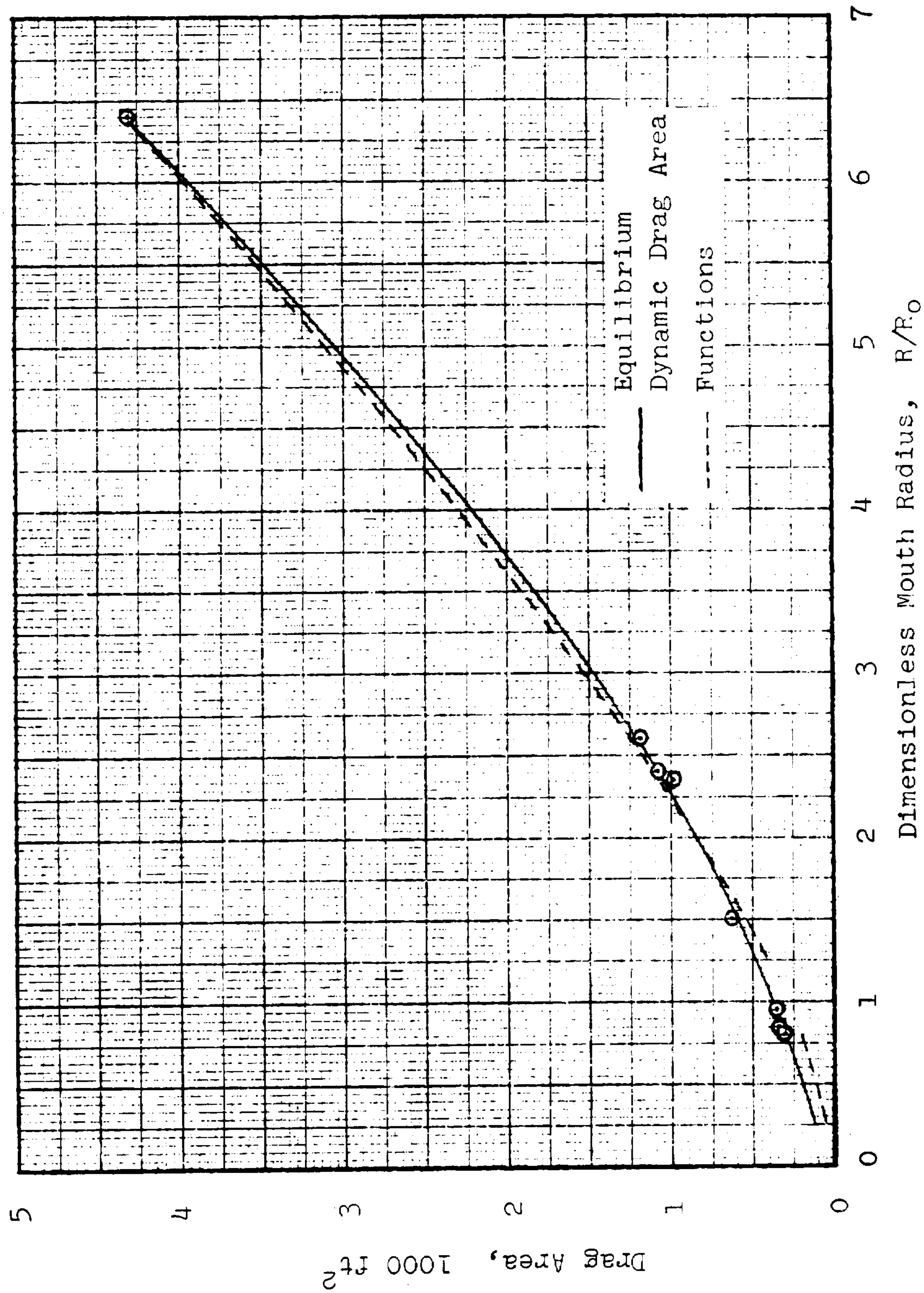

Fig. 49. Drag Area Versus Dimensionless Mouth Radius

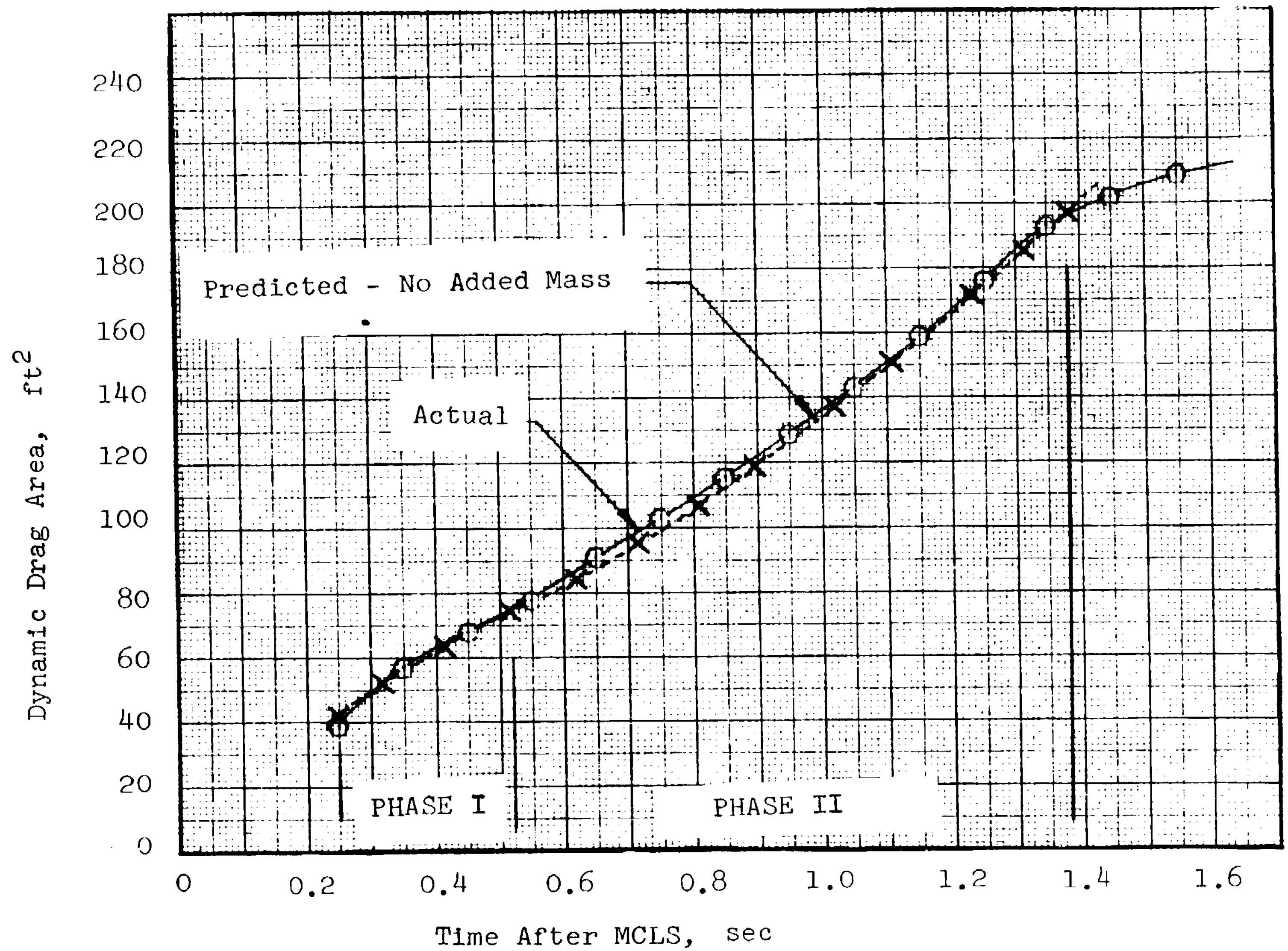

Fig. 50. Comparison of Actual Dynamic Drag Area with Computer Result During First Stage Inflation

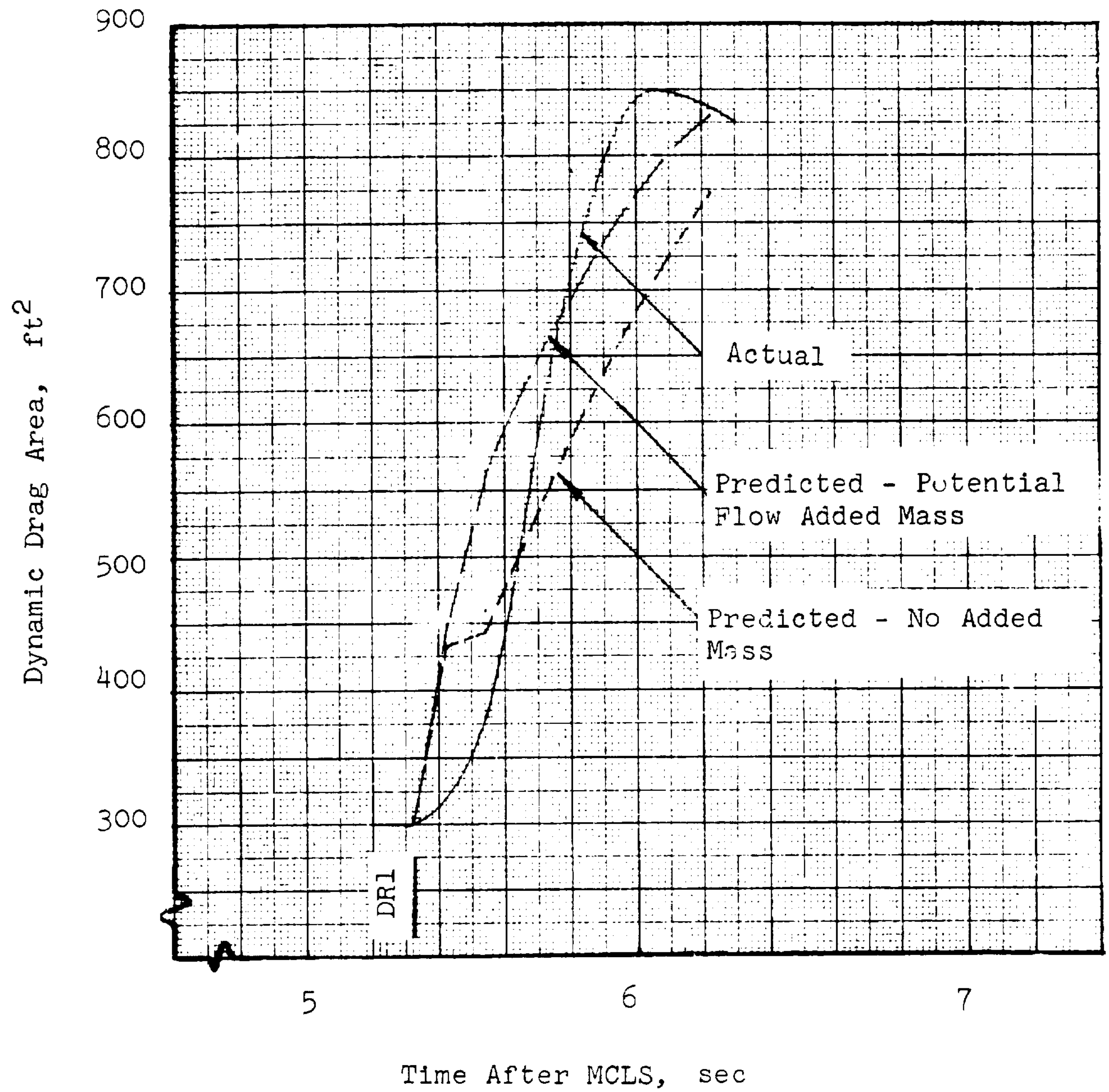

Fig. 51 . Comparison of Predicted and Actual Dynamic Drag Areas

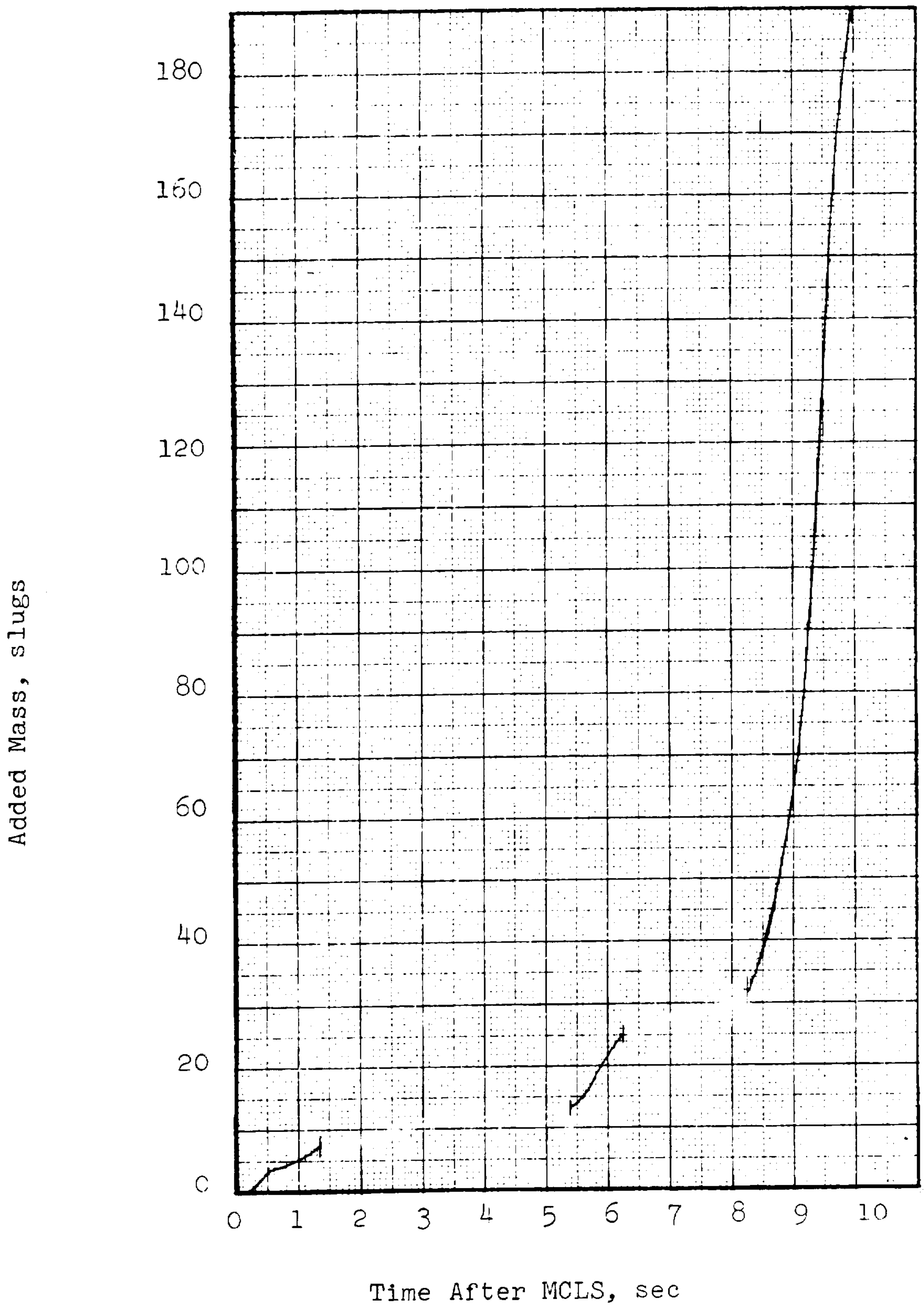

Fig. 52. Potential Theory Added Mass Versus Time After MCLS

As mentioned above, first stage loads were obtained using no added mass. The first two phases used $C_DS_c = 5363\ (R/R_o)^{1.3}-10$, and the third phase used an empirical C_DS-time relationship. The first stage loads and trajectory information appear in Figures 53, 54 and 55.

Excellent first stage loads and trajectory predictions have been made. The peak opening load was close to the measured peak and the predicted and actual dynamic pressures correlated well. However, predicted flight path angles lagged the actual. This problem has been attributed to imprecise $d\bar{s}/d\bar{R}$, a result of inaccurate film analysis of projected radius. The second stage loads and trajectory information appear in Figures 56, 57 and 58. For clarity, only those curves for which the added mass factor is 0.0, 1.0, and 2.0 are shown.

It can be seen that the larger the added mass, the greater the peak load and the earlier the peak load time. The predicted loads are low because the dynamic pressures are low. The lower than actual dynamic pressure has been caused by the following:

a) At disreef, the dynamic pressure was about 1 psf lower than actual. The continuing $d\bar{s}/d\bar{R}$ inaccuracy caused greater dynamic pressure discrepancies during the second stage.

b) Because an instantaneous Phase IV was assumed (by Rust, and therefore, here), the predicted loads rise at disreef unlike the actual (the assumption means that the inlet diameter instantaneously increases to the condition of tangency). It can be seen that the impulse of the predicted riser load is about twice the actual, causing an excess dynamic pressure loss of 1.0 - 1.5 psf, a significant amount

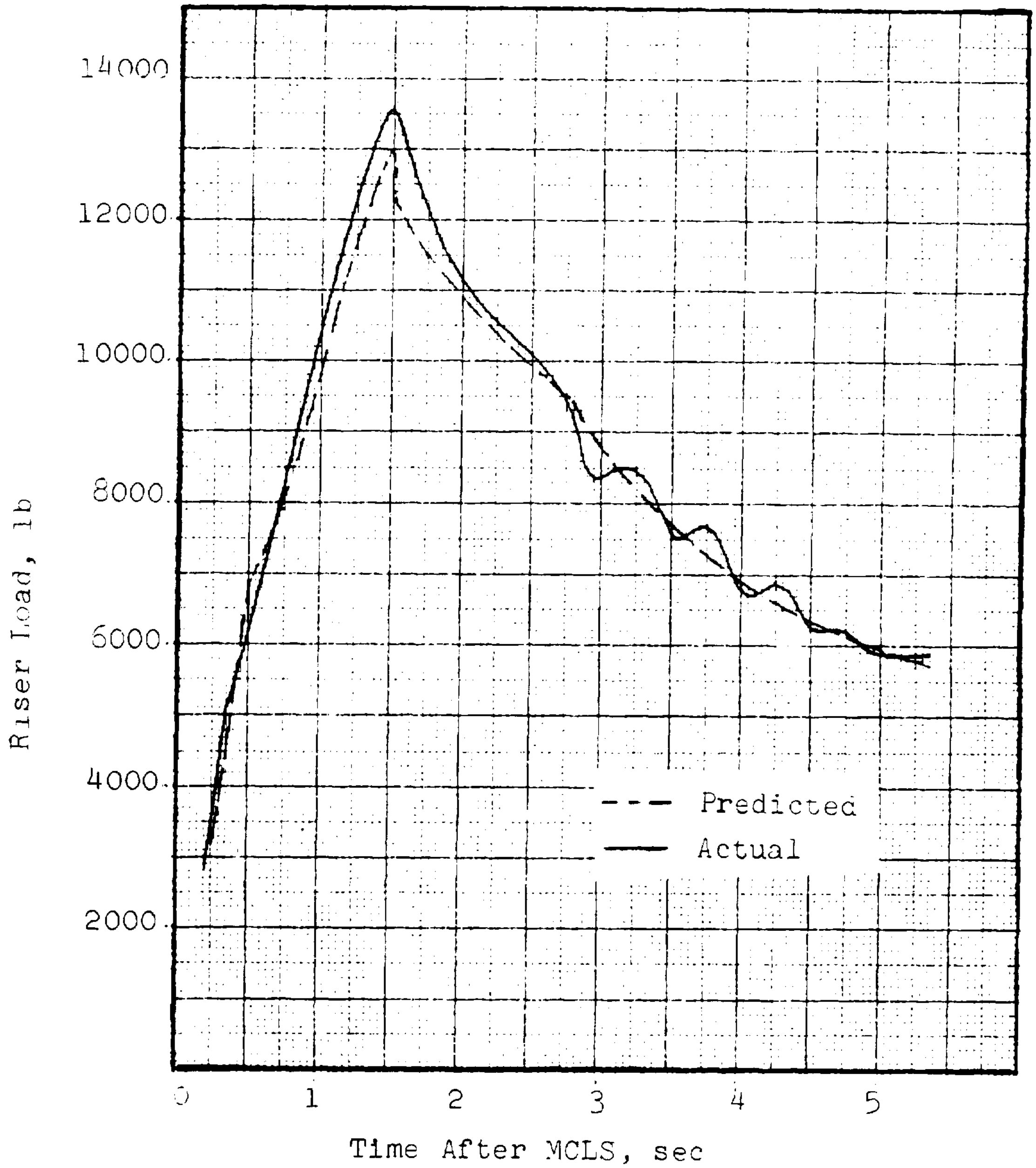

Fig. 53. Comparison of Predicted and Actual Riser Load for First Reefing Stage

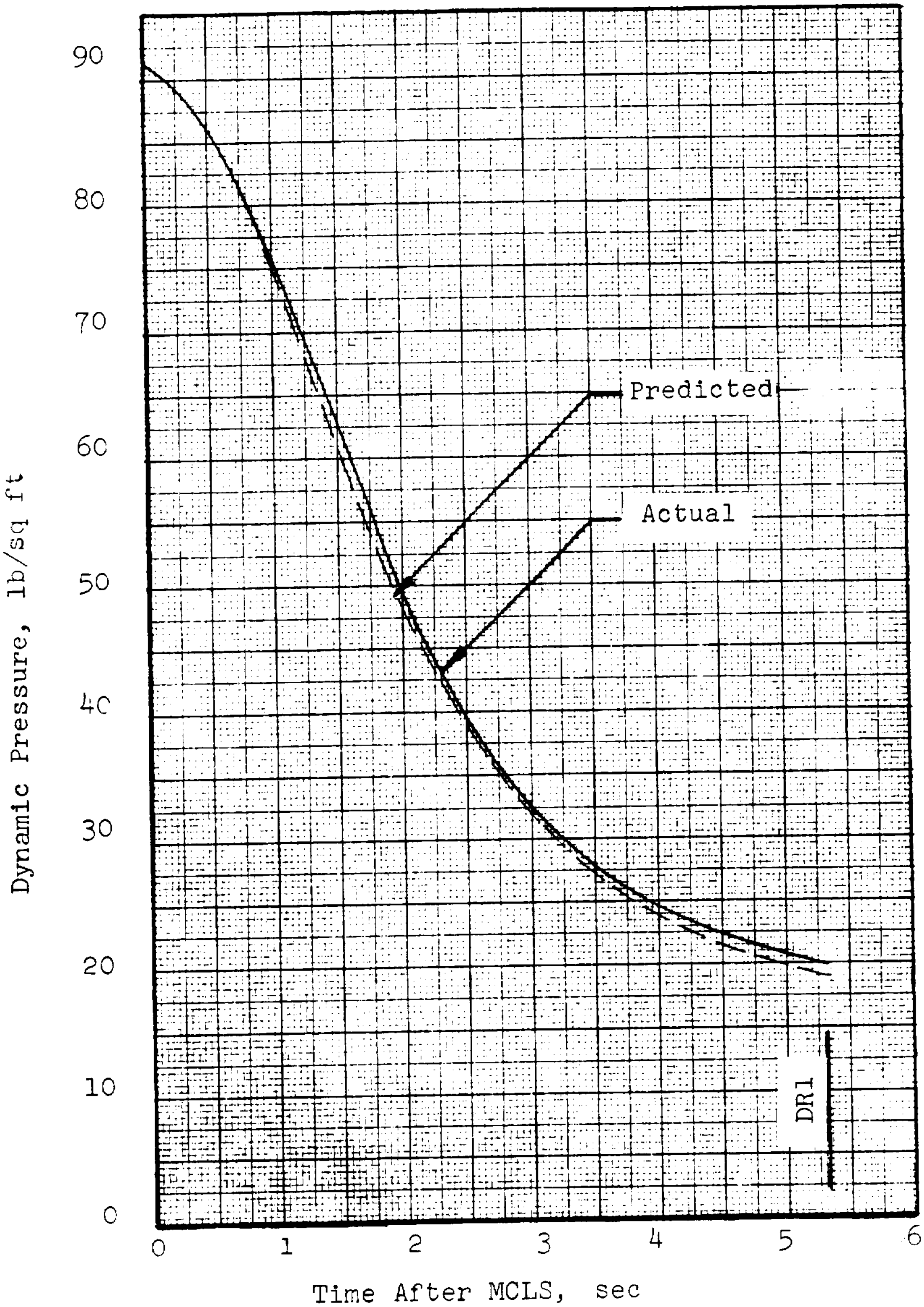

Fig. 54. Dynamic Pressure Versus Time After MCLS

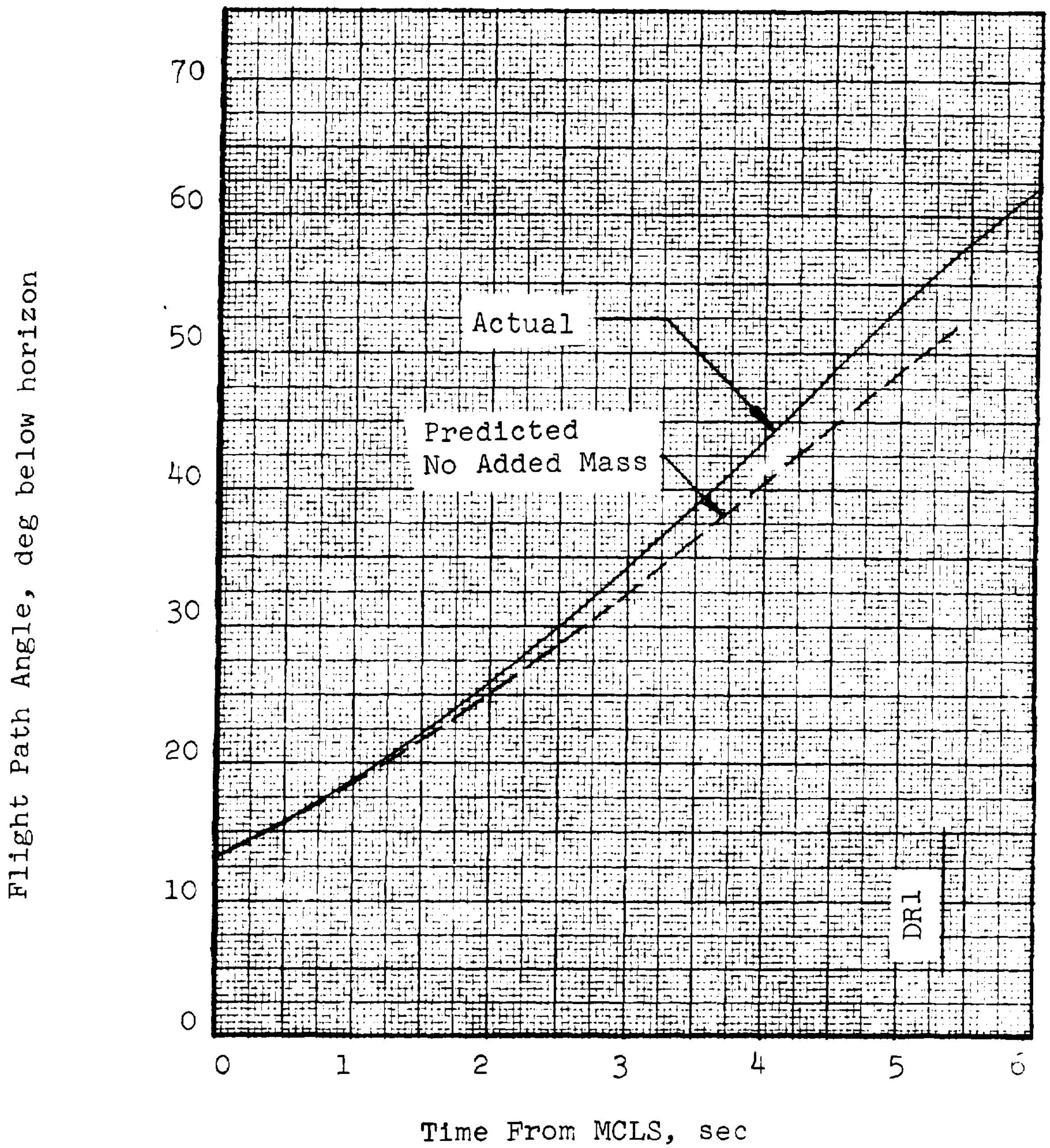

Fig. 55. Comparison of Predicted and Actual Flight Path Angles

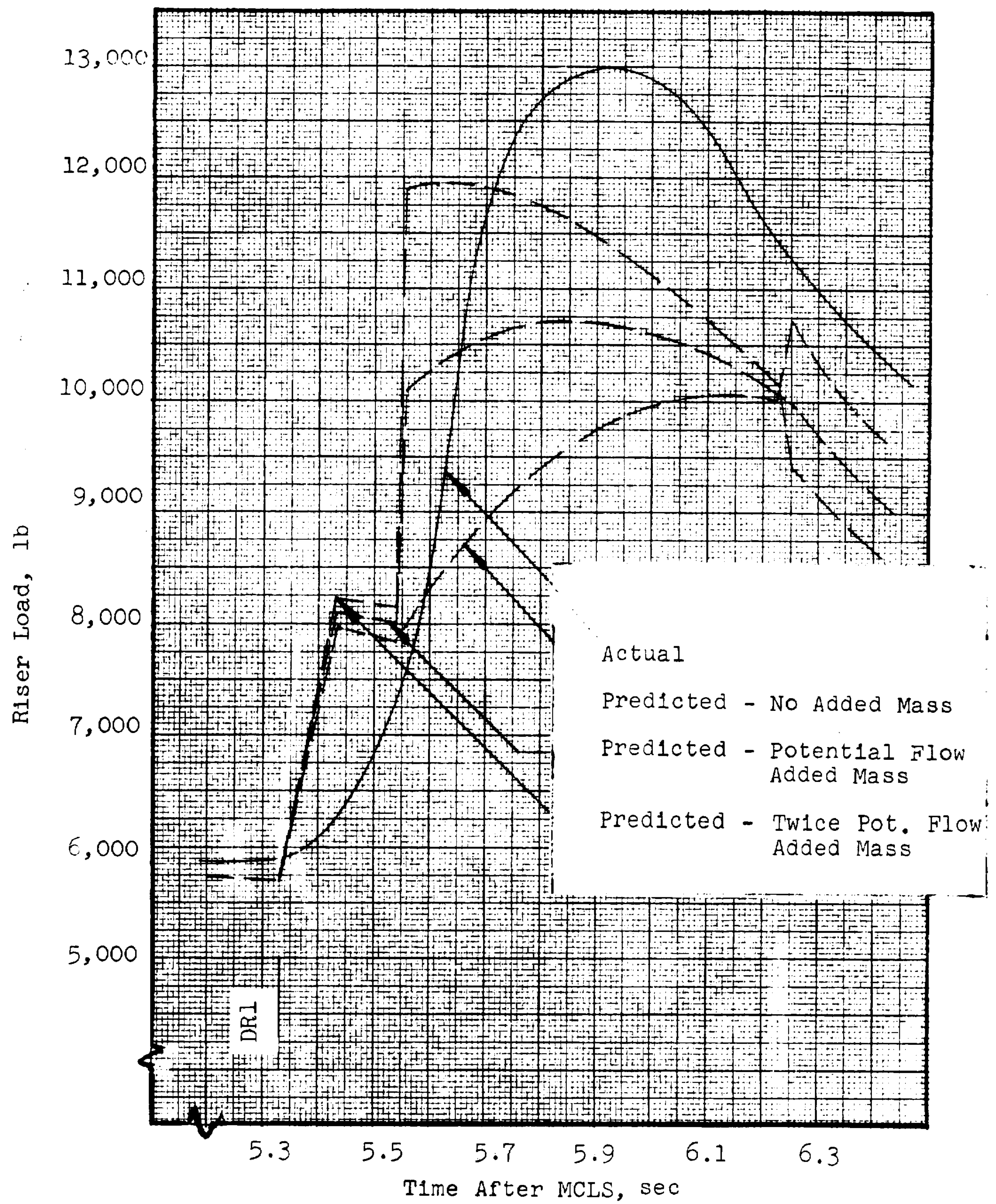

Fig. 56. Comparison of Actual and Predicted Second Stage Loads

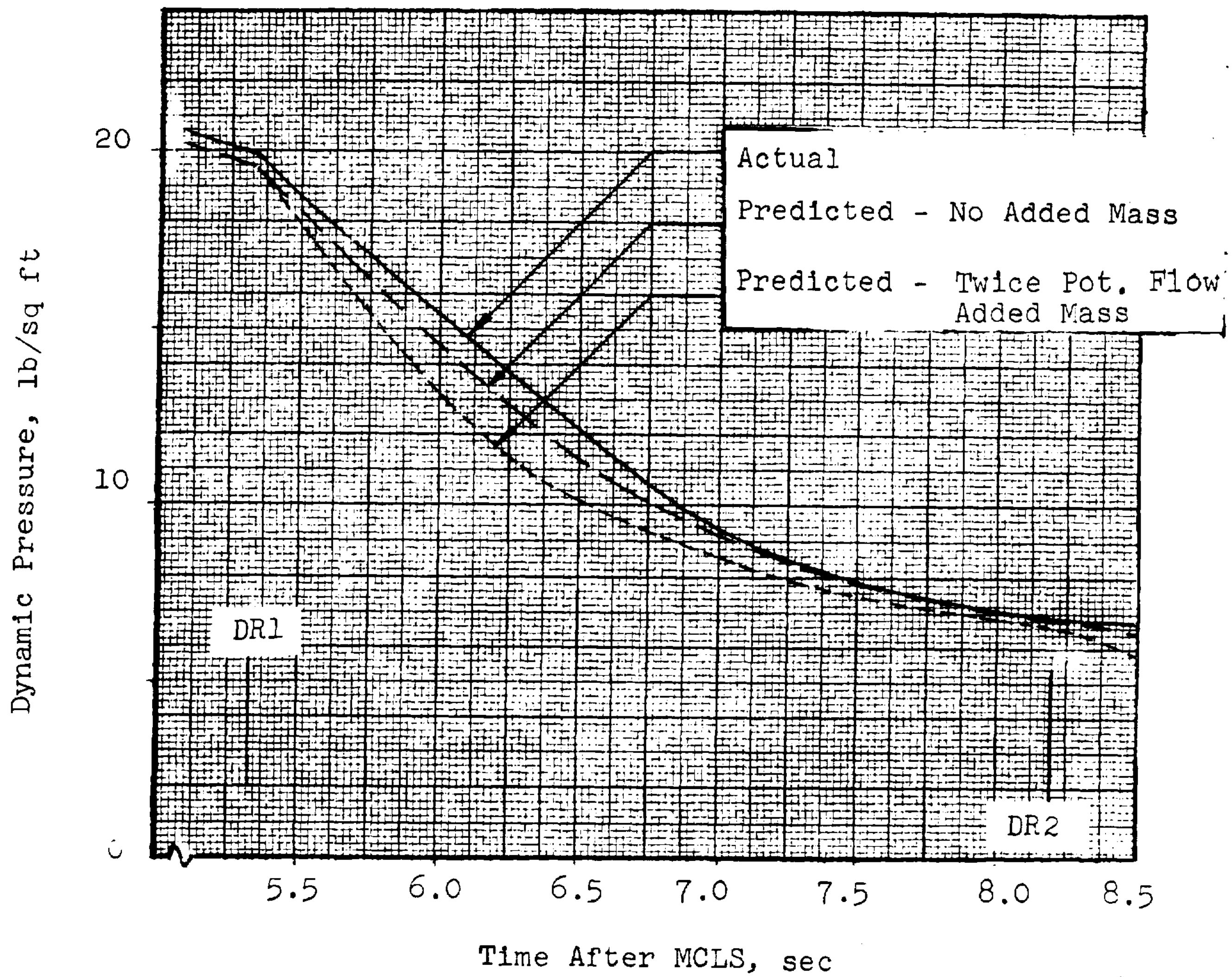

Fig. 57. Comparison of Predicted and Actual Dynamic Pressures

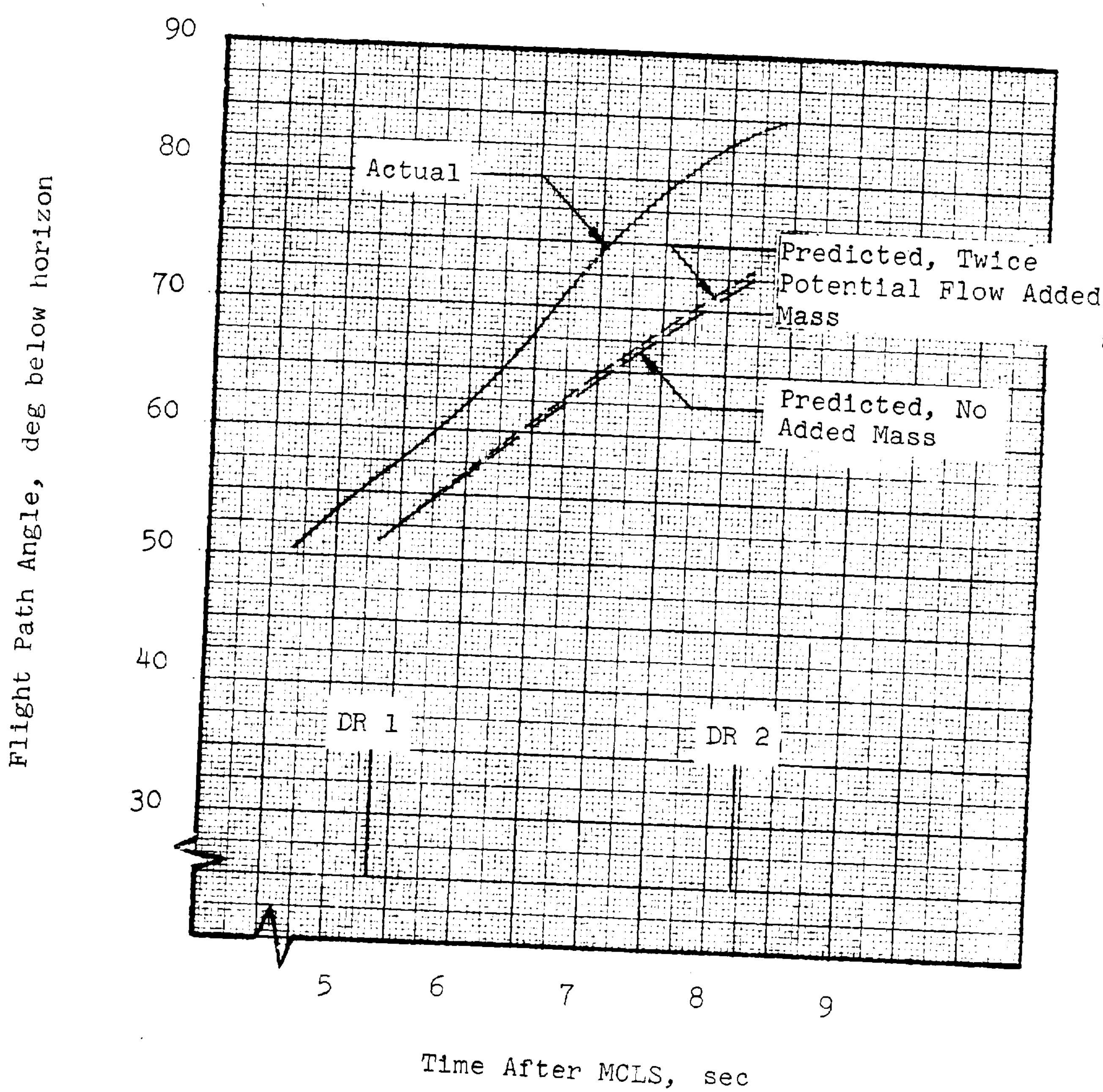

Fig. 58. Comparison of Predicted and Actual Flight Path Angles During Second Stage

considering the large drag areas. Subsequent development of the Shape/Distance Method should include removal of the assumption that Phase IV is instantaneous.

When using the projected radius - time method of determining $d\bar{s}/d\bar{R}$ outlined in Section 4.3.3.1.3, it is important to curve fit the input radius-time data. At first, actual radius-time points were provided to the computer, which calculated dR_p/dt from the points. Because the added mass effects are very sensitive to the slope dR_p/dt, results were as in Figure 59. That is to say, the use of a discontinuous dR_p/dt resulted in discontinuous loads. The smooth curve in Figure 59 resulted from using a continuous dR_p/dt function obtained from a curve fit of the data.

The third stage loads reflect this phenomenon, for there was not time to curve fit the data. Again, loads are presented for added mass factors of 0.0, 1.0, and 2.0. It can be seen in Figure 60 that the load peak times become earlier as the added mass factor increases. Once again loads are low because dynamic pressure (Figure 61) is low. As in the second stage, a distinct Phase IV is needed.

4.3.4 Summary

To fulfill the need for a satisfactory analytical model of the parachute inflation process, and in order to better understand and predict the loads observed during the process, a start was made at developing the Shape/Distance Opening Load Prediction Method during the Apollo analysis study.

The method which has been developed for the prediction of opening loads for a single Apollo main parachute was adapted from the work of Rust.[29] Rust's theory was chosen because, of all the approaches studied, it provided the best combination of completeness, lack of restrictive assumptions, simplicity, and applicability to the Apollo parachutes.

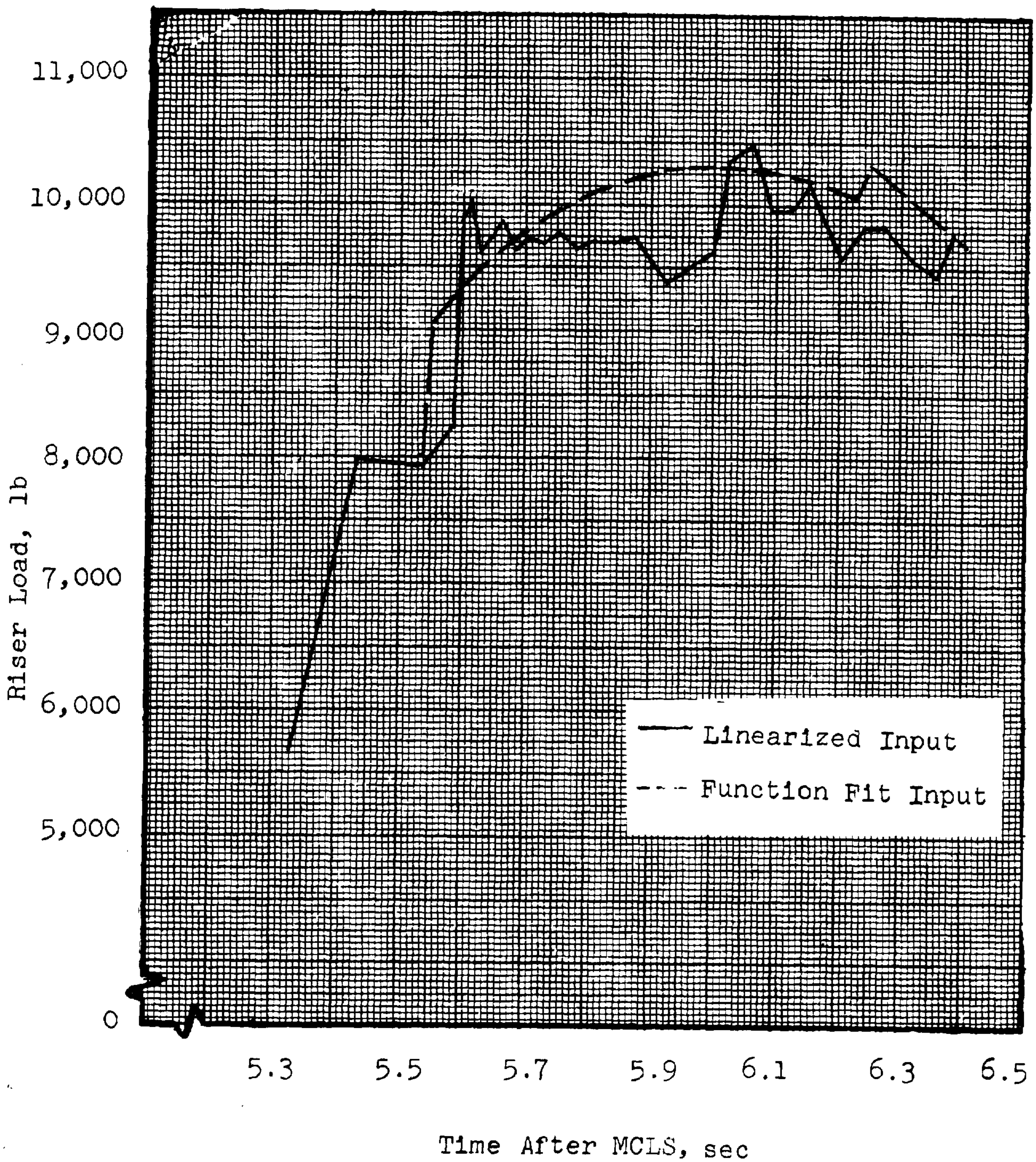

Fig. 59. Comparison of Computer Resultant Loads with Linearized dR_p/dt Input and with Function Fit dR_p/dt

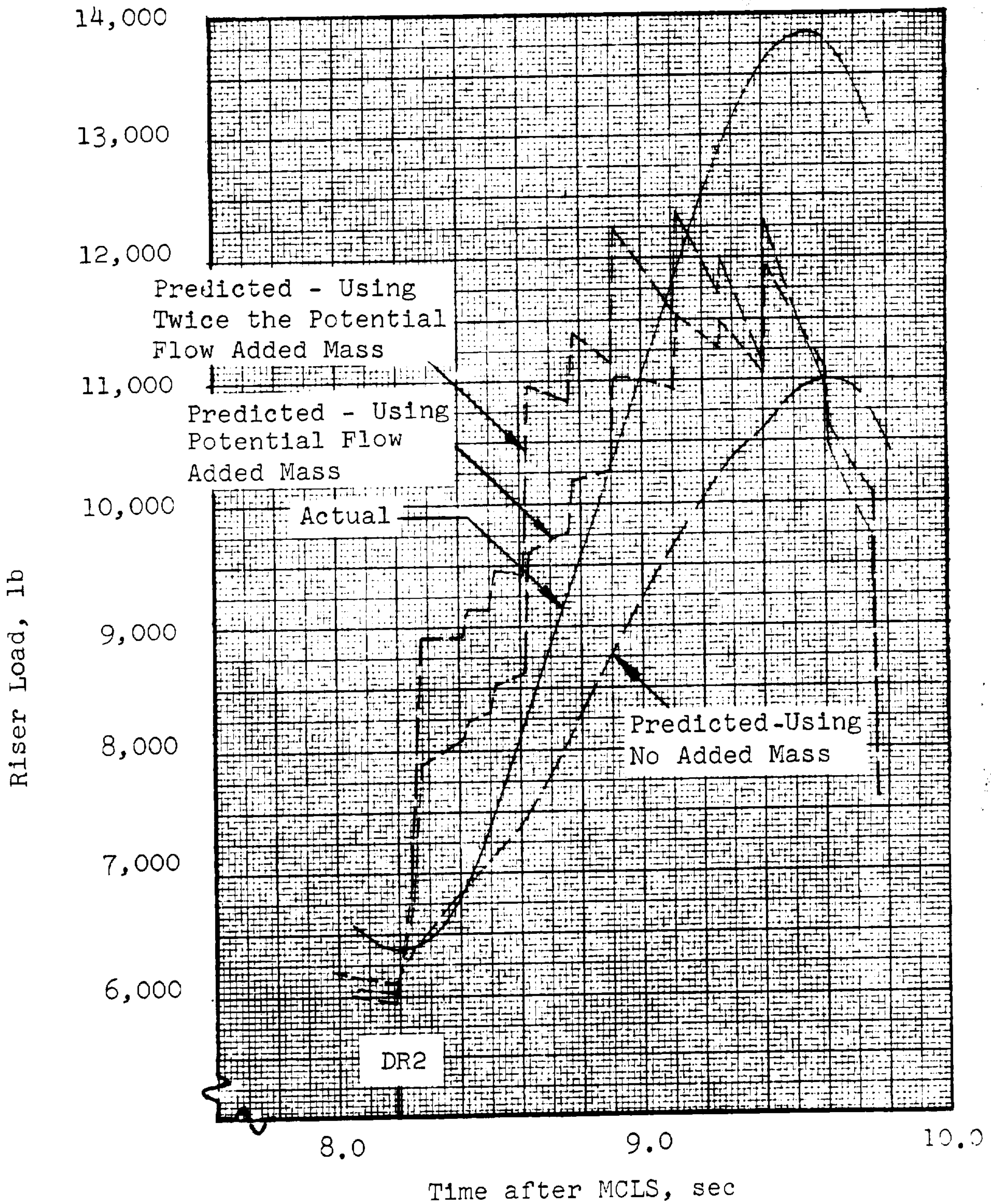

Fig. 60. Comparison of Predicted and Actual Third Stage Loads

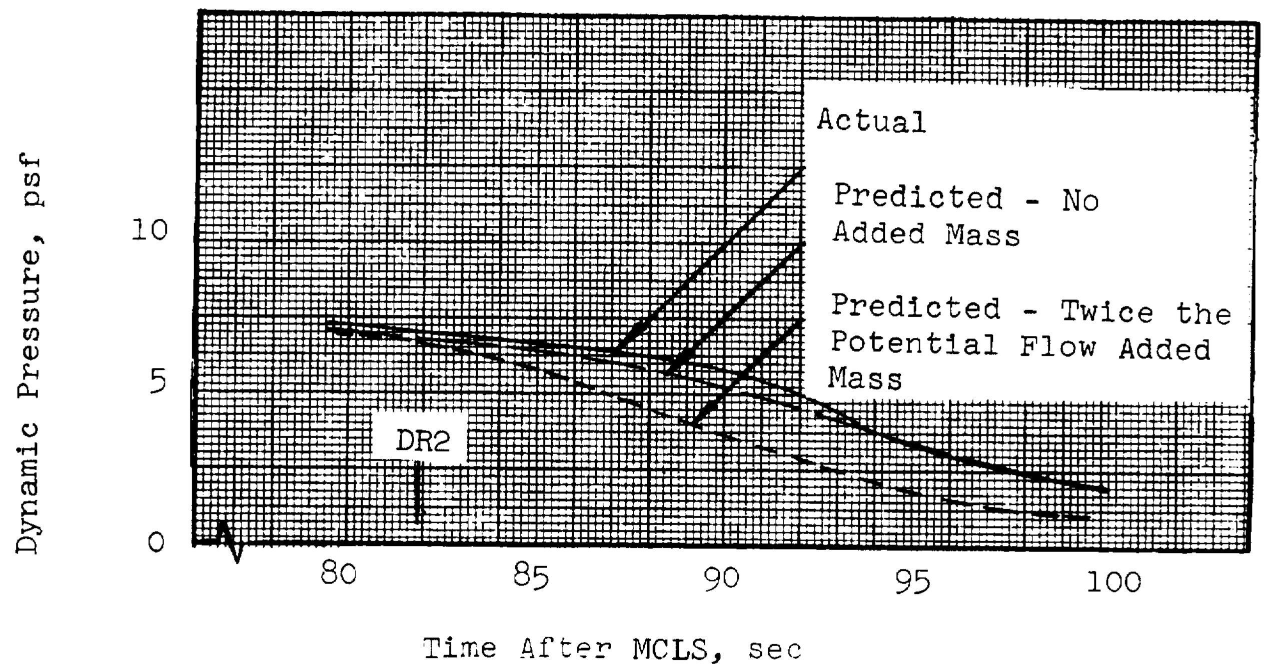

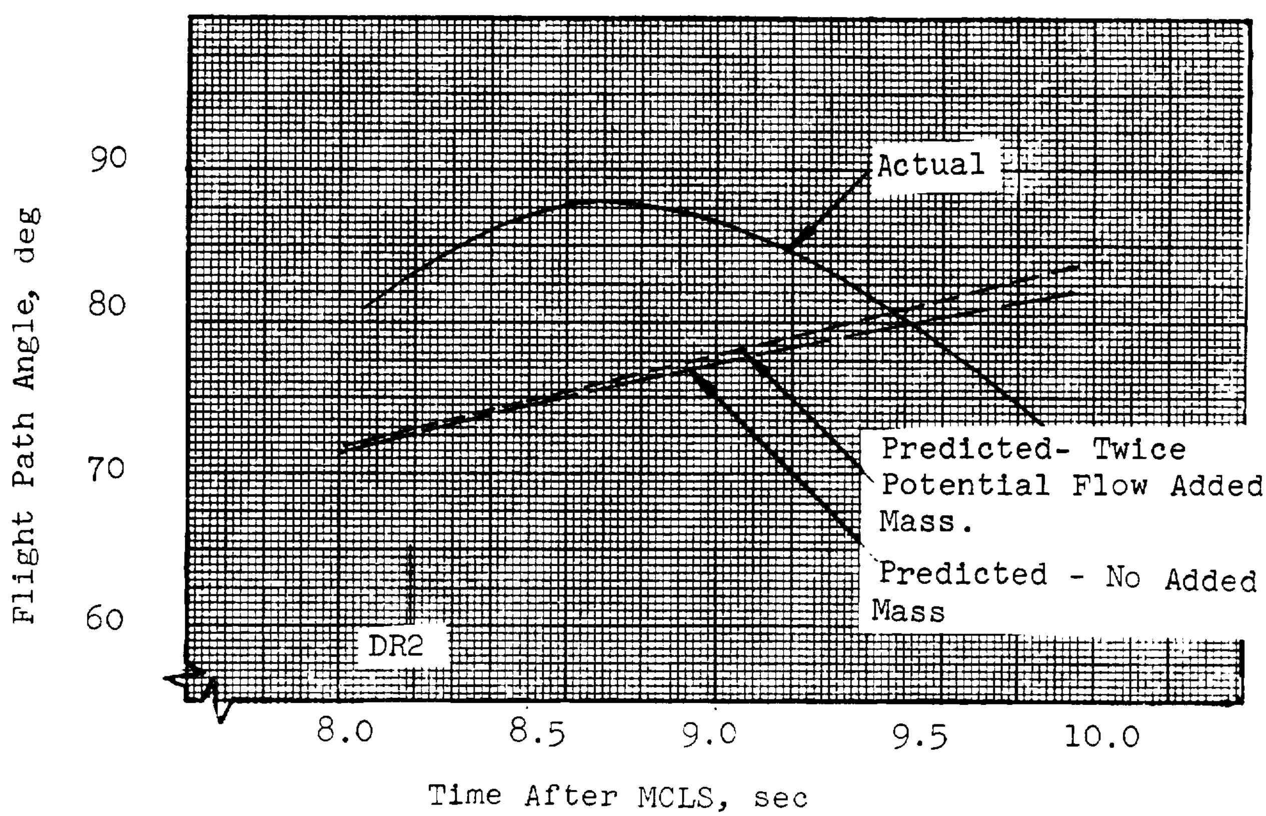

Fig. 61. Comparison of Predicted and Actual Dynamic Pressures and Flight Path Angles for Third Stage Inflation

Good progress has been made in that (1) the method has been programmed for the computer in a form that accommodates many of the special features of the Apollo system, including reefing, and (2) all input data have been estimated for the Apollo main parachute. While initial results are encouraging, difficulties in estimating the input data arose because of the inadequacy of information on certain of the basic parachute parameters.

4.4 SUPPLEMENTARY STUDY

When the Mass/Time Method had been established for single parachute tests, and the Shape/Distance Method had been brought to its present state of development, there were still some questions of interest which had not been answered.

These questions were:

a) How can the Mass/Time Method be applied to cluster cases?

b) What is the effect of including the added mass terms in the flight path angle equation derived in Section 6.3?

c) Are Rust's basic assumptions valid?

While there were other questions remaining, it was realized that these three important ones could be answered by a short supplementary study. This study was carried out and is described here.

4.4.1 Approach

The technical approach was to answer all three questions jointly. It was realized that this could be done with several modifications of the computer program for the Mass/Time Method.

The first modification was the incorporation of the added mass term in the flight path angle equation, in a manner similar to its incorporation in the velocity equation. Thus, the flight path angle equation was changed from:

$$m\dot{\gamma} = - \frac{mg \cos \gamma}{V}$$

to:

$$(m + m_a)\,\dot{\gamma} = - \frac{mg \cos \gamma}{V}$$

The second modification was the incorporation of Rust's basic assumptions. The assumptions included were:

a) That parachute added mass and drag area are unique functions of the state of parachute opening (for a specific parachute at a specific altitude).

b) That the state of parachute opening is a unique function of the distance the parachute has traveled since the beginning of inflation (in any particular stage).

While it was believed that these assumptions were valid from an engineering point of view, their validity had not been demonstrated during the present study. It was reasoned that a good way to prove their validity would be to incorporate them in the computer program for the Mass/Time Method and see how they worked. To include the two assumptions noted, it sufficed to express drag area as a function of the distance traveled since the beginning of the stage for which the loads were being calculated. Because added mass was already expressed as a function of drag area in the Mass/Time Method, added mass automatically became a function of the distance traveled since the beginning of the stage. Another consequence of this modification was that a given parachute would open in a fixed distance. This is the same assumption that was made in the Mass/Time Method to determine filling time. But here, as in the Shape/Distance Method, filling time does not need to be predetermined; rather, the filling time is determined by the method as a side result of the opening load and trajectory calculations. It was this fact that allowed the modified method to be used in cluster cases. The two difficulties posed to the Mass/Time Method by the cluster case that could not be readily accommodated were the determination of drag areas and filling times. The aerodynamic interference in the cluster case affects the drag area. And the effect of nonsynchronous disreefing is to make the filling time harder to determine than in the single parachute case. Of course, these same difficulties were successfully solved during the development of the Mass/Time Method for single parachutes; and the approach to solving them in the cluster case would be the same as it was in the single parachute case. Unfortunately, there was not sufficient time at end of the Mass/Time Method study to pursue the iterative procedure required to determine drag areas and filling times(or the filling distance constant K_f) for the cluster case. So, as stated above, the modified Mass/Time Method, because it would not require predetermined filling times, was regarded as a fairly quick means of looking at the cluster case. The problem of determining drag area could not be avoided as in the case of filling time. Therefore the scheme established in the Mass/Time Method for single parachutes for determining drag area was used in the cluster case. As expected, use of the single chute parameters caused the accuracy of the calculated loads to be poor.

Using the approach outlined above, the modified Mass/Time Method was formulated and applied to several of the tests for which data were available. These tests included the six single chute tests on which the Mass/Time Method had been used, three two-chute cluster, ICTV tests, and one three-chute cluster, PTV test. The modified method was applied to the single chute tests, both with and without the changed flight path angle equation. The set of calculations without the changed equation showed that the method was working properly, and therefore that Rust's basic assumptions would provide a good engineering approach. The set with the changed equation showed that, within the context of Apollo main parachutes, the change did not affect the opening loads significantly. The modified method was then applied to the cluster cases. The method worked reasonably well on the cluster cases, considering that no correction was attempted for the aerodynamic interference. The method was able to handle the clustered parachutes in that it predicted fairly accurate filling times. However, the opening loads were generally too high, indicating the necessity of a reduction in drag area due to aerodynamic interference. It should be pointed out that one set of general parameters was determined, with the aid of results developed in the Mass/Time Method study, and these general parameters were then applied to all tests studied, single and cluster cases. Furthermore, there was no time remaining to modify these parameters. Therefore the results to be presented in Section 4.4.3 represent the very first attempt at predicting loads with the modified Mass/Time Method. It is expected, therefore, that these results could be significantly improved upon thorough development of the general parameters for application to the cluster cases.

4.4.2 Modified Mass/Time Method

The technical approach of the modified Mass/Time Method is outlined above. The modifications of the computer program have been indicated in a most general form, though they are presented in detail in Reference 41. What remains is to describe the general parameters used by the program. These parameters were determined on the basis of results of the Mass/Time Method study, and represent the first attempt at their determination.

a) Filling Distance. The distance required for a parachute to open in one of its stages was expressed as a function of the drag area growth. This is quite similar to the approach taken in the Mass/Time Method. Figures 62, 63 and 64 show the graphs used to determine opening distance in the first, second and third stages, respectively. These figures show filling distance as a function of area growth. To use them, the area growth for each stage must be known. For example, in Test 80-3R1, the drag area grew from 320 sq ft at the end of Stage 1 to 1067 sq ft at the end of inflation in Stage 2 (1067 = (1186)(0.80), where 1186 sq ft was the drag area at the end of Stage 2, based on the reefing ratio.) Therefore, using Figure 63 and an area growth of 747 sq ft (= 1067-320) in second stage, a filling distance of 132 ft is determined in second stage of Test 80-3R1. The equations of the lines in Figures 62, 63 and 64 are in the computer program so it can make these calculations. It has also been given the capability of calculating how far the vehicle has traveled since the beginning of opening, by integrating the velocity (and "remembering" where it started.) It is noted that this representation of the filling distance would appear to contradict the work in Section 4.2. However, use of the linear filling distance function merely represents a less sophisticated approximation than the approach used in Section 4.2. This linear approximation was chosen for expediency.

b) Drag Area. Drag area was determined as a linear function of the distance traveled in Stages 1 and 2. In Stage 3, drag area was expressed by the equation

$$C_D S(s) = 1100 + 3200 \{(s - 22)/103\}^3, \qquad 65 \leq s \leq 103$$

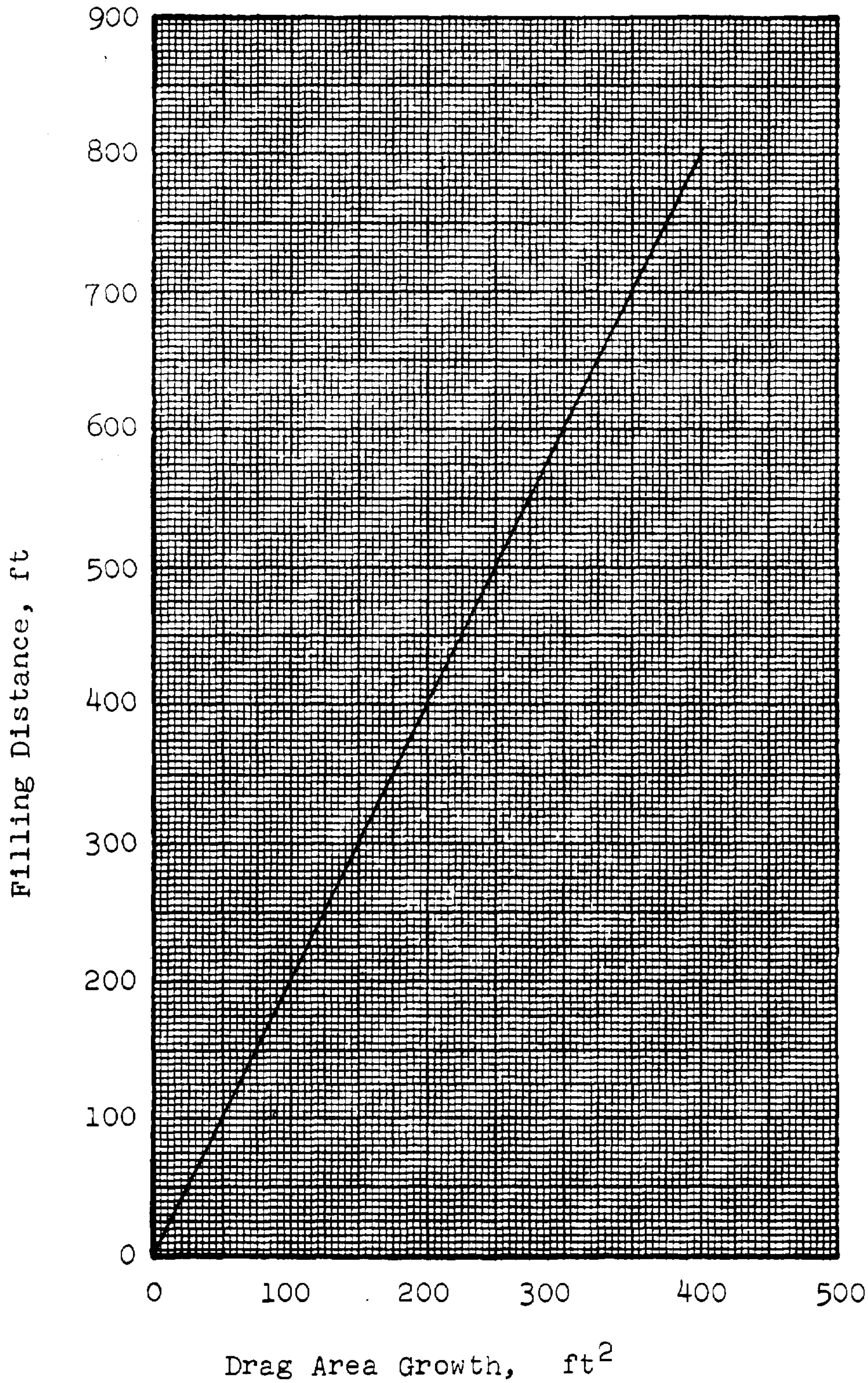

Fig. 62 . First Stage Filling Distance

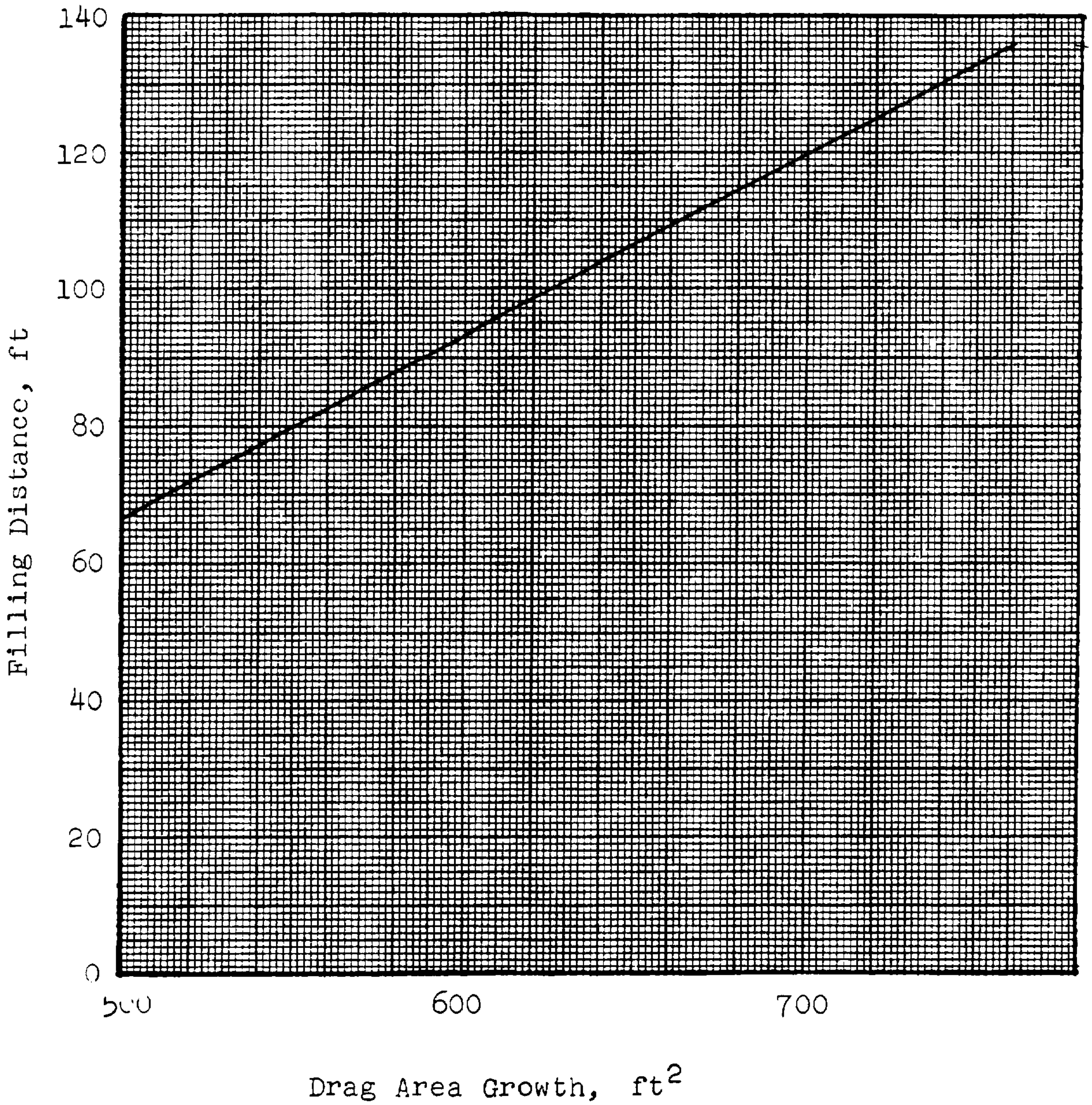

Fig. 63. Second Stage Filling Distance

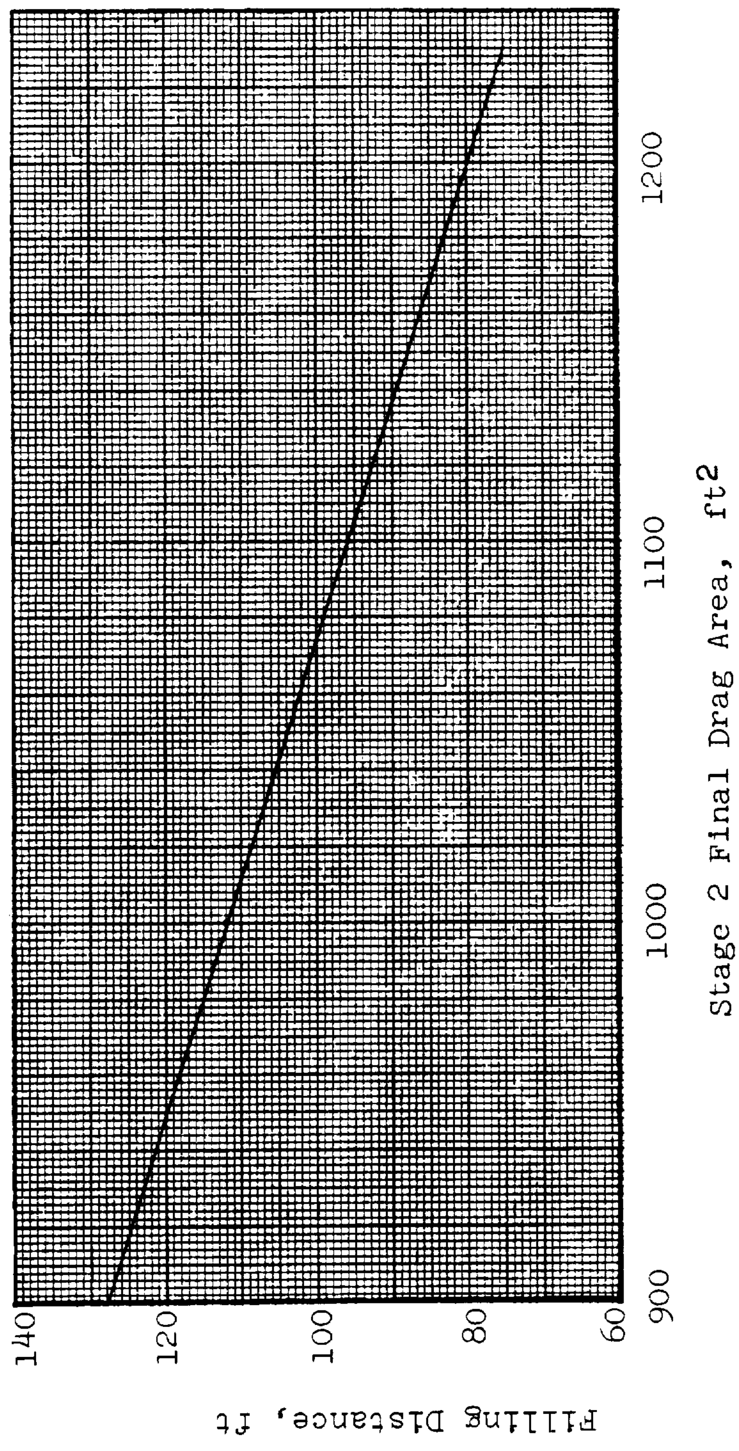

Fig. 64. Third Stage Filling Distance

where **s** is the distance traveled since passing a reference point 103 ft before the completion of filling. The cause of this fairly complicated means of expressing C_DS as a function of distance was that, while it was assumed that all parachutes inflated to a full open drag area of 4300 sq ft, there were variations in the area growth to full open, because the final drag area in Stage 2 was varied from test to test. Further complication was met in expressing the drag area for values of s less than 65 ft. The approximation used here was to make the drag area growth proportional to the distance traveled since the beginning of inflation, the constant of proportionality being a quotient; the numerator was 1260 sq ft minus the final drag area in Stage 2 ($C_DS(65)$=1260 sq ft) and the diameter was the distance required to travel from the beginning of inflation to the point at which **s** is 65 ft. This complicated expression was unfortunate in that it caused numerical difficulties of the sort described in Section 4.2.2, because it resulted in a discontinuity in m_a. However, it was felt that the problem did not significantly affect the peak loads calculated. Nevertheless, this is probably one area where improvement in the modified Mass/Time Method is possible. Also, for **s** greater than 103 ft, C_DS was set equal to 4300 sq ft. This caused another discontinuity in m_a and invalidated all calculations after the lead chute reached full open. This is not a serious problem though, since the full open load on the lead chute is always greater than those on the lag chutes, and is therefore the full open load of interest to the designer.

The drag area values at times outside the inflation interval were determined in the manner specified for the Mass/Time Method.

c) Added Mass. As in the Mass/Time Method, a value of 0.66 was used for K_a. This neglected aerodynamic interference between canopies in a cluster.

While the general parameters for the modified Mass/Time Method were more complicated than those for the unmodified Mass/Time Method, the use of the former was simplified by the incorporation of these parameters into the computer program. Therefore, all that must be specified are initial conditions, drag area values at the end of inflation in each stage and at the end of each stage, and reefing cutter times.

4.4.3 Results

It was stated in Section 4.4.1 that once the general parameters described in Section 4.4.2 had been determined, one calculation for each of ten tests was made. These calculations are presented here and represent the first attempt to calculate loads with the modified Mass/Time Method for each of these ten tests. The calculations are presented in Figures 65 through 74 in the form of time histories of calculated riser force versus time histories of measured force.

4.4.4 Discussion of Results

As stated above, using the added mass term in the flight path angle equation only affects the calculated loads insignificantly. There is no effect in Stages 1 and 2 because the added mass terms are neglected there. The effect in Stage 3 is to reduce the loads by a small amount, typically 0.2 percent. This effect is so small because, by the time the system has reached third stage, it is in almost vertical descent and the flight path angle change rate itself is very small.

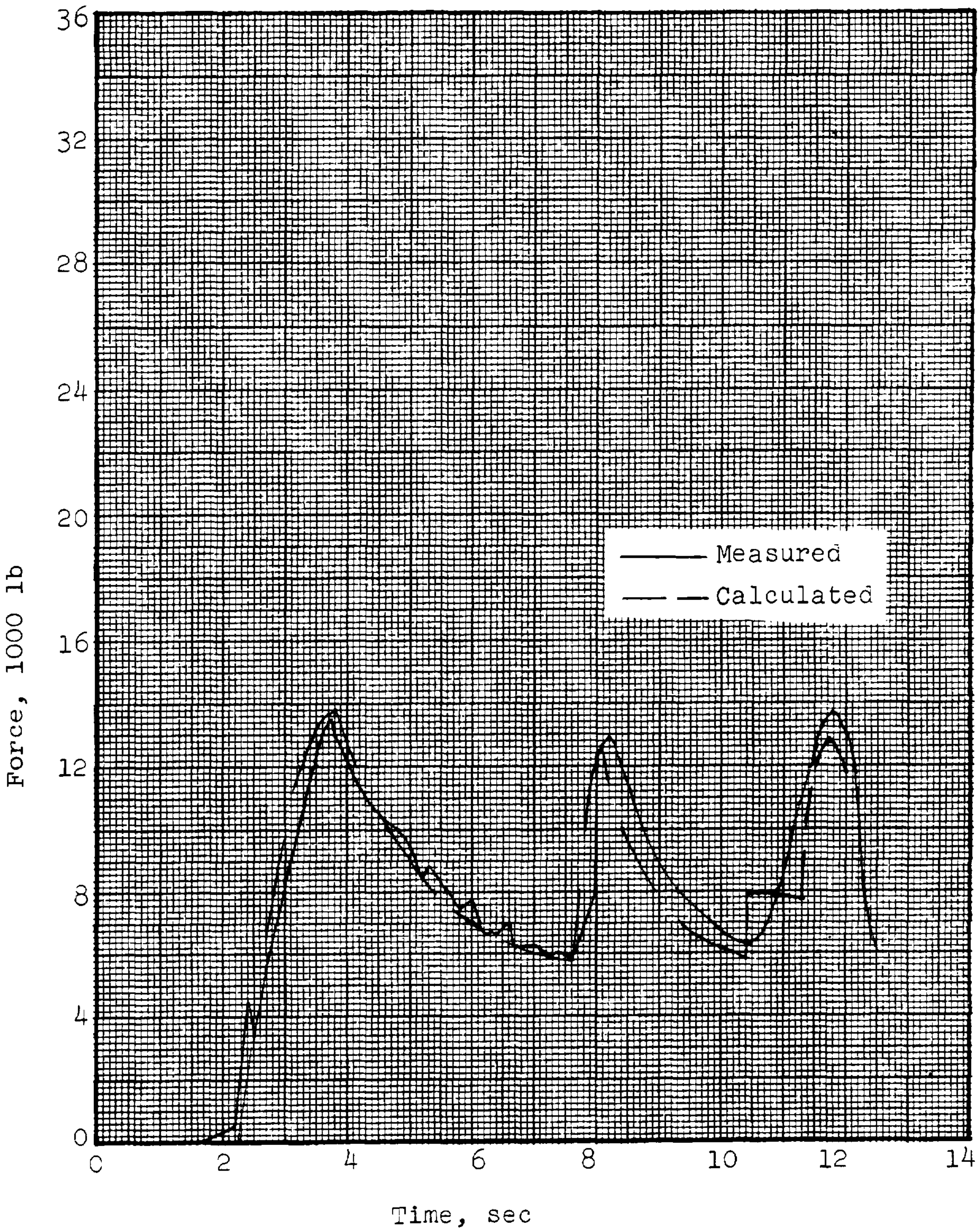

Fig. 65. Modified Mass/Time Method, Test 80-1R

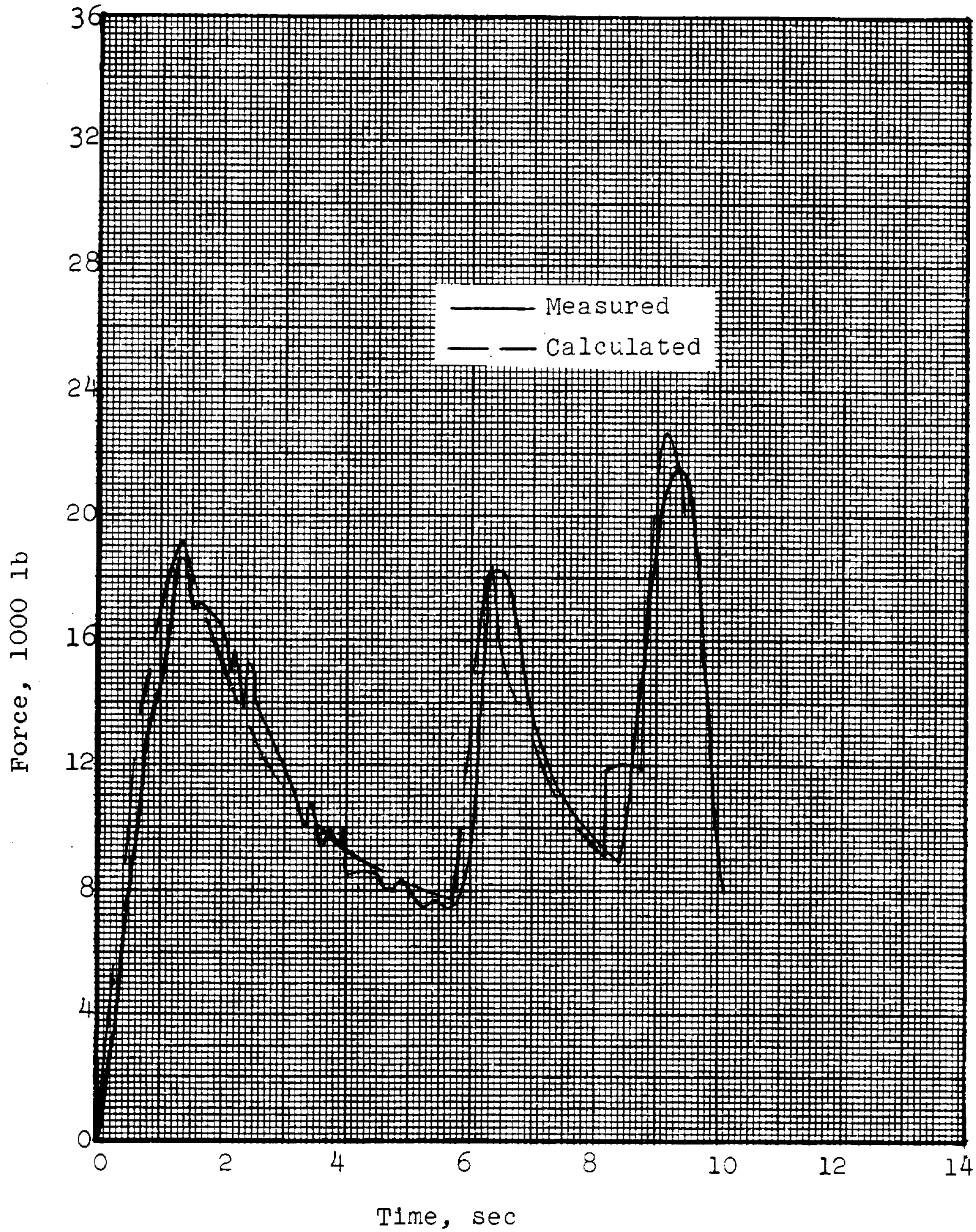

Fig. 66. Modified Mass/Time Method, Test 80-2

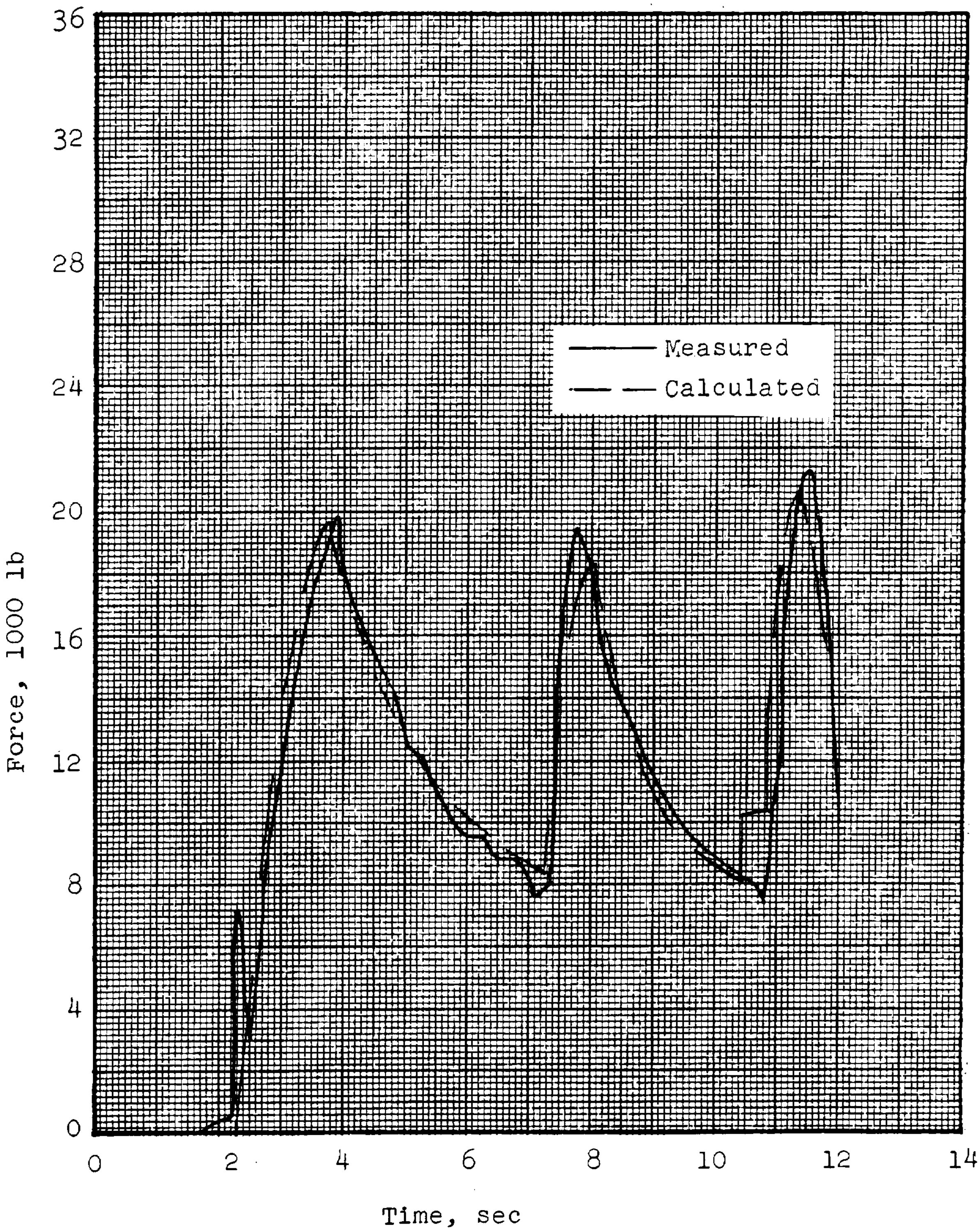

Fig. 67. Modified Mass/Time Method, Test 80-3R1

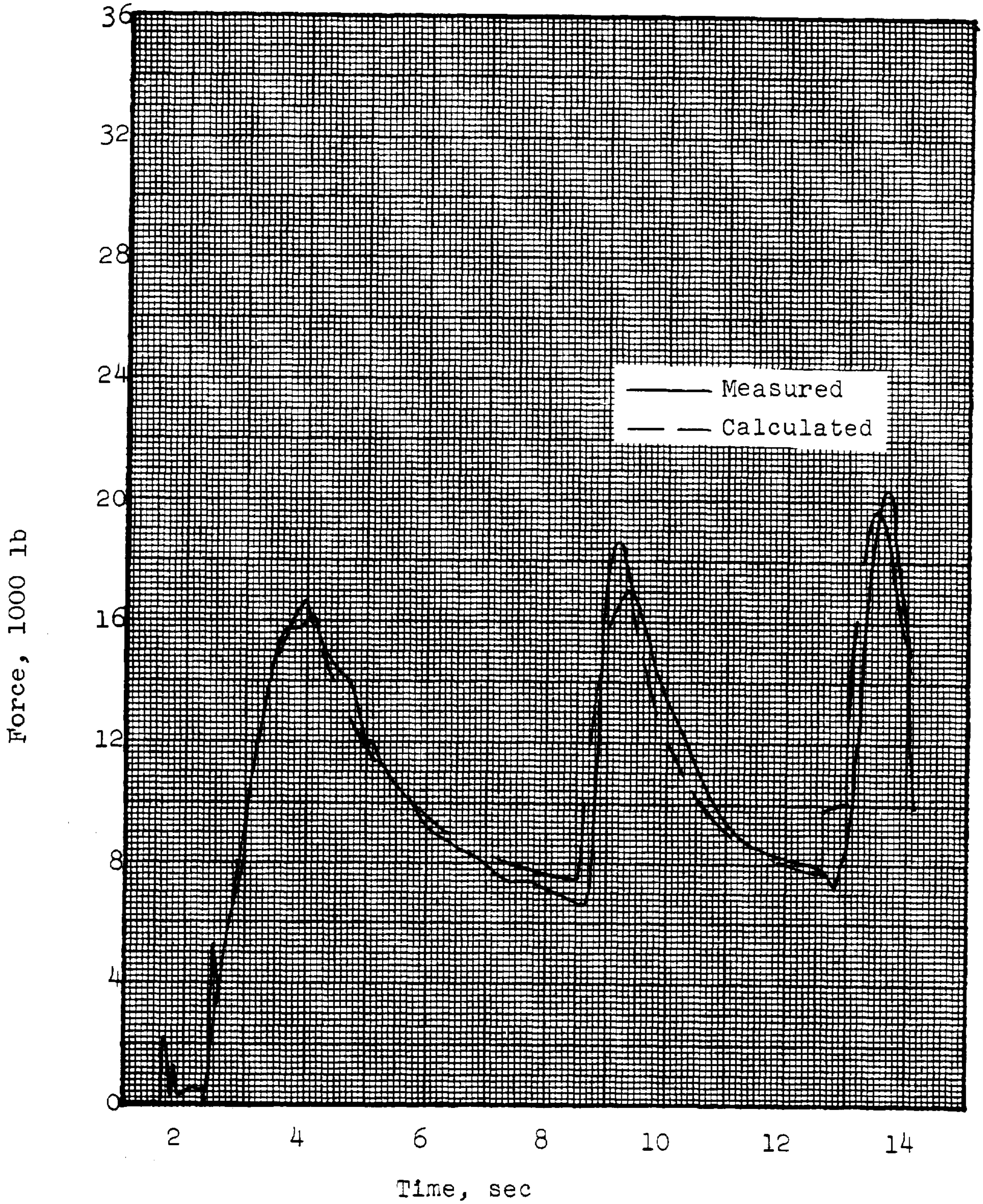

Fig. 68 . Modified Mass/Time Method, Test 80-3R2

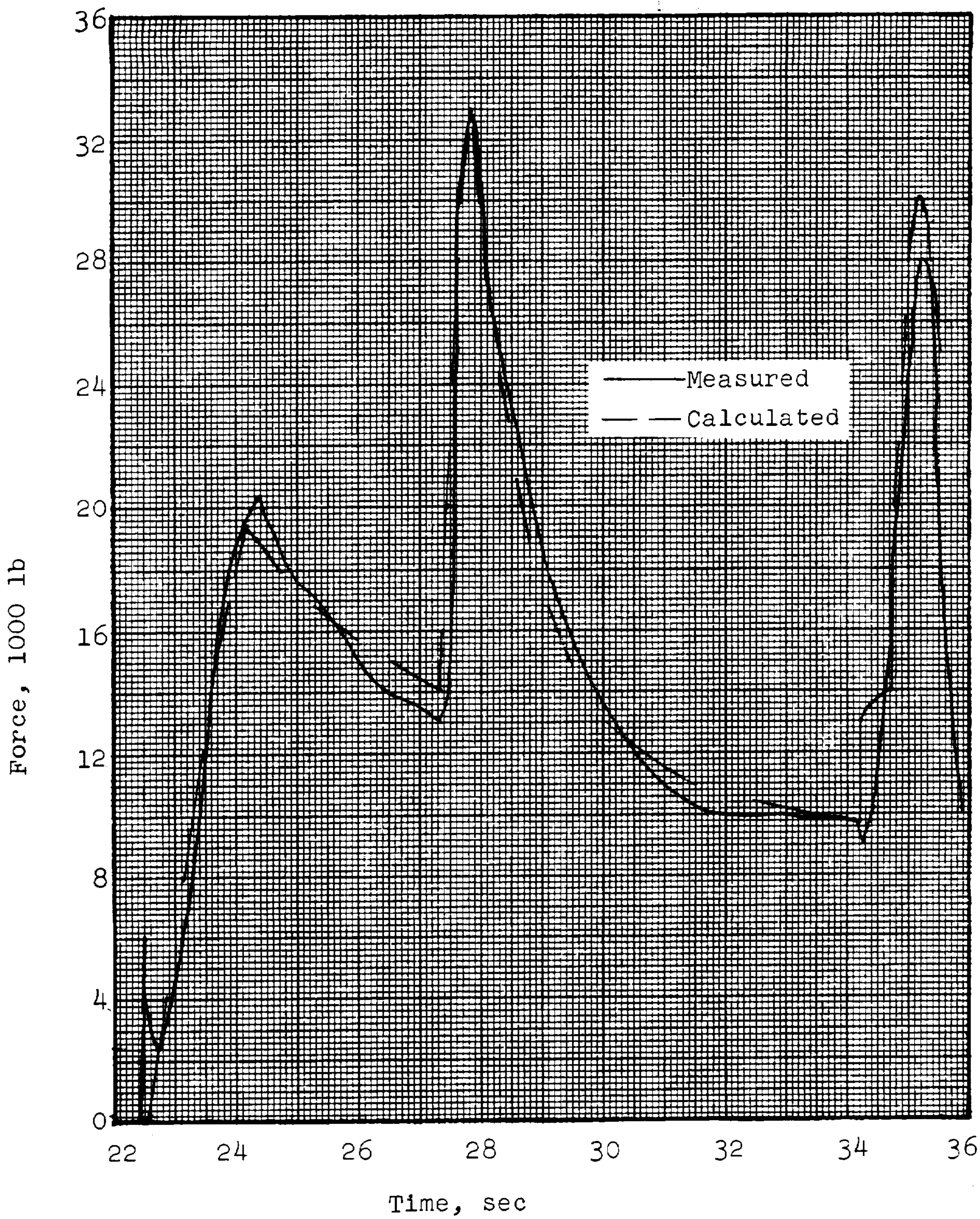

Fig. 69. Modified Mass/Time Method, Test 82-2

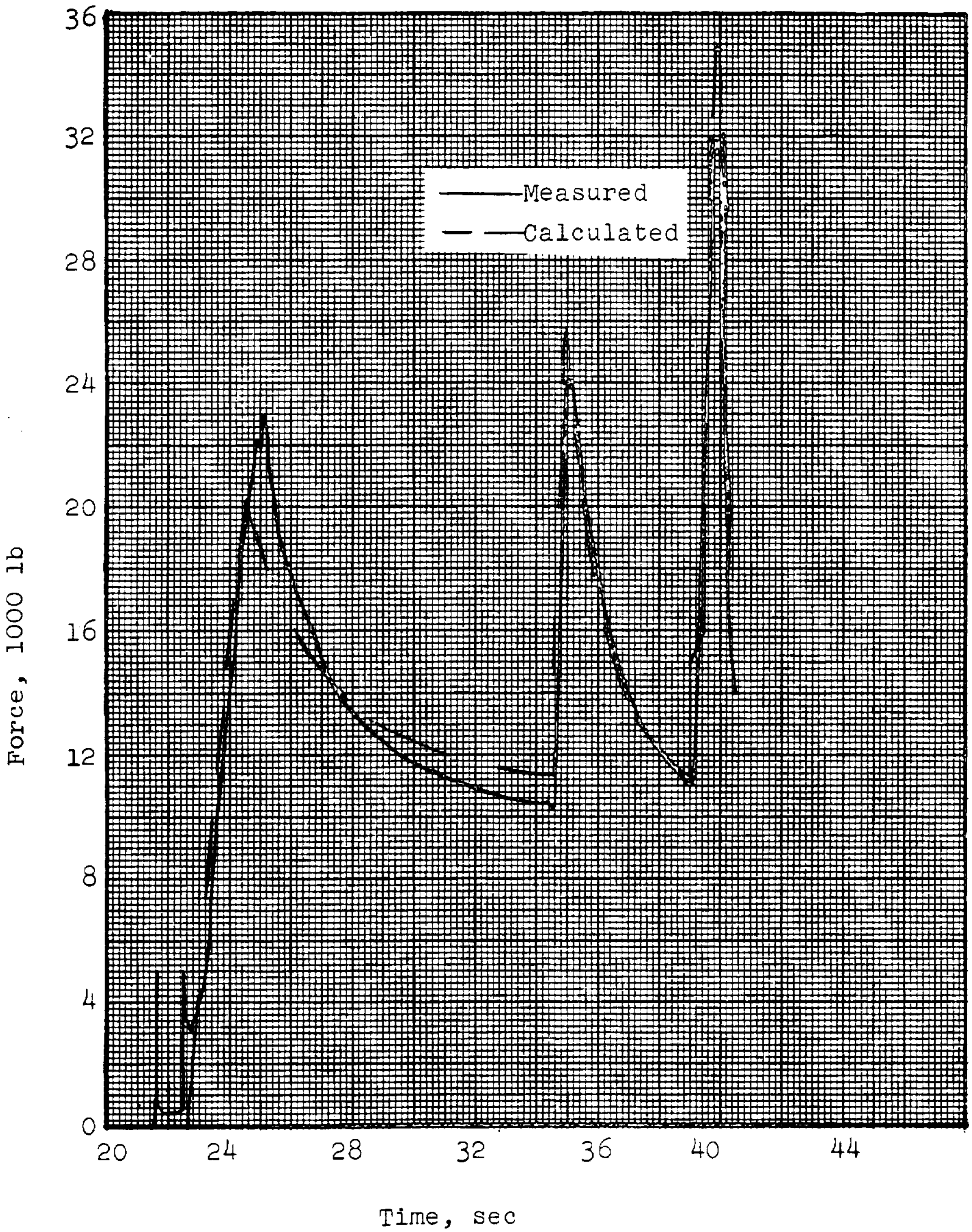

Fig. 70. Modified Mass/Time Method, Test 82-4

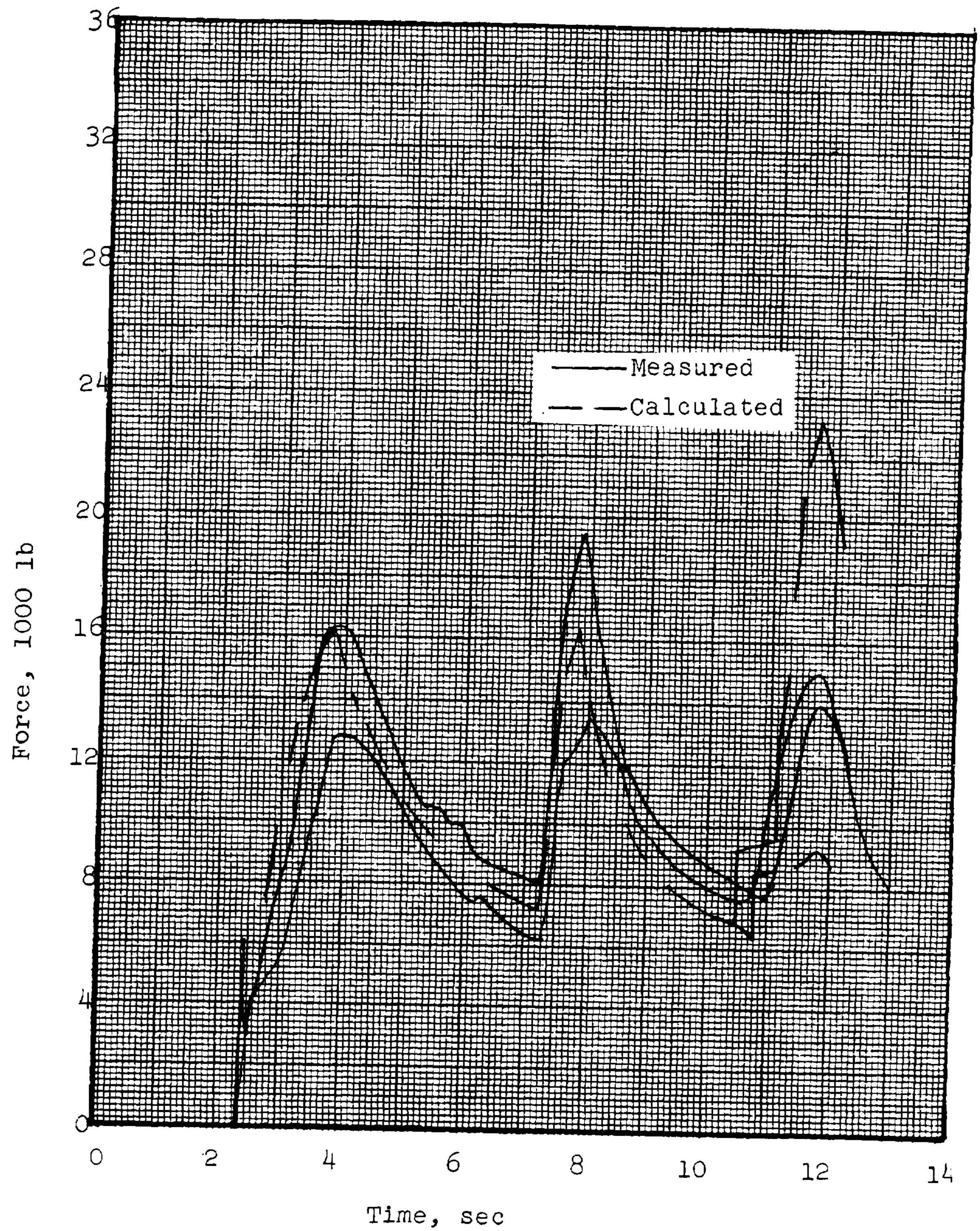

Fig. 71. Modified Mass/Time Method, Test 81-1

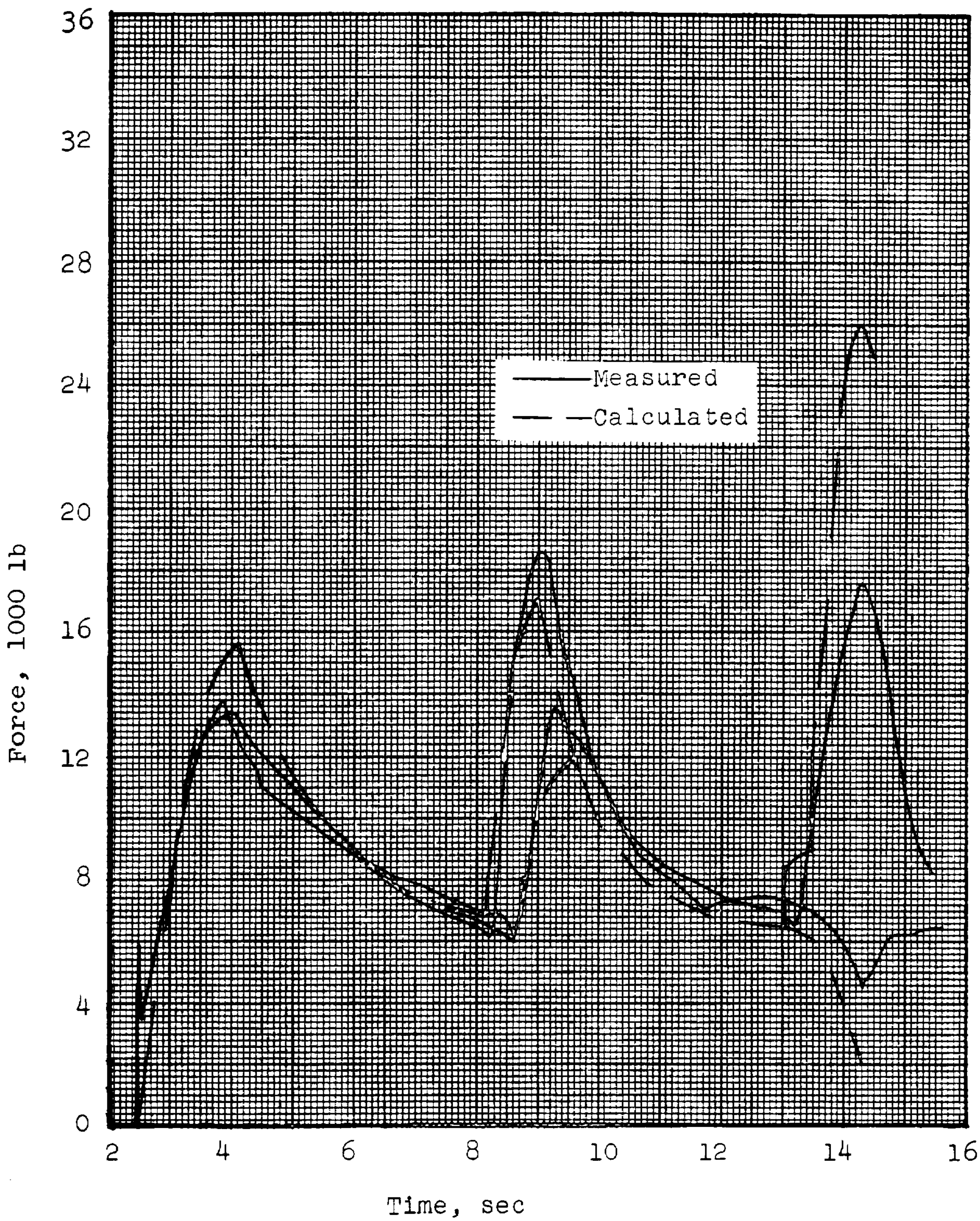

Fig. 72. Modified Mass/Time Method, Test 81-2

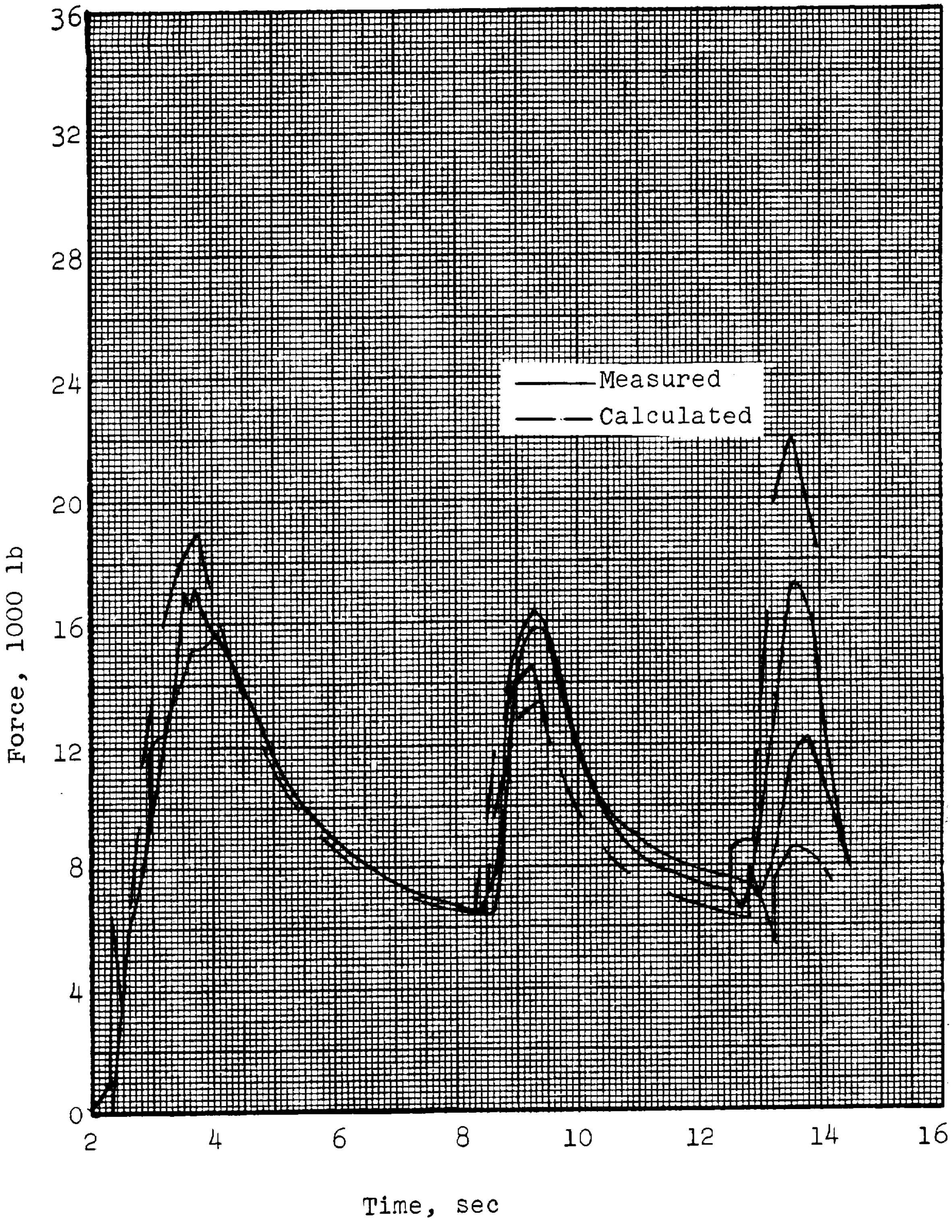

Fig. 73. Modified Mass/Time Method, Test 81-4

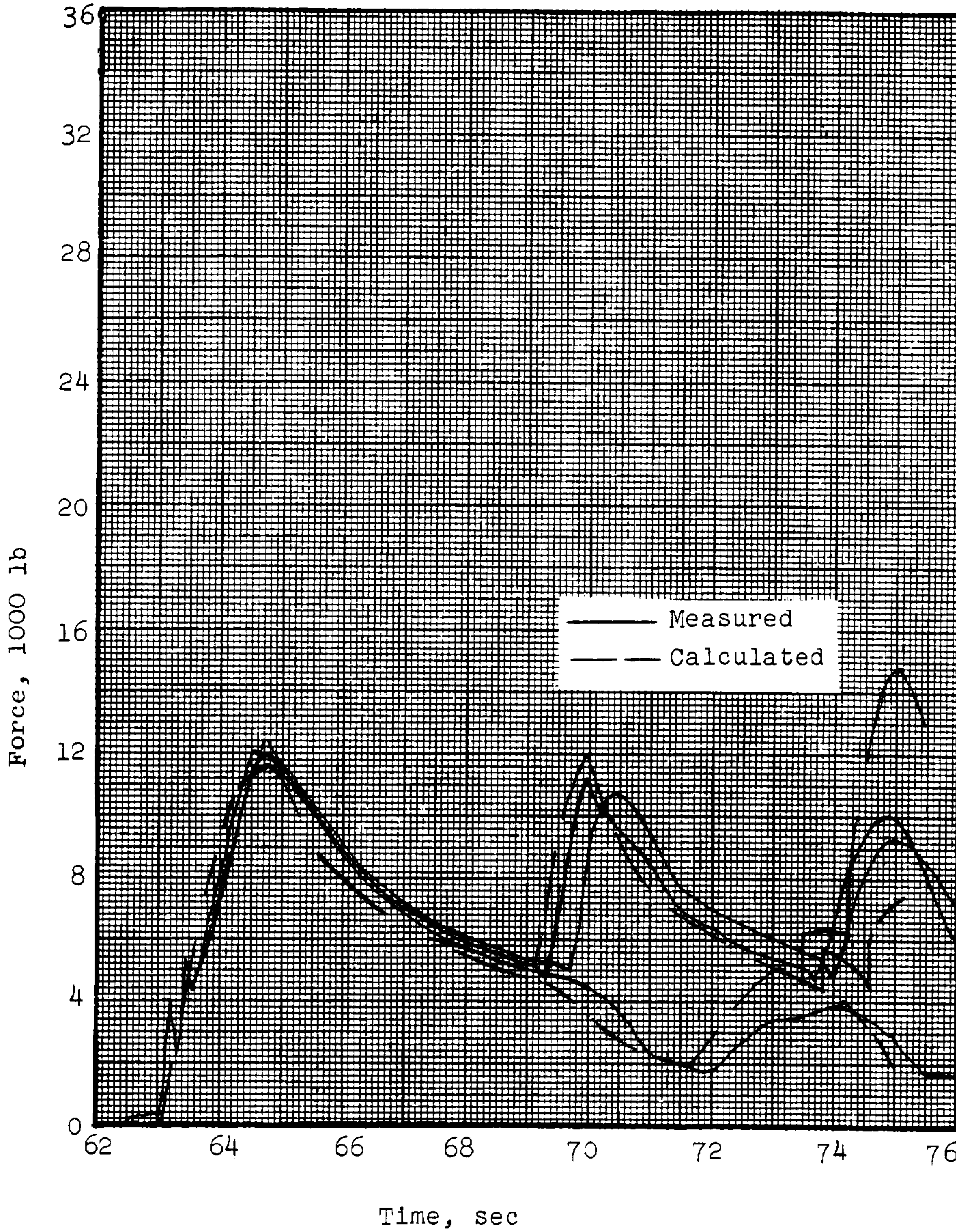

Fig. 74. Modified Mass/Time Method, Test 84-1R

Figures 65 through 74 demonstrate that the basic assumptions from Rust's analysis are valid from an engineering point of view. Surprisingly, the results obtained with the modified Mass/Time Method are slightly more accurate than those from the unmodified Mass/Time Method, for Stages 1 and 2. The same fact is not true for third stage, but Figures 65 through 70 show that the modified Mass/Time Method is acceptably accurate there too, especially for a first attempt. Figures 71 through 74 show quite encouraging results for the cluster cases. These results are very good for the first and second stages; calculated filling times are very close to measured filling times and most loads are within 10 percent of the measured values. The results in third stage are poor in that, while the filling times are accurate, the calculated loads are inaccurate. The nature of the inaccuracy seems to be that the calculated peak load for the lead chute is high, while the peak load for the lag chute is low in third stage. The former is probably due to the neglecting of aerodynamic interference in the determination of drag area and filling distance; the latter is probably because, when added mass terms are considered, each parachute has a strong effect on the loads of the others in the cluster through the mechanism of vehicle acceleration.

While the application of the modified Mass/Time Method to cluster cases is not presently justified by its accuracy, the results show it to be quite promising as an approach. And, it is felt that the necessary adjustments in the parachute parameters would be sufficient to make it an acceptably accurate method. The data in Section 2.3 indicate the types of adjustments that are required.

Main parachute loads for an Apollo design case, as predicted by the modified Mass/Time Method, are presented in Appendix C. This case, referred to as Case 410, is a normal entry case for which one drogue chute and two main parachutes operate. For this case, the predicted maximum opening loads for the first two stages are $F_{r_1} = 19{,}240$ lb and $F_{r_2} = 19{,}410$ lb. These loads are approximately 3.9 percent higher and 9.9 percent lower, respectively, than the corresponding loads from the final Apollo ELS loads report.[3]

SECTION 5.0
PARACHUTE OSCILLATIONS STUDY

In the large number of development tests for the Apollo parachute system conducted by Northrop Ventura, it has been observed that parachutes may oscillate during descent. These oscillations may be described as follows:

a) Longitudinal - This type of oscillation occurs along the longitudinal axis of the module- parachute system. Thus, it is a reciprocative movement in one dimension between the Apollo module and the canopy system. This is shown in Figure 75 (a).

b) Rotative - In this case the longitudinal axis of the parachute system rotates about the path of descent in two or three dimensions (precession). It is not necessary to assume rigid body behavior for the module-parachute system. The rotative oscillation is shown in Figure 75 (b).

It is also possible to have combinations of both. In some cases of severe longitudinal oscillations, repeated overinflation occurs. In Test 99-5R this phenomenon occurred in the drogue programmer chute with subsequent failure.

These longitudinal oscillations were discussed by Knacke[43] in a recent paper. Knacke pointed out that Apollo drop tests have shown the amplitude of the oscillations depends upon the ratio of the forebody, canopy mouth characteristic lengths.

The danger in the presence of rotative oscillations rests in two facts. The first is that the descent speed of the system is a function of the angle of attack of the module to the air

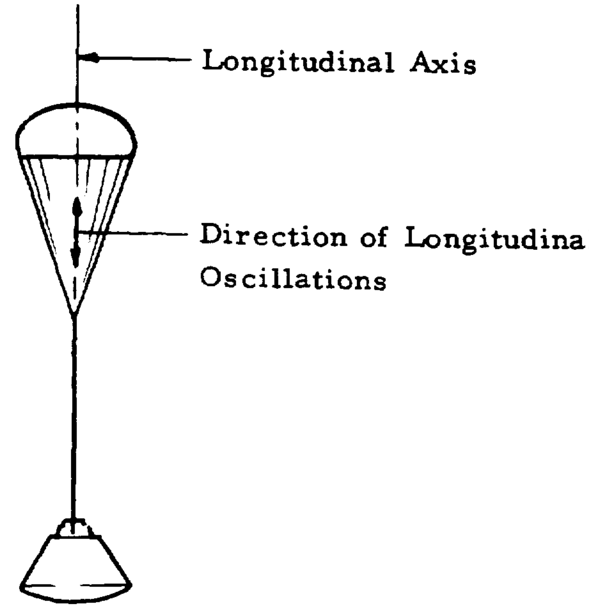

(a) Longitudinal

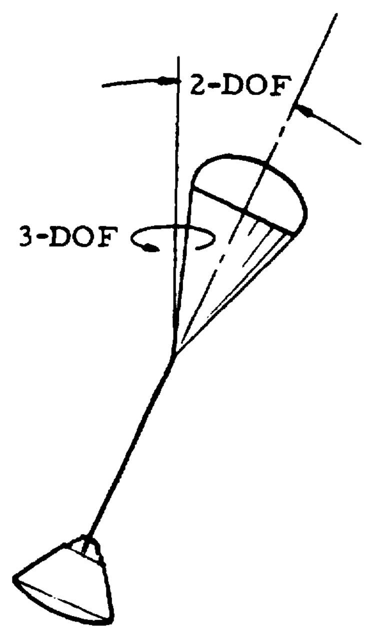

(b) Rotative

Fig.75. System Oscillation Modes

flow. If the rotative oscillations increased enough in amplitude to expose a smaller cross sectional area of the module to the free stream for a long enough time, the dynamic pressure forces on the parachute canopy could become large enough to cause failure. The second fact is that high rotation rates could cause line foul up of the deployed parachutes, which could also result in system failure.

In view of the possible consequences due to oscillations, more information concerning their cause is desired. However, the scope of the problem must be reduced to one type of oscillation. Because of their mathematical tractability, the longitudinal oscillations will be the ones to be considered. However, as the problem is developed for the longitudinal case, many of the concepts will be seen to apply to the rotative case. In the stochastic field solution presented in outline the concepts are identical for the longitudinal and rotative cases. In the work that is to follow, the word oscillations will always mean longitudinal oscillations unless otherwise specified.

5.1 OBJECTIVE

The objective of this study is to explain the cause of the longitudinal canopy oscillations observed in the Apollo parachute test program. This explanation will consist of proposing a physical model that is analyzed mathematically, then comparing the results of these calculations to experimental data. The mathematical analysis will start from first principles in order to point out assumptions that have been implicit in previous analytical work.

In addition to this simple straightforward mathematical analysis, it is desired to formulate a much more fundamental mathematical approach to the problem of the turbulent wake, the turbulent canopy flow and their interactions with one another. This fundamental mathematical approach should consider the basic characteristics of turbulence, i.e., its randomness, its eddy energy distribution with respect to frequency, its decay times, etc. It must be emphasized that only by considering this most fundamental and general of mathematical treatments of the turbulent wake can any advances in understanding be made. Thus, the basic objective of this study is to show how a simple mass-spring-dashpot system can predict canopy oscillations within an order of magnitude, but that a much more realistic physical and mathematical model is needed to predict and explain the details of the turbulent wake, the canopy oscillations and the interdependence of the two.

5.2 METHOD OF PROCEDURE

It is desired to make the mathematical solutions as general as possible. This will ensure the wide applicability of the solutions and provide the greatest physical insight into the oscillation phenomenom. Therefore, two methods of solution will be presented. The first is based on the very simple mass-spring-dashpot analysis and the second is based on random field theory. (Random field theory, when applied to continuous fluids, is called turbulence, or stochastic, three dimensional, vector field physics.) The first method will be used to determine the forebody wake frequency, f_w. The observed experimental frequency, f_e, obtained from drop tests will be used to compare against the calculated values of the canopy response frequency, f_k, and f_w. Numerical results will be presented for the calculations based upon the mass- spring - dashpot (msd) analysis. The random field model will be presented in functional form because of the unavailability of an experimentally determinable function. A general discussion will follow the presentation of the mathematical models and their comparison to the experimental data. Recommendations for future investigations, both theoretical and experimental, will be given at the very end of the study.

At this point, some general characteristics of the two mathematical methods to be used should be pointed out. Msd analysis has one very desirable characteristic. This is that order of magnitude results can be quickly provided from the drop test data already available. However, by the same token, order of magnitude often is not a close enough estimate. Another disadvantage is that msd uses the concept of dimensional analysis in this study. However, dimensional analysis does not apply to systems with many characteristic parameters, all of which are influencing the phenomenon to be analyzed. For example, the wake behind an aircraft is caused by a variety of parts, each with a different characteristic length. To find the energy distribution of the eddies in the wake using dimensional analysis and one characteristic length would be impossible. Therefore, dimensional analysis must be used in systems where there is clearly only one characteristic parameter.

The random field approach has two good characteristics. The first is that the solutions are much better than order of magnitude in exactness. The second is that the method does not break down when the system becomes complicated. However, extensive additional data in the form of a correlation function must be obtained before it can be used. These data are obtained in air with hot wire anemometers which are not very easy to use. In addition, after the data are obtained they must go through an extensive reduction process to be able to yield the desired function, the correlation function. It is because of the unavailability of the correlation function that quantitative answers have not been presented in the random field models. Nevertheless, the method is felt to be so powerful that its mathematical formulation is outlined and strongly recommended as the next step in any parachute experimental or analytical techniques.

5.3 DETERMINATION OF THE CANOPY RESPONSE FREQUENCY, f_k

It is important to point out that the existence of the canopy oscillation frequency, f_k, that is to be calculated does not in general depend upon the presence of a turbulent wake generated by some forebody. In fact, wind tunnel experiments have shown that a canopy will oscillate at the same frequency with or without a forebody. The forebody provides a turbulent wake that either can cause an increase in the oscillation amplitude of the canopy or act as a trigger for the oscillations. These conditions exist only if the wake can give the canopy energy at the frequencies that the canopy is responsive to. These responsive frequencies of the canopy are at its fundamental frequency and higher harmonics. In effect, imagine the parachute system as a band pass filter. A narrow frequency band exists as an output. However, the magnitude of the output is increased if the input is increased at the band pass frequency.

The preceding discussion on the response of the parachute system by the turbulent wake forcing function contains an implicit assumption. This assumption is that the energy of the turbulent wake forcing function, E(f.f), is the same order as the energy of the canopy response, E(c.r.). (The forcing function is assumed to contain some energy at the band pass frequency of the parachute system.) The canopy response frequency, f_k, can be a true function of the canopy material and geometry constraints only in this case. One only needs to consider the other possibilities to be convinced of this. Assume that $E(f.f) \gg E(c.r.)$. In this case, the high energies of the forcing function would drive the canopy at the characteristic frequency of the forcing function.

This means that the characteristic parameters of the response system are so overpowered as to become negligible constraints to the forcing function. In the band pass filter analog, the forcing function would not detect the filter. Now assume $E(f.f.) \ll E(c.r.)$. This case becomes trivial except if E(f.f.) is large enough to become a "trip" for the onset of the oscillations. This trip can only occur if some of the energy of the forcing function is at the response frequency of the parachute system.

Summarily, the drop test conditions must be checked to ensure E(f.f.) = order of E(c.r.) before any conclusions are drawn from oscillation test data. This is simply a comparison of the loads to which the parachute system was designed versus the test loads it will experience in the drop test. In the drop tests analyzed in this study, the test dynamic pressures were always of the same order as the design q of the parachute system. This means that the analysis presented herein is valid insofar as the parachute system is characterized by its constraints of mass, spring constant, viscosity, etc. It is important that in any mathematical oscillation analysis to be conducted, this implicit assumption be realized as a necessary mathematical condition.

5.3.1 Classical Mass - Spring - Dashpot Model

5.3.1.1 Physical Model Formulation. One may represent the parachute system as a member of the classical family of all mechanical dynamic systems. This means that one can ascribe to the parachute system the elements; mass, M, a spring constant, k, and a viscous damping coefficient, ν. This system is then brought under the influence of some external force that would be a function of time, F(t). The physical model that could be constructed from these four elements could behave as a linear, quasi-linear (where the constant terms become a function of the independent parameter, e.g., $\nu \frac{dx}{dt}$ becomes $\nu(t) \frac{dx}{dt}$, or nonlinear system. For the purpose of this first model formulation, a linear system will be assumed. If it is found that this model is unsatisfactory in adequately representing the parachute system behavior, then quasi-linear or nonlinear effects will have to be considered.

The breakup of the elements of the parachute system is as follows. The mass of the canopy material and the geometrically enclosed air mass will be used as a first estimate for the system mass, M. The viscous damping coefficient, ν , will be represented by the damping effects of the air surrounding the canopy system. Material interactions such as cloth bending moments will be ignored. The spring constant, k, will be represented by the spring characteristics of the nylon suspension lines. The spring constant associated with the compressibility of the air will be neglected. It should be noted that the strongest test of the linearity assumption will be in assuming the nylon spring constant to be linear. It is known that the stress-strain curve for the suspension lines is not a straight line. This difficulty will be circumvented for the linear system approximation by taking the tangent to the load elongation curve at the load in question. The validity of this procedure will be checked based on the quantitative results of Section 5.3.1.3 and their correlation to experiment.

The forcing function, F(t) used in this section will be considered to be from the turbulent air inside and behind the canopy. For the sake of generality, F(t) will be assumed to be a periodic function of time. A more specific dimensional analysis expression will be described in the latter part of Section 5.3.1.2.

The preceding physical model is pictorially presented in Figure 76 in mechanical analog form.

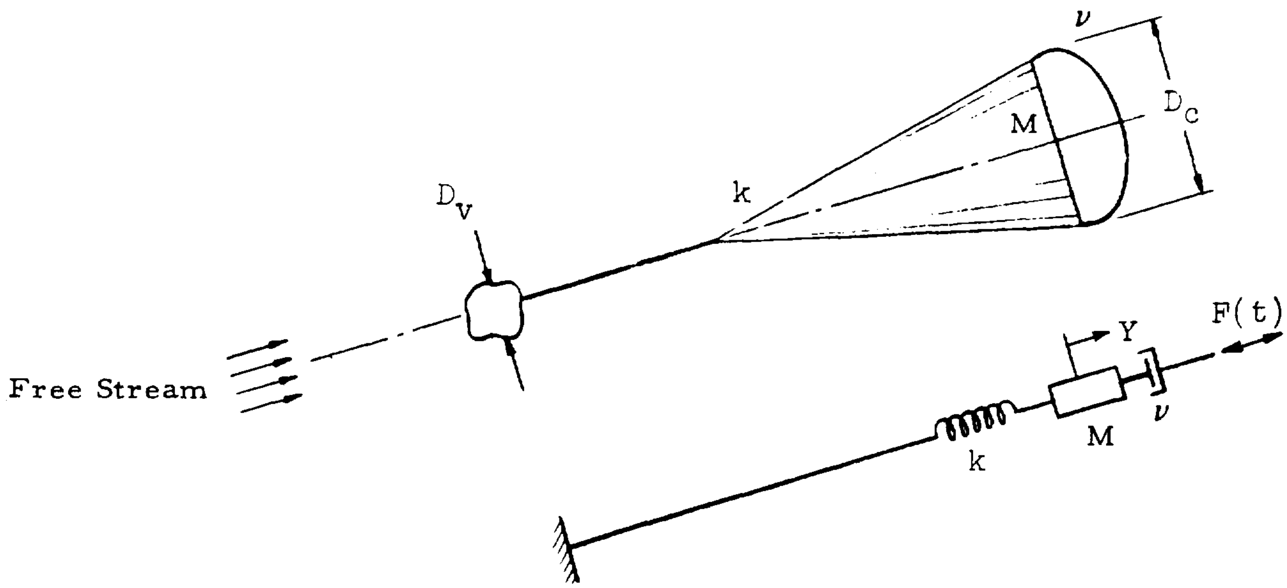

Fig. 76. Mechanical Analog to Apollo Parachute System

5.3.1.2 Mathematical Model Formulation. The differential equation of motion for the viscously damped spring-mass system driven by F(t) can be written as

$$M \frac{d^2Y}{dt^2} + \nu \frac{dY}{dt} + kY = F(t) \tag{38}$$

where Y is the linear displacement as shown in Figure 76. The steady state solution of Equation (38) is the particular solution. This is just a steady state harmonic oscillation at the frequency of the driving force with the displacement vector lagging the force vector by some angle θ. If F(t) is assumed to be

$$F(t) = B \sin \omega t \tag{39}$$

the particular solution can be assumed to be

$$Y = A \sin(\omega t - \theta) \tag{40}$$

where ω is the frequency of the harmonic oscillations. The steady state, nondimensional solution of Equation (38) is

$$\frac{A}{A_o} = \frac{1}{\left[\left[1 - \left(\frac{\omega}{f_k}\right)^2\right]^2 + \left[2\xi\left(\frac{\omega}{f_k}\right)^2\right]\right]^{\frac{1}{2}}} \tag{41}$$

$$\tan\theta = \frac{2\xi\left(\frac{\omega}{f_k}\right)}{1 - \left(\frac{\omega}{f_k}\right)^2} \tag{42}$$

where

f_k	=	$\sqrt{k/M}$	=	natural frequency of undamped oscillations
ξ	=	ν/ν_c	=	damping factor
ν_c	=	$2Mf_k$	=	critical damping coefficient
A_o	=	B/k	=	zero frequency deflection of spring-mass system by a steady force, B.

It is obvious that the importance of damping is mainly in the attenuation effects upon A/A_o near $\omega = f_k$. Furthermore, since it is desired to reduce or eliminate the longitudinal oscillations, it is necessary to have either

$$\omega \ll f_k \tag{43}$$

or

$$\omega \gg f_k \tag{44}$$

Inequality (43) represents the case of very small inertia and damping terms, thus a small phase angle θ. The magnitude of the force of the forcing function is then nearly equal to the spring force.

Inequality (44) represents the case of θ nearing 180° and the force magnitude of $F(t)$ is spent in trying to overcome the large inertia force.

The condition of $\omega \cong f_k$ represents that the forcing function frequency is almost that of the system's fundamental frequency and unwanted resonance is occurring.

To determine whether or not this resonant condition is responsible for the Apollo parachute oscillations, some calculations must be made for ω and f_k. The expression for f_k is known from the definition but the expression for ω is as yet unknown.

To this end, it is necessary to consider the physical origin of $F(t)$. Using dimensional reasoning, the characteristic velocity v , (the free stream velocity) and a characteristic length, L, can be combined to give an angluar frequency,

$$\omega = \frac{v}{L} \tag{45}$$

Hence,

$$F(t) = B \sin \left(\frac{v}{L} t \right)$$

It is left to determine what physical part of the system L represents. In the case of a forebody-generated turbulent wake, L would represent the characteristic length of the forebody that was in the plane of the projected normal to the direction of movement. The presence of a forebody wake that generates the forcing function will be discussed in detail in Section 5.4. In this section, the assumption will be made that there is no forebody. Since it has been shown that parachutes oscillate regardless of the presence of the forebody, the forcing function must originate in or behind canopy. Hence, a likely choice for L would be the canopy mouth diameter, D_c, for the fully open canopies. Some mean characteristic length, taken between the maximum diameter and the mouth diameter could be used for the reefed canopies. (It is obvious that the radius of the canopy mouth also could be used for the calculation of the forcing function. In that case the numerical answers would be off by a factor of two from the case of using D_c as the characteristic length. In this case the correlation of calculated values to experiment would depend upon the trend of the variation of calculated values for different canopies. This trend would then be compared to the trend of the experimental frequency observed for the different canopies. For a correlation to result the calculated values of frequency for the different canopies would have to vary in the same way as the experimental values.) The forcing function could be due to the trapped circulating air within the canopy, or the shed vortices behind the canopy, or a combination of both. In this study the forcing function characteristic length for shed eddies and the flow inside the canopy are of the same order of magnitude. Therefore, the characteristic length D_c can be used.

$$F(t) = B \sin \left(\frac{V}{D_c} t \right)$$

To verify the hypothesis that the forcing function is due to the turbulent eddies that are of the characteristic length of the canopy a calculation must be made to show that the forcing function frequency is of the same order of magnitude as the response frequency f_e. Again it is only necessary to show order of magnitude correlations because the eddy energy is not concentrated at one frequency but spread over a range of frequencies. This range of high energy eddy frequencies is typically one order of magnitude around the characteristic frequency. This spread effect is shown in Section 5.4.1.

Calculations for the forcing function frequency ω are shown in Table 28 for the different tests. It should be noted that ω correlates in all cases within an order of magnitude to the observed experimental frequency f_e.

Table 28. Comparison of Frequencies

DROP TEST 84-4 — PTV - DROGUE CHUTE

Drogue 1	1st Reefed Stage							
v (ft/sec)	560	560	560	555	555	550	545	540
f_w (hz)	13.7	13.7	13.7	13.6	13.6	13.5	13.3	13.1
f_e (hz)	19	16	16	18	18	17	17	18
w (hz)						13.6		
f_k (hz)	= 10 @ mean load = 10.4 @ max load							

DROP TEST 85-2 — BP - DROGUE CHUTE

Drogue 1	Full Open					
v (ft/sec)	271	267	262	260	256	253
f_w (hz)	3.4	3.3	3.3	3.3	3.3	3.1
f_e (hz)	7	6	4	4	4	4
w (hz)				3.8		
f_k (hz)	= 7.4 @ max load					

DROP TEST 85-5 — BP - DROGUE CHUTE

Drogue 1	1st Reefed Stage					
v (ft/sec)	512	493	470	455	438	429
f_w (hz)	6.4	6.4	6.4	5.8	5.4	5.4
f_e (hz)	10	9	9	8	8	8
w (hz)			11.4			
f_k (hz)	= 9.7 @ max load					

Table 28 Continued. Comparison of Frequencies

DROP TEST 85-5 — BP - DROGUE CHUTE

Drogue 1 — Full Open Stage

v (ft/sec)	382	366	354	344	334
f_w (hz)	4.8	4.6	4.5	4.4	4.2
f_e (hz)	7	7	8	8	7
w (hz)			5.1		

f_k (hz) = 5.1 @ max load

DROP TEST 84-1R — PTV - DROGUE CHUTES

Drogue 1 — 1st Reefed Stage

v (ft/sec)	630	600	550	500	480	460	440	430	420
f_w (hz)	15.4	14.7	13.5	12.1	11.7	11.3	10.8	10.5	10.3
f_e (hz)	14	14	14	14	14	14	13	13	13
w (hz)				11.2					

f_k (hz) = same as Drogue 2

Drogue 2 — 1st Reefed Stage

v (ft/sec)	630	600	550	500	480	460	440	430	420
f_w (hz)	15.4	14.7	13.5	12.1	11.7	11.3	10.8	10.5	10.3
f_e (hz)	17	17	17	16	15	14	14	13	13
w (hz)				11.2					

f_k (hz) = 11.7 @ mean load
= 13.4 @ max load

Table 28 Continued. Comparison of Frequencies

DROP TEST 83-6			PTV - DROGUE CHUTES			
Drogue 1	1st Reefed Stage					
v (ft/sec)	510	500	485	475	465	455
f_w(hz)	12.5	12.1	11.9	11.6	11.4	11.1
f_e(hz)	16	16	15	15	15	15
w (hz)		11.2				
f_k(hz)	= same as Drogue 2					
Drogue 2 -	1st Reefed Stage					
v (ft/sec)	same as Drogue 1					
f_w(hz)	same as Drogue 1					
f_e(hz)	18	18	18	18	18	18
f_k(hz)	= 10.0 @ mean load 10.1 @ max load					

DROP TEST 99-3			ICTV - DROGUE CHUTE	
Drogue 1	1st Reefed Stage			
v (ft/sec)	806	798	750	737
f_w(hz)	43	42	40	39
f_e(hz)	20	19	20	20
w (hz)	20			
f_k(hz)	= 18.6 @ max load			

Table 28 Continued. Comparison of Frequencies

DROP TEST 84-1R — PTV - DROGUE CHUTE

Drogue 1	Full Open					
v (ft/sec)	377	207				
f_w (hz)	9.0	7.3				
f_e (hz)	10	9				
w (hz)	5.4					
f_k (hz)	= 7.1 @ max load					

DROP TEST 84-4 — PTV - DROGUE CHUTE

Drogue 1	Full Open					
v (ft/sec)	534	507	483	462	445	431
f_w (hz)	13					10.6
f_e (hz)	14	13	13	11	11	12
w (hz)		7.4				
f_k (hz)	= 9.2 @ max load					

DROP TEST 83-6 — PTV - DROGUE CHUTE

Drogue 1	Full Open			
v (ft/sec)	441	388	362	347
f_w (hz)	11.0			8.5
f_e (hz)	12	11	12	11
w (hz)		5.5		
f_k (hz)	= 7.2 @ max load			

Table 28 Concluded. Comparison of Frequencies

DROP TEST 84-1R		PTV - MAIN PARACHUTE		
	1st Reefed Stage			
v (ft/sec)	232	181	156	140
f_w(hz)	5.7	4.1	3	3.4
f_e(hz)	5	4	3	3
w (hz)		4.3		
f_k(hz)	= 3 to 6 @ max load and for different assumed air masses.			

DROP TEST 84-4		PTV - MAIN PARACHUTE		
	1st Reefed Stage			
v (ft/sec)	239	205	180	169
f_w(hz)	5.9	5	4.4	4.1
f_e(hz)	5	5	3	4
w (hz)		4.7		
f_k(hz)	= 2.5 to 4.6 @ max load and for different assumed air masses.			

5.3.1.3 Calculation of Values of f_k. The calculated values of f_k, k and M must first be determined. To determine k, the spring constant, one must use the curve of load versus elongation for the combined parachute riser and suspension lines. An example of this type of curve is shown in Figure 77 for the drogue parachutes. The k dependence upon compressibility effects of the air will be discussed in Section 5.3.2.1. As was mentioned before, since the curve is nonlinear, k is the slope of the tangent to the curve at some loading point. This loading is the tensile force in the cable riser at a particular time during the descent. Thus in a typical calculation, a mean load on the Apollo drogue parachute of 13,300 lb gives a k = 5000 lb/ft. The mean load value is obtained by taking the mean of the fluctuating forces from the force versus time trace over the increment of time being considered. An example of the force versus time traces is shown in Figure 78. (The mean load at any time is the midpoint between the maximum and minimum load fluctuation.)

To find M, the total mass of the system, the mass of the canopy, M_c, must be added to the total mass of the included air, M_a. Hence, $M = M_c + M_a$. The value of M_c is known from available manufacturing data, but M_a must be estimated. This estimation in its most accurate form must consider all the air mass that can oscillate with the canopy. Therefore, M_a would include some of the air mass in front of, behind, and around the sides of the canopy. To account for this peripheral air, one must consider that the domain of influence of the canopy diminishes nonlinearly through the surrounding turbulent flow field. For an order of magnitude analysis, however, the geometrical estimation of the air only within the inflated canopy will be determined and used as the value for M_a.

The results of these straightforward calculations for f_k are listed in Table 28. The calculations for f_k were performed in some of the tests for both mean loads and maximum loads. This was done to observe how sensitive f_k is to the load. In addition, in the table for the Parachute Test Vehicle (PTV) using the first reefed stage of the Apollo main parachutes, there is a range presented for f_k. This range is calculated to show the sensitivity of f_k to the canopy air mass used in the calculations. The higher value represents the air mass contained in the reefed canopy approximated by a sphere, the diameter of which was the canopy mouth diameter. The lower value is the canopy approximated by a sphere with a diameter equal to the maximum canopy diameter.

It is now desired to compare the calculated frequency, f_k, with the observed experimental frequency, f_e. The section that follows describes the method used for obtaining f_e from the experimental data.

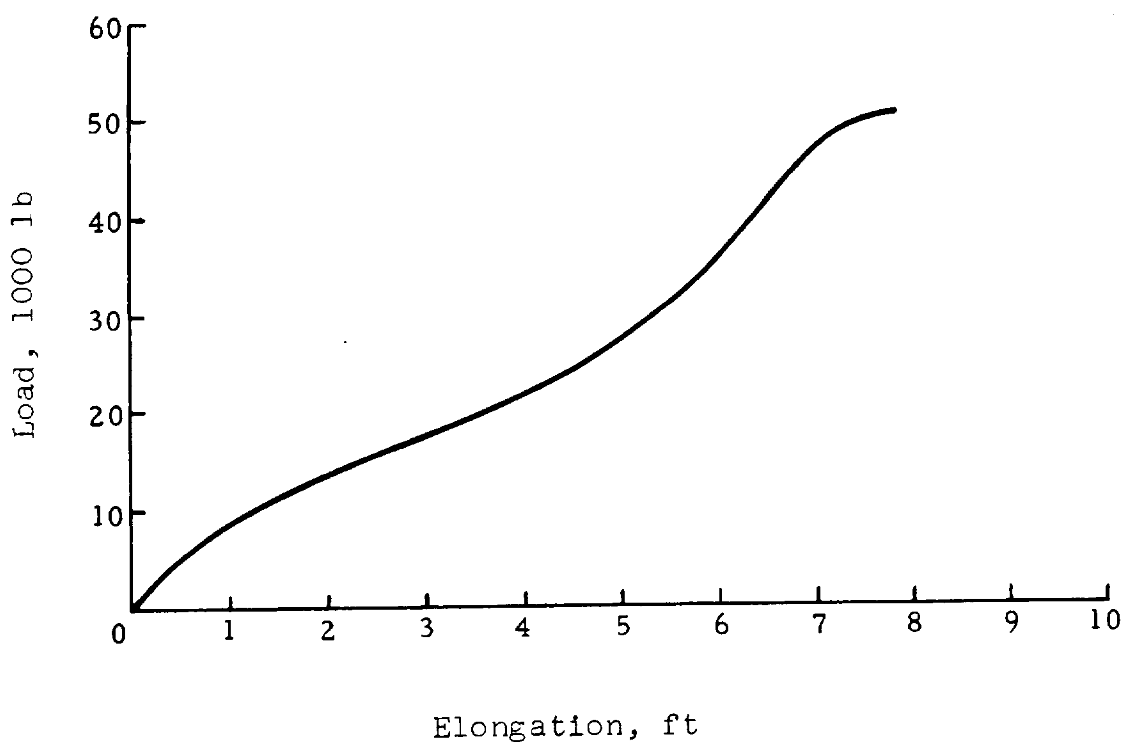

Fig. 77. Typical Nylon Load - Elongation Curve

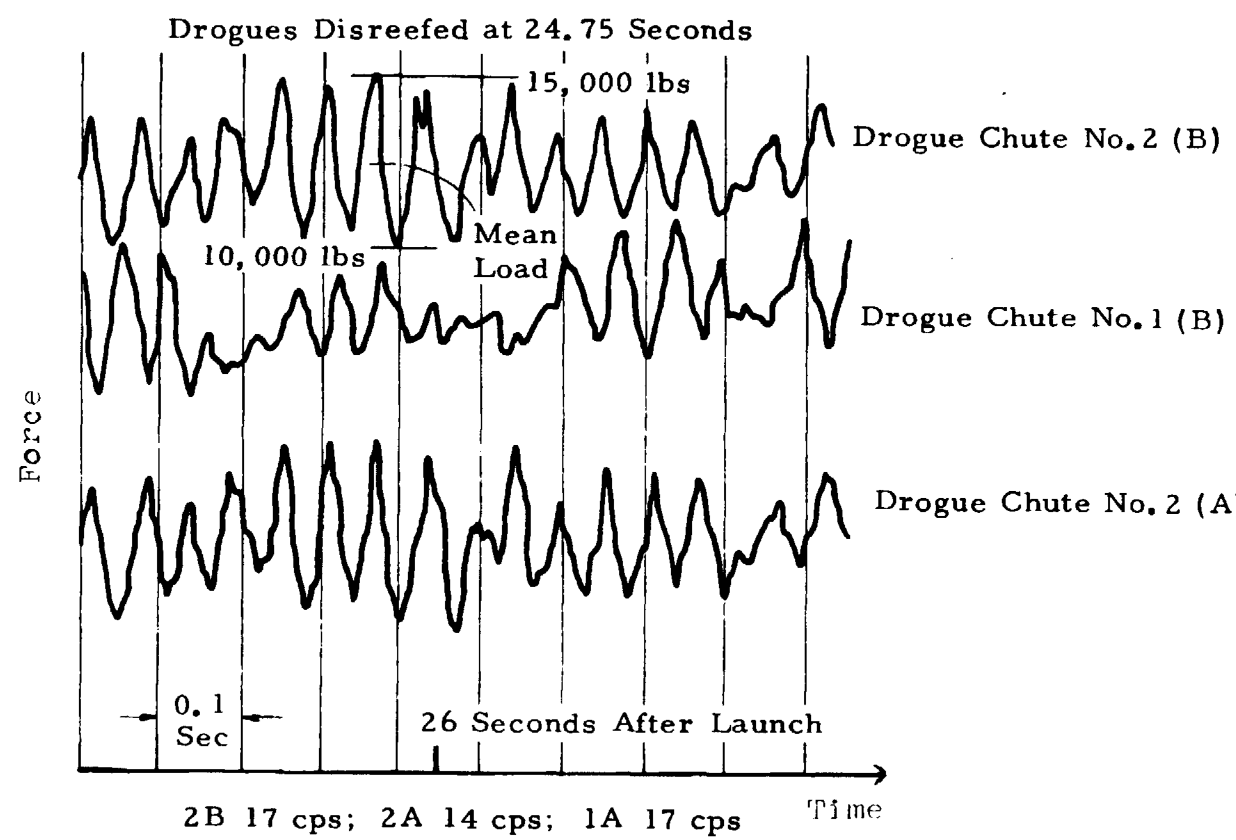

Fig. 78. Typical Drogue Chute Force-Time Trace

5.3.1.4 <u>Determination of f_e from Data</u>. The telemetry data of force versus time was surveyed to find the drop tests in which canopy oscillations occurred. The onboard and offboard films for the tests that contained oscillations were analyzed to select only those cases in which the oscillations were longitudinal.

For this set of telemetry data, the zero crossings of the force versus time data were counted to yield frequency of oscillation versus time. The mean frequency for one-second intervals was then recorded. It was a simple matter to relate time from opening to descent velocity through the computer output of the Askania data. Thus, the mean frequency of oscillations, f_e, was obtained versus the mean descent velocity v, for one-second intervals. For the particular example of f_k = 11.7 cps, calculated from Test 84-1R drogue chute 2, the corresponding values of f_e are as follows:

<u>Drogue 2 Test 84-1R</u>

v	(ft/sec)	630	600	550	500	480	460	440	430	420
f_e	(hz)	17	17	17	16	15	14	14	13	13

Tables of the calculated values of f_k and the experimental f_e are given in Table 28 for Tests 83-6, 84-1R, 84-4, 85-2, 85-5 and 99-3.

5.3.1.5 <u>Discussion of Results</u>. It is seen from the comparison of the f_k to f_e that the cumulative assumptions for f_k have yielded answers that are much better than order of magnitude accuracy. Since each assumption is a potential source of error, it is left up to further investigations to show what and how much of an effect each assumption has on the comparison of dimensional theory to experiment in canopy oscillations. This theory can provide a valuable tool for the designer who has to know beforehand at what frequencies his parachute systems will oscillate. In addition, this analysis was carried out for a variety of canopies, giving in each case very good correlation to the observed experimental values.

It should be pointed out that the analytical results are to be taken as correlating very well in order of magnitude only, even though in all of the cases, f_k and f_e are within a few tens of percent of each other. It is best to be conservative in the claims made about an analytical method until the detailed effects of the assumptions can be found experimentally to substantiate the method. It is felt, however, that the general assumptions made are valid and true representations of the problem.

5.3.2 Random Field Model for the Forcing Function

It was stated previously that the dimensional analysis method does not include consideration of the micro-structure of the physical phenomena for F(t). In simple cases where there is one characteristic length, the dimensional analysis could give answers for F(t) that were as close to reality as those given by the random field model. However, a demonstrative example is found in thermodynamics where the pressure of a perfect gas on a piston can be calculated from perfect gas laws or by considering the changes in momentum of all of the gas molecules hitting the piston surface. Either method gives the same answer; however, the second method gives a more fundamental understanding of the process involved. The worth of the much more complicated second method is not evident in the simple, what's-the-pressure-on-the-piston problem. However, if the gas in the system became so dilute as to stop being a continuum, or the gas molecules were really vapor metal, or again if there were pinholes through the surface of the piston, it would become solvable only by the fundamental method. An analogous fundamental system will now be described as an aid to solving more sophisticated oscillation problems that depend on more complicated versions of M, k, ν, and $F(t)$ and more complicated interactions of these.

5.3.2.1 Physical Model The problem at hand is to consider what is happening to the parachute canopy while it is oscillating. The answer to this question was partially developed in the basic functional form and is written here again as

$$G \quad (M, k, \nu, F(t)) = 0 \tag{38}$$

However, in this model the mass and spring constants are functions of the fluid viscosity and the forcing function, while the forcing function is a function of the viscosity and so-on. The physical model that would yield such functional interdependencies is as follows: The fluid flows in front, within, and behind the canopy are in turbulent motion. All of the eddies associated with these flows are of a size that, in a very general way, depend upon the dimensions of the canopy. (This is again for the case of no forebody.) In this way, the four variables M, k, ν, $F(t)$ depend upon the nature of the turbulence.

The mass, M, that must now be considered for the calculation of f_k, depends upon how much mass is swept into and out of the domain of influence of the parachute by the turbulent field. Thus, at any particular time, there will be eddies breaking away from the stagnated air flow behind the canopy or pumping high energy air into the wake, thereby reducing the added mass of the canopy. Therefore, the added mass depends upon the domain of influence of the canopy, and this domain of influence depends in turn upon the turbulent field. For example, a slotting system that pumps high energy free stream air into the turbulent wake would reduce the domain of influence of the parachute.

The spring constant, k, is a function of the canopy material and the compressibility of the air, the latter dependence being influenced by the nature of the flow field. However, unless the turbulent eddy velocities approach the speed of a pressure wave through the fluid, the change in k because of the turbulent field can be considered to be of second or higher order.

It is well known that the turbulent air mass within the influence of the canopy has an artificial viscosity. Thus, the damping that is experienced because of the artificial fluid viscosity is dependent upon the nature of the turbulent flow field. In fact, the artificial viscosity can be directional in an inhomogeneous turbulent flow. This means that oscillations in one direction would be damped more than oscillations in another direction. This phenomenon is based upon an eddy having a dynamic "memory". This "memory" tends to resist the motion that would disturb it. Another turbulent flow characteristic is that there are time scales associated with the eddies. This means that a given homogenous eddy field will tend to damp some frequencies and reinforce or transmit other frequencies.

The forcing function $F(t)$ has already been assumed to be solely dependent upon the turbulent field under the canopy's influence. The dependence of M, k, ν, and $F(t)$ upon the flow field has now been shown and must be considered mathematically in the following subsection.

5.3.2.2 Mathematical Model Formulation. The mathematical model must make a basic assumption in order to become tractable.

This assumption is that the known functional form of the auto-correlation function exists. In fact, such information concerning the auto-correlation function, if known, would have represented a sophisticated experimental project. Since the auto-correlation function is not known, the worth of this Section 5.3.2.2 lies not in the quantitative results, but as a technique to be outlined now and used in the future. In the future, it would be sufficient to determine the form of the velocity auto-correlation function through experiment in the turbulent flow areas in and about the canopy. In the case where a forebody is generating a wake, the best obtainable data would result from the determination of the correlation function in the wake, and in and around the canopy, while the flow in the canopy is under the influence of the wake. Section 5.4.2 will discuss the wake correlation measurements in more detail.

Summarily then, the functional form of the auto-correlation function is a necessary step in the determination of the kinetic energy distribution through the frequency range of the eddies. The energy distribution then shows one what the forcing function looks like. The forcing function, in turn, shows how the turbulent air mass interacts with the parachute system during canopy oscillation.

The outline of the formal mathematical development follows. The Fourier decomposition of the fluctuating velocity field $\underline{v}\ (\underline{x})$ is

$$\underline{v}\ (x_1,\ x_2,\ x_3) = \int_{-\infty}^{\infty} e^{i\underline{k}\underline{x}}\, d\underline{Z}\ (\underline{k}) \tag{46}$$

where $\underline{k}$ = wave number in $k_1,\ k_2,\ k_3$ and $\underline{v} = v_1,\ v_2,\ v_3$.

Since the derivative of the function $\underline{Z}$ ($\underline{k}$) is not finite, Equation (46) is a stochastic Fourier-Stieltjes integral of a generalized kind. This representation is necessary to take account of the fact that when the energy spectrum is continuous, the function $\underline{Z}$ ($\underline{k}$) is not in general of bounded total variation. The increment $d\underline{Z}$ ($\underline{k}$) is a random variable since its value at $\underline{k}$ depends on the particular realization of the velocity distribution $\underline{v}$ ($\underline{x}$) and one is interested in average properties.

Taking the inverse transform of Equation (46) gives

$$d\underline{Z}\ (\underline{k}) = \frac{1}{2\pi} \int_{-\infty}^{\infty} e^{-i\underline{kx}}\ \underline{v}\ (\underline{x})\ d\underline{Z},$$

and taking $*$ to mean complex conjugate,

$$\lim_{d\underline{k} \to 0} E \left\{ \frac{dZ_i^*\ (\underline{k}) \cdot dZ_j\ (\underline{k})}{dk_1 dk_2 dk_3} \right\} = \frac{1}{(2\pi)^3} \int_{-\infty}^{\infty} R_{ij}(\underline{r})\ e^{-i\underline{k}\cdot\underline{r}}\ d\underline{r}$$

Where $E\{\}$ represents the expected value and R_{ij} is the correlation function in tensor form.

Also, $\underline{r}$ = separation vector between two points x and x'.

The Fourier transform of the correlation tensor R_{ij} ($\underline{r}$) is the energy spectrum function Φ_{ij} ($\underline{k}$) which represents the distribution of kinetic energy over wave space for the turbulent field. Mathematically, this is

$$\Phi_{ij}\ (\underline{k}) = \frac{1}{(2\pi)^3} \int_{\infty}^{\infty} R_{ij}\ (\underline{r})\ e^{\ i\underline{kr}}\ d\underline{r} \qquad (47)$$

and this is related to the fluctuating velocity field by

$$\int_{-\infty}^{\infty} \Phi_{ij} (\underline{k}) \quad d\underline{k} = E \{ v_i \ (\underline{x}) \ v_j \ (\underline{x}') \} \tag{48}$$

and

$$E \left\{ v_i(\underline{x}) \ v_j \ (\underline{x}') \right\} = \int_{-\infty}^{\infty} \int_{-\infty}^{\infty} e^{i\underline{x} \cdot (\underline{k}-\underline{k}')} \ E \{ dZ_i(\underline{x}') \ dZ_j(\underline{x}) \} \tag{49}$$

The solution of Equation (47) represents the distribution of turbulent energy with respect to wave number. Therefore, Equation (47) would be used to find the frequency at which most of the energy of the turbulent flow was concentrated. The maximum energy can be considered as the prominent forcing function $f(t)$ on the canopy at that frequency. It is noted that to obtain the energy spectrum function, $\Phi_{ij} (\underline{k})$, it is necessary to know the correlation function, $R_{ij}(\underline{r})$. The correlation function is determinable from experiment. In summation, to find the forcing function on the canopy for a turbulent flow, it is necessary to determine the energy spectrum function which in turn depends upon the correlation function. The fundamental requirement to carry this mathematical treatment to a quantitative answer is therefore the determination of the auto-correlation function, $R_{ij} (\underline{r})$ by experiment.

This completes the outlines of the mathematical method. (The reader is referred to an excellent paper on this topic by the mathematician S. Chandrasekhar, "The Invarient Theory of Isotropic Turbulence in Magneto-Hydrodynamics"[44] and the section "Some Linear Problems" in the book, The Theory of Homogeneous Turbulence, by G. K. Batchelor.[45])

5.4 THE FOREBODY TURBULENT WAKE FREQUENCY, f_w

It was previously mentioned that having a forebody is not a necessary condition to have the canopy oscillate, since the forcing function, $F(t)$, is due to the turbulent air flows in and about the canopy. It was also mentioned that the parachute system acts like a band pass filter in that, of all the forcing function frequencies it comes across, it is responsive to only a few. From this point onward, "parachute system" is taken to mean the complete response function, f_k'. This implies that M, k, ν and $F(t)$ combined are the new system with a response frequency f_k' and an external forcing function, the forebody wake, f_w. It is physically obvious why this redefinition is necessary, since the forebody wake will now also interact with the turbulent flows that are under the canopy influence. In addition it can readily be seen from a dimensional analysis point of view that the maximum forebody wake-canopy flow interactions take place when the time scales of the forebody wake and the canopy turbulent flows match. Section 5.4, therefore, asks the question, is the energy in the turbulent forebody wake at the responsive frequency, f_k', of the parachute system? The following sections deal with this question in detail.

5.4.1 Dimensional Analysis Model

5.4.1.1 Physical Model Formulation. As the forebody moves through the fluid medium, a turbulent wake is generated behind it, and a part or all of the parachute system moves through this wake. This turbulent wake has an energy distribution through the frequencies of its eddies that depends directly upon the forebody shape. Therefore, if the body is geometrically clean, i.e., it has only one characteristic length, then the energy distribution of the eddies will be in the shape of a concentrated peak at the frequency that is proportional to the inverse of the forebody's characteristic length. As the forebody becomes more unclean geometrically; e.g., as the geometry of an aircraft, then the energy distribution of eddies in the wake is spread over many frequencies. A graphical representation of these statements is shown in Figure 79 .

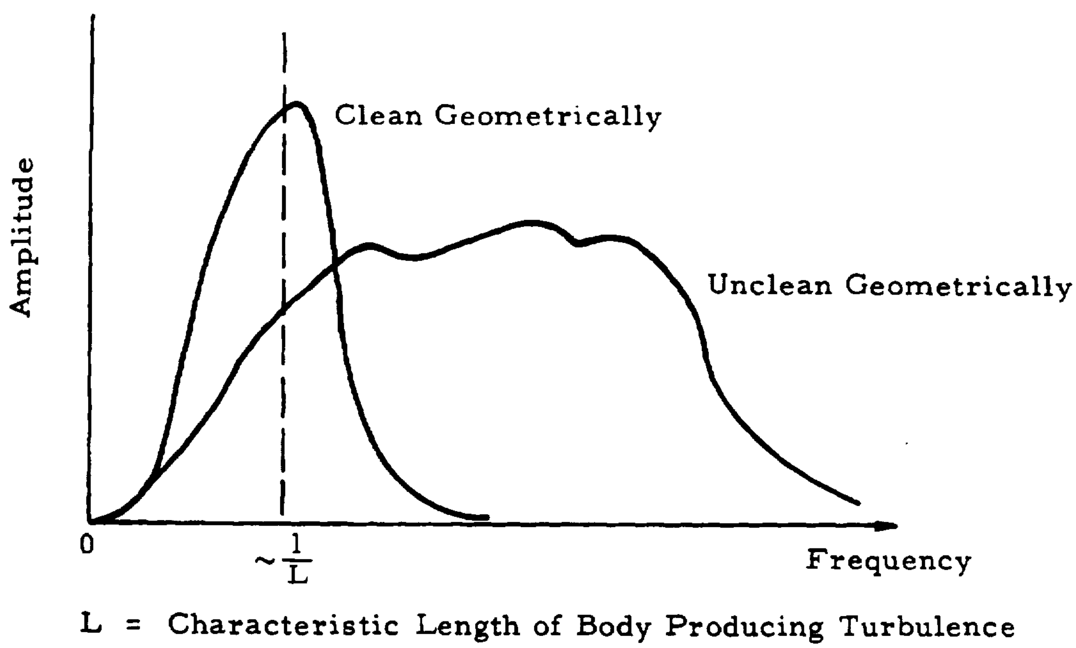

Fig. 79. Typical Turbulent Energy Distribution for Clean and Unclean Geometrical Shapes

In the case of the "more-than-one-characteristic-length" forebody with its more-than-one associated wake frequencies, beat frequencies are produced as upper and lower sidebands. (There is an upper limit to the frequency possible in a particular fluid. This upper limit is set by viscous dissipation and is called the Kolmogoroff microscale. The lower limit is, of course, the plane wave.) Therefore, even though a wake analysis would show the frequencies, f_w, to be much greater than the response frequency, f_k' or f_k, the lower sideband must be investigated before a conclusion about the influence of f_w on f_k' (or f_k) could be reached. In the case of a clean forebody with one characteristic length, this beat frequency phenomenon becomes of secondary importance as a possible source of energy for the response system. This is because the upper sidebands become too high and the lower sidebands become too low. The effect of viscosity and unequal pressure distributions in the wake is to never allow a single shape peak at only one frequency to occur, such as the Dirac delta function. This means that there will always be beat frequencies produced.

In addition to viscosity, a turbulent characteristic known as "vortex stretching" tends to transfer energy from low frequency eddies to higher frequency eddies. Vortex stretching is the inertial smearing of frequencies while viscosity is a molecular smearing. While this frequency band broadening is going on, the peak intensities also are being reduced, so that a typical turbulent flow field would decay with time as shown in Figure 80.

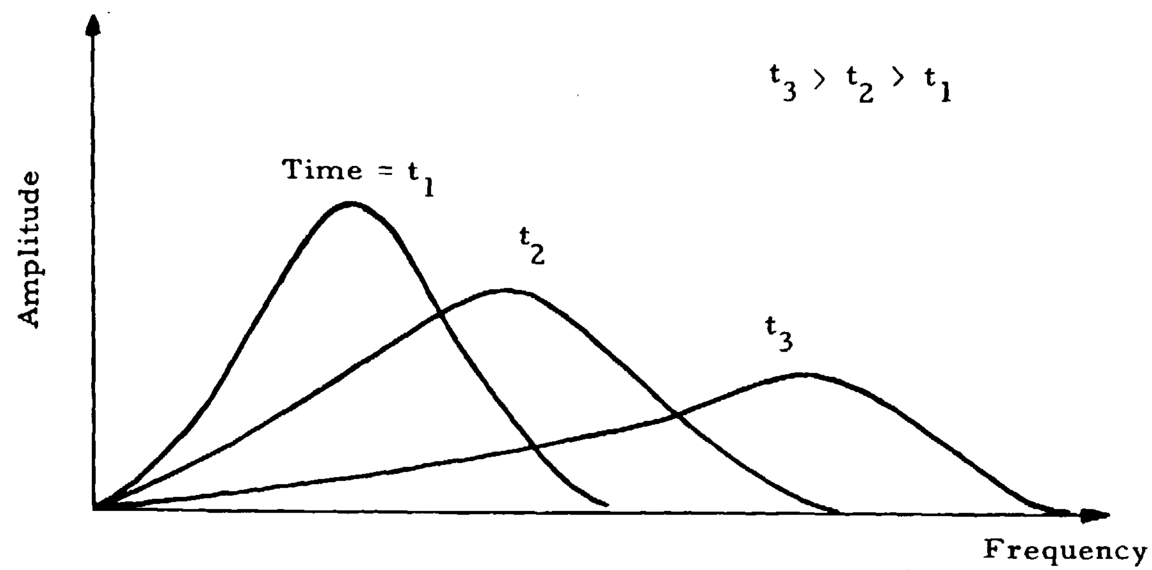

Fig. 80. Turbulent Decay with Respect to Time

Thus, if the parachute system were far enough behind the forebody, it would see a changed turbulent wake from the one originally generated. However, this decay process does not begin to occur until somewhere around 150 to 200 forebody characteristic lengths behind the forebody.

For the later mathematical analysis the assumption of homogeneity must be made for the wake. Typically, a wake will become homogeneous beyond fifteen characteristic lengths of the forebody. Homogeneity is therefore a valid assumption to use to calculate the energy spectrum behind the module. In summation for Section 5.4.1.1, the physical flow system can be described as a homogeneous, nondecaying, turbulent wake that is generated by a forebody. This wake interacts with the turbulent fluid contained by the canopy, which in turn interacts with the parachute canopy.

5.4.1.2 Dimensional Analysis Mathematical Model. A clean forebody shape is assumed for this section, otherwise, the dimensional analysis would have difficulty handling the nonlinearity of the inertial and viscous interactions between different size eddies. Hence, for a single characteristic length, the form for the wake frequency is

$$f_w = \frac{1}{2\pi} \frac{v}{D_V} \tag{50}$$

This form of f_w will be used as the dimensional estimate of the shed vortices in the forebody wake.

5.4.1.3 Experimental Results. The experimental values of v and D_V to be substituted into Equation (50) were obtained from previous sections. For the example of 84-1R, a comparison of f_w to f_k is shown in Table 28. $D_V = 70$ in. is the diameter of PTV. The rest of the data are shown in Table 28.

It is evident that the shed vortices from the forebody supply energy to the parachute system. Thus, the turbulent wake only aggravates the oscillation problem. It should also be noted that the ratio of D_c/D_v is order (1) for the first reefed stage, the exact condition that would cause maximum interference between the wake and the parachute system.

5.4.2 Random Field Model

5.4.2.1 Physical Model. This model has been described generally in the introduction to Section 5.4 so that its description here will be brief. The fundamental idea is that the forebody wake does not directly influence the canopy, but rather, that the wake directly influences the trapped turbulent flow in and behind the canopy. Generally then, if the turbulence characteristics in the influence region of the canopy were much different from the turbulence characteristics of the wake, the wake turbulence influence on the canopy would be modified greatly or its influence might not even be detectable. (It is implicitly assumed that the intensity of both flow fields is of the same magnitude.) With this physical picture in mind, the general mathematical formulation can now be presented.

5.4.2.2 General Mathematical Model Formulation. Only a brief outline of the mathematical analysis will be presented here. This section, as Section 5.3.2.2, suffers because of the absence of a specific functional form for the correlation function measured in the forebody wake (so that quantitative results are not available). The mathematical outline is as follows:

a. Homogeneity must be assumed.

b. A Fourier decomposition and formation of the expression for the correlation function must be accomplished.

c. The energy spectrum function must be obtained. (These three parts are exactly the same as the analysis presented in Section 5.3.2.2).

d. This energy function is then the forcing function for the stagnated canopy air which can be represented as a nonlinear differential equation for a mass-spring-dashpot system.

e. Once the response of the mass-spring-dashpot system has been found, this response in turn becomes the forcing function for the canopy.

f. The canopy is represented as a linear mass-spring-dashpot system and its response to the forcing function of the stagnated air is found.

5.5 CONCLUDING REMARKS

The cause of parachute oscillations has been analyzed without a forebody and with a forebody by the classical mass spring dashpot system and by the description of a stochastic system analysis. The msd model gives a very good method by which a designer can find the oscillation frequency of the parachute. The testing of the validity of the msd model shows it to hold for a variety of cases. These range from PTV drogue chutes reefed and unreefed to the simulated Apollo modules reefed main parachutes. This model shows that the parachutes being designed at the present time have very strong interactions with the wake of the forebody.

Just in the light shed by the quantitative answers of the msd analysis, it is suggested that the method developed in this report be used in the design of parachutes to avoid the wake-canopy interaction. This can be done by designing the canopy system away from frequency resonance with the forebody wake or the canopy's turbulent field.

The development of a quantitative answer for the stochastic model was impossible because of the nonexistence of the wake and canopy flow data needed to form the auto-correlation function. If the needed velocity correlation measurements were taken and the stochastic model developed, it would give a powerful analytical tool for predicting the physics of the turbulent flows, and the dynamics of all the canopy oscillations, not just the longitudinal ones. Used in conjunction with the msd shortcut method, the stochastic method would give a complete understanding of the system in both the micro and macro levels.

SECTION 6.0

INVESTIGATION OF PARACHUTE INFLATION PROCESS

The study documented in this section took as its objective the development of concrete ideas on how the parachute inflation process could be analyzed by analytical and/or numerical analysis techniques (as opposed to empirical techniques). To develop these ideas, the equations governing the fluid motions and canopy deformations were studied. Only by working with these equations was it believed that analysis methods would be developed that could predict detailed information on the shape, pressure, stress and strain distributions throughout the entire parachute during the complete inflation process. This approach was taken because this information, if it could be predicted, would be of great value to parachute designers during the development of new parachute designs.

6.1 REVIEW OF PERTINENT LITERATURE

The first attempt to study the parachute inflation process by examining transient fluid motions appears to have been an investigation by Weinig[22] in 1951. Weinig studied the case of a decelerating, expanding sphere traveling in an incompressible fluid. For this case, Weinig was able to derive relatively simple expressions for the velocity potential in the fluid surrounding the sphere. He then derived expressions for the components of the velocity throughout the fluid flow field and the pressure acting on the surface of the sphere. By integrating the pressure over the surface of the sphere, Weinig showed that there are fluid forces which resist both lineal deceleration and dilatation type motions. Weinig developed the following expressions for the ideal fluid forces along the flight path and normal to the surface of the sphere, respectively:

$$F_v = \frac{2\pi}{3} R^2 \rho \left(R \frac{dv}{dt} + 3\, v\, u\right) \tag{51}$$

$$F_u = 4\pi R^2 p_\infty - \pi R^2 \rho \left(v^2 + 6\, u^2 + 4\, R \frac{du}{dt}\right) \tag{52}$$

where

F_v	=	fluid force on sphere in direction of flight path,
F_u	=	fluid force normal to surface of sphere,
ρ	=	fluid density,
p_∞	=	fluid pressure at infinity,
R	=	radius of sphere,
$u = dR/dt$	=	dilatation velocity of sphere,
v	=	lineal velocity of sphere, and
d/dt	=	time rate of change.

Weinig then modified these equations by dropping the first term on the right-hand side of Equation (52) and by incorporating several additional terms in both equations to account for drag type (nonideal fluid) forces. Finally, he proposed a scheme for solving the parachute inflation process using two momentum equations which featured fluid forces of the types given by his modified fluid force equations. These equations featured eleven aerodynamic constants which he proposed could be experimentally determined. Although Weinig's final equations may never find a practical application, the instructive value of his analysis is considered noteworthy.

An analysis of the dynamic stress in an inflating parachute was presented by Asfour[31] in 1966. He proposed that the maximum stress in a canopy is related in a particular way to the radial component of the velocity in concentric slices of air contained within the canopy at a "stagnation plane" that moves from the apex of the canopy to the skirt during the inflation process. Asfour postulated that at the instant a concentric slice reaches its maximum diameter, the radial component of the air inflow is decelerated by a transient hoop stress occurring in the ring of canopy cloth that bounds the slice. He developed an expression for evaluating this stress, designated as "snap stress," and related it to both diameter and filling time. A review of the method indicates that it has limited usefulness. In particular, it is now known that Apollo ringsail parachutes do not inflate in the same manner that Asfour postulated; see for example, the stress-time study presented in Section 4.0 of Volume II.

A theoretical model of the parachute inflation process was presented by Roberts[32] in 1968. He developed a set of six governing equations for the deformation dynamics of a parachute structure under arbitrary pressure loading conditions. Associated with these 6 equations, which were simultaneous second order partial differential equations, were 6 auxiliary equations, 12 boundary conditions, and 13 initial conditions. Roberts indicated that it would be required to couple these equations with the equations of fluid dynamics, but he failed to indicate how this might be done for a case having practical interest. However, he did recognize that this would be required, and he did give an expression for the pressure distribution on one side of a two-dimensional parabolic shell.

A technique for obtaining the internal loads, stresses and strains of an inflating parachute, based on a limited amount of test data, is presented in Section 4.0 of Volume II. This technique does require rather good data on the profile shape and riser force as a function of time throughout the inflation process. Knowing these two items of data, it is shown that the parachute canopy distribution of differential pressure can be estimated over the entire canopy at any instant during the inflation. The technique is applied to the Apollo main parachute by analyzing the state of the canopy at 12 discrete instants of time during an inflation for which the required shape and riser force data were available. This analysis produces a stress-time history for essentially every structural element in the parachute. The disadvantage of this new stress-time technique is that good flight test data must exist before it can be applied.

6.2 BACKGROUND DISCUSSION

Spacecraft parachutes function for periods of time that range from seconds to minutes. For example, the periods of operation for the Apollo drogue, pilot and main parachutes for a normal entry are one minute, two seconds, and five minutes, respectively. The manner in which a parachute performs throughout its period of operation is of great interest to a parachute designer. However, the brief moments during the opening of the parachute hold the greatest interest to the parachute designer. This is because the largest loads are usually experienced by the parachute during its opening. If a parachute is going to burst, that would be the time.

What is the nature of the opening process? From the standpoint of an aerodynamicist, the following observations may be made. First, the process is completely transient: the flight velocity, the flight path angle, the added mass, the parachute shape, and the parachute dimensions all change during the process. Second, the canopy is porous, both due to its geometrical (built-in) porosity and due to the inherent porosity of the cloth out of which the canopy is constructed. Furthermore, this porosity is nonuniform in its distribution over the surface of the canopy; also, it changes as a function of the loading during the process. Third, the shape of the canopy is such as to induce flow separation both at the "sharp leading edge" of the skirt and at the "blunt" rearward, or apex portion of the canopy. Fourth, the process is, at least to a certain extent, stochastic in nature; it does not always work the same way every time. Some of the fluid, parachute, vehicle and planetary properties that are, or may be, important in a parachute opening process are listed in Table 29.

Table 29. Properties That Are, or May Be, Important in a Parachute Opening Process

A. FLUID PROPERTIES

1. Density
2. Temperature
3. Compressibility
4. Viscous Dissipation

B. PARACHUTE PROPERTIES

1. Aerodynamics
2. Parachute Type and Dimensions
3. Material Density
4. Material Porosity
5. Material Elongation Characteristics
6. Material Bending Characteristics
7. Reefing Time Intervals

C. VEHICLE PROPERTIES

1. Mass and Inertia
2. Aerodynamics
3. Riser Attachment (arrangement and location)
4. Wake

D. PLANETARY PROPERTIES

1. Gravitational Constant
2. Fluid Density Gradient

It may be observed that powerful mathematical techniques are available for analyzing processes; in particular, modern control theory. However, modern control theory is not suited to the task of analyzing the parachute opening process. This is because the governing equations for the parachute opening process are partial differential equations. Modern control theory is based on a rationale which uses ordinary differential equations and is, unfortunately, not suited to this task.

The partial differential equations of the parachute opening process are (1) the equations that govern the motions of the fluid, and (2) the equations that govern the motions of the parachute structure. These equations must be treated as a simultaneous set. Depending on the complexity of the mathematical model, these equations may include terms that account for some or all of the properties listed in Table 29. Also, initial conditions must be specified with the governing set of partial differential equations in order to completely specify a specific process.

The problem posed in the foregoing paragraphs is indeed formidable. It is therefore appropriate to give consideration to what might be an acceptable model, both from the standpoint of being physically relevant and from the standpoint of being mathematically solvable. Many of the properties listed in Table 29 often have little importance and can sometimes be disregarded without undue loss of generality. On the other hand, certain properties must be included in any worthwhile model. Therefore, a good question to ask might be: Is there a simple model that would be both physically relevant and mathematically tractable?

A simple model for the process could be made by assuming that the parachute consists simply of a canopy and many suspension lines, and that it is axisymmetrical. The canopy properties could be idealized by assuming zero material density, constant canopy porosity, infinite elongation stiffness, and zero bending stiffness. A simple model for the fluid could be obtained by assuming that the fluid is everywhere incompressible and irrotational. The latter assumptions, the assumptions of potential flow, permit the fluid motions to be expressed in terms of Laplace's equation. A number of techniques are available for finding solutions to this equation, and it is therefore apparent that this would be an attractive approach.

There is little doubt that an approach based on Laplace's equation can be used to obtain meaningful solutions to the parachute opening process. It is also quite certain that these solutions can include effects due to material density, variable canopy porosity, material stiffness, etc. Such solutions can provide predictions for the motions of the fluid around the parachute as well as the motions of the parachute itself.

The approach described above is distinctly limited by the fluid model; i.e., the assumptions of incompressibility and irrotationality. Fortunately, there may be a way to circumvent this limitation. In particular, another approach for the fluid model is suggested by the success of recent studies in which the equations for time dependent fluid motions have been solved by numerical techniques. In this approach, the partial differential equations for the fluid motions are rewritten as finite difference equations. The space occupied by the fluid is divided into cells and the equations are solved by "stepping" forward in time. Even effects due to compressibility and viscous dissipation (including shock waves) may be numerically evaluated using finite difference techniques.

The following subsections continue this discussion. Section 6.3 presents the results of a study on the added mass terms that appear in the momentum equations along and normal to the flight path of an inflating parachute. Section 6.4 presents the results of a rather detailed study of the inflation process based on potential flow analysis. Finally, Section 6.5 briefly discusses the applicability of finite difference methods to the task of obtaining numerical solutions of the parachute inflation process.

6.3 MOTION EQUATIONS STUDY

The importance of added mass in the momentum equation taken tangent to the flight path was apparently first pointed out in 1946 by Scheubel.[12] Added mass has been used in practically all analyses of the parachute opening process since that time--but primarily in the momentum equation taken tangent to the flight path. How added mass should be included in the momentum equation taken normal to the flight path is not altogether obvious. Almost without exception, statements of this equation, when written for application to the parachute opening process, have not featured an added mass term. Two questions were therefore formulated. First, how should added mass be included in the momentum equation taken normal to the flight path? And second, how is the added mass that appears in this equation related to the added mass that appears in the momentum equation taken tangent to the flight path?

The concept of added mass (apparent mass, hydrodynamic mass, etc.) comes originally from the classical hydrodynamics literature. It is discussed as a part of the general topic of the unsteady motion of a body through a fluid in the hydrodynamics texts of Lamb,[46] Basset,[47] Milne-Thompson[48] and others. These texts show that if an incompressible, acyclic potential flow* is assumed, the effects of the surrounding fluid on a moving body can be represented by a fluid inertia tensor. It is only within the restrictions of this simplified fluid model that the concept of added mass has a precise meaning. The added mass terms discussed here are the only element of the inertia tensor required to describe fluid effects for simple ballistic motion.

* Acyclic potential flow is defined as potential flow in which the region occupied by the fluid is simply connected.

An undesirable feature of acyclic potential flow is that it predicts no steady state forces. As an approximation, steady state drag is therefore normally added to the unsteady forces predicted by potential flow theory.

The motion of a parachute system center of gravity during inflation is usually described by conservation of momentum equations taken tangent and normal to the flight path.

$$m \frac{dv}{dt} = m\ g\ \sin\ \theta - D + F_v$$
$$m\ v \frac{d\theta}{dt} = m\ g\ \cos\ \theta + F_w \tag{53}$$

where

m = system mass
g = gravitational acceleration
D = steady state drag
F_v = unsteady fluid force tangent to flight path
F_w = unsteady fluid force normal to flight path
v = flight path velocity
θ = flight path angle (positive downward)

In order to obtain solutions to these equations, an inflation equation is also needed to describe the rate of change of some characteristic parachute dimension, R. The inflation equation is not considered here.

The problem is thus one of finding the unsteady fluid force components F_v and F_w. It is assumed that the position of all points on the parachute can be described in terms of the center of gravity position and the parachute dimension, R. This essentially means that the parachute passes through the same family of axisymmetric shapes during every inflation.

Hydrodynamicists have long used the Lagrange equations to derive expressions for forces and moments imposed on a body as it moves through an incompressible, inviscid fluid. The application of these equations to a body of changing shape like an inflating parachute is somewhat unusual, but the basic principles are the same as for a fixed shape body. Consider an inflating parachute in ballistic motion as illustrated in the adjoining sketch.

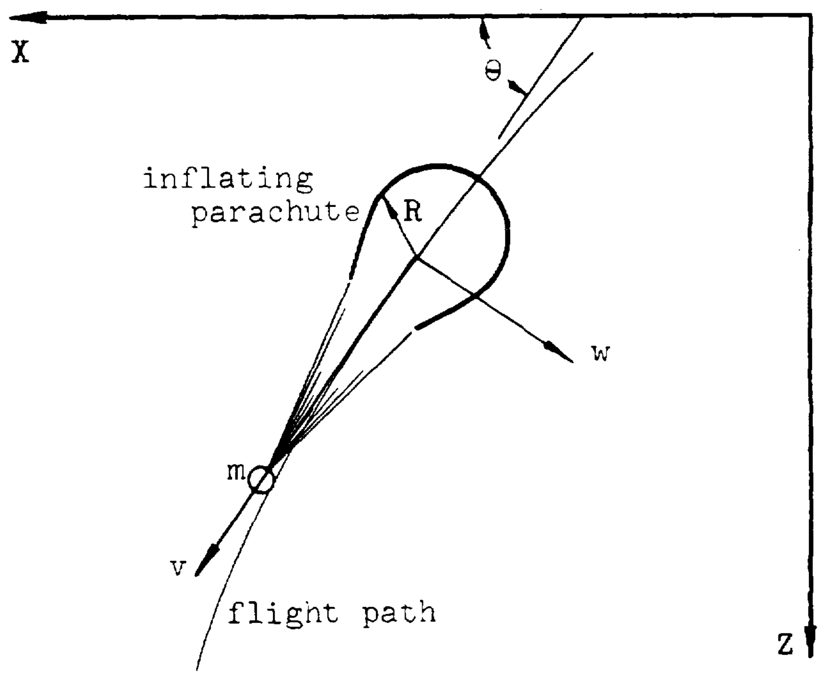

Assume the flow about the parachute to be incompressible, acyclic, potential flow, and let the parachute geometry be entirely specified by the characteristic dimension R. For this case, it may be shown that the kinetic energy of the surrounding fluid can be expressed in the form

$$T = \tfrac{1}{2}A_1 v^2 + A_2 v \frac{dR}{dt} + \tfrac{1}{2}A_3 \left(\frac{dR}{dt}\right)^2 + \tfrac{1}{2}A_4 \left(\frac{d\theta}{dt}\right)^2 \qquad (54)$$

where the coefficients A_1, A_2, A_3 and A_4 are different functions of the characteristic dimension R.

Forces in the X and Z directions are calculated from the Lagrange equations as

$$F_X = -\frac{d}{dt}\left(\frac{\partial T}{\partial \dot{X}}\right)$$
$$= -\frac{d}{dt}\left(A_1 \; v \cos\theta + A_2 \frac{dR}{dt} \cos\theta\right)$$

$$F_Z = -\frac{d}{dt}\left(\frac{\partial T}{\partial \dot{Z}}\right)$$
$$= -\frac{d}{dt}\left(A_1 \; v \sin\theta + A_2 \frac{dR}{dt} \sin\theta\right)$$

where $\quad v = \frac{dX}{dt} \cos\theta + \frac{dZ}{dt} \sin\theta$

Taking the derivatives and resolving the forces into components tangent and normal to the flight path gives the following relations for F_v and F_w:

$$F_v = -\left[A_1 \frac{dv}{dt} + \frac{dA_1}{dR} \frac{dR}{dt} v + A_2 \frac{d^2R}{dt^2} + \frac{dA_2}{dR}\left(\frac{dR}{dt}\right)^2\right]$$
$$F_w = -\left[A_1 \; v \frac{d\theta}{dt} + A_2 \frac{dR}{dt} \frac{d\theta}{dt}\right] \qquad (55)$$

The coefficients $A_1 = A_1(R)$ and $A_2 = A_2(R)$ are different, but related, added masses of the parachute canopy.

By inspection of the expression for F_v, it is seen that A_1 is the familiar added mass associated with acceleration of fluid by the canopy due to the acceleration of the system center of gravity along the flight path. It could in fact be defined as the force induced by the fluid per unit acceleration along the flight path. It is also seen that A_2 is a similar mass term but is apparently associated with acceleration of the fluid by the parachute canopy relative to the system center of gravity due to the change in the canopy shape. It could be defined as the force induced by the fluid along the flight path per unit acceleration of the parachute dimension, R. The other terms in the F_v expression are momentum type terms familiar to propulsion engineers. They occur because the parachute shape, and hence added mass, is variable during inflation.

It is seen from the F_W expression that added mass terms also appear in the trajectory angle equation. This fact has apparently been missed in much of the parachute literature.

Denoting s as the distance along the flight path and recognizing that $R = R(s)$, the ballistic equations can be written,

$$\frac{d}{dt}\left[v\,(m + m_a)\right] = m\,g\,\sin\theta - D$$

$$(m + m_a)\,v\,\frac{d\theta}{dt} = m\,g\,\cos\theta \qquad (56)$$

where $m_a = A_1 + A_2\,\frac{dR}{ds}$. This is not an especially convenient form for obtaining numerical solutions, but it shows that the total added mass effect can be written as $m_a = m_a(s)$. For all dynamically similar inflations of a given parachute, m_a is equal to the fluid density times the same function of s.

The above discussion is not intended as a rigorous description of all forces on a parachute during inflation. It is intended merely to clarify the concept of added mass and its use in ballistic equations. Including real fluid effects such as compressibility and viscosity obviously makes the problem much more difficult. Hopefully, first order effects can be included in added mass coefficients, as they are in the steady state drag coefficient.

6.4 APPLICATION OF POTENTIAL FLOW ANALYSIS

The results of a study, on applying potential flow analysis to predict the flow about an inflating parachute canopy, are presented in this section. A solution algorithm is developed for solving the inflation process based on both aero and structural dynamics equations. This algorithm sequentially solves for the instantanteous velocity potential, internal loads, canopy acceleration, pressure distribution, added mass, drag, lineal acceleration, and flight path angle rate. Knowing these quantities, a new canopy shape, canopy deformation rate, lineal velocity and flight path angle of the parachute system are computed. The process is repeated over and over, each computation cycle being advanced in time by a small amount until the inflation process is complete. In this manner, a detailed history is obtained for essentially every parameter of the inflation process.

The fluid equations for potential flow are presented and briefly discussed in Section 6.4.1. A method of solving for the velocity potential of a deforming canopy is described in Section 6.4.2. An equation for the pressure difference acting across a canopy surface in terms of aerodynamic parameters is derived in Section 6.4.3. A similar equation for the pressure difference across a canopy surface in terms of structural parameters is derived in Section 6.4.4. The two pressure difference equations are solved in Section 6.4.5 to give the pressure distribution over the canopy surface and a canopy acceleration vector. Also presented in Section 6.4.5 are equations for computing the transport velocity of the flow through the canopy surface, the added mass, and a drag force. Finally, an algorithm for computing the complete inflation process is presented in Section 6.4.6.

6.4.1 Fluid Equations

The equations of motion for an incompressible, irrotational fluid are presented, without being derived, in the following discussion. The reader interested in a thorough development of these equations is referred to References 46-48.

The continuity equation of an incompressible fluid is

$$\partial q_x/\partial x + \partial q_y/\partial y + \partial q_z/\partial z = 0$$

or simply

$$\nabla \cdot \underline{q} = 0 \tag{57}$$

where x, y, z are fixed cartesian coordinates and q_x, q_y, q_z are the components of the fluid velocity vector $\underline{q}$. Equation (57) applies for both steady and unsteady fluid motions. If the fluid motion is everywhere irrotational, then it may be shown to possess a velocity potential, ϕ. Equation (57) can then be written in the form of Laplace's equation,

$$\partial^2\phi/\partial x^2 + \partial^2\phi/\partial y^2 + \partial^2\phi/\partial z^2 = 0$$

or simply

$$\nabla^2\phi = 0 \tag{58}$$

The meaning of ϕ is given by the relations

$$q_x = \partial\phi/\partial x, \quad q_y = \partial\phi/\partial y, \quad q_z = \partial\phi/\partial z$$

or simply

$$\underline{q} = \nabla \phi \tag{59}$$

The velocity potential ϕ is a scalar quantity; in general, $\phi = \phi(x, y, z; t)$. Equation (58) is referred to as the potential equation, and the analysis of flows that satisfy this equation is referred to as potential flow analysis.

Potential flow analysis consists very largely of finding solutions to Equation (58) that satisfy specified boundary conditions. For an opening parachute, two types of boundary conditions are required. One specifies a compatibility condition at the surface of the canopy and the other specifies conditions far away from the parachute. The compatibility condition at the surface of the canopy is

$$(\nabla \phi_c - \underline{u}_c) \cdot \underline{n} = w_c$$

where $\nabla \phi_c$ is the velocity of the fluid at the canopy surface, $\underline{u}_c$ is the velocity of the canopy surface, and w_c is the transport velocity of the fluid through the surface. The symbol $\underline{n}$ denotes the outward unit normal to the surface. The second boundary condition is

$$\nabla \phi_\infty = 0 \qquad (60)$$

This states that the fluid velocity at limitingly large distances from the parachute (in any direction) is zero. The subscript ∞ denotes infinity.

It is convenient to define a coordinate system that moves with the parachute. Let this be a cartesian system $O'x'y'z'$ with origin O' at the apex of the parachute. Also, let the parachute be symmetrical and let the axis of symmetry lie along the z' axis. At time t, let the moving coordinate system $O'x'y'z'$ coincide with the fixed coordinate system $Oxyz$. The situation is illustrated in Figure 81.

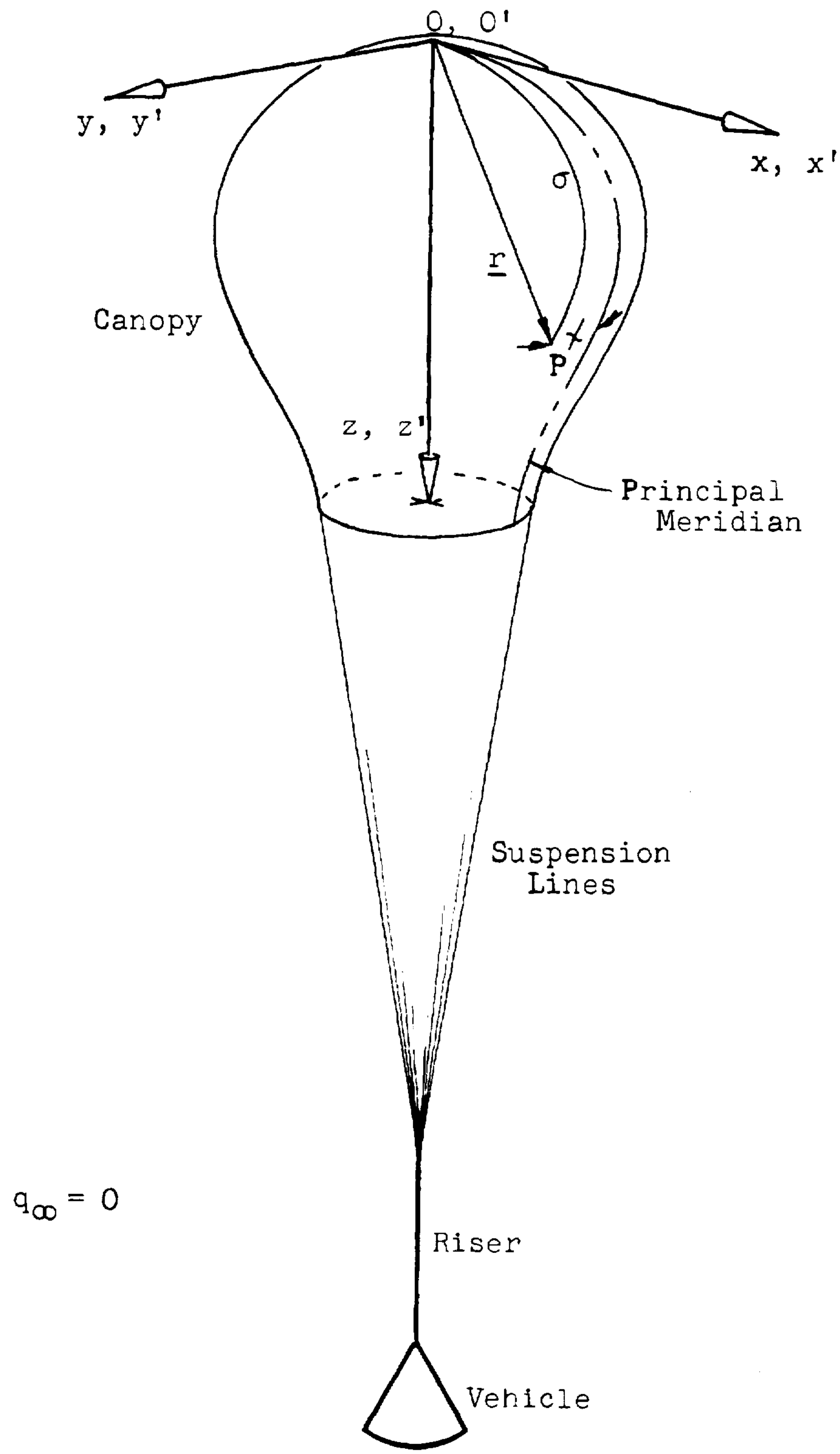

Fig. 81. Schematic of Parachute Showing the Fixed Coordinate System Oxyz and Moving Coordinate System O'x'y'z' at Time t.

A Point P on the canopy surface may be specified as

$$P = P(\sigma, \chi; t)$$

where σ is the curvilinear distance along the surface of the canopy from the apex (or meridional distance), χ is the azimuth angle of the point with respect to the principal meridian, and t is time. The principal meridian is shown in Figure 81; it is a curve on the canopy surface that lies in the $x'z'$ plane. The position of Point P may be denoted by a position vector

$$\underline{r}_P = \underline{r}\,(\sigma, \chi; t)_P$$

Likewise, the velocity of Point P relative to $O'x'y'z'$ may be denoted by a velocity vector

$$\dot{\underline{r}}_P = \dot{\underline{r}}\,(\sigma, \chi; t)_P$$

where the overdot denotes differentiation with respect to time; i.e., $\dot{\underline{r}} = d\underline{r}/dt$. Finally, the acceleration of Point P relative to $O'x'y'z'$ may be denoted by an acceleration vector,

$$\ddot{\underline{r}}_P = \ddot{\underline{r}}\,(\sigma, \chi; t)_P$$

where the double overdot denotes double differentiation with respect to time; i.e., $\ddot{\underline{r}} = d^2\underline{r}/dt^2$.

Let the velocity of the moving origin, O', with respect to the fixed origin, O, be the vector $\underline{v}$ that lies along the z and z' axes. The velocity of the canopy with respect to the fixed coordinate system $Oxyz$ is then

$$\underline{u}_c = \underline{v} + \dot{\underline{r}}$$

The compatibility condition at the surface of the canopy may now be written as

$$(\nabla \phi_c - \underline{v} - \dot{\underline{r}}) \cdot \underline{n} = w_c \tag{61}$$

In summary, the motions of an incompressible, irrotational fluid are governed by one equation, the so-called potential equation, Equation (58). Associated with this equation are two boundary conditions: a compatibility condition at the surface of the canopy, Equation (61); and a condition at infinity, Equation (60).

6.4.2. Solving for the Velocity Potential

Reference 47 presents a solution for the flow of an incompressible, irrotational fluid about a spherical bowl. This solution is obtained by distributing doublets over the surface of an indefinitely thin, bowl shaped shell. It is also shown in this reference that the velocity potential for the flow around an arbitrarily shaped, indefinitely thin sheet can be expressed by the equation

$$\phi\ (P') = \iint_A \frac{h \cos \alpha}{\xi^2}\ dA \qquad (62)$$

where ϕ is the velocity potential at any field Point P', h is the doublet strength per unit area, and A is the surface area of the sheet. The quantities α, ξ, and dA are defined in in the adjoining sketch. (Point P is at dA and $\underline{n}$ is the outward unit normal of dA.) Equation (62) is valid for Point P' anywhere except in the sheet that contains the doublets.

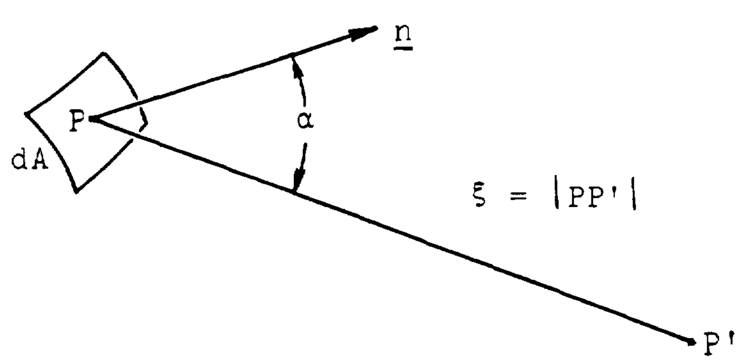

It is shown in Reference 47 that Equation (62) has the equivalent form

$$\phi = \iint h \, d\,\Omega \tag{63}$$

where $d\,\Omega = \cos\alpha \; dA/\xi^2$ is the solid angle subtended by dA as "seen" by Point P'. With this equation, it may be shown that the velocity potential on the inside surface of the sheet (subscript i) is greater than the velocity potential on the outside surface of the sheet (subscript o) by $4\,\pi h$. That is,

$$\phi_i - \phi_o = 4\pi h \tag{64}$$

The velocity potential given by Equation (62) is a well behaved function except at the sheet. For the case at hand, this is the canopy. Equation (61) requires evaluation of $\nabla\phi$ at the canopy, and because ϕ is discontinuous at the canopy, care must be taken in performing this evaluation.

A velocity potential of the form given by Equation (62) automatically satisfies Equations (58) and (60). Hence, the problem reduces to that of solving for the doublet distribution h that satisfies Equation (61). It is shown in Appendix B that Equation (61) may be expanded and rewritten as

$$\partial\phi/\partial n = \dot{R} \sin\phi - (\dot{Z} + v) \cos\phi + w_c \tag{65}$$

where $\partial\phi/\partial n$ is the gradient of ϕ normal to the surface, and $\dot{R}$ and $\dot{Z}$ are the time rates of change of the canopy coordinates. A schematic of the canopy illustrating the angle ϕ and other pertinent quantities is illustrated in the sketch on the next page.

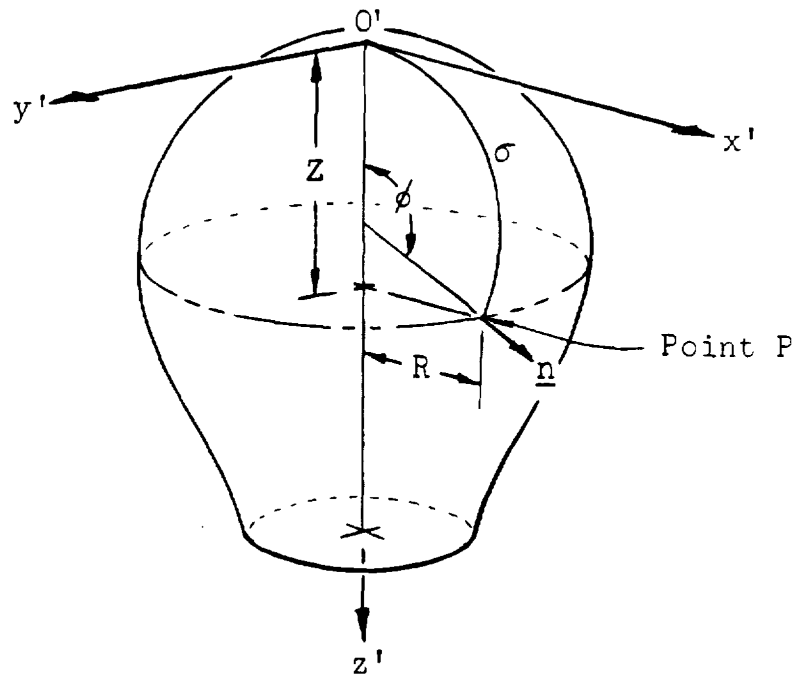

It is shown in Appendix B how Equation (62) can be used to solve for a doublet distribution vector, $\underline{h}$. This vector has n components and is written as*

$$\underline{h} = (h(\sigma_1),\ h(\sigma_2),\ \ldots,\ h(\sigma_n))^T \qquad (66)$$

The first component $h(\sigma_1)$ is the doublet strength in the region of the canopy apex; the second component $h(\sigma_2)$ is the doublet strength in an annular region surrounding the apex; and so forth until the last component $h(\sigma_n)$ which is the doublet strength in an annular region adjacent to the canopy skirt.

---

* In Equation (66) and subsequent equations, time dependence is ignored in the interest of keeping the notation simple.

A plot of doublet strength h versus meridional distance σ might look like the curve labeled "numerical solution" in the adjoining sketch.

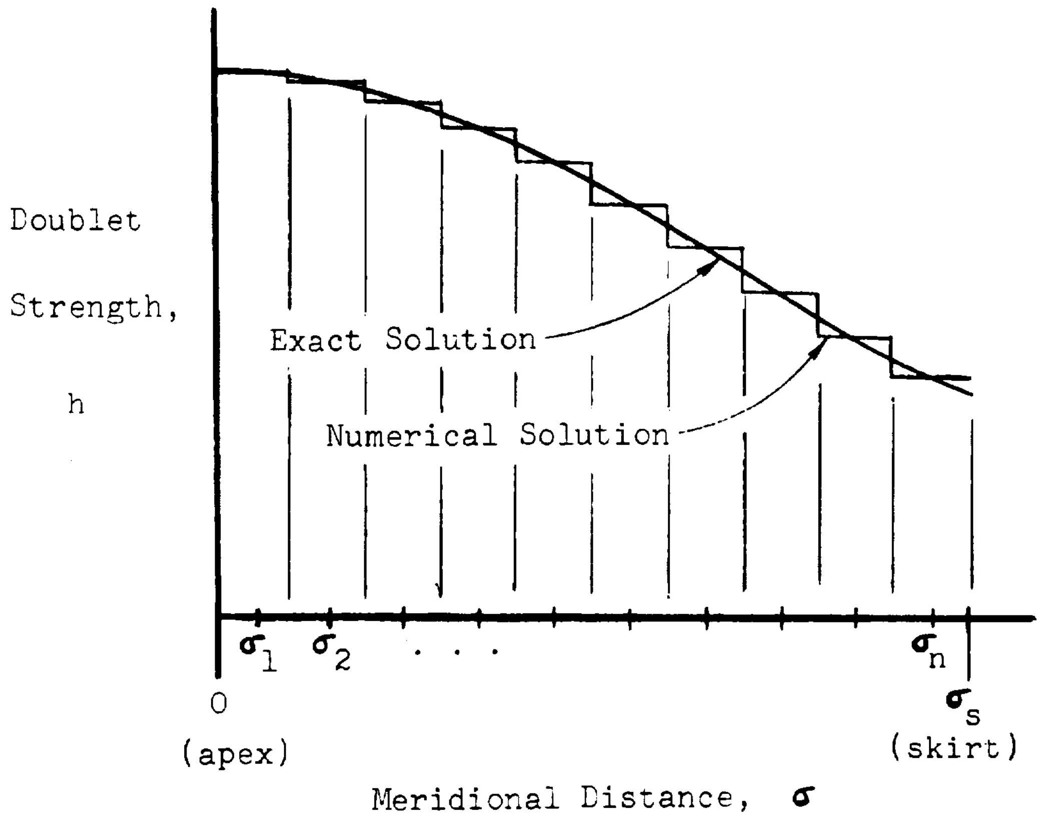

Once the doublet distribution is known, the velocity potential at any Point P', on or off the canopy surface, can be solved for by using Equation (62). Likewise, once the velocity potential is known, it is a relatively simple task to compute the velocity of the fluid at Point P' by using Equation (59).

6.4.3 Aerodynamic Pressure Equation

Of even greater interest than the velocity of the fluid is the differential pressure Δp that acts across the canopy. In order to evaluate Δp, the transient pressure equation must be used. This equation is

$$p = p_\infty + \rho(\partial \emptyset/\partial t) - \tfrac{1}{2}\rho \; (\underline{q} - \underline{v})^2 + \tfrac{1}{2}\rho v^2 \tag{67}$$

The differential pressure at the meridional distance σ is

$$\Delta p(\sigma) = p_i(\sigma) - p_o(\sigma)$$

where $p_i(\sigma)$ and $p_o(\sigma)$ are the inside and outside pressures acting on the canopy at the meridional distance σ, respectively. It follows that

$$\Delta p = \rho \partial/\partial t(\emptyset_i - \emptyset_o) - \tfrac{1}{2}\rho \left\{(\underline{q}_i - \underline{v})^2 - (q_o - \underline{v})^2\right\}$$

By utilizing Equation (64) and by carrying out the operations indicated in the last term, this equation may be simplified to the form

$$\Delta p = 4\pi\rho \; (\partial h/\partial t) - \tfrac{1}{2}\rho \left\{(q_i{}^2 - q_o{}^2) - 2\;(\underline{q}_i - \underline{q}_o)\cdot \underline{v}\right\}$$

This may be further simplified by noting that

$$\underline{q}_i - \underline{q}_o = 2(\partial \emptyset_i/\partial\sigma)\;(\underline{m})$$
$$q_i{}^2 - q_o{}^2 = 0 \tag{68}$$

to give the following form

$$\Delta p = 4\pi\rho \; (\partial h/\partial t) + 2\;\rho v\;(\partial\emptyset_i/\partial\sigma)\sin\emptyset \tag{69}$$

The pressure distribution over the canopy may be conveniently represented by a pressure distribution vector $\underline{\Delta p}$

$$\underline{\Delta p} = (\Delta p\ (\sigma_1),\ \Delta p\ (\sigma_2),\ \ldots,\ \Delta p\ (\sigma_n))^T \qquad (70)$$

where the notation already used in Equation (66) is again employed. In the discussion that follows, this notation will be commonly used. It will even be used to denote canopy shape, velocity and acceleration vectors. In particular, the canopy shape, velocity and acceleration vectors are defined, respectively, as*

$$\begin{aligned} \underline{r} &= (\underline{r}\ (\sigma_1),\ \underline{r}\ (\sigma_2),\ \ldots,\ \underline{r}\ (\sigma_n))^T \\ \underline{\dot{r}} &= (\underline{\dot{r}}\ (\sigma_1),\ \underline{\dot{r}}\ (\sigma_2),\ \ldots,\ \underline{\dot{r}}\ (\sigma_n))^T \qquad (71) \\ \underline{\ddot{r}} &= (\underline{\ddot{r}}\ (\sigma_1),\ \underline{\ddot{r}}\ (\sigma_2),\ \ldots,\ \underline{\ddot{r}}\ (\sigma_n))^T \end{aligned}$$

Equation (69), when expressed in this notation, becomes

$$\underline{\Delta p} = 4\pi\rho\ \partial\underline{h}/\partial t + 2\rho v\ \underline{(\partial\phi/\partial\sigma)\ \sin\phi} \qquad (72)$$

An approximate expression for $\partial\underline{h}/\partial t$ is provided by Equation (B23) of Appendix B as follows:

$$\partial\underline{h}/\partial t = -\ (\underline{\underline{A}})^{-1}\ (\underline{\ddot{r}}_n - \dot{v}\cos\underline{\phi}) \qquad (73)$$

The quantity $(\underline{\underline{A}})^{-1}$ is a known $n \times n$ matrix and $\underline{\ddot{r}}_n$ is the component of the canopy acceleration normal to the surface. Substituting the right hand side of Equation (73) into Equation (72) gives the following relation for the pressure difference

---

* It should be realized that these vectors are defined with respect to the moving coordinate system O'x'y'z'. The actual velocity and acceleration are $(\underline{\dot{r}} + \underline{v})$ and $(\underline{\ddot{r}} + \underline{\dot{v}})$.

vector

$$\underline{\Delta p} = -4\pi\rho\,(\underline{\underline{A}})^{-1}\,(\ddot{\underline{r}}_n - \dot{v}\cos\underline{\phi}) + 2\rho v\underline{(\partial\phi/\partial\sigma)\sin\phi} \qquad (74)$$

Equation (74) provides an expression for the pressure difference across the canopy surface in terms of aerodynamic parameters. The next subsection provides a similar expression for the pressure difference in terms of structural parameters.

6.4.4 Structural Dynamic Pressure Equation

A numerical method for determining the shape and internal load distribution of a parachute for a given construction, canopy pressure distribution and riser load is developed in Section 3.0 of Volume II. Finite elements are used in the mathematical model to represent the parachute structure, and an iterative process is used to find the unique shape and internal load and strain distribution that satisfies the equilibrium and boundary conditions. The parachute structure consists of horizontal elements (sails or horizontal ribbons) which carry the circumferential loads and meridional members (radial tapes and suspension lines) which carry the meridional loads. The geometry of the radial tapes is governed by the following equation:

$$\Delta p_{se} = \left[\frac{P_R}{2\,RR_\phi\,\sin\pi/b} + \frac{N_\theta\,\sin\phi}{R\,\cos\pi/b}\right]\sqrt{1 - \sin^2\pi/b\,\sin^2\phi} \qquad (75)$$

where Δp_{se} is the static equilibrium pressure difference acting across the canopy surface and other symbols are defined as follows. P_R is the longitudinal load in the radial tape, and R_ϕ is the radius of curvature of the radial tape. N_θ is the transverse load in the radial tape per unit length along the tape, and the number of radial tapes in the parachute is denoted by b.

Equation (75) is for static equilibrium. The corresponding equation for dynamic equilibrium is

$$\Delta p = \Delta p_{se} + \mu \left[(\ddot{r} + \dot{v})_n + g \; (\sin \Theta \cos \phi - \cos \Theta \sin \phi \cos \chi) \right] \tag{76}$$

where $(\ddot{r} + \dot{v})_n$ is the magnitude of the canopy acceleration normal to the surface, $g \; (\sin \Theta \cos \phi - \cos \Theta \sin \phi \cos \chi)$ is the component of the acceleration due to gravity in the direction normal to the canopy surface, and μ is the mass per unit area of canopy surface. The latter equation may be simplified somewhat by dropping the asymetrical gravity term and by replacing $\dot{v}_n$ with $\dot{v} \cos \phi$ to give

$$\Delta p = \Delta p_{se} + \mu \left[\ddot{r}_n + \dot{v} \cos \phi + g \sin \Theta \cos \phi \right] \tag{77}$$

Finally, this equation, when written in the vector notation described in the previous subsection, becomes

$$\underline{\Delta p} = \underline{\Delta p}_{se} + \underline{\underline{M}} \left[\ddot{\underline{r}}_n + \dot{v} \cos \underline{\phi} + g \sin \Theta \cos \underline{\phi} \right] \tag{78}$$

where $\underline{\underline{M}}$ is the $n \times n$ diagonal matrix,

$$\underline{\underline{M}} = \text{diag} \; (\mu(\sigma_1), \mu(\sigma_2), \ldots, \mu \; (\sigma_n)) \tag{79}$$

Equation (78) provides an expression for the structural dynamic pressure difference across the canopy surface in terms of structural, inertial and gravitational parameters. Its counterpart in terms of aerodynamic parameters is Equation (74).

6.4.5 Pressure Distribution and Other Quantities

Equations (74) and (78) provide two equations in two unknowns: $\underline{\Delta p}$ and $\ddot{\underline{r}}_n$. These equations may be solved by first eliminating either unknown and solving for the other. The most easily eliminated unknown is $\underline{\Delta p}$. Setting the right hand sides of the two equations equal to each other and collecting terms gives

$$\underline{\underline{B}}\,\ddot{\underline{r}}_n = -\underline{C} \qquad (80)$$

where

$$\underline{\underline{B}} = 4\,\pi\rho\,(\underline{\underline{A}})^{-1} + \underline{\underline{M}}$$

and

$$\underline{C} = \underline{\Delta p}_{se} + \underline{\underline{M}}\left[\dot{v}\cos\underline{\phi} + g\sin\theta\cos\underline{\phi}\right] - 2\,\rho v\,\underline{(\partial\phi/\partial\sigma)\sin\phi}$$

It follows from Equation (80) that the canopy normal acceleration vector can be solved for directly with the equation

$$\ddot{\underline{r}}_n = -\,(\underline{\underline{B}})^{-1}\,\underline{C} \qquad (81)$$

where $(\underline{\underline{B}})^{-1}$ is the inverse of $\underline{\underline{B}}$.

After solving for $\ddot{\underline{r}}_n$ with Equation (81), either Equation (74) or Equation (78) may be used to solve for the differential pressure distribution vector $\underline{\Delta}p$.

Once the differential pressure distribution is known, it is a relatively simple matter to compute the transport velocity, w_c. This computation is made by using the following equation taken from Reference 5:

$$w_c = C\sqrt{2\,\Delta p/\rho} \qquad (82)$$

where C is defined as the effective porosity of the canopy material. Reference 5 gives plots of C for various canopy materials as a function of altitude and pressure difference. By evaluating Equation (82) at $\sigma_1, \sigma_2, \ldots, \sigma_n$, a transport velocity vector, w_c is evaluated

$$\underline{w}_c = (w_c(\sigma_1), \quad w_c(\sigma_2), \ldots, \quad w_c(\sigma_n))^T \tag{83}$$

The added mass can also be evaluated once the pressure distribution is known. To do this, note that Equation (74) shows the pressure difference, $\underline{\Delta p}$ to be the sum of two terms: a "transient" term, and a "steady state" term. That is, Equation (74) may be rewritten as

$$\underline{\Delta p} = (\underline{\Delta p})_{tr} + (\underline{\Delta p})_{ss} \tag{84}$$

where the transient pressure difference is

$$(\underline{\Delta p})_{tr} = -4\pi\rho \; (\underline{\underline{A}})^{-1} \; (\ddot{\underline{r}}_n - v \cos \underline{\phi})$$

and the steady state pressure difference is

$$(\underline{\Delta p})_{ss} = 2 \rho v \; \underline{(\partial\phi/\partial\sigma) \sin \phi}$$

The added mass is due only to the transient term and is related to $(\Delta p)_{tr}$ through the relation

$$\frac{d}{dt}(m_a v) = \iint (\Delta p)_{tr} \cos \phi \, dA \tag{85}$$

Analysis shows that m_a may be approximately solved for using the following equation which is essentially equivalent to Equation (85)

$$m_a(t) = \frac{1}{v} \int_0^t \left[\sum_{j=1}^{m} (\Delta p)_{tr_j} \cos \phi_j A_j \right] dt + m_a(0) \tag{86}$$

The notation used in this equation is explained in Appendix B.

If $t = 0$ is when the canopy first starts to inflate, then the term $m_a(0)$ may be dropped; i.e., $m_a(0) = 0$ for this case.

The steady state term in Equation (84) provides no net force according to a momentum conservation principle known as d'Alembert's paradox. This would appear to be unreasonable because the integral of $(\Delta p)_{ss} \cos \phi$ over the canopy area quite obviously produces a net force in the direction of $-\underline{k}$; viz.,

$$\iint_A (\Delta p)_{ss} \cos \phi \, dA > 0 \tag{87}$$

This dilemma is resolved by noting that d'Alembert's paradox applies only if the force known in wing theory as "leading edge thrust" develops at the skirt edge of the canopy. It is considered a certainty that this so-called leading edge thrust does not occur on a parachute canopy. Therefore the steady state force computed in Equation (87) may be interpreted as a drag force. Denoting this force by D, it follows that an approximate relation for computing this quantity is

$$D = \sum_{j=1}^{m} (\Delta p)_{ss_j} \cos \phi_j \, A_j \tag{88}$$

Equation (88) probably gives a lower bound for the drag actually experienced by the canopy.

6.4.6 Solution Algorithm

A solution algorithm, which employs the analytical concepts developed in the foregoing subsections as a basis for predicting the parachute inflation process, may now be discussed in a preliminary way. The main elements of the computation are reasonably clear, and a description of the computational steps involved may be outlined. A flow diagram for a solution algorithm that predicts the process by stepping forward in time is illustrated in Figure 82. The computational steps indicated in this figure are briefly discussed below.

1) The parachute structure is specified in detail. This specification includes all dimensional, mass and elastic properties of all components of the parachute. In addition, the distribution of the canopy geometric porosity is specified. Also, the mass and drag coefficient of the vehicle are given.

2) The starting conditions at the initial time, say $t = 0$, are specified. These consist of the flight velocity v, the flight path angle Θ, the canopy shape vector $\underline{r}$, and the canopy velocity vector $\underline{\dot{r}}$. In addition, estimates of the initial riser force F_r, the initial transport velocity vector $\underline{w}_c$, and the initial acceleration of the system $\dot{v}$ are specified. (These estimates are for use in the first computation cycle only.)

3) The velocity potential ϕ is computed using Equation (62) with doublet distribution as described in Appendix B.

4) The static equilibrium pressure difference vector $\underline{\Delta p}_{se}$ is computed by using the procedure described in Section 3.0 of Volume II.

5) The canopy normal acceleration vector $\underline{\ddot{r}}_n$ and the pressure difference vector $\underline{\Delta p}$ are computed using Equations (81) and (78).

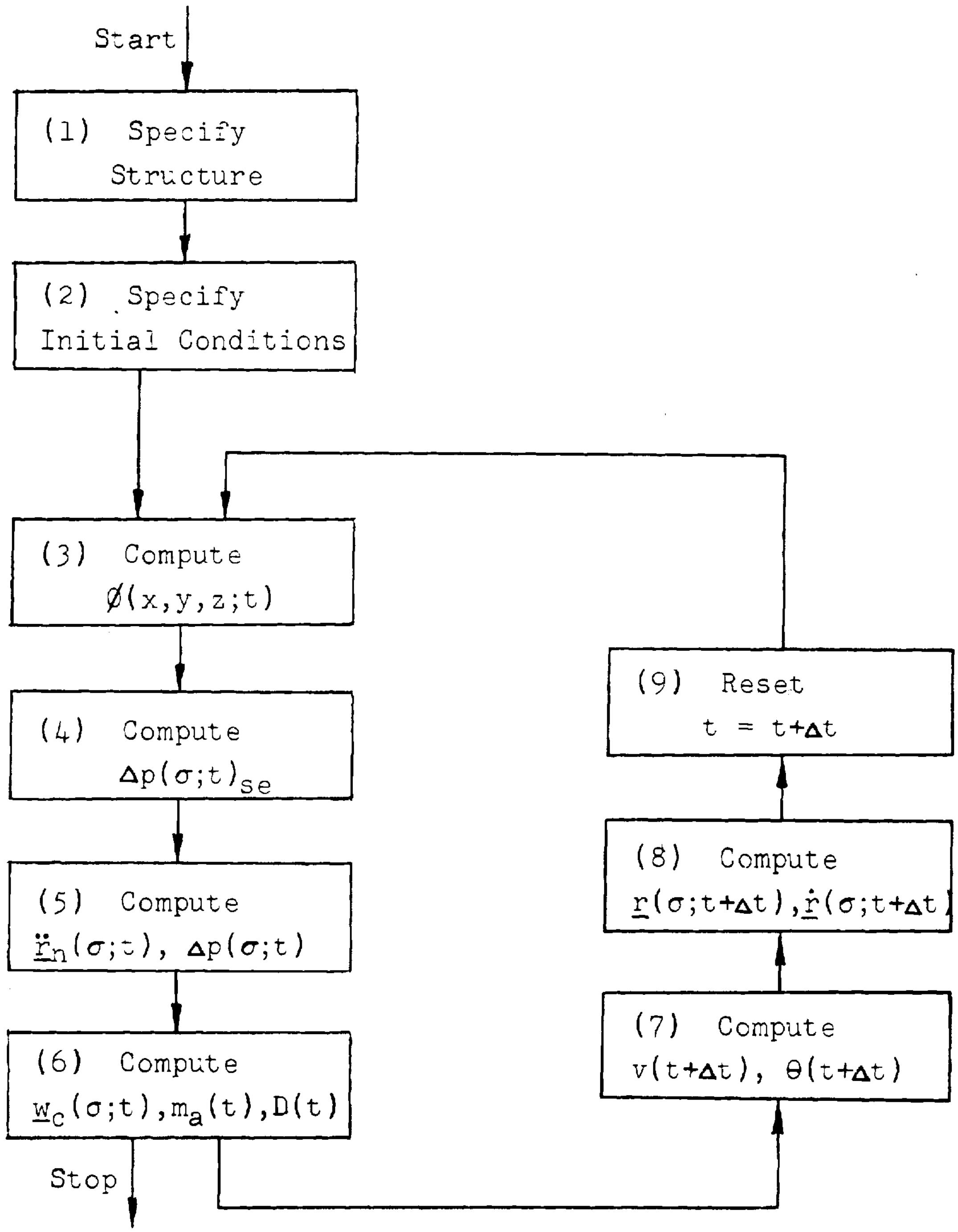

Fig. 82. Flow Diagram of Solution Algorithm

6) The transport velocity vector $\underline{w}_c$, the added mass m_a, and the drag D are computed using, respectively, Equations (83), (86) and (88).

7) The flight velocity v and the flight path angle θ are computed at time $t + \Delta t$ using the equations

$$v\,(t + \Delta t) = v\,(t) + \dot{v}\,(t)\,\Delta t$$

$$\theta\,(t + \Delta t) = \theta\,(t) + \dot{\theta}\,(t)\,\Delta t$$

where the system acceleration $\dot{v}$ and the flight path angle rate $\dot{\theta}$ are computed with Equations (56). Also, the riser force F_r is computed with the equation

$$F_r = m_v(g \sin \theta - \dot{v}) - D_v$$

8) The canopy shape and velocity vectors are computed at time $t + \Delta t$. These computations use the following equations:

$$\underline{r}\,(t + \Delta t) = \underline{r}\,(t) + \dot{\underline{r}}\,(t)\,\Delta t + \tfrac{1}{2}\,\ddot{\underline{r}}_n(t)\,\Delta t^2$$

$$\dot{\underline{r}}\,(t + \Delta t) = \dot{\underline{r}}\,(t) + \ddot{\underline{r}}_n\,(t)\,\Delta t$$

9) The time $t + \Delta t$ is reset to t and the computations are continued by returning to Step (3).

Steps (3) through (9) are repeated until a test indicates that the canopy shape vector $\underline{r}$ is no longer changing with time. When this is found to be the case, the inflation process is complete, and the computations are stopped.

The solution algorithm described above is somewhat involved, and it is quite evident that a high speed digital computer will be required to implement the computations required by the method. This means that a computer program will have to be prepared. With a functioning computer program, the complete inflation process may be predicted. Included among the parameters that may be predicted would be the stress-time history for every structural element in the parachute system during its entire opening. That such information will be of great interest to a parachute designer is quite apparent. However, the accuracy and ultimate usefulness of these predictions, which will be based on potential flow theory, can not be assessed at this time.

6.5 FINITE DIFFERENCE METHODS

To solve for the pressure distribution over a parachute canopy during the opening process is a very difficult problem in fluid mechanics. The shape of the canopy influences the fluid flow and vice versa, so that there are mutually interacting nonlinear systems. However, since the advent of high speed, large memory electronic computers, it has become possible to solve complicated problems in fluid mechanics using numerical techniques. The greatest amount of work in fluid mechanics has been in the field of compressible flows with shocks, large distortions and time dependent processes in several dimensions. Recently, incompressible flows have been investigated and the most recent of these are incompressible flows with a free surface. The numerical methods used to solve fluid mechanics problems are almost as many in number as the investigators using the numerical methods. The principal methods based on the variety of problems treated and acceptability by researchers, are the Particle in Cell (PIC), the Fluid in Cell (FLIC), Marker and Cell (MAC), AFTON, Landshoff, Lax, Rusanov, and the Lax-Wendroff methods.

To demonstrate how the numerical methods may be applied to solving the parachute opening process, a brief description of the PIC method is presented because of its generality.

In the numerical methods now used, all of the systems subdivide the fluid into small cells. The partial differential equations for the fluid model are then approximated in finite difference form. There are two general ways of representing the coordinate systems that are used in formulating these finite difference equations. The first is Lagrangian in which the coordinate system moves with particles of the fluid. The second is Eulerian in which the coordinate system is fixed with respect to ground. The former method produces equations that remain valid only so long as there are no large fluid distortions, and the latter method produces equations that cannot resolve the fine structure of the flow. The PIC method combines the two coordinate systems to eliminate these disadvantages. Thus there are two computing meshes, an Eulerian and a Lagrangian. As stated by F. H. Harlow:[49]

> "The domain through which the fluid is to move is divided into a finite number of computational cells which are fixed relative to the observer. This is the Eulerian mesh. In addition, the fluid itself is represented by particles or mass points which move through the Eulerian mesh, representing the motion of the fluid. This is the Lagrangian mesh. Associated with the mesh points of each system are certain variables whose history the calculation develops. Thus, for each Eulerian cell there is kept the velocity, the internal energy, and the total mass of each kind of material. For the Lagrangian mesh of particles, individual masses and positions are kept."

In applying the PIC method, it would be required that a computer program be written to solve the finite difference equations, together with the boundary conditions. This computer program would generate the solution by computing the fluid velocities, pressures, internal energies, etc., throughout the fluid at sequential instants of time. Preliminary ideas on the application of the PIC method to the parachute opening process follow.

The initial conditions for the fluid (velocity, pressure, internal energy, etc.,) would be specified at the mesh points in the fluid, and the parachute in its initial geometry would be given as a starting boundary condition to the computer. The characteristics of the canopy -- including its type, configuration, dimensions, material properties and porosity distribution -- would also be modeled and given to the computer.

The solution would be generated by first stepping forward in time by a very small time increment and then computing new values for the fluid properties, and the canopy position and velocity. This process is identically repeated many times, and in this way, the solution is generated. Initially, it would be desirable to use relatively few mesh points and a fixed geometry canopy. Next, it would be desirable to increase the number of the mesh points and use a slowly deforming canopy. After experience is gained with these computational problems, the full problem featuring a deforming canopy whose shape is determined by its interaction with the fluid could be undertaken.

Many finite difference methods have been successfully used to solve a wide variety of nonsteady fluid flow problems. The Particle in Cell method is a method that is suited to solving the parachute opening process. A solution based on the PIC method could include the effects of compressibility, viscosity and rotationality. Such a solution would be free of certain basic limitations inherent in potential flow analysis, and it would therefore be expected that it could provide a more accurate analysis of the parachute opening process.

SECTION 7.0
MEASUREMENTS REQUIRED IN SUPPORT OF THE LOAD PREDICTION METHODS

The types of measurements that are required to support the further development of the load prediction methods being developed for Apollo type parachutes are discussed in this section.

7.1 SHAPE/DISTANCE OPENING LOAD METHOD

Two different types of data are needed in order to use the Shape/Distance Opening Load Method. The first type of data consists of the initial flight conditions (velocity, altitude and flight path angle), the vehicle weight, the vehicle drag, and the gravitational constant. The second type of data are certain canopy shape characteristics, the canopy added mass, and the canopy drag area. This discussion is concerned with the measurement of the latter type of data only.

The canopy shape characteristics consist of the eccentricity of the ellipsoidal crown, the radii defining the phases, the airball length versus projected radius (for Phase I), and the inflation parameter, $d\bar{s}/d\bar{R}$. Some of these characteristics have been estimated from Apollo flight test films. However, because of the obliqueness of the camera line of sight to the canopy axis, the canopy profile shapes could not always be ascertained. Furthermore, the lack of an accurate reference length made the results obtained from film analysis somewhat uncertain.

The canopy added mass versus radius is needed. With an Apollo main parachute this mass is significant. At present, this is obtained by assuming an equivalent, imporous ellipsoid and using a potential flow theory relationship.

The canopy drag area as a function of projected radius is also needed. At present, steady state values at different reefing ratios are used. However, because the shape of an inflating canopy at a given mouth radius is very different from the shape of a canopy in steady state with the same mouth radius, this approach is considered inadequate.

In brief, the input data for the Shape/Distance Load Prediction Method are now being estimated on the basis of rather limited information; i.e., the existing Apollo flight test data. This has not proved to be entirely satisfactory because these test data do not permit the canopy characteristics to be accurately determined. Even more important, the available flight test data do not permit the added mass effects to be separated from the drag effects. Therefore, it is considered essential that special tests be conducted for the explicit purpose of obtaining the specific items of data needed by the Shape/Distance Opening Load Method. The needed data are:

1) Canopy Shape Characteristics
    a) Crown eccentricity versus projected radius $\bar{R}$,
    b) Projected radii at the start and end of each phase of inflation,
    c) Airball length versus $\bar{R}$ (for Phase I), and
    d) Inflation parameter $d\bar{s}/d\bar{R}$ versus $\bar{R}$.
2) Canopy added mass versus $\bar{R}$
3) Canopy drag area versus $\bar{R}$

7.2 PARACHUTE INFLATION POTENTIAL FLOW THEORY

When developed, the inflation theory presented in Section 6.0 will provide detailed predictions of the parachute opening process. These predictions will include extensive information on the canopy shape, the canopy differential pressure distribution, the canopy internal loading and the fluid flow field during the complete process. These items of information, which will be given by the theory, should be compared with measured quantities to the extent that such comparisons can be made.

The parachute inflation theory given in Section 6.0 is based on a potential flow analysis which rests on several assumptions. In particular, this potential flow analysis assumes that the fluid is both incompressible and irrotational. The assumption that the fluid is incompressible is entirely reasonable where the application of the theory is to parachutes operating at low Mach numbers. However, the assumption that the flow is everywhere irrotational is questionable. Namely, there may be both a vehicle wake and a canopy wake; and both of these regions, which would impinge on the canopy, may be quite rotational. How much error will be introduced by the irrotationality assumption of the potential flow analysis in unknown at this time.

There are few measurements that can be easily obtained during a parachute inflation process. Those presenting the least difficulty are shape-time, flight velocity-time and riser force-time data. These are valuable items of data and should be given first priority. The canopy differential pressure distribution, the canopy internal loading and the fluid flow field (each a function of both space and time) would be even more valuable as items of data to compare with the predictions that will be made by potential flow theory. However, these latter quantities are quite difficult to measure. Apparently less difficult to measure than these quanitities are the added mass and drag of the parachute canopy at different points during the inflation process. For this reason, added mass-time and drag-time data should be given second priority. It follows that third priority would be canopy differential pressure distribution, canopy internal loading and fluid flow field data.

7.3 ADDED MASS CONCEPT AND MOTION EQUATIONS

A body moving through a fluid induces motions in the fluid which are of the nature of parting motions for the fluid particles in front of the body and closing-in-behind motions for the fluid particles in back of the body. If the body is moving at constant velocity, these motions in the fluid dissipate energy and produce a force on the body, referred to as drag, which opposes the body's motion. If in addition to having velocity, the body is also accelerating, the parting and closing-in-behind motions of the fluid are accelerated and the body experiences another fluid force directly associated with these fluid accelerations. That is, in addition to the drag force and the D'Alembert force required to accelerate the mass of the body, there is an additional force associated with accelerating the parting and closing-in-behind motions in the fluid. The effect of these fluid accelerations is to make the body appear to have a mass larger than its actual mass. The difference between the apparent mass of the body and the actual mass of the body is referred to as the apparent added mass, or simply, the added mass. The added mass of a body is, in general, dependent on the size and shape of the body, the direction of the body's acceleration (with respect to body axes), and the fluid density.

A typical body moving in a fluid-filled space has fluid forces and moments acting upon it which may be thought of as being of two types: (1) those due to the translational and rotational velocities of the body, and (2) those due to the translational and rotational accelerations of the body. These different forces and moments can be identified with respect to the six components of velocity and the six components of acceleration for the typical (constant shape) body. Texts on hydrodynamics by Lamb,[46] Basset[47] and Milne-Thomson[48] give complete derivations of the six equations that govern the trajectories of typical bodies.

For a nontypical (varying shape) body such as an opening parachute, it is required to add one or more equations to the basic six trajectory equations in order to form a complete governing set. For such a case, added mass type terms due to the shape variation(s) are required in both the additional equation(s) and the basic six trajectory equations. A complete analytical statement for the motions of a body such as an opening parachute is quite complex, and the task of measuring the many added mass terms that appear in such a statement would be unreasonably difficult if not impossible. Fortunately, at least for the case of Apollo type parachutes, it is possible to make a number of simplifying assumptions and in this way materially reduce the complexity of an analytical statement that describes the process.

The Apollo parachutes are essentially symmetrical about their longitudinal axes during opening. It is observed that they produce negligible lift or sideforce. They stay aligned with the flight path; i.e., the angle of attack and angle of sideslip are small enough to be neglected. Also, their roll motions about their axes of symmetry are negligible. And finally, they are observed to open in nearly the same general manner every time--independent of altitude, flight speed, flight path angle, etc. The net result of these and other simplifying circumstances is that only two of the six basic trajectory equations are required: the momentum equation taken tangent to the flight path and one momentum equation taken normal to the flight path. Also, because the shape changes during opening are always essentially the same for any given parachute, only one additional equation is required in order to analytically define the opening process. This equation may be a drag area-time relationship such as the one used in the Mass/Time Opening Load Method (given as Equation (21) in

Section 4.2) or a radius-distance relationship such as the one used in the Shape/Distance Opening Load Method (see discussion on page 164 of Section 4.3). Other relationships are also possible.

The two trajectory equations for an opening parachute are shown in Section 6.3 to be the following momentum equations taken tangent and normal to the flight path, respectively:

$$\frac{d}{dt}\left[(m + m_a)v\right] = m\,g\,\sin\theta - D \tag{89}$$

$$(m + m_a)\,v\,\frac{d\theta}{dt} = m\,g\,\cos\theta \tag{90}$$

where

m = system mass,

m_a = added mass,

v = system velocity,

θ = flight path angle (positive downward),

D = drag force, and

t = time.

The added mass, m_a appears in both Equation (89) and Equation (90). At first glance, it would appear that either equation could be used as a basis for estimating m_a from ordinary flight test data. On further inspection, this proves not to be true. The reasons for this are explained as follows.

Ordinary flight test data include many items of data. For the Apollo flight tests, for example, these data items typically include v, dv/dt, θ and the dynamic drag area, $(C_DS)_{dyn}$. For an opening parachute, the latter quantity is related to the added mass by the relation

$$(C_DS)_{dyn} = \left[D + \frac{d(m_a v)}{dt}\right] /q \qquad (91)$$

where q is the flight dynamic pressure. In order to evaluate m_a from either Equation (89) or Equation (91), the aerodynamic drag force, D must be known. Without data on how D varies during the opening process, neither Equation (89) nor (91) may be used as a basis for estimating the added mass quantity, m_a.

The typical flight test also provides data on the riser force, F_r, and it might be asked if it could be used to aid in evaluating m_a. It may be shown that F_r is related to m_a by the equation

$$F_r = \left[m_c \frac{dv_c}{dt} - g\ m_c \sin\theta\right] + \left[\frac{d(m_a v_c)}{dt} - D_c\right] \qquad (92)$$

where m_c is the canopy mass, v_c is the canopy velocity and D_c is the canopy drag. Ordinary flight test data allow the first bracket in Equation (92) to be evaluated. However, data on how D_c varies during the opening process are required in order to evaluate m_a. Thus, it is seen that Equation (92) is also inappropriate for providing a basis for evaluating the added mass, m_a, from ordinary flight test data.

The objections associated with using Equations (89), (91) and (92) do not apply in the case of Equation (90). This equation does not have a drag term, and therefore m_a may be solved for directly in terms of known quantities; viz.,

$$m_a = (m\ g\ \cos\ \theta)\ /\ v\ \frac{d\theta}{dt}\ -\ m \qquad (93)$$

It may be noted that this equation is quite inappropriate when θ is large; say $\theta \doteq 90$ deg. For such a case, small errors in either θ or $d\theta/dt$ produce large errors in m_a. Therefore, consider the equation for the most favorable case when θ is small and $d\theta/dt$ is large. This is the case when the parachute system is deployed along a flight path that is nearly horizontal. For this case, Equation (93) may provide a basis for evaluating m_a provided $d\theta/dt$ can be determined with sufficient accuracy. However, this is not likely because of the second difference nature of the $d\theta/dt$ values that are obtained from ordinary flight test data. In particular, the flight path angle, θ, which is listed in the flight test data tabulations every 0.2 sec, is a first difference type quantity. Hence, $d\theta/dt$, which must be computed by taking first differences of the listed values for θ, is in reality a second difference type quantity. It is well known that numerically-evaluated second difference quantities have poor accuracy. Therefore, it is reasonable to expect that any estimates of m_a based on Equation (93) would be quite inaccurate, even for the most favorable case. This expectation was checked by using Apollo flight test data to make numerical evaluations of $d\theta/dt$. The result was as expected; the computed values of $d\theta/dt$ were quite inconsistent, and any hope of using Equation (93) to estimate m_a had to be abandoned.

Ordinary flight test data such as the data obtained in the Apollo flight tests apparently do not permit the added mass of an opening parachute to be directly evaluated. Therefore, attention is given to testing techniques that are suited to measuring m_a directly.

7.4 TECHNIQUES FOR MEASURING ADDED MASS

Section 6.3 derives the following relation for the added mass of an opening parachute

$$m_a = A_1 + A_2 \frac{dR}{ds} \qquad (94)$$

Here, A_1 denotes the added mass associated with acceleration of the fluid by the canopy due to the acceleration of the system center of gravity along the flight path. A_2 denotes a similar mass term, but this term is associated with acceleration of the fluid by the canopy relative to the system center of gravity due to canopy shape changes. R denotes a variable characteristic parachute dimension, such as the projected radius of the canopy, and s denotes distance along the flight path.

Equation (94) indicates that m_a is composed of two components. Both components vary throughout the opening process. The first component, A_1 is dependent only on the shape; i.e., $A_1 = f(R)$. (In this discussion, dependence on density is disregarded.) The second component, $A_2 \frac{dR}{ds}$ is dependent on both the shape and the rate of change of the shape; i.e., $A_2 \frac{dR}{ds} = f(R, dR/ds)$. Thus, is may be observed that the added mass of a parachute canopy of fixed shape is simply A_1. This quantity may be measured by conducting special tests which employ a fixed shape canopy, either in a wind tunnel or in free flight. A technique for measuring A_1 is discussed in the following two subsections.

7.4.1 Measuring A_1 in the Wind Tunnel

Consider a parachute supported in a wind tunnel as shown in Figure 83. The canopy construction includes special internal reefing lines such that the shape is made to represent an instant of a normal opening. The riser goes upstream to a pulley and passes out of the tunnel to an eccentric arm on a motor-driven flywheel. The tunnel velocity is maintained constant during the test. Instrumentation includes a riser force

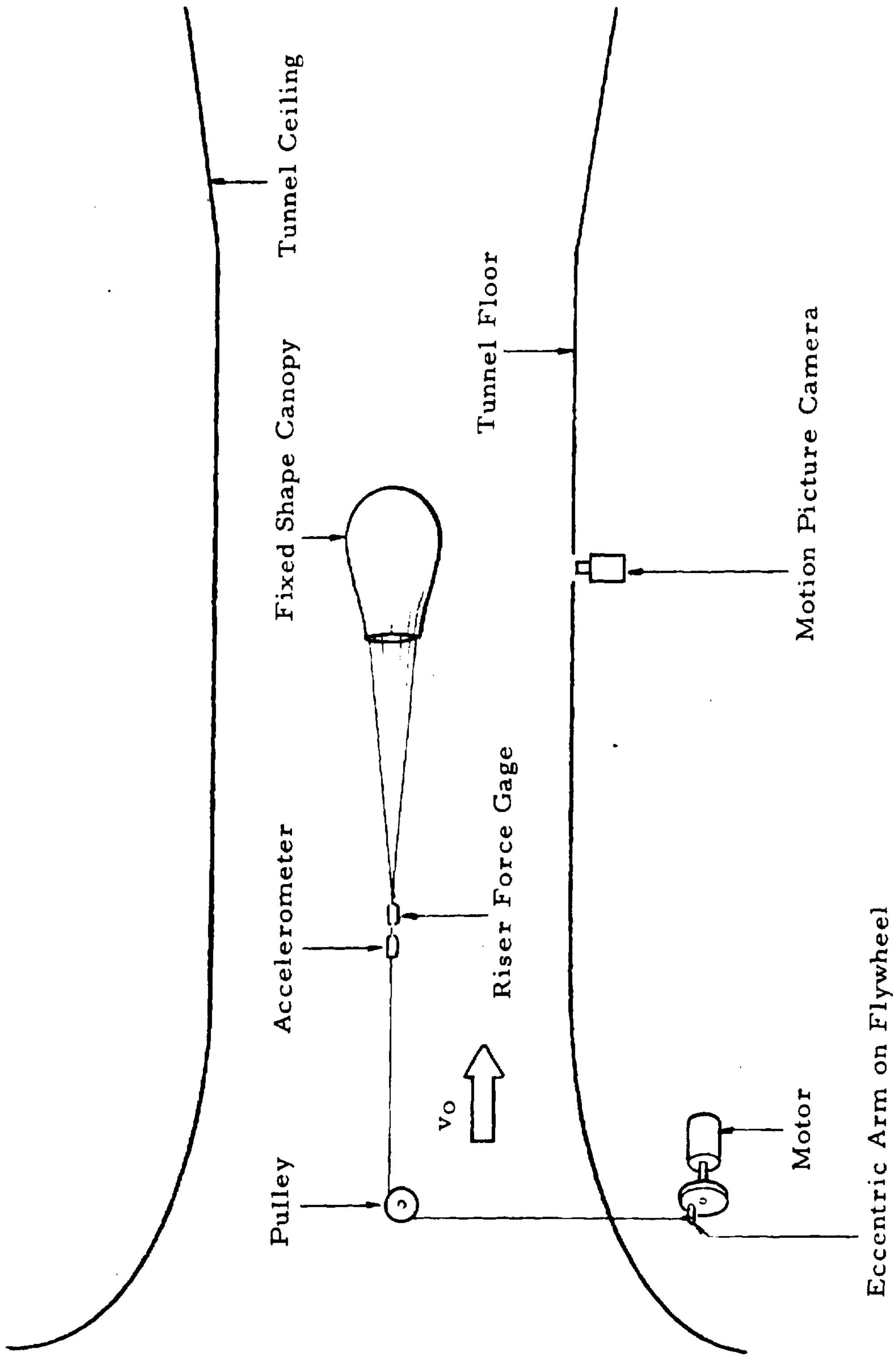

Fig. 83. Test Arrangement for Measuring A_1 In the Wind Tunnel

gage and an accelerometer located just below (upstream) the confluence point and a motion picture camera. Common timing marks are provided to the riser force-accelerometer recorder and the motion picture camera.

To conduct a test with the arrangement illustrated in Figure 83, the motor speed is adjusted until the canopy oscillates fore-and-aft at a high enough velocity to make the riser force vary significantly from its mean value, say ± 10 percent. The velocity of the oscillation is measured by integrating the accelerometer output and checked by differentiating the position data provided by the camera coverage. Let the velocity of the canopy with respect to the free stream air be denoted by

$$v = v_o + u\, e^{i\omega t} \tag{95}$$

where v_o is the free stream velocity, u is the amplitude of the oscillation velocity, $i = \sqrt{-1}$, ω is the angular frequency of the oscillation, and t is time.

The force at the force gage is, according to theory,

$$F_r = (A_1 + m_c)\frac{dv}{dt} + D_c \tag{96}$$

where m_c is the mass of the canopy and suspension lines, and D_c is the drag of these same two components. The drag D_c may be expressed as

$$D_c = (C_D S)_c\, \tfrac{1}{2}\, \rho\, v^2 \tag{97}$$

From Equation (95) it may be noted that velocity squared is

$$v^2 = v_o{}^2 + 2v_o u\, e^{i\omega t} + u^2\, e^{i2\omega t} \tag{98}$$

Likewise,

$$\frac{dv}{dt} = i\omega u e^{i\omega t} \tag{99}$$

Substituting quantities from Equations (97) - (99) into

Equation (96), it may be shown that the riser force may be written as

$$F_r = \left[(C_D S)_c \tfrac{1}{2} \rho v_o^2 \right] + \left[(C_D S)_c \rho v_o u + i \omega (A_1 + m_c) u \right] e^{i\omega t} + \ldots \qquad (100)$$

This equation shows that the riser force, F_r will oscillate in some manner about the average value.

The precise manner in which F_r varies with time during a test will be recorded. A Fourier analysis can be performed on this riser force-time data and in this way the observed relationship can be expressed as

$$F_r = F_O + \left[F_1 + i F_2 \right] e^{i\omega t} + \ldots \qquad (101)$$

where F_O is the average value, F_1 is the amplitude of the cos ωt component of F_r, and F_2 is the amplitude of the sin ωt component of F_r. Next, the measured quantities F_O, F_1, F_2 can be equated to the corresponding quantities in Equation (100) to give the three equations

$$F_O = (C_D S)_c \tfrac{1}{2} \rho v_o^2 \qquad (102)$$

$$F_1 = (C_D S)_c \rho v_o u \qquad (103)$$

$$F_2 = \omega (A_1 + m_c) u \qquad (104)$$

The canopy drag area, $(C_D S)_c$ may be computed using Equations (102) and (103), and the added mass term, A_1 may be computed using Equation (104). The latter computation would employ the relation

$$A_1 = F_2/\omega u - m_c \qquad (105)$$

It may be observed from this equation that the mass of the canopy and suspension lines should be kept as small as possible in relation to the added mass in order to improve the accuracy of the computation. Also, it may be observed that both ω and u should be varied from test to test, and that in this way A_1 may be obtained under somewhat different conditions. Such tests should show that A_1 is independent of ω and u.

The important test variables for this type of testing are canopy shape (corresponding to different instants of the opening), canopy type (ringsail, ribbon, etc.,) forebody shape, and free stream velocity. The latter variable is important when its variation produces changes in the streamline field in and around the canopy.

7.4.2 Measuring A_1 in Free Flight

There are two good reasons for wanting to measure parachute added mass with free flight tests. First, there is apparently no other way of measuring the added mass of large parachutes such as the Apollo main parachutes. (Wind tunnels large enough to test full open, Apollo main parachutes do not exist.) There are definite indications that large ringsail parachutes behave differently than medium sized or small ringsail parachutes,[51] and therefore it is believed that information on added mass scale effects would be desirable. Second, there is apparently no other way of measuring the added mass of even medium sized parachutes such as the Apollo drogue chutes at high dynamic pressures. (Wind tunnels large enough to test Apollo drogue chutes can not operate at high enough dynamic pressures to correctly simulate the Apollo deployment conditions.) The dependency of added mass on porosity, which is strongly dependent on dynamic pressure, is well known.[35] It is therefore believed that information on how parachute added mass varies at high dynamic pressure would be desirable.

Measuring A_1 in free flight tests may be accomplished using a procedure similar to the wind tunnel technique described above. Now however, the mechanism for producing the harmonic variations in the riser force must be packaged within the vehicle. A specific arrangement is illustrated in Figure 84. Shown in this figure are a fixed shape canopy, a fin-stabilized bomb, and a falling weight mechanism contained within the vehicle. This falling weight mechanism is a weighted device that descends through the body of the bomb at variable velocity. In this way, the D'Alembert force of the body is made to oscillate about its average value. The instrumentation consists of a riser force gage and an accelerometer, both located just below the confluence point of the suspension lines, and a pitot tube for measuring the static and stagnation pressure of flight. With this arrangement, data can only be taken for a short period of time, say for six to twelve oscillations, but this should be adequate. (The alternative of providing a power supply and motor to drive a flywheel and eccentric similar to the arrangement described for the added mass wind tunnel tests is probably not feasible.)

The important test variables for this type of testing are canopy shape, canopy type, forebody shape, free stream dynamic pressure and Mach number. The latter variable is probably important for flight Mach numbers greater than 0.7.

7.4.3 Measuring A_2 in the Wind Tunnel

The quantity A_2 is the added mass associated with accelerations of the fluid by the canopy relative to the system center of gravity due to canopy shape changes. It is estimated that A_2 is equal to approximately one-half of A_1. The added mass is $m_a = A_1 + A_2\ dR/dS$. Because the average value of dR/dS during a typical opening is generally between 0.1 and 0.01, it is evident that the contribution of the A_2 term is relatively unimportant. Furthermore, it

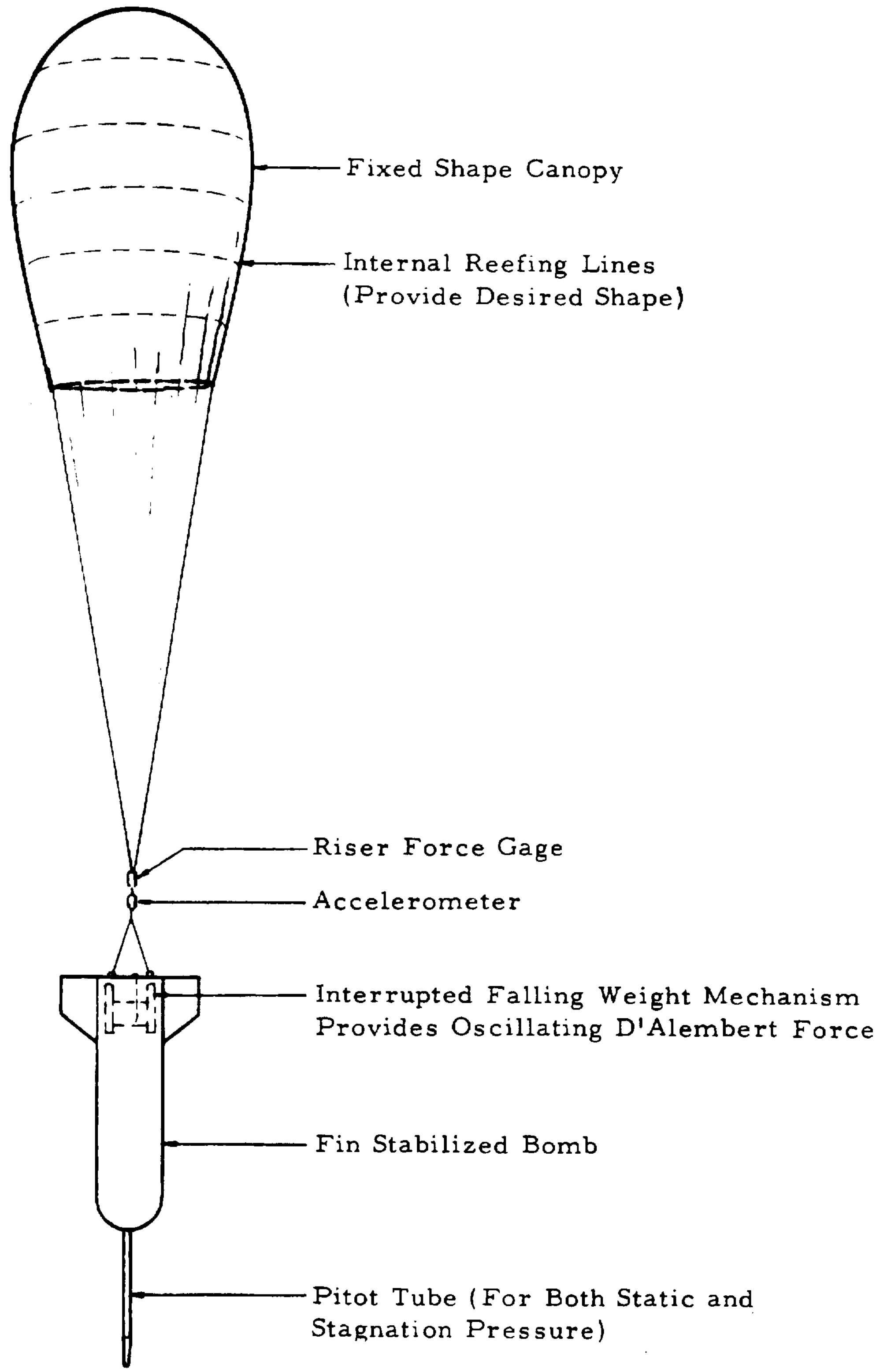

Fig. 84. Test Arrangement for Measuring A_1 In Free Flight

appears that A_2 can be estimated in terms of A_1 with fair accuracy. This being the case, there is little reason for measuring A_2. However, a possible experimental technique for measuring A_2 is instructive regardless of its practicality.

Figure 85 shows an arrangement for measuring A_2 in a wind tunnel. Along each radial of the parachute is a flexible rib. In the center of the canopy is an umbrella mechanism which includes spokes to each of the ribs and an air cylinder to alternately push and pull on the spokes and in this way make the parachute radius oscillate about an average value. The ribs, spokes and air cylinder are so arranged that the shape changes are realistic in relation to the actual opening process. Instrumentation includes a riser force gage and a motion picture camera. Obtaining A_2 from the data is quite similar to the procedure described earlier for computing A_1 and is not presented. Suffice it to observe that analysis indicates it is feasible to measure A_2 with the test arrangement shown in Figure 85. This leads to an interesting final comment on the problem of measuring added mass. Whereas, at least for the case of an opening parachute, it is apparently impossible to measure m_a directly, it is possible to measure A_1, A_2 and dR/ds separately, and then evaluate m_a by means of the relation

$$m_a = A_1 + A_2 dR/ds$$

7.5 PROGRAM PLAN FOR MEASURING ADDED MASS

This section describes a program for measurement of the parachute canopy parameters required for use in the loads prediction methods described in Sections 4.0 and 6.0. It encompasses a two-part plan designed to follow a logical sequence of 1) wind tunnel testing to obtain the required canopy measurements and confirm the adequacy of the instrumentation, and 2) limited flight tests to obtain further canopy measurements and to correlate wind tunnel results.

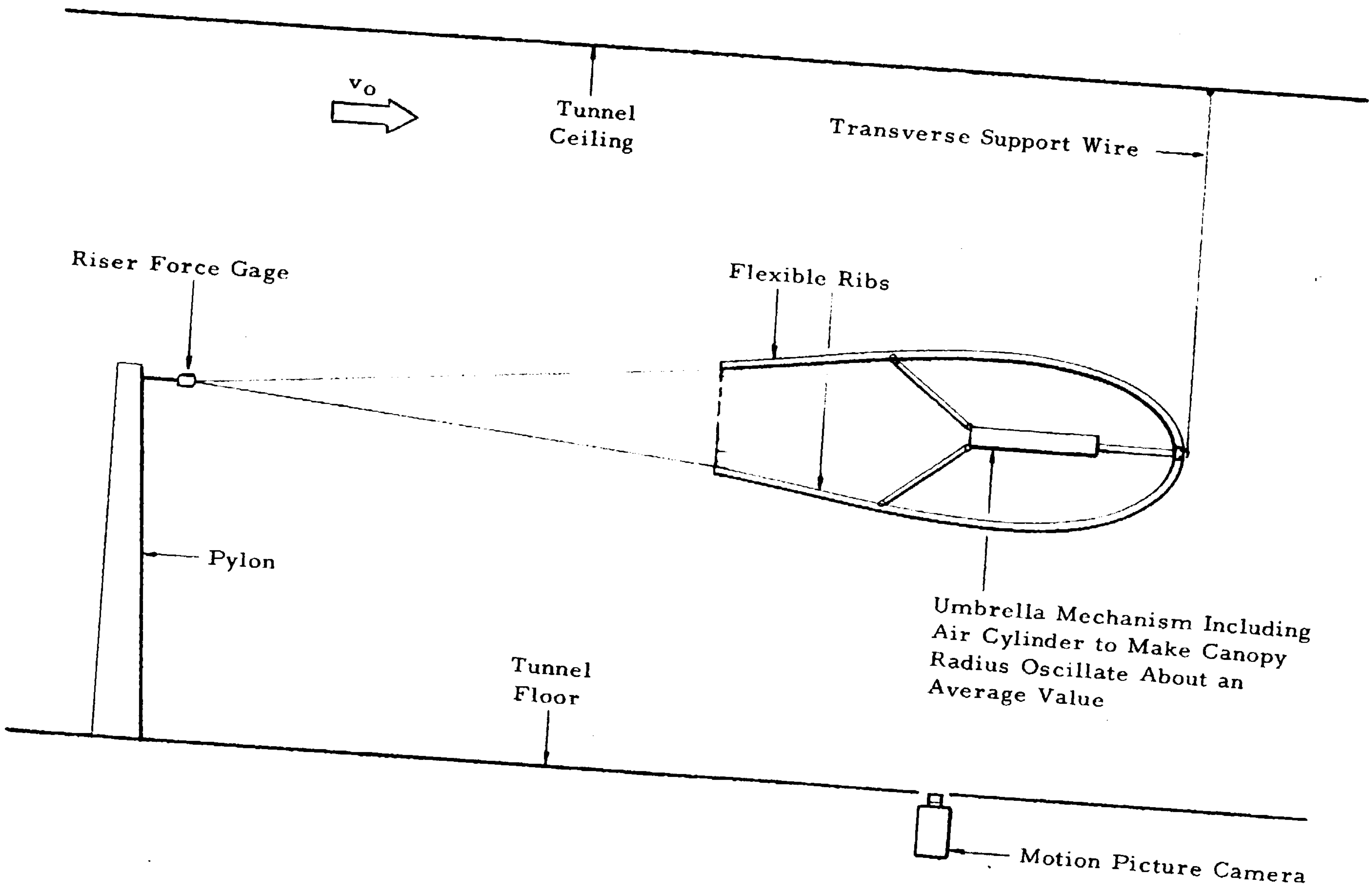

Fig. 85. Test Arrangement for Measuring A_2 In the Wind Tunnel

The experimental program strongly interacts with and depends on the theoretical methods for predicting canopy loads, and one of its most important results would be to confirm the accuracy of the theoretical methods.

7.5.1 Wind Tunnel Phase

Preliminary Considerations A wind tunnel program will be worthwhile for obtaining useful measurements of canopy parameters during the opening process.

(Consideration was given to the El Centro Whirl Tower as an alternative to the wind tunnel for making the canopy measurements discussed above. The primary advantages of the Whirl Tower are (1) the facility of observation which it affords for tests that may be conducted under finite mass conditions and (2) the relatively low cost and simplicity of testing. However, the Whirl Tower is not appropriate for testing large parachutes having reefed stages because the time available for opening is not sufficient to allow disreefing. It would be necessary to open the parachute directly to the stage being tested. This procedure is unattractive in that it does not represent the true opening process, and no further consideration was given to the use of the Whirl Tower in the program.)

Modeling Considerations Because of the practical limitations associated with scaling the parachute opening process, it is important in wind tunnel testing to use the largest possible model. For the Apollo main parachute, the largest wind tunnels available should be utilized. The Ames 40 x 80-foot Tunnel and the Langley 30 x 60-foot Tunnel both can accommodate large parachute models. The Ames Tunnel is capable of operating at dynamic pressures up to 100 psf, while the Langley Tunnel is limited to about 60 psf. Because of its larger size and dynamic pressure range, the Ames 40 x 80-foot Tunnel is the most suitable for Apollo parachute testing.

Prior experience has shown that to avoid undesirable tunnel blockage effects, the drag area of the parachute model should be limited to 15 percent of the test section area. For a test section area of 3200 ft^2 and a C_{D_0} of about 0.8, the maximum allowable D_0 is about 28 ft. This means that one-third scale models of the main parachute and full scale drogue chutes can be tested. Tests of a one-third scale model and a reefed full scale model of an early main parachute design were successfully carried out in the Ames Tunnel in 1963.[52]

Parachute model canopies should be scaled geometrically to preserve porosity and strain effects. Unfortunately, at least for the case of many components in the Apollo main parachute, this is not possible. For example, the 1.1 oz sail cloth used in the Apollo main parachutes is the lightest cloth obtainable and therefore cannot be scaled. Because of this limitation, the sails of a one-third scale model of an Apollo main parachute will be too stiff. It is believed that this will affect the canopy porosity and hence the pressure distribution. However, the effect of this stiffness mismatch on the pressure distribution is believed to be small. In particular, the wind tunnel tests of Reference 52 showed that there were close similarities between the shapes of a full scale ringsail parachute and a one-third scale model constructed from the same canopy materials. Since the shapes were similar, it follows that the pressure distributions on the canopies were similar, and hence that the flows about the canopies were similar.

<u>Program Outline</u> A wind tunnel test program is recommended to provide drag, opening shape and added mass data for the Shape/Distance Opening Load Method and to aid the development of the parachute opening theory described in Section 6.0. This program is outlined in Table 30 and discussed briefly below.

Table 30. Outline of Recommended Wind Tunnel Tests

Test Type	Wind Tunnel Model		Comments
1. Restrained Shape Oscillating	1/3-scale main parachute (D_o = 28 ft)	20% Shape Restraint 40% " " 60% " " 80% " " No	Model oscillated during test (see Fig. 84)
2. Infinite Mass Opening	1/3-scale main parachute (D_o = 28 ft)	Stage 1 Opening Stage 2 " Stage 3 "	Model opens normally

Two types of tests are recommended. These will be restrained shape, oscillating tests and infinite mass, opening tests. For both types of tests, a one-third scale main parachute model (D_o = 28 ft) will be employed. The oscillating tests will utilize internal reefing lines to control the canopy shape during the testing to correspond to 20, 40, 60, 80 and 100 percent of full-open. The opening tests will employ reefing lines and reefing line cutters in order to simulate the Stage 1, 2 and 3 opening processes. The same test setup may be used for both types of tests.

7.5.2 Flight Test Phase

Preliminary Considerations It is recommended that the flight tests be primarily low altitude (2500 ft), single parachute drops of one-third scale main parachute models and secondarily high altitude (10,750 ft), single parachute drops of full scale Apollo ringsail parachutes. This is felt to be reasonable in view of the complexity of the test instrumentation and techniques that will be involved and the likelihood that interpretation of the data may be difficult. Good profile data are needed for the development of the Shape/Distance Opening Load Method, and the low altitude tests will be well-suited to obtaining this type of data. Because some doubts may exist regarding the validity of the reduced scale parachute tests, the full scale tests are recommended to provide corroborative data.

Instrumentation The instrumentation for the flight tests will be as follows:

1) Riser force,
2) Ground-based motion picture cameras of focal length such that good resolution is obtained,
3) Onboard camera to record axial views of the parachute during inflation, and
4) Airborne motion picture camera coverage for the full scale flight tests

All transducer outputs will be recorded by an oscillograph carried onboard the drop test vehicle, and dynamic pressure will be measured by an onboard pitot tube.

Test Conditions The scaling laws derived in Section 3.2 for velocities and masses are,

$$v_1/v_o = (r_1/r_o)^{\frac{1}{2}} \qquad \text{(duplicates Froude number)}$$

$$m_1/m_o = (\rho_1/\rho_o)(r_1/r_o)^3 \qquad \text{(duplicates added mass ratio)}$$

where subscript 1 denotes the model and subscript o denotes the full scale parachute. These expressions may be used to compute test conditions for the model parachute. The required velocity and vehicle mass for a one-third scale parachute model at an altitude of 2500 ft that simulates a main parachute at an altitude of 10,750 ft and a velocity of 330 ft/sec (a critical, high altitude abort condition), are as follows:

Parachute	Altitude	Velocity	Vehicle Weight
Full scale main	10,750 ft	330 ft/sec	6500 lb
1/3-scale main	2,500	190	313

In regard to model stiffness, a similar problem occurs in flight testing as in wind tunnel testing. Namely, the model is too stiff. Testing the model parachute at the lower altitude tends to offset this effect. This is because the density at 2500 ft is approximately 30 percent higher than at 10,750 ft. In other words, by testing the one-third scale model at 2500 ft, the state of strain in this model will more closely simulate the state of strain in the full scale parachute than if it were also tested at 10,750 ft.

An outline of the recommended flight tests is presented in Table 31.

Table 31. Outline of Recommended Aerial Flight Tests

Test Type	Flight Test Model		Comments
1. Restrained Shape, Oscillating	1/3-scale main parachute (D_o = 28 ft)	20% Shape Restraint 40% " " 60% " " 80% " " No " "	Model oscillated during test (see Fig. 85)
2. Finite Mass, Normal Opening	1/3-scale main parachute (D_o = 28 ft)	Stage 1 Opening Stage 2 " Stage 3 "	Model opens normally
3. Finite Mass, Normal Opening	Full scale parachute (D_o = 28 ft)	Stage 1 Opening Stage 2 " Stage 3 "	Parachute opens normally

SECTION 8.0
SUMMARY

This report presents the results of a one-year study conducted for the purpose of analyzing Apollo parachute loads* data, upgrading loads prediction methods, and investigating advanced prediction methods. This includes a thorough analysis of an extensive amount of flight test data on the Apollo drogue and main parachutes tested between 1962 and 1969. These data were used to upgrade the pertinent load prediction methods for both the drogue and main parachutes and to develop improved semi-empirical methods directly applicable to Apollo type spacecraft parachutes. In addition, there is presented an investigation of vehicle-parachute interactions, a new parachute inflation theory, and concepts for new parachute test techniques. Also included are brief statements of analytical voids that represent barriers to the further advancement in the technology of loads predictions as well as identification of means for removing these barriers.

Introduction (Section 1.0)

The background and scope of the investigation herein reported are briefly indicated. Associated with this report is a companion report, Volume II, which presents the results of a concurrent study on parachute structural analysis methods.

Upgrading the Apollo Loads Prediction Methods (Section 2.0)

The loads prediction methods used in the Apollo parachute development program are briefly summarized. Except for the calculation of snatch loads, these methods are empirically based. The approach used in calculating Apollo parachute loads was to calculate

* Unless otherwise indicated, the word "loads" in this report refers to the longitudinal loads transmitted through the parachute riser.

the flight conditions at the time each stage of inflation was programmed to occur and to predict loads on the basis of these flight conditions. Two approaches were used. One employed C_DS-time data in a two-degree-of-freedom trajectory computation. The other employed the opening load factor method. In addition to longitudinal opening loads, the snatch forces, circumferential inflation control line and reefing line loads were computed.

A study of the loads prediction methods used in the Apollo parachute development program included a detailed analysis of the Block I, Block II and Block II (H) flight test data and the methods used at Northrop Ventura between 1962 and 1969 to make loads predictions. Specific improvements made as a result of this study are indicated below.

Drogue Chute - At reefed opening, variations in the opening load factor, $(C_K)_r$, are accounted for by variations in the following five parameters: type of vehicle (a wake effect), whether or not the load is in excess of limit load, type of deployment, number of drogue chutes inflating, and Mach number. Other parameters expected to contribute to variations in $(C_K)_r$, such as flight path angle, could not be analyzed because they were not varied by significant amounts in the tests. When the influence of the five parameters is treated as additive, it is found that the values of $(C_K)_r$ measured in the Block II (H) tests can be represented by an expression of the following form:

$(C_K)_r$ =	1.00	(plus the following as they apply)
	+0.00	(if ICTV is used)
	+0.21	(if BP is used)
	+0.18	(if PTV is used)
	+0.07	(for loads in excess of limit load)
	+0.05	(for mortar deployment)
	+0.05	(if only one drogue chute inflates)
	+0.02	(for Mach number in excess of 0.75)

Thus, the baseline is an ICTV test with two static line-deployed drogue chutes at operational loads and operational Mach numbers.

At disreef opening, the type of vehicle used has the largest effect on the disreef opening load factor, $(C_K)_o$. Larger factors occur when an ICTV is used than when a PTV is used -- a trend that is opposite that observed for reefed opening. Three parameters affecting the disreef opening load factors of the Apollo drogue chutes are 1) the inverted fill distance parameter $(v\Delta t)^{-1}$, 2) the drag area ratio $(C_DS)_r/(C_DS)_o$ and 3) the fill time ratio $\Delta t/t_{fill}$. Good correlation with test data is shown for the first parameter. Correlation for the second parameter cannot be shown directly, because, in the Apollo development program, $(C_DS)_r/(C_DS)_o$ was held fairly constant. Correlation for the third parameter is made difficult by the unavailability of accurate times. Also, its effect may be of the same magnitude as the parameters ignored in the analytical model; viz., losses due to friction and the effects of material elasticity. The data obtained with the BP vehicle follow the same trends obtained with the ICTV but exhibit greater scatter.

<u>Pilot Chute</u> - By using calculated flight conditions at pilot chute canopy stretch in posttest analysis (rather than Askania-measured flight conditions), the scatter in the empirically determined opening load factors is reduced. The reduction in C_K scatter is from 0.86 ± 0.04 to 0.85 ± 0.02 for five of the six tests in which pilot chute loads were measured in the Apollo development program. Also, calculating the main parachute pack deceleration during pilot chute opening, and then basing a pilot chute opening load factor on the calculated dynamic pressure of the pack at the instant of peak pilot chute load, results in factors of 1.06 ± 0.02 in four of the six tests. This range of C_K agrees with the value given in Reference 5 which shows an opening load factor of 1.05 for ringslot parachutes in infinite mass applications.

Main Parachute - The method used for predicting the loads of the main parachutes in the Apollo development program employs a point-mass computer program for the two reefed stages and a special adaptation of the opening load factor method for the third stage. The reefed opening load computations are made with inputs derived empirically from prior Apollo tests including drag area and filling time. Aerodynamic interference between canopies in a cluster is taken into account by introducing deployment and disreef time differentials obtained from tests, and by applying a loss factor to the lag canopy drag area calculation. Also, the computer output is modified by factors to account for effects due to vehicle dynamics and data scatter.

The opening load calculation for the third stage is performed with the aid of five empirical data graphs from which drag areas, filling times and effective unit canopy loadings are obtained in a series of trial solutions for the opening load factors of the lead, lag and lag-lag canopies of the cluster. Nonuniform opening effects are accounted for by introducing a disreef time differential for the second stage and relating it to the filling time of the lead canopy at the peak load instant.

A comparison of loads predicted by the method with test results indicates that its accuracy is approximately $\pm$ 10 percent. Analysis of its empirical basis reveals the possibility of obtaining only a slight improvement in accuracy through better and more complete data utilization.

Background Studies on Improved Load Prediction Methods (Section 3.0)

A review of the technical literature is presented on both the analysis of the parachute opening process and the loads developed during the process. The rapid, early development of the understanding and mathematical theories for the process are traced, and various prediction methods are discussed briefly. Several related topics that support the understanding of the load prediction problem are reviewed briefly. The contributions of Scheubel, O'Hara, Heinrich, Rust and Noreen are identified as outstanding. In addition to providing improved understanding of the parachute inflation process, the literature review emphasizes the importance of added mass in load prediction methods. Another result of the literature review is recognition that the load prediction method developed by Rust in 1965 is the most complete method so far proposed, especially for parachutes with reefing.

The parachute opening process is investigated by studying relationships among the variables as they appear in the differential equations which govern the process. It is shown that the so-called scaling laws given by Barton are equivalent to a correlation parameters approach. In this approach, certain nondimensional quantities must be the same on different tests in order for the data from the tests to be equivalent. Two different sets of correlation parameters are identified for the two cases: 1) the constant flight path angle case, and 2) the variable flight path angle case.

New Load Prediction Methods (Section 4.0)

A new method for predicting the deployment and fill times for the Apollo parachutes is given. The new method calls for calculating the trajectories of both the vehicle and the parachute from the time deployment is initiated to the time of line stretch. Formerly, this time interval could only be estimated on the basis of previous tests. The new method also calls for calculating fill time by using the constant fill distance principle. Values of fill distance for the first stage of the Apollo drogue chutes are presented for several reefing ratios. It is shown that the new method gives significantly more accurate predictions of fill time than the old method which employed a constant value.

Two new methods for making main parachute load predictions are presented. These are denoted as the Mass/Time Method and the Shape/Distance Method (also referred to as the Rust Method). The Mass/Time Method was chosen for development because it offered a way of obtaining a simple engineering method of making parachute load and trajectory predictions. The Shape/Distance Method was chosen for development for several reasons: 1) it featured an analytical approach that would make its extension to the case of clustered parachutes reasonably straightforward, 2) it was developed by Dr. Rust specifically for application to reefed parachutes such as those in the Apollo system, and 3) the details of the method were already worked out.

The Mass/Time Method is developed to a useful level for all three stages of an individually operating Apollo main parachute. Improvements in accuracy in Stages 1 and 2 result from using actual filling times and drag areas rather than synthetic values (as had previously been used). Also, improvements are derived by employing a two-part drag area growth curve; viz., one part for the initial inflation interval and one part for the continued growth during the reefed interval. Accuracy improvements in Stage 3 are realized when the canopy added mass terms are included in the parachute force equation. The added mass and drag area parameters are empirically determined, as are the filling distance constants for each stage. The inclusion of added mass during Stage 3 is accomplished with a computer program which was developed during the study. It is noted that this represents the first successful attempt at calculating a time history of opening load for Stage 3 (as opposed to calculating only the peak load for this stage). The characteristic accuracy of the Mass/Time Method for single parachute tests is $\pm$ 5 percent (the characteristic accuracy of the previous method is approximately $\pm$ 10 percent). The initial results of an investigation of clustered parachutes, in which the Mass/Time Method was used to predict the loads observed in a two-parachute cluster test, are encouraging.

The Shape/Distance Method development was implemented by preparing a computer program to predict the opening loads for a single Apollo main parachute. The equations used in this method feature several functions that must be determined experimentally. These functions are added mass and drag area as a function of projected radius. Because these functions are not known and cannot be determined from the available flight test data, they had to be estimated. The loads predictions that resulted when these estimates were incorporated into the computer program did not compare favorably with test data. Modifications were made to the added mass and drag area estimates, and the calculated load histories improved substantially. However, the accuracy of the load predictions provided by the Shape/Distance Method has not yet achieved a satisfactory level. Added mass and drag area data must be obtained experimentally before the method can be reduced to a useful engineering tool.

A modification was made to the Mass/Time Method by incorporating into it the basic assumptions of the Shape/Distance Method. The resulting modified Mass/Time Method was tested by making several computer runs, and it was found to be as accurate as the unmodified Mass/Time Method. Included as test cases were all six of the single parachute tests previously computed with the unmodified Mass/Time Method. It was concluded on the basis of these test cases that the basic assumptions of the Shape/Distance Method are valid. An important advantage of the modified Mass/Time Method is that it is directly applicable to cluster cases because it does not require predetermined filling time estimates. To show that this is true, it was applied to several cluster cases (three two-parachute tests and one three-parachute test) with drag area and added mass data from the single parachute tests. The results obtained showed that reasonably accurate cluster loads could be predicted for Stages 1 and 2, but that the Stage 3 load predictions were not acceptably accurate. This was taken to indicate that the aerodynamic interference effects are important and must be accounted for when Stage 3 cluster loads are being predicted.

Parachute Oscillations Study (Section 5.0)

The cause of longitudinal parachute oscillations is analyzed without a forebody and with a forebody by the classical mass-spring-dashpot system and by the description of a stochastic system analysis. The msd model gives a good method by which a designer can find the oscillation frequency of the parachute. The testing of the validity of the msd model shows it to hold for a variety of cases. These cases range from a PTV with drogue chutes reefed and unreefed to a B/P with reefed main parachutes. This model shows that the parachutes being designed at the present time have strong interactions with the wake of the forebody.

Study on Parachute Inflation Process (Section 6.0)

The results of a study undertaken to develop concrete ideas on how the parachute inflation process can be analyzed by analytical and/or numerical techniques (as opposed to empirical techniques) is presented. An analysis of the added mass type fluid forces acting on an inflating parachute canopy indicates that the same added mass term should appear in both the momentum equation taken tangent to the flight path and the momentum equation taken normal to the flight path. A potential flow study shows how the velocity potential can be determined for an inflating parachute canopy, and that to solve for the distribution of the differential pressure acting across an accelerating canopy surface, two simultaneous vector equations must be solved. Equations for evaluating other quantities such as the transport velocity of the fluid through the canopy surface, the canopy added mass, and the canopy drag are given. A solution algorithm for computing the complete parachute inflation process is given, and it is observed that a high speed digital computer will be required to implement it. An alternative approach to potential flow theory would be to use finite difference methods to solve the partial differential equations governing the motions of a compressible, viscous fluid under the transient conditions of an inflating parachute.

Measurement of Added Mass and Drag Area (Section 7.0)

The types of measurements needed to aid further development of load prediction methods for Apollo type spacecraft parachutes are described. Primarily, these are added mass and drag area measurements because the nonexistence of added mass and drag area data stands as a barrier to the development of accurate load prediction methods. The concept of added mass is discussed, and it is explained why this quantity cannot be determined from typical flight test data. A measurement technique that employs a longitudinally oscillating parachute canopy is described, and a test plan which utilizes this technique is presented. This plan describes tests that may be made in the NASA/Ames 40 x 80-foot wind tunnel and at the DOD/El Centro Parachute Test Facility to acquire the needed data.

SECTION 9.0
CONCLUSIONS

The conclusions of the one-year study on prediction methods for the loads of Apollo type spacecraft parachutes presented in this report are as follows:

1) A rigorous review of test data going back through six years of ELS aerial drop test information, and the application of several different longitudinal loads prediction methods, confirms that the traditional opening load factor method used on Apollo is reasonably accurate and conservative. (Small changes in C_K values and area growth curves are warranted and would have the effect of minor change only in certain Apollo parachute loads predictions.) This affirmative data audit gives increased confidence to the margins of safety for the Apollo ELS parachutes that existed at the start of the study.

2) The drogue chute opening load factor at reefed opening is a function of five parameters: vehicle wake, load level as related to design load, type of deployment, number of drogue chutes, and Mach number when greater than 0.75. (Other parameters such as flight path angle could not be analyzed because they were not varied by significant amounts in the Apollo development program.)

3) At drogue disreef, the parameter having the largest effect on the drogue chute opening load factor is the forebody shape (wake effect).

4) Drogue chute load link oscillations (dynamics) can cause large unpredictable variations in the riser load. A careful review of the data indicates that load link dynamics occurred on seven different ICTV tests: Tests 48-1, 48-4, 48-5, 48-1R, 99-3, 99-4 and 99-5.

5) An extensive analysis of the main parachute test data, and the associated load prediction methods used in the Apollo development program, leads to the conclusion that only a negligible improvement in accuracy can be obtained by refining these methods further.

6) An improved correlation of main parachute opening load data is obtained when measured area growth and calculated flight conditions are used (instead of synthetic area growth and Askania flight conditions).

7) A careful analysis of the opening load factor for the Apollo pilot chutes indicates that, within the measured range, this factor is 0.85 $\pm$ 0.02 (instead of 0.86 $\pm$ 0.04 as formerly believed).

8) A review of the technical literature on parachute opening loads indicates that the contributions of Scheubel, O'Hara, Rust and Noreen are outstanding.

9) The Mass/Time Opening Load Method developed in the present study is an improved method for calculating single Apollo main parachute loads and trajectories. Its accuracy for single parachute cases is estimated to be $\pm$ 5 percent (compared to approximately

± 10 percent for the previous method). This method utilizes the types of data that are obtained in typical flight tests, and it is amenable to further refinement. In particular, a modification of the Mass/Time Method appears to have the potential of being able to predict parachute cluster loads.

10) The Shape/Distance Method shows promise of becoming a useful engineering tool for predicting opening loads. Its development could not be completed because certain added mass and drag area data for Apollo type parachutes were not available.

11) An analysis of the longitudinal oscillations that are observed to occur in Apollo parachutes indicates that they are caused by strong interactions with the wake of the forebody. The oscillation frequencies of the Apollo parachutes, as predicted on the basis of a simple mass-spring-dashpot model, appear to match the test data.

12) The flow about an inflating parachute may be analyzed with the aid of potential flow analysis by using a mathematical model that features doublets distributed over an idealized canopy shaped surface. A solution algorithm for computing the complete inflation process is apparently feasible, although quite involved, and a high speed digital computer will be needed in order to carry out the required computations.

13) An alternative to using potential flow analysis for computing the flow about an inflating parachute is to use finite difference methods. These methods are suited to solving the partial differential equations governing the motions of a compressible, viscous fluid under transient conditions such as those of an inflating parachute.

14) The added mass of a parachute canopy cannot be inferred from typical flight test data. However, it may be measured either in a wind tunnel or in free flight by making special measurements. (Added mass and drag area measurements should be made with large sized models; the NASA/Ames 40 x 80-foot wind tunnel and the DOD/El Centro Parachute Test Facility are suited to making the needed tests.)

SECTION 10.0
RECOMMENDATIONS

Based on the analysis results of a one-year study of loads prediction methods for Apollo type spacecraft parachutes, it is recommended that:

1) Future load predictions for the reefed Apollo drogue chutes be based on an opening load factor evaluated by using the five-component formula presented in this report.

2) Further basic analytical work in depth or refinements of the existing Apollo main parachute loads prediction methods not be undertaken. (Any immediate need for new loads predictions on the Apollo program should be fulfilled by the existing method as an adequate and conservative technique. The modified Mass/Time Method should be phased in when verification exists as to its accuracy and reliability.)

3) The system velocity test data (Askania), when analyzed in the future, be refined by using a computer to calculate the precise system velocity at canopy stretch in post-test review of predicted versus actual loads. (By this means, the apparent scatter in loads data points can be reduced with the result that the accuracy of subsequent loads predictions can be improved.)

4) The new method of predicting deployment and fill times that was developed in this study be adopted in place of the data method previously used in the event that there is a requirement for further Apollo loads prediction work.

5) The load links used in the future to measure riser loads should be mounted in such a way that they cannot oscillate and thus induce large errors in the load measurement.

6) The coupling between the parachute and the vehicle-canopy wakes, which can cause large amplitude longitudinal oscillations in the parachute structure, be included as a design consideration at the time any new parachute configuration is being conceived.

7) The added mass term denoted in this study as m_a be included in both momentum equations when parachute trajectory and opening load computations are made in the future.

8) The work being done at the close of the study to adapt the Mass/Time Method to the case of clustered parachutes be continued by further utilizing the existing Apollo test data.

9) A test program be undertaken to measure the added mass and drag area of Apollo type parachute canopies as a function of inflation state; also, that the development of the Shape/Distance Method, which was constrained during the study by not having these types of data, be continued when the data from this test program becomes available.

10) The potential flow algorithm for the parachute inflation process, which is described in this report, be implemented by having a suitable computer program prepared.

11) The use of finite difference methods be further investigated as a practical means of solving the parachute inflation process.

12) A test program be undertaken to obtain the velocity correlation measurements needed to develop a stochastic model of the forebody-parachute wake interaction process.

APPENDIX A
EQUATIONS FOR THE PARACHUTE PARAMETERS STUDY

Development of Basic Equations

The force equations tangent and normal to the flight path for the opening parachute shown in Figure 24 (page 113) are

$$d/dt \left[(c_a \rho r^3 + m)v \right] = W \sin\theta - D \qquad (A1)$$

$$(c_a \rho r^3 + m)v(d\theta/dt) = W \cos\theta \qquad (A2)$$

where $c_a = c_a(r)$ is a dimensionless parachute added mass coefficient defined as $c_a = m_a/\rho r^3$.

The canopy volume rate of change dV/dt can be approximated by an equation of the form

$$dV/dt = c_f r^2 v \qquad (A3)$$

where $c_f = c_f(r)$ is a dimensionless net inflow coefficient. The canopy volume V can be eliminated from this equation by differentiating the volume relation,

$$V = c_v r^3 \qquad (A4)$$

where $c_v = c_v(r)$ is a dimensionless volume coefficient. Performing this elimination gives the result

$$dr/dt = c_c v \qquad (A5)$$

where $c_c = c_c(r)$ is a dimensionless coefficient defined as $c_c = c_f/(rc_v' + 3c_v)$. The prime denotes differentiation with respect to r; i.e., $c_v' = dc_v/dr$.

Equations (A1), (A2) and (A5) are three equations in the three dependent variables: v, Θ and r. These equations may be simplified. To do this, it is first required to carry out the differentiation indicated on the left hand side of Equation (A1); viz.,

$$(r^3 c_a' + 3c_a r^2)\ \rho\ v(dr/dt) + (c_a \rho\ r^3 + m)(d_v/dt) = W \sin \Theta - D \qquad (A6)$$

Next, the dr/dt term in Equation (A6) is eliminated with the aid of Equation (A5). This gives the equation

$$(c_a\ \rho\ r^3 + m)(dv/dt) = W \sin \Theta - D - c_b\ \rho\ r^2 v^2 \qquad (A7)$$

where $c_b = c_b(r)$ is a dimensionless coefficient defined as $c_b = (rc_a' + 3c_a)c_f/(rc_v' + 3c_v)$. Next, the drag term D in Equation (A7) is expanded as

$$D = (\pi\ r_o^2 c_{Dp} + \pi r_v^2 c_{Dv})(\tfrac{1}{2}\ \rho\ v^2)$$

where $c_{Dp} = c_{Dp}(r)$ is the parachute drag coefficient based on the parachute nominal area πr_o^2, and c_{Dv} is the vehicle drag coefficient based on the vehicle area πr_v^2. Noting also that $W = gm$, Equation (A7) may be written as

$$(c_a \rho\ r^3 + m)(dv/dt) = g\,m \sin \Theta - (\tfrac{1}{2}\ \pi\ r_o^2 c_{Dp} + \tfrac{1}{2}\ \pi\ r_v^2 c_{Dv} + r^2 c_b)\ \rho v^2 \qquad (A8)$$

Equations (A8), (A2) and (A5) can now be rewritten as

$$\dot{v} = (g\,m \sin \Theta - (\tfrac{1}{2}\ \pi r_o^2 c_{Dp} + \tfrac{1}{2}\ \pi r_v^2 c_{Dv} + r^2 c_b)\ \rho v^2)/(c_a \rho r^3 + m) \qquad (A9)$$

$$\dot{\Theta} = g \cos \Theta/v\ (1 + m_a/m) \qquad (A10)$$

$$\dot{r} = c_c v \qquad (A11)$$

where the dots denote differentiation with respect to t.

Using the vector notation, $\underline{x} = (v, \theta, r)^T$, these equations can be simply represented as

$$\dot{\underline{x}} = \underline{f}(\underline{x}, \underline{c}(\underline{x}), g, m, \rho) \qquad \text{(A12)}$$

where $\underline{c}(\underline{x})$ is a vehicle-parachute characteristics vector defined as $\underline{c}(\underline{x}) = (c_a, c_b, c_c, c_{Dp}, C_{Dv}, r_o, r_v)$. The vector $\underline{c}$ $(\underline{x})$ is, in general, a function only of r, but it is shown here as a function of $\underline{x}$ for the sake of notational simplicity. The quantities g, m, ρ are constants in this analysis.

The initial conditions associated with Equation (A12) are

$$\underline{x}(0) = (v_i, \theta_i, r_i)^T \qquad \text{(A13)}$$

where v_i, θ_i, r_i are the flight velocity, the flight path angle and the radius of the parachute at $t = 0$ when the opening process is assumed to start.

The Transformed Equations

The results developed in the foregoing paragraphs may be extended by nondimensionalizing the variables. To do this, the dependent variables in Equations (A9) - (A11) are replaced by the nondimensional variables U, θ, R which are defined as

$$U = v/v_o$$

$$\theta = \theta$$

$$R = r/r_o$$

Here, v_o is taken to be the full-open, equilibrium velocity associated with g, m and ρ. Also, the independent variable t is replaced by the nondimensional variable T defined as

$$T = v_o t/r_o$$

Associated with the new dependent variables is a new state vector

$$\underline{X} = (U,\ \theta,\ R)^T$$

Substituting the nondimensional variables just introduced into Equations (A9) - (A11) gives the following transformed set of equations:

$$\dot{U} = \frac{\sin\theta}{(1+\nu)/FN^2} - \frac{(\frac{1}{2}\pi C_{Dp} + \frac{1}{2}\pi R_v^2\ C_{Dv} + C_b R^2)U^2}{C_a(1+\nu)/\nu} \qquad \text{(A14)}$$

$$\dot{\theta} = \cos\theta/FN^2 U \qquad \text{(A15)}$$

$$\dot{R} = C_c U \qquad \text{(A16)}$$

where the dots now denote differentiation with respect to T, and where

$$FN = v_o/\sqrt{r_o g}$$

$$\nu = c_a \rho_o r_o^3/m_o$$

The quantities $C_a = C_a(R)$, $C_b = C_b(R)$, $C_c = C_c(R)$, $C_{Dp} = C_{Dp}(R)$ are identical to $c_a = c_a(r)$, $c_b = c_b(r)$, $c_c = c_c(r)$, $c_{Dp} = c_{Dp}(r)$ except that their arguments are changed to R in place of r; and, $C_{dv} = c_{Dv}$. The quantities FN and ν (nu) are referred to as Froude number and added mass ratio, respectively. The transformed initial conditions are

$$\underline{X}(0) = (U_i,\ \theta_i,\ R_i)^T \qquad \text{(A17)}$$

Equations (A14) - (A16) can be represented by a transformed vector equation

$$\dot{\underline{X}} = \underline{F}(\underline{X},\ \underline{C}(\underline{X}),\ FN,\ \nu) \qquad \text{(A18)}$$

where $\underline{C}$ $(\underline{X})$ is a nondimensional vehicle-parachute characteristics vector defined as $\underline{C}(\underline{X}) = (C_a, C_b, C_c, C_{Dp}, C_{Dv}, R_v)$. This vector is, in general, a function of R only, but it is shown here as a function of $\underline{X}$ for notational simplicity. The quantities FN and ν are constant by definition throughout any one opening process.

Fixing the Froude number and the added mass ratio, say as FN_o and ν_o is equivalent to specifying two equations in four unknowns (g is assumed fixed); viz., the equations

$$FN_o = v_o / \sqrt{r_o g}$$

$$\nu_o = c_a \rho_o r_o^3 / m_o$$

provide two relations between the four variables: v_o, r_o, M_o, ρ_o. Inspection of these equations shows that there are four ways in which a unique set of variables may be specified.

1) Specify r_o, ρ_o (and solve for v_o, m_o),
2) Specify r_o, m_o (and solve for v_o, ρ_o),
3) Specify v_o, ρ_o (and solve for r_o, m_o), and
4) Specify v_o, m_o (and solve for r_o, ρ_o).

APPENDIX B
THE DOUBLET DISTRIBUTION

Additional Notation

Let a Point P on the canopy surface be defined by a position vector

$$\underline{r}_P = (R \cos\chi,\ R \sin\chi,\ Z)(\underline{i},\ \underline{j},\ \underline{k})^T \tag{B1}$$

where R and Z are the relations

$$R = (x_P'^2 + y_P'^2)^{\frac{1}{2}}$$

$$Z = z_P'$$

At time t, let the quantities R and Z be specified as a function of σ, the curvilinear distance along the meridian of the canopy from the apex to Point P. That is, let

$$\left.\begin{aligned} R &= f_1\ (\sigma;\ t) \\ Z &= f_2\ (\sigma;\ t) \end{aligned}\right\} \quad 0 \leq \sigma \leq \sigma_s \tag{B2}$$

where subscript s denotes the skirt. Also, at time t, let the velocity of Point P be defined by a velocity vector

$$\dot{\underline{r}}_P = (\dot{R} \cos \chi,\ \dot{R} \sin \chi,\ \dot{Z})(\underline{i},\ \underline{j},\ \underline{k})^T$$

and let $\dot{R}$ and $\dot{Z}$ be similarly specified as a function of σ at time t; i.e., let

$$\left.\begin{aligned} \dot{R} &= g_1\ (\sigma;t) \\ \dot{Z} &= g_2\ (\sigma;t) \end{aligned}\right\} \quad 0 \leq \sigma \leq \sigma_s$$

Consider the set of unit vectors ($\underline{l}$, $\underline{m}$, $\underline{n}$) at Point P on the canopy surface as shown in Figure B1. Vectors $\underline{l}$, $\underline{m}$, and $\underline{n}$ are defined as being tangent to the parallel, tangent to the meridian, and normal to the surface at Point P respectively. It is evident that

$$\begin{aligned} \underline{l} &= (1/R)\, \partial \underline{r}/\partial \chi \\ \underline{m} &= \partial \underline{r}/\partial \sigma \\ \underline{n} &= \underline{l} \times \underline{m} \end{aligned} \tag{B3}$$

Analysis that utilizes Equation (B1) can be performed to show that these vectors can be expressed in terms of other quantities as follows:

$$\begin{pmatrix} \underline{l} \\ \underline{m} \\ \underline{n} \end{pmatrix} = \begin{pmatrix} -\sin \chi & \cos \chi & 0 \\ R'\cos \chi & R'\sin \chi & Z' \\ Z'\cos \chi & Z'\sin \chi & -R' \end{pmatrix} \begin{pmatrix} \underline{i} \\ \underline{j} \\ \underline{k} \end{pmatrix} \tag{B4}$$

where the primes denote differentiation with respect to σ; i.e.,

$$\begin{aligned} R' &= dR/d\sigma = \cos \phi \\ Z' &= dZ/d\sigma = \sin \phi \end{aligned}$$

where ϕ is the angle between $\underline{n}$ and $-\underline{k}$

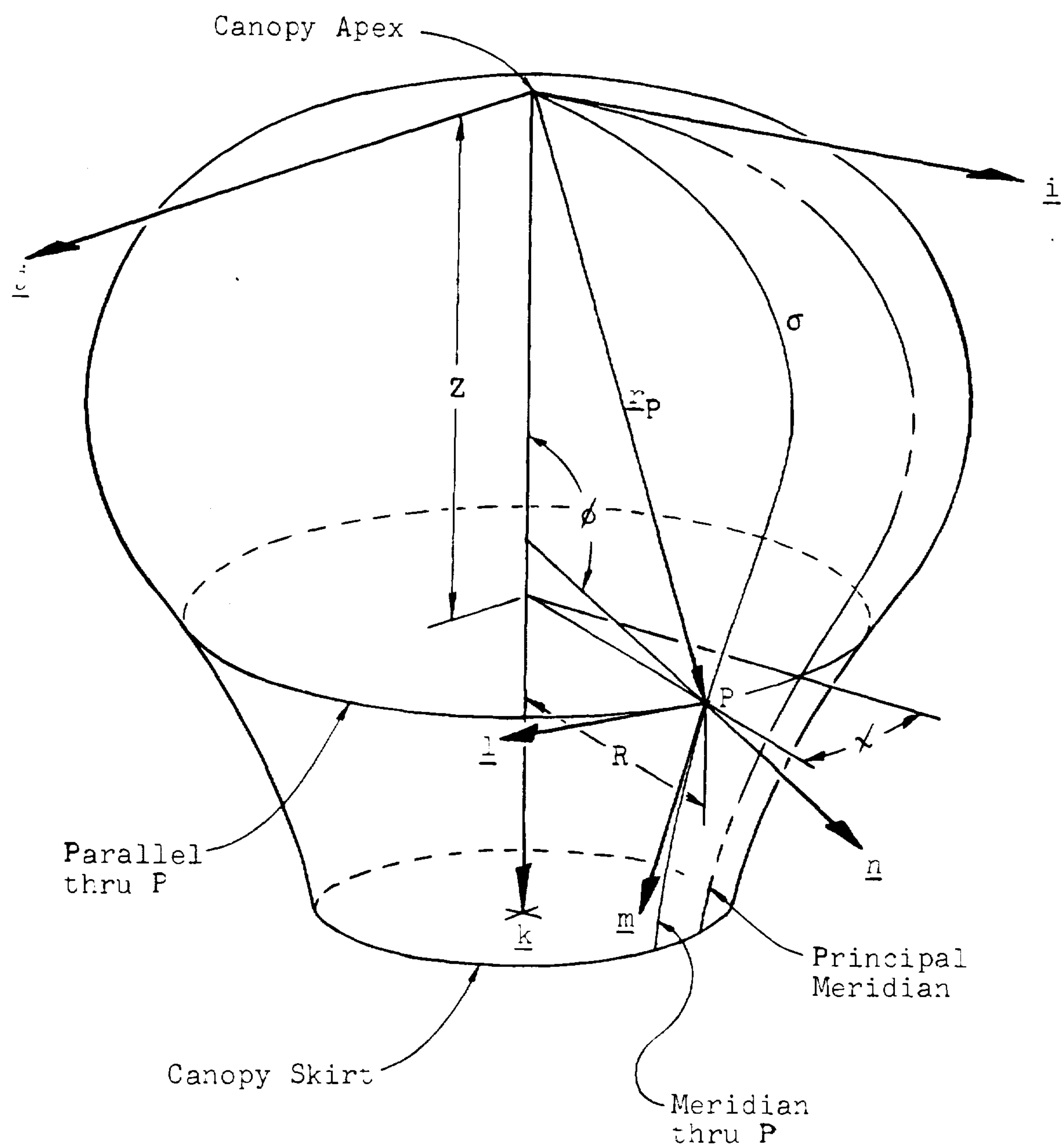

Fig. B1. Sketch Illustrating Additional Notation

In addition to the Point P, which may be anywhere on the canopy surface, let there be identified a Point Q on the principal meridan of the surface defined by the vector

$$r_Q = (R_Q, 0, Z_Q)\ (\underline{i}, \underline{j}, \underline{k})^T \qquad \text{(B5)}$$

where

$$R_Q = f_1\ (\sigma;t) \qquad 0 < \sigma < \sigma_s$$

$$Z_Q = f_2\ (\sigma;t)$$

Functions f_1 and f_2 are, of course, the same as those in Equations (B2).

In order to solve for the strength of the doublet distribution over the surface of the canopy, it is required that an integration be performed over the entire canopy surface. This is accomplished numerically by subdividing the canopy surface area into a large number of subareas $A_1, A_2, \ldots, A_m$. Let the centroids of these subareas be identified as $P_1, P_2, \ldots, P_m$, and let the meridional distances of these points be denoted as σ_j, $j = 1, 2, \ldots, m$. Also, let these subareas be arranged in the manner shown in Figure B2. This figure shows how the smoothly contoured surface is replaced by a pattern of approximately equal sized, trapezoidal subareas. The edges of adjacent subareas are contiguous, being straight line segments that approximate a portion of either a meridian or a parallel. In addition, let the principal meridian pass through a centroid in each annular group of subareas, and let these centroids be identified as the Points $Q_1, Q_2, \ldots, Q_n$, and denote the meridional distances to these points as σ_k, $k = 1, 2, \ldots, n$.

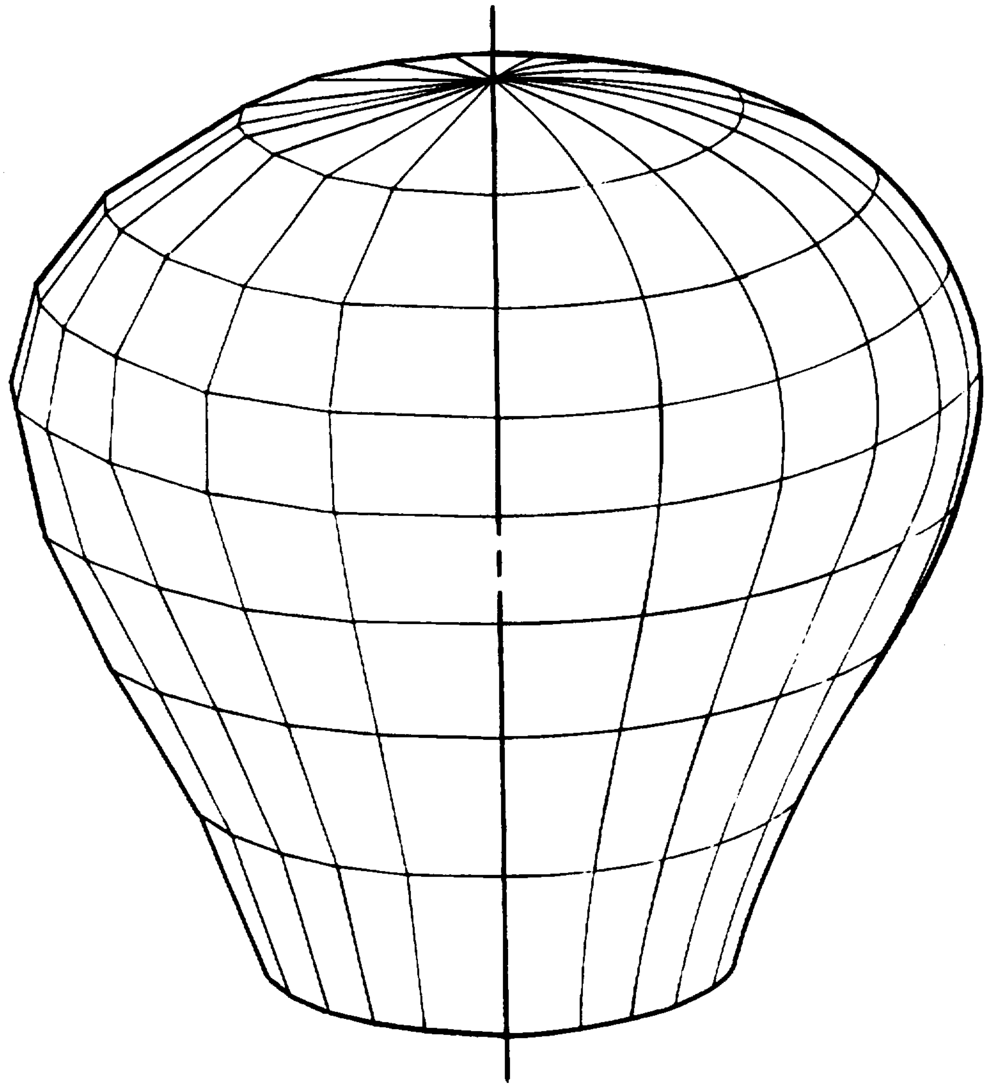

Fig. B2. Schematic Illustrating How Idealized Canopy Surface (on Right) Is Approximated by Configuration of Trapezoidal Subareas (on Left).

The Compatibility Equation

The compatibility condition at the surface of the canopy, given by Equation (61) in Section 6.4.1, is

$$(\nabla \phi_c - \underline{v} - \underline{\dot{r}}) \cdot \underline{n} = w_c \qquad (B6)$$

Noting that the left hand side may be expanded as

$$(\nabla \phi_c - \underline{v} - \underline{\dot{r}}) = \Big[(\partial\phi/\partial R - \dot{R}) \cos \chi,\ (\partial\phi/\partial R - \dot{R}) \sin \chi,$$
$$(\partial\phi/\partial Z - \dot{Z} - v) \Big] (\underline{i},\ \underline{j},\ \underline{k})^T \qquad (B7)$$

and that

$$\underline{n} = (Z' \cos \chi,\ Z' \sin \chi,\ -R')(i,\ j,\ k)^T \qquad (B8)$$

it may be shown that Equation (B6) can be alternatively expressed as

$$q_n = \dot{R} \sin \phi - (\dot{Z} + v) \cos \phi + w_c \qquad (B9)$$

where $q_n = \underline{q} \cdot \underline{n}$ is the component of the fluid velocity normal to (and at) the canopy surface. Equation (B9) may also be written as

$$\partial\phi/\partial n = \dot{R} \sin \phi - (\dot{Z} + v) \cos \phi + w_c \qquad (B10)$$

where $\partial/\partial n$ denotes the gradient normal to (and at) the canopy surface.

Substituting the right hand side of Equation (62) into Equation (B10) gives the following equation:

$$\frac{\partial}{\partial n} \iint_A \frac{h \cos \alpha}{\xi^2}\, dA = \dot{R} \sin \phi - (\dot{Z} + v) \cos \phi + w_c \qquad (B11)$$

At any given instant of time, the quantities on the right hand side of Equation (B11) are known functions of σ . Likewise, for any given σ, the quantities α and ξ (associated with dA) are known. Hence, Equation (B11) contains only one unknown, the doublet strength h which is a function of σ. This equation provides a basis for determining $h(\sigma)$, and the description of a numerical method for accomplishing this follows.

Equation (A11) may be rewritten as

$$\frac{\partial}{\partial n_Q} \int_{A_k}\int \frac{h(\sigma_P)\cos\alpha_P}{|QP|^2}\, dA_P + \frac{\partial}{\partial n_Q} \int\int_{(A_k)^c} \frac{h(\sigma_P)\cos\alpha_P}{|QP|^2}\, dA_P$$

$$= \left[\dot{R}\sin\phi - (\dot{Z} + v)\cos\phi + w_c\right]_Q \quad \text{(B12)}$$

where A_k is the subarea associated with Point Q_k (and hence the meridional distance σ_k), and $(A_k)^c$ is the complement of A_k, defined as all the canopy area except A_k. In other words, the first integral is taken over only the subarea identified with Point Q_k, and the second integral is taken over all the other subareas.

At this point, another simplifying assumption is made. It is assumed that the doublet strength is constant over each subarea. Also, because of symmetry, the doublet strength of each subarea in the same annular group is, of course, the same. This assumption will permit the left hand side of Equation (B12) to be replaced by a simple summation.

It has been shown by Latham[50] that the first quantity on the left hand side of Equation (B12) can be evaluated explicitly; viz.,

$$\frac{\partial}{\partial n_Q} \iint_{A_k} \frac{h\,(\sigma_P)\,\cos\alpha_P}{|QP|^2}\, dA_P = -\,K_k h(\sigma_k) \tag{B13}$$

where the quantity K_k is evaluated with the equation

$$K_k = 2\left[\frac{\sin\gamma_1}{d_1} + \frac{\sin\gamma_{2-}}{d_2} + \frac{\sin\gamma_{2+}}{d_2} + \frac{\sin\gamma_3}{d_3}\right] \tag{B14}$$

The adjoining sketch defines the γ and d type quantities that appear in this equation.

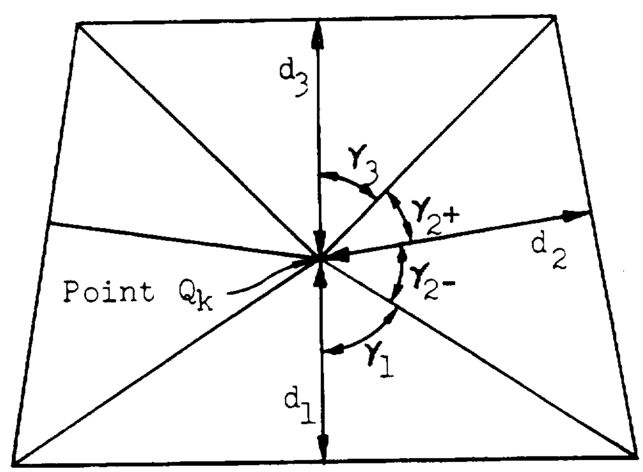

Plan view of subarea A_k

The second quantity on the left hand side of Equation (B12) can be simplified by differentiating under the integral sign. Performing this operation gives

$$\frac{\partial}{\partial n_Q} \iint_{(A_k)^c} \frac{h(\sigma_P) \cos \alpha_P}{|QP|^2} \, dA_P = -2 \iint_{(A_k)^c} \frac{h(\sigma_P) \cos \alpha_P \cos \alpha_Q}{|QP|^3} \, dA_P \quad \text{(B15)}$$

where α_Q is the angle between $\underline{PQ}$ and $\underline{n}_Q$.

It follows that Equation (B11) can now be approximated as

$$-\sum_{j=1}^{m} h\ (\sigma_j)\ G\ (A_j,\ \sigma_k)\ A_j = H\ (\sigma_k) \quad \text{(B16)}$$

where

$$G\ (A_j,\ \sigma_k) = K_k/A_j, \qquad j = k$$

$$= \frac{2 \cos \alpha_P \cos \alpha_Q}{|QP|^3}, \qquad j \neq k$$

and

$$H\ (\sigma_k) = \left[\dot{R} \sin \phi - (\dot{Z} + v) \cos \phi + w_c\right]_{\sigma_k} \quad \text{(B17)}$$

Equation (B16) is an algebraic statement of the compatibility condition at meridional distance σ_k, $k = 1, 2, \ldots,$ n.

Solving for the Doublet Strength

Equation (B16) is actually n equations; i.e., one equation exists for each value of c_k, k = 1, 2, ..., n. These n equations may be written as one vector equation in the form

$$- \begin{vmatrix} a_{11} & a_{12} & \cdots & a_{1n} \\ a_{21} & a_{22} & \cdots & a_{2n} \\ \cdot & \cdot & & \\ a_{n1} & a_{n2} & \cdots & a_{nn} \end{vmatrix} \begin{vmatrix} h(\sigma_1) \\ h(\sigma_2) \\ \cdot \\ h(\sigma_n) \end{vmatrix} = \begin{vmatrix} H(\alpha_1) \\ H(\sigma_2) \\ \cdot \\ H(\sigma_n) \end{vmatrix} \qquad \text{(B18)}$$

where the typical term in the matrix is

$$a_{jk} = G(A_j, \sigma_k) A_j$$

By adopting the following notation

$$\underline{\underline{A}} = (a_{jk})$$
$$\underline{h} = (h(\sigma_1), h(\sigma_2), \ldots\ldots, h(c_n))^T$$
$$\underline{H} = (H(\sigma_1), H(\sigma_2), \ldots\ldots, H(\sigma_n))^T$$

it follows that Equation (B18) may be rewritten as

$$-\underline{\underline{A}}\,\underline{h} = \underline{H} \qquad \text{(B19)}$$

Thus it is seen that a doublet distribution vector, $\underline{h}$ may be solved for directly with the equation

$$\underline{h} = -(\underline{\underline{A}})^{-1}\,\underline{H} \qquad \text{(B20)}$$

where $(\underline{\underline{A}})^{-1}$ is the inverse of $(\underline{\underline{A}})$.

The Time Rate of Change of the Doublet Strength

The equation for the differential pressure across the canopy surface includes a term which is the time rate of change of the doublet strength; i.e., $\partial \underline{h}/\partial t$. This term is evaluated by differentiating Equation (B20).

$$\begin{aligned} \partial \underline{h}/\partial t &= - \frac{\partial}{\partial t} (\underline{\underline{A}})^{-1} \underline{H} \\ &= - \partial (\underline{\underline{A}})^{-1}/\partial t \, \underline{H} - (A)^{-1} \partial H/\partial t \end{aligned} \quad \text{(B21)}$$

The first term on the right hand side of the latter equation is assumed small in relation to the second term, and Equation (B21) is approximated as

$$\begin{aligned} \partial \underline{h}/\partial t &= - (\underline{\underline{A}})^{-1} \partial \underline{H}/\partial t \\ &= - (\underline{\underline{A}})^{-1} \frac{\partial}{\partial t} \underline{\left[\dot{R} \sin\phi - (\dot{Z} + v) \cos\phi + w_c\right]} \\ &= - (\underline{\underline{A}})^{-1} \underline{\left[\ddot{R} \sin\phi - (\ddot{Z} + \dot{v}) \cos\phi\right]} \\ &\quad - (\underline{\underline{A}})^{-1} \underline{\left[(\dot{R} \cos\phi + (\dot{Z} + v) \sin\phi) \, d\phi/dt + \dot{w}_c\right]} \end{aligned}$$

The last bracket in the latter equation is assumed small in relation to the first bracket, and the expression for $\partial \underline{h}/\partial t$ is further approximated as

$$\begin{aligned} \partial \underline{h}/\partial t &= - (\underline{\underline{A}})^{-1} \underline{\left[\ddot{R} \sin\phi - (\ddot{Z} + \dot{v}) \cos\phi\right]} \\ &= - (\underline{\underline{A}})^{-1} \underline{\left[\ddot{r}_n - \dot{v} \cos\phi\right]} \end{aligned} \quad \text{(B22)}$$

where $\ddot{r}_n$ is the magnitude of the component of the canopy acceleration that is normal to the canopy surface. The latter equation may be alternatively written as

$$\partial \underline{h}/\partial t = - (\underline{\underline{A}})^{-1} (\ddot{\underline{r}}_n - \dot{v} \cos\phi) \tag{B23}$$

where $\ddot{\underline{r}}_n$ is the component of the canopy acceleration normal to the surface.

Equation (B23) is an approximate expression that was obtained by dropping several terms. The complete expression is Equation (B21). A solution based on the complete expression would be a worthwhile refinement of the present analysis.

APPENDIX C

STUDY RESULTS RELATED TO APOLLO ELS PROGRAM

The opening loads methods analyzed in this report are related to those used in the Apollo ELS development program as illustrated in Figure C1. This figure shows that the primary loads method used during the development of the Apollo ELS was the opening load factor method. Also, the area growth method was used to predict Stage 1 and 2 opening loads for the main parachutes. During the study reported herein, the specific Apollo parachute load calculation methods developed and continuously improved during the Apollo program were reviewed and, in most cases, improved. This appendix presents, on an example basis, the opening loads now predicted for the main parachute to illustrate these improvements in the prediction methods. These loads are then compared with those given in the final loads report for the Apollo Block II (H) ELS, Reference 3. In addition, the main parachute loads predicted for the first two stages by the modified Mass/Time Method are given.

It is emphasized that the loads presented in this appendix are the product of three essential factors:

1) Specific parachute load prediction methods developed and continuously improved during the Apollo ELS program,

2) The profoundly important NASA/MSC, NAR and Northrop analysis ground rules which defined design cases and various empirical and analytically determined factors and constants used in the analysis, e.g., data scatter factors, command module dynamics factors, and

3) The refinement of empirical data during the study reported herein.

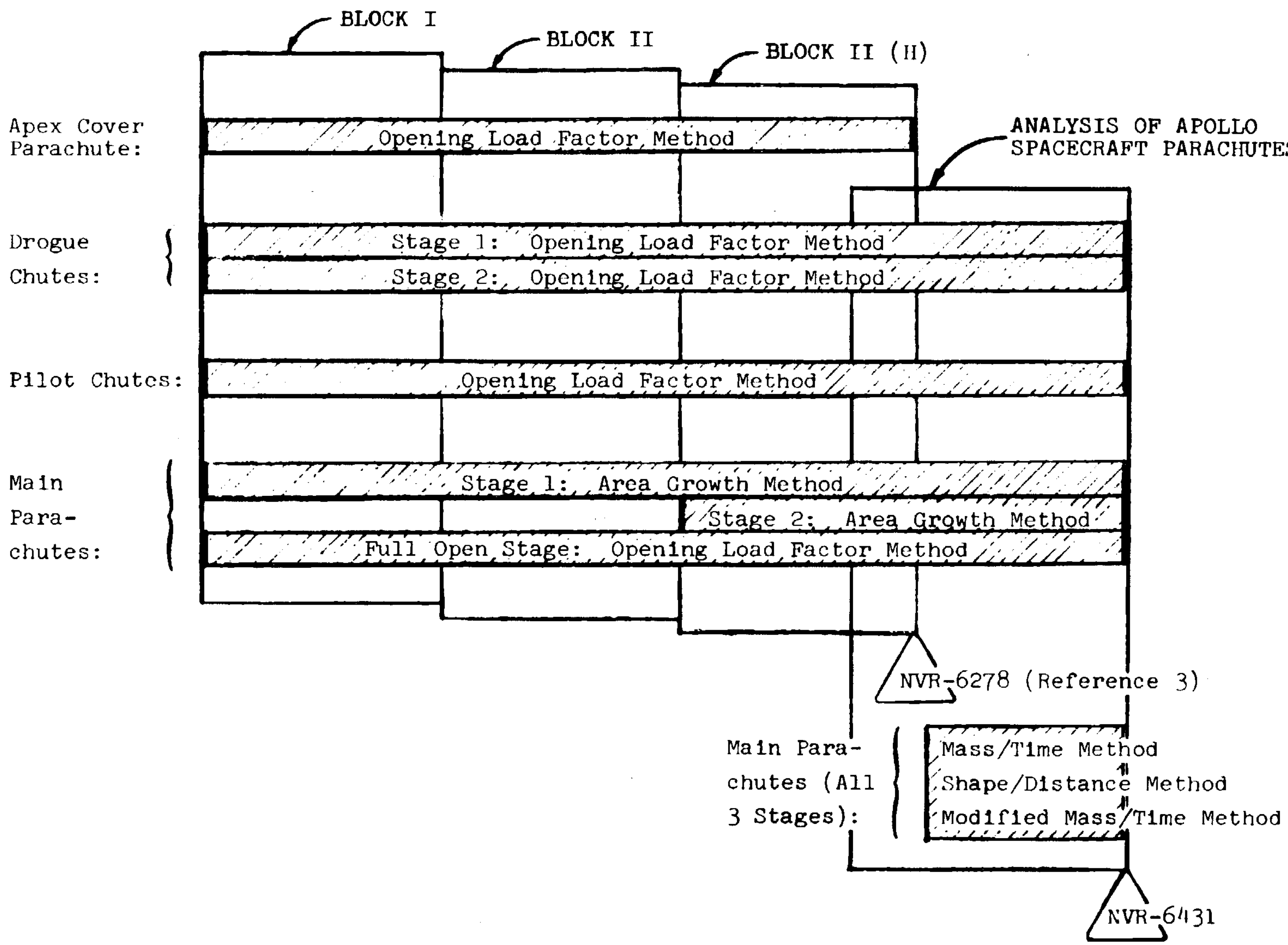

Fig. C1. Schematic Illustrating Progression of Load Prediction Methods During Total Apollo ELS Program

Study Results Used in the Final Apollo ELS Loads Report

Program overlap between the Block II (H) program and the study reported herein allowed several results to be integrated into the final Apollo ELS loads report, Reference 3. These results, which were of the nature of data analysis refinements, were presented as Figures 6-5 and 6-7 of Reference 3. Figure 6-5, which presented main parachute opening load factor versus effective unit canopy loading for Stage 3, was prepared during the study reported herein, subsequently modified, and is now presented in its modified form as Figure 19. Figure 6-7 presented, in effect, the dynamic drag area of lag parachutes at the time of lead parachute maximum load versus the dimensionless time parameter, $\Delta t_{d2}/t_{f_{oL}}$. This figure, which was a modification of a previous figure, is now presented as Figure 21.

Study Results Illustrated with Example Calculations

Results of the study reported herein are illustrated, on an example basis, for the main parachute loads of one Apollo design case. This case, identified as Case 410, is a normal entry case for which one drogue chute and two main parachutes operate. (This is the critical case for entry and limiting with respect to extending the present ELS system to higher velocities and/or payloads.) For this case, the following conditions, taken from Reference 3, apply: vehicle weight, 12,960 lb; flight dynamic pressure at canopy line stretch, 85.0 lb/ft^2; flight path angle, -90 deg; altitude, 10,750 ft; time from drogue chute disconnect to lead MCLS, 1.6 sec; time from drogue chute disconnect to lag MCLS, 1.8 sec.

Stage 1 Maximum Load - Using Figure 31 and the 80 percent reduction factor discussed on page 149, the drag area at the completion of the rapid initial filling may be shown to be 257 ft^2 for the lead parachute. The fill time, found with the aid of Figure 17, is 1.89 sec. The lag parachute, which achieves

MCLS 0.2 sec after the lead parachute, ia analyzed by the method given in Reference 3 (a vehicle dynamics factor of 1.05 and a scatter factor of 1.10 are used). These data, when used as input values to the 2-DOF trajectory program GT03, produce a maximum Stage 1 opening load (lead parachute), F_{r_1} = 18,650 lb.

Stage 2 Maximum Load - Using Figure 31 and the 90 percent reduction factor discussed on page 149, the drag area at the completion of the rapid filling is determined to be 1026 ft^2 for the lead parachute. Stage 2 fill time is found with the aid of Figure 15 (b) to be 1.108 sec. All other parameters are determined by the methods given in Reference 3 (a combined vehicle dynamics-scatter factor of 1.05 is used). These data, when used as input values to the 2-DOF trajectory program GT03, produce a maximum Stage 2 opening load (lead parachute), F_{r_2} = 18,350 lb.

Stage 3 Maximum Load - The method used to predict Stage 3 loads is explained in detail in Section 2.3. This method, when applied to the conditions of this example, produces a maximum Stage 3 opening load (lead parachute), F_o = 18,680 lb.

The three opening loads given above are shown in Table C1, together with the corresponding values taken from the final Apollo ELS loads report, Reference 3. Whereas the new values for Stages 1 and 3 are approximately 0.8 percent higher, the new value for Stage 2 is approximately 14.8 percent lower than the corresponding load from Reference 3.

Stage 1 and 2 Loads Predicted by the Modified Mass/Time Method

The maximum opening loads for Stages 1 and 2 were calculated with the modified Mass/Time Method for the same example case to provide another comparison. This method, although not yet developed for application to Stage 3 cluster loads, has shown good agreement ($\pm$ 5 percent accuracy) for single main parachutes and fair agreement ($\pm$ 10 percent accuracy) for the parachutes in

Stages 1 and 2 of 2- and 3-chute clusters of main parachutes. This method predicts F_{r_1} = 19,240 lb and F_{r_2} = 19,410 lb. These loads are approximately 3.9 percent higher and 9.9 percent lower, respectively, than the corresponding loads from Reference 3.

Table C1. Main Parachute Load Calculations for Example Case 410 (Normal Entry, One Drogue Chute and Two Main Parachutes)

Source	F_{r_1}	F_{r_2}	F_o
Baseline loads from final Apollo ELS loads report[3]	18,250 lb	21,540 lb	18,540 lb
Loads used in final Apollo ELS stress report[53]	20,250	23,400	22,000
Loads predicted on basis of results reported herein	18,650 (1)	18,350 (1)	18,680 (1)
Loads calculated by modified Mass/Time Method	19,240	19,410	–

NOTES: (1) These loads, multiplied by a 1.35 safety factor, are referred to in Appendix B of Volume II as "New Load" in an example margin of safety calculation for the Apollo ELS main parachutes.

REFERENCES

1. Mullins, W. M., Reynolds, D. T., Lindh, K. G. and Bottorff, M. R., "Investigation of Prediction Methods for the Loads and Stresses of Apollo Type Spacecraft Parachutes, Volume II - Stresses," NVR-6432, June 1970, Northrop Ventura, Newbury Park, Calif.

2. Torgerson, R. E., "Contract End Item Detail Specification Performance/Design Requirements - Apollo Block II Parachute Subsystem, Earth Landing System," Spec. No. SS-00003, Rev. 3, 1 October 1969, Northrop Ventura, Newbury Park, Calif.

3. Finck, R. D. and Gran, W. M., "Loads and Stability Analysis for Critical Operational Cases - Apollo Block II Heavyweight ELS," NVR-6278, Sept. 1968, Northrop Ventura, Newbury Park, Calif.

4. French, K., "Inflation of a Parachute," AIAA Journal, Vol. 1, No. 11, Nov. 1963, pp. 2615-2617.

5. Chernowitz, G., ed., "Performance of and Design Criteria for Deployable Aerodynamic Decelerators," ASD-TR-61-579, Dec. 1963, AFFDL, Wright-Patterson Air Force Base, Ohio (AD 429 971).

6. Moeller, J. H., "Opening Shock Factor Analysis for Predicting Peak Disreef Loads for Clustered Parachutes and Evaluation of Apollo Main Parachute Design Loads," NVR-3949, Sept. 1965, Northrop Ventura, Newbury Park, Calif.

7. Wildhack, W. A., "Optimum Time of Delay for Parachute Opening," Journal of Aeronautical Sciences, Vol. 9, No. 6, June 1942.

8. Pflanz, Erwin, "Determination of the Decelerating Forces during the Opening of Cargo Parachutes," ATI-26111, July 1942, USAF Translation of German Report No. ZWB-4894.

9. Pflanz, Erwin, "Retarding Forces During Unfolding of Cargo Parachutes," ATI 20126, Sept. 1943, USAF Translation of German Report No. ZWB-1706.

10. Hallenbeck, Capt. G. A., "The Magnitude and Duration of Parachute Opening Shocks at Various Altitudes and Air Speeds," Army Air Force Memorandum ENG-49-696-66, July 1944.

11. von Karman, T., "Notes on Analysis of the Opening Shock of Parachutes at Various Altitudes," ATI 200-814, 1945.

12. Scheubel, Franz N., "Notes on Opening Shock of a Parachute," Progress Report No. IRE-65, April 1946, Foreign Exploitation Section, Intelligence (T-2).

13. O'Hara, F., "Notes on the Opening Behavior and the Opening Forces of Parachutes," Royal Aeronautical Society Journal, Vol. 53, Nov. 1949, pp. 1053-1062.

14. Heinrich, H. G., "Some Research Efforts Related to Problems of Aerodynamic Deceleration," WADD TN-60-276, Nov. 1961, Wright-Patterson Air Force Base, Ohio.

15. Heinrich, H. G. and Bhateley, I. C., "A Simplified Analytical Method to Calculate Parachute Opening Time and Opening Shock," paper presented to Symposium on Aerodynamic Deceleration, July 1961, Univ. of Minn., Minn.

16. Chernowitz, C., ed., "Performance of and Design Criteria for Deployable Aerodynamic Decelerators," ASD-TR-61-579, Dec. 1963, AFFDL, Wright-Patterson Air Force Base, Ohio, pp. 149-164.

17. Bhateley, I. C., "Dynamics of Opening of Reefed Parachutes," M. S. Thesis, Sept. 1961, Department of Aeronautical Engineering, University of Minn., Minn.

18. Buchanan, K. B., "The Physical Process of Parachute Inflation," paper presented to Symposium on Aerodynamic Deceleration, July 1965, Univ. of Minn., Minn.

19. Heinrich, H. G. and Noreen, R. A., "Analysis of Parachute Opening Dynamics with Supporting Wind Tunnel Experiments," Paper No. 68-924 presented to AIAA 2nd Aerodynamic Deceleration Systems Conference, Sept. 1968, El Centro, Calif.

20. Heinrich, H. G., "Experimental Parameters in Parachute Opening Theory," Shock and Vibration Bulletin No. 19, Feb. 1953, Research and Development Board, Department of Defense, pp. 114-121.

21. Heinrich, H. G., "The Opening Time of Parachutes Under Infinite Mass Conditions," paper presented to the 6th Aerospace Sciences Meeting, Jan. 1968, New York, N. Y.

22. Weinig, F. S., "On the Dynamics of the Opening Shock of a Parachute," TR-6, Feb. 1951, USAF Office of Aeronautical Research, Wright Air Development Center, Ohio (AD 84 500).

23. Foote, J. R. and Scherberg, M. G., "Dynamics of the Opening Parachute," paper presented to Second Midwest Conference on Fluid Mechanics, May 1952, Ohio State Univ., Ohio.

24. Foote, J. R. and Giever, J. B., "Study of Parachute Opening - Phase I," TR 56-253, Sept. 1956, Wright Air Development Center, Ohio.

25. Foote, J. R. and Giever, J. B., "Study of Parachute Opening - Phase II," TR 56-253, June 1958, Wright Air Development Center, Ohio.

26. French, K. E., "The Initial Phase of Parachute Inflation," Paper No. 68-927 presented to AIAA 2nd Aerodynamic Deceleration Systems Conference, Sept. 1968, El Centro, Calif.

27. Berndt, Rudi J., "Experimental Determination of Parameters for the Calculation of Parachute Filling Times," paper presented to WGLR-DGRR Annual Meeting, Sept. 1964, Berlin, Germany.

28. Schilling, D. L., "A Method for Determining Parachute Opening Shock Forces," Report No. 12543, Aug. 1957, Lockheed Aircraft Corporation, Burbank, Calif.

29. Rust, L. W., Jr., "Theoretical Investigation of the Parachute Inflation Process," NVR-3887, July 1965, Northrop Ventura, Newbury Park, Calif.

30. Bloetscher, F., "Aerodynamic Deployable Decelerator Performance Evaluation Program - Phase II," AFFDL-TR-67-25, June 1967, Wright-Patterson Air Force Base, Ohio.

31. Asfour, K. J., "Analysis of Dynamic Stress in an Inflating Parachute," Journal of Aircraft, Vol. 4, No. 5, Sept. - Oct. 1967, pp. 429-434.

32. Roberts, Bryan W., "A Contribution to Parachute Inflation Dynamics," Paper No. 68-298 presented to AIAA Second Aerodynamic Decelerator Systems Conference, Sept. 1968, El Centro, Calif.

33. Rust, L. W., Jr., "Determination of the Apparent Mass Factor (K)," IOC 2230/65-14, 3 Feb. 1965, Northrop Ventura, Newbury Park, Calif.

34. Ibrahim, S. K., "The Potential Flowfield and the Added Mass of the Idealized Hemispherical Parachute," AIAA Aerodynamic Deceleration Systems Conference, Sept. 1966, New York, N. Y., pp. 10-16.

35. Ibrahim, S. K., "Experimental Determination of the Apparent Moment of Inertia of Parachutes," FDL-TDR-64-153, Dec. 1964, Wright-Patterson Air Force Base, Ohio.

36. Scherberg, M. and Rhode, R. V., "Mass Distribution and Performance of Free Flight Models," NACA TN 268, Oct. 1927.

37. Kaplun, S., "Dimensional Analysis of the Inflation Process of Parachute Canopies," AE Thesis, California Institute of Technology 1951, (AD 90633).

38. French, K. E., "Model Law for Parachute Opening Shock," AIAA Journal, Vol. 2, No. 12, Dec. 1964, pp. 2226-2228.

39. Barton, R. L., "Scale Factors for Parachute Opening," NASA TN D-4123, Sept. 1967.

40. LaSalle, J. and Lefschetz, S., Stability by Liapunov's Direct Method, 1st ed., Academic Press, New York, 1961, pp. 21-26.

41. McEwan, A. J., Huyler, W. C. Jr., Mullins, W. M., and Reynolds, D. T., "Descriptions of Computer Programs for the Analysis of Apollc Spacecraft Parachutes," NVR-6428, June 1969, Northrop Ventura, Newbury Park, Calif.

42. Neustadt, M., Eriksen, R. E., and Guiteras, J. J., "Apollo Recovery System Dynamic Analysis," NVR-3528, April 1964, Northrop Ventura, Newbury Park, Calif. (Note: This report is proprietary to the Space and Information Division of the North American Rockwell Corp.)

43. Knacke, T. W., "The Apollo Parachute Landing System," TP-131, Paper presented at AIAA Second Aerodynamic Decelerator Systems Conference, Sept 1968, El Centro, Calif.

44. Chandrasekhar, S., "The Invariant Theory of Isotropic Turbulence in Magneto-Hydrodynamics," Proc. Roy. Soc. A., 1951.

45. Batchelor, G. K., The Theory of Homogeneous Turbulence, Cambridge University Press, 1960.

46. Lamb, H., Hydrodynamics, 6th Ed., Dover Publications, 1945.

47. Basset, A. B., A Treatise on Hydrodynamics, Vol. I, Dover Publications, 1961.

48. Milne-Thompson, L. M., Theoretical Hydrodynamics, 5th Ed., MacMillian Co., New York, 1968.

49. Harlow, F. H., "The Particle-in-Cell Method for Numerical Solution of Problems in Fluid Dynamics," Proceedings of Symposia in Applied Mathematics, Vol. 15, L.A.D.C. 5288, 1963, Los Alamos, New Mexico.

50. Private Communication from Dr. R. W. Latham of the Northrop Corporate Laboratories, 7 April 1969.

51. Ewing, E. G., "Recent Ringsail Parachute Developments and Some Advanced Landing System Concepts," Unpublished paper presented at the NASA Manned Spacecraft Center, 27 Sept. 1965, Houston, Texas.

52. Groat, J. F. Jr., and Nash-Boulden, S. S., "Analysis of Apollo Main Parachute Wind Tunnel Test Using Full, Half and Third Scale Models," NVR-2928, Jan. 1964, Northrop Ventura, Newbury Park, Calif.

53. Utzman, C., Mullins, W., Reynolds, D., Farnsworth, R. and Labbe, J., "Strength Analysis - Apollo Block II Earth Landing System, Weight Accommodation Program," NVR-6112A, Sept. 1968, Northrop Ventura, Newbury Park, Calif. (p 13).